UNIVERSITAT DE BARCELONA

Compound F: A novel nuclear receptor modulator and its potential application on hematologic malignancies

Eugenia Ruiz Cánovas

Compound F: a novel nuclear receptor modulator and its potential application on hematologic malignancies

Memòria presentada per Eugènia Ruiz Cánovas per optar al grau de doctora per la Universitat de Barcelona.

Eugènia Ruiz Cánovas

Programa de doctorat en Biotecnologia

Octubre 2018

Director:	Director:	Supervisor:
Jaume Mercadé Roca	Eva Estébanez Perpiñá	Carlos Balsalobre Parra

ABSTRACT

Compound F has been reported to possess important antioxidant, anti-inflammatory, anti-diabetic and anti-cancer effects, among other interesting properties. Although Compound F has been extensively investigated, its underlying mechanism of action has not been elucidated yet. In this thesis we describe a novel modulation of several nuclear receptors carried out by Compound F and other ABCs. Focusing on steroid receptors, we also report a direct interaction between Compound F and the glucocorticoid and androgen receptor. Despite the nature of the modulation has not been fully clarified, we propose that it could explain at least some of Compound F bioactivities. Precisely, amid all these potential applications of Compound F, we have centered in the treatment of hematologic malignancies. We report the deleterious effects of Compound F on different cell models of hematologic malignancies, concentrating on acute myeloid leukemia. Current findings also suggest that Compound F could have additive effects in combination with standard of care drugs. An important drawback for the use of Compound F in health applications is its poor water solubility and its low bioavailability. Here, we have developed an albumin-based nanoparticle formulation that overcomes this problem. Additionally, a primary evaluation of its toxicity and pharmacokinetic parameters after intravenous and oral administration to mice has been performed.

ACKNOWLEGDEMENTS

No PhD thesis happens without the personal and professional support of many people, and this one is not an exception. During this period, I have required assistance and encouragement many times, but thanks to those who have been by my side this thesis has been an enriching experience. Now, I feel profoundly grateful and would like to share some of my happiness.

I would like to start showing gratitude to Greenaltech and its founders, Olga, Jordi and Jaume; and also to Joan, for allowing me to pursue a PhD in an industrial environment. I want to especially thank Jaume, who has trusted me to handle this project and has always pushed me to be more creative and optimistic.

In the final stage of this adventure I have had the luck that Eva enrolled in the project and accepted to co-direct this thesis. I am deeply indebted with her for finding time to give me inestimable advice. I would also like to thank Alba, who together with Eva, have introduced me into the world of SPR and crystallography.

I would also like to thank the Biomed division of Leitat, especially José Luis and Sílvia. Thank you, José, for always be willing to share your knowledge and for you unwavering support in interpreting many unexpected results. Thank you, Sílvia, for doing your best in providing us with all the cell cultures we asked for.

I am grateful with Annabel and her Nuclear Receptor Research Group at UB. It meant a lot that you let me access your lab and learn from your team. I want to specially mention Joan, who taught me to perform qPCR assays (and the art of labcoat tuning). I also want to thank Carme, who, together with Annabel, have given us (and still are) invaluable support and counseling.

I could not have properly characterized our nanoparticles without access to a DLS equipment. For that, I must thank the Smart Nanobiodevices Research Group at IBEC. Special thanks to Angel, who has had infinite patience to measure colorful samples.

At last, but not least, I would like to thank all the current and former team members of Greenaltech. I strongly appreciate the contributions of the ones that have personally collaborated with this project: Borja, Noelia and Tania. I am particularly grateful with Xavi (or McÁlvarez Consulting) for his invaluable support in the chemical aspects of the project. Infinite thanks to Derek, MT, Cristina and Dani: Bio molones forever. Derek, thanks for always making us laugh, even in the hardest moments. Cristina, despite influencing me to drink more and more coffee, I admire how you always find a reason to smile. MT and Dani, you have always been my pillars inside and outside GAT. MT, I will never forget our funny

trips to Camps carrying all the cultures, or the endless evenings in the lab singing the latest *Chlamydomonas* hit. Dani, after countless hours in the lab, at the gym and at "Deutsch Unterricht", you still make that everything looks like an amusing game (and you cook delicious). Thank you, guys, for giving me the energy to go through my PhD.

I no seria jo sinó acabés barrejant llengües per poder arribar a tothom a qui tinc coses a agrair. En especial, als meus pares, per donar-m'ho tot. Gràcies per estimar-me, per animar-me i donar-me suport sempre i per valorar la importància de la meva educació. I també per tots els tuppers que m'han permès sobreviure durant la tesi! Gràcies a la Cristina, perquè tot i estar una mica boja, sempre ens arrenca un somriure (per sota del nas). I gràcies al Foc, per passar tantes hores fent-me companyia mentre treballava!

Moltes gràcies LCP, perquè tot i que passi el temps, ens seguim fent costat. Sobretot gràcies Pep, Míriam, Alba i Raquel, sense vosaltres no seria el mateix. Us estimo lliures. Míriam, a tu t'haig d'agrair especialment el teu suport com a dissenyadora gràfica. Ets la millor!

Durant aquest període de tesis hi ha hagut molts moments durs, però he tingut la sort de tenir sempre el suport del Gerard. Gràcies per tot el que hem compartit.

Isa, sóc afortunada de tenir una super compi de pis i veïna de lab. I sobretot, una gran professora d'immunos! Gràcies al Ferran i a la Laia, també, per escoltar tots els drames de doctorands. Us dec un gelat en algun destí tropical.

Tampoc em puc oblidar de donar les gràcies al Cosp i a l'Anna, per aquests sopars estadístics tan útils (i bons).

All of you have contributed to make me a better professional and person than I would have been without your influence. Thank you.

CONTENTS

LIST OF FIGURES ..... **V**

LIST OF TABLES ..... **IX**

ABBREVIATIONS ..... **XI**

INTRODUCTION **1**

COMPOUND F 3

Health benefits of Compound F 3

OBJECTIVES 5

CHAPTER 1. Assessment of Compound F modulation of nuclear receptors: a focus on GR **7**

INTRODUCTION 9

THE NUCLEAR RECEPTOR SUPERFAMILY 9

ABCs and NRs 11

THE GLUCOCORTICOID RECEPTOR 11

Structure of the glucocorticoid receptor 11

GR isoforms 12

GR function and regulation 14

GR ligands 20

Compound F bioactivities and glucocorticoids 22

MATERIALS AND METHODS 25

EXTRACTION AND PURIFICATION OF ABCs 25

NR-TRANSACTIVATION TR-FRET ASSAYS 25

GR AND PXR COMPETITIVE BINDING TR-FRET ASSAYS 26

NR-COREGULATOR INTERACTION TR-FRET ASSAY 27

INDUCTION OF MMTV PROMOTER ACTIVITY (TR-FRET ASSAY) 28

TR-FRET DATA TREATMENT 28

SURFACE PLASMON RESONANCE 29

GR expression and purification 29

Sensor surface preparation 30

Binding detection....30
Affinity and kinetics analysis....31
GFP-GR TRANSLOCATION ASSAY....32
NATIVE GR STUDIES IN HaCat CELLS....32
Cell culture....32
Protein extraction....33
Western blotting....33
EXPRESSION ANALYSIS IN MOUSE MACROPHAGES....34
IL8 DETERMINATION IN MONOCYTES....36
TNFα DETERMINATION IN MONOCYTES....36
TNFα DETERMINATION IN MACROPHAGES....37
STATISTICAL ANALYSIS....37
RESULTS....39
INFLUENCE OF ABCS ON NRs TRANSCRIPTIONAL ACTIVITY....39
Transactivation inhibition on subfamily NR3....40
Transactivation inhibition on retinoid receptors....46
PPARγ inhibition....48
COMPOUND F COMPETITIVE BINDING TO GR AND PXR....50
COMPOUND F INFLUENCE ON NRs–COREGULATOR INTERACTION....52
BINDING AFFINITY OF COMPOUND F AND COMPOUND F3 TO AR AND GR....55
Compound F binding to GR....55
Compound F binding to AR....57
Compound F3 binding to GR....58
Compound F3 binding to AR....59
INHIBITION OF MMTV PROMOTER ACTIVITY BY COMPOUND F....61
COMPOUND F INFLUENCE ON GR-MEDIATED REGULATION OF INFLAMMATION....63
Expression of GC-transactivated anti-inflammatory genes....63
Effect on LPS-induced inflammation....64
Effect on PMA-induced inflammation....67
EFFECT OF COMPOUND F ON GR NUCLEAR TRANSLOCATION....71
Effect on GFP-GR translocation....71

Effect on native GR translocation 73
MODULATION OF GR EXPRESSION AND DEGRADATION BY COMPOUND F 76
DISCUSSION 77
CHAPTER 2. Evaluation of Compound F activity on cell models of hematologic malignancies 89
INTRODUCTION 91
HEMATOLOGIC MALIGNANCIES 91
Classification 91
Current drugs and treatments 94
COMPOUND F EFFECTS ON HMs 101
Formulation of Compound F for *in vivo* administration 101
MATERIALS AND METHODS 103
EXTRACTION AND PURIFICATION OF ABCS 103
IN VITRO ASSAYS 103
Cell viability assay: IC50 determinations 103
Apoptosis, cytotoxicity and viability assay 104
Cell cycle analysis by flow cytometry 105
COMPOUND F FORMULATION IN ALBUMIN NANOPARTICLES 105
Nanoparticles preparation 105
Nanoparticle analysis and characterization 105
IN VIVO EXPERIMENTATION 106
Animal models 106
Repeated dose toxicity study 107
Pharmacokinetic studies 108
STATISTICAL ANALYSIS 110
RESULTS 111
CYTOTOXICITY EVALUATION OF COMPOUND F ON HM CELL LINES 111
Assessment of the cytotoxic activity of Compound F on different HM cell lines 111
Comparison with the cytotoxicity of other ABCs on THP1 114
Cytotoxic activity of Compound F in combination therapy 116

INDUCTION OF APOPTOSIS BY COMPOUND F 124
EFFECT OF COMPOUND F ON MONOCYTES' CELL CYCLE 127
COMPOUND F FORMULATION IN ALBUMIN NANOPARTICLES 129
Nanoparticles characterization and scalability 129
Stability of Compound F-albumin nanoparticles 132
REPEATED DOSE TOXICITY STUDY OF F-BSA NPs 136
Maximum tolerated dose (MTD) assessment 136
Hematologic profiles 136
Biochemical analysis 140
Biodistribution 141
PHARMACOKINETICS OF COMPOUND F IN MICE 143
DISCUSSION 149
GENERAL DISCUSSION AND FUTURE PROSPECTS 163
CONCLUSIONS 169
REFERENCES 173

LIST OF FIGURES

Figure 1. Functional classification of the NR superfamily. 10
Figure 2. GR domain structure and PTMs 12
Figure 3. Alternative processing of the GR gene, located on chromosome 5q31–32 13
Figure 4. Overview of GR mechanisms of action and regulation 15
Figure 5. Construct used for expressing AncGR2(LBD)....30
Figure 6. Fluorescent detection of GAL4(DBD)-NR(LBD) transcriptional activity 40
Figure 7. Inhibition curves of different ABCs on NR3C....42
Figure 8. F and F3 inhibition curves of ERs and ERRs 45
Figure 9. F inhibition curves of retinoid receptors 47
Figure 10. PPARγ inhibition curves....48
Figure 11. Layout of the competitive binding TR-FRET assay....50
Figure 12. GR and PXR ligand displacement by F 51
Figure 13. Layout of the GR-coregulator interaction TR-FRET assay....52
Figure 14. F effects on NR-coactivator interaction. 53
Figure 15. Dexamethasone binding to AncGR2(LBD) 56
Figure 16. F binding to AncGR2(LBD) 57
Figure 17. F and dexamethasone binding to AR(LBD). 58
Figure 18. F3 binding to AncGR2(LBD) 59
Figure 19. F3 binding to AR(LBD) 60
Figure 20. Inhibition of MMTV promoter transactivation caused by Compound F....61
Figure 21. Fluorescent detection of MMTV promoter activity....62
Figure 22. Induction of the anti-inflammatory genes Gilz and Mkp1 in macrophages 64
Figure 23. IL8 secretion of LPS-stimulated monocytes after treatment with F....65
Figure 24. Effect of F on LPS-induced inflammation in macrophages....66
Figure 25. IL8 secretion of PMA-stimulated monocytes after treatment with F....68

Figure 26. TNFα secretion in monocytes after treatment with PMA, DEX and F 69

Figure 27. TNFα expression and secretion in macrophages after treatment with PMA, DEX and F 70

Figure 28. Quantification of F effect on GFP-GR nuclear translocation 72

Figure 29. Effect of F on GFP-GR nuclear translocation 73

Figure 30. Effect of F on GR nuclear translocation in HaCat cells 75

Figure 31. Effect of F on GR expression in HaCat cells 76

Figure 32. Overview of hematopoiesis and cell types affected by HMs.....93

Figure 33. General classification of HMs based on the origin of the disease and cell types involved.....94

Figure 34. F and DEX reduce cell viability of several HM cell lines: TF-1 (AML), CCFR-CEM (ALL), MV-4-11 (biphenotypic AML+ALL) and MM1s (MM) 113

Figure 35. F reduces cell viability of several HM cell lines with higher efficacy than DEX: HL-60 (AML), K562 (CML), Ramos (NHL) and U937 (NHL) 114

Figure 36. Some ABCs reduce cell viability of THP1 with higher efficacy than DEX 115

Figure 37. Cytotoxic activity of F and its metabolite F3 in combination with cytarabine...117

Figure 38. Isobologram analysis of the interaction of cytarabine with F or F3 119

Figure 39. Cytotoxic activity of F in combination with different cytotoxic drugs in MV-4-11 cells 120

Figure 40. Cytotoxic activity of F in combination with ATRA, calcipotriol and rosiglitazone in MV-4-11 cells 122

Figure 41. Viability, cytotoxicity and apoptosis curves of MV-4-11 treated with F for different periods of time.....125

Figure 42. Viability, cytotoxicity and apoptosis curves of MV-4-11 treated with staurosporine 126

Figure 43. Evolution of estimated IC50 of F on MV-4-11 over time.....126

Figure 44. Influence of F on THP1 cell cycle 127

Figure 45. Cell cycle analysis by flow cytometry of the incubation of THP1 with F.....128

Figure 46. Scheme of the electrical double layer on the surface of a negatively-charged particle 129

Figure 47. Characterization of F-BSA NPs prepared at different w/w ratios 131

Figure 48. Characterization of different batches of F-BSA NPs at 1:5 w/w ratio.....132

Figure 49. Stability of F in different batches of F-BSA nanoparticles at 1:5 w/w ratio 134

Figure 50. Stability of DLS parameters in different batches of F-BSA nanoparticles at 1:5 w/w ratio 135

Figure 51. Progression of body weights along the RDT study 136

Figure 52. Findings in the hematologic profiles of mice after the RDT study.....138

Figure 53. Biochemical blood parameters of mice at the end of the RDT study.....142

Figure 54. Pharmacokinetic profiles of F and its metabolites after an IV bolus administration 146

Figure 55. Pharmacokinetic profiles of F and its metabolites after oral administration 147

LIST OF TABLES

Table 1. Main studied post-translational modifications on GR and their characteristics. 17

Table 2. Functional classes of coregulators (coactivators and corepressors) reported to interact with GR 19

Table 3. F effects comparable to a GR agonist. 22

Table 4. F effects comparable to a GR antagonist. 22

Table 5. Parameters in LanthaScreen™ Coregulator Assays for the different NRs studied. .27

Table 6. Tested run conditions in the surface plasmon resonance. 31

Table 7. Primers used in the qPCR for the determination of mRNA levels in macrophages.35

Table 8. Estimated parameters for the GR inhibition curves of different ABCs 43

Table 9. Estimated parameters for the AR inhibition curves of different ABCs....44

Table 10. Estimated parameters for PR inhibition curves of different ABCs 44

Table 11. Estimated parameters for the antagonist effect of different ABCs on MR....45

Table 12. Estimated parameters for the antagonist effect of F and F3 on NR3A and NR3B. 46

Table 13. Estimated parameters for the antagonist effect of F on retinoid receptors 47

Table 14. Estimated parameters for the PPARγ inhibition curves of different ABCs....49

Table 15. Estimated parameters of GR and PXR ligand displacement by F 51

Table 16. Estimated parameters for the effect of F on NR-coactivator interaction....54

Table 17. SPR-derived parameters of F-GR and F-AR binding 58

Table 18. SPR-derived parameters of F3-GR and F3-AR binding 60

Table 19. Estimated parameters for inhibition curves of TNFα secretion....69

Table 20. Current available treatments for hematologic malignancies 96

Table 21. Treatment groups in the repeated dose toxicity assay. 107

Table 22. Treatment groups in the intravenous and oral kinetics assay. 108

Table 23. Characteristics of tested HM cell lines. 111

Table 24. Estimated parameters for the cytotoxicity curves of dexamethasone on HM cell lines. 112

Table 25. Estimated parameters for the cytotoxicity curves of F on HM cell lines. 113

Table 26. Estimated parameters for the cytotoxicity curves of different ABCs on THP1 cell line. 116

Table 27. Estimated parameters for the cytotoxicity curves of the combination of cytarabine with F or F3 in two cell lines. 118

Table 28. Estimated parameters for the cytotoxicity curves of the combination of different cytotoxic drugs with 0.5µM F in MV-4-11 cells. 121

Table 29. Combination indexes (CI) of the interaction of different cytotoxic drugs with 0.5 µM F on MV-4-11 121

Table 30. Estimated parameters for the cytotoxicity curves of the combination of F with NR ligands drugs in MV-4-11 cells. 123

Table 31. Hematologic profiles of mice at the end of the RDT study 139

Table 32. Standard deviations of average measures in Table 31. 140

Table 33. Concentrations of F3 in brains and pancreas from mice subjected to the RTD study 142

Table 34. Estimated pharmacokinetic parameters of F and its metabolites after an intravenous bolus administration 144

Table 35. Estimated pharmacokinetic parameters of F and its metabolites after a single-dose oral administration 145

ABBREVIATIONS

5FU	5-fluorouracil
A	Compound A
ABC	ATP-binding cassette
Act	Activation
ALL	Acute Lymphoblastic Leukemia
AML	Acute Myeloid Leukemia
APL	Acute Promyelocytic Leukemia
AR	Androgen receptor
ATL	Adult T-cell leukemia
ATRA	All-trans retinoic acid
B	Compound B
Bla	Beta-lactamase
BM	Bone marrow
BSA	Bovine serum albumin
CaPT	Calcipotriol
CE	Cytoplasmic extract
CF	Competition factor
CI	Combination index
CLL	Chronic lymphoid leukemia
CML	Chronic myeloid leukemia
COX	Cyclooxygenase
Dex	Dexamethasone
DBD	DNA binding domain
DHFR	Dihydrofolate reductase
Disp	Displacement
DLS	Dynamic Light Scattering
DMA	Dimethylacetamide
DMEM	Dulbecco's Modified Eagle's medium
DMSO	Dimethyl sulfoxide
DR	Daunorubicin
ER	Emission ratio
ESI	electrospray ionization source
FBS	Fetal Bovine Serum
FD	Freeze-drying
F	Compound F
F2	Compound F2
F3	Compound F3
F4	Compound F4
GC	Glucocorticoid
GCB	Gemcitabine
GILZ	Glucocorticoid-induced leucine zipper
GR	Glucocorticoid Receptor

GRA	Granulocytes count
GRA%	Granulocytes percentage
GRE	Glucocorticoid response element
GST	Glutathione S-transferase
h	Hour
HCT	Hematocrit
HGB	Hemoglobin
HL	Hodgkin's lymphoma
HMs	Hematologic malignancies
HRE	Hormone response elements
HSA	Human serum albumin
IC50	Half maximal inhibitory concentration
IL	Interleukin
L	Compound L
LBD	Ligand binding domain
LLD	Lenalidomide
LPS	Lipopolysaccharide
LYM	Lymphocytes count
LYM%	Lymphocyte percentage
MCH	Mean corpuscular hemoglobin
MCHC	Mean corpuscular hemoglobin concentration
MCV	Mean corpuscular volume
MDR	Multidrug resistance
MF	Mometasone furoate
MID	Medium size cells count
MID%	Medium size cells percentage
Min	Minute
Mkp1	Mitogen-activated protein kinase phosphatase 1
MM	Multiple myeloma
MPD	Mean particle diameter
MPV	Mean platelet volume
MR	Mineralocorticoid receptor
MTD	Maximum Tolerated Dose
MTX	Methotrexate
N	Compound N
NCoR	Nuclear receptor corepressor
NE	Nuclear Extract
NEAA	Non-Essential Amino Acid
NGFIB	Nerve Growth factor IB
NHL	Non-Hodgkin's lymphoma
NLCs	Nanostructured lipid carriers
NO	Nitric oxide
NOR1	Neuron-derived orphan receptor 1
Nos2	Nitric oxide synthase 2
NP	Nanoparticle
NR	Nuclear receptor

NURR1	Nuclear receptor related 1
PB	Peripheral blood
PBS	Phosphate buffered saline
PCT	Platelet percentage
PDI	Polydispersity index
PDWcv	Platelet distribution width coefficient of variation
PDWs	platelet distribution width Standard deviation
PEG	Polyethylene glycol
PEL	Primary effusion lymphoma
PLT	Platelet count
PMA	Phorbol 12-myristate 13-acetate
PTM	Post transcriptional modification
PP	Polypropylene
PPAR	Peroxisome Proliferator-Activated Receptor
PR	Progesterone receptor
PXR	Pregnane X receptor
RBC	Red blood cell count
RDWcv	Red cell distribution width coefficient of variation
RDWs	Red cell distribution width Standard deviation
RDT	Repeated dose toxicity
ROS	Reactive oxygen species
RGZ	Rosiglitazone
RT	Room temperature
RU-486	Mifepristone
SD	Standard deviation
SEPS	Self-emulsifying phospholipid suspensions
SLNs	Solid lipid nanoparticles
SMRT	Silencing mediator for retinoid and thyroid hormone receptors
S-SNEDDS	Self-nanoemulsifying drug delivery systems
TNFα	Tumor necrosis factor α
TR-FRET	Time-resolved fluorescence resonance energy transfer
TRF	Transcription factor
UAS	Upstream Activator Sequence
VD	Vacuum-drying
Y	Compound Y
w/w	Weight/weight
WBC	Total white blood cell count
WCE	Whole Cell Extract

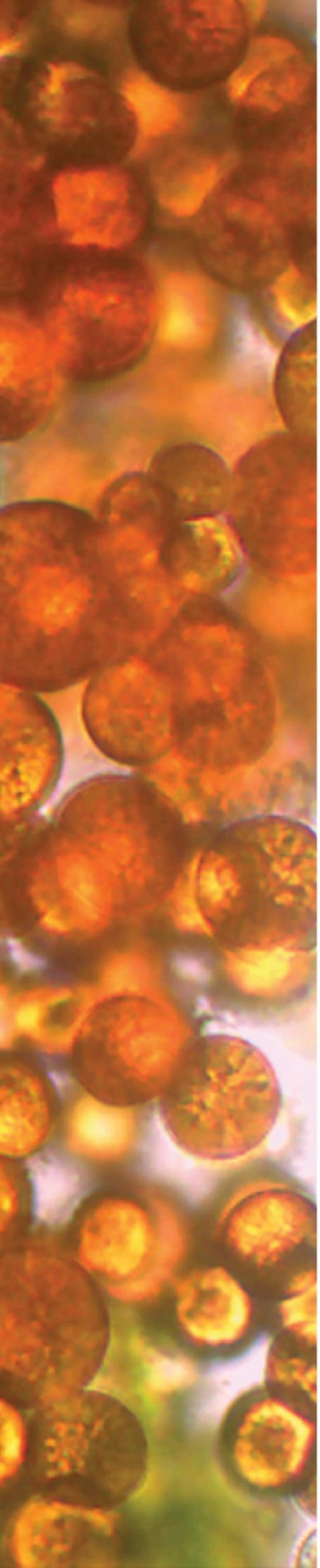

INTRODUCTION

COMPOUND F

Compound F (F) is found in many microalgae and macroalgae. It possesses a unique chemical structure that includes an allenic bond and many oxygenic functional groups. Purified F is highly susceptible to degradation due to high temperatures, low pH and light exposure.

F has been shown to possess many beneficial properties for humans. Therefore, it has recently attracted considerable attention and is now one of the most studied molecules of its family (from now on family ABCs). Potential and actual applications are discussed in the following section.

F-containing algae are largely consumed worldwide. When ingested, F is thought to be metabolized to Compound F2 (F2) by intestinal or pancreatic cells, which is later converted to Compound F3 (F3) in the liver. All these metabolites have also started to be studied and, to the moment, have shown similar beneficial properties to F.

Health benefits of Compound F

In the past decade, F and its metabolites have been extensively studied for their potential applications in human health as antioxidant, anti-inflammatory, anti-cancer, anti-obesity, anti-diabetes and anti-malarial; and in hepatoprotection, skin protection, bone protection, neuroprotection and ocular protection. However, no mechanism of action has been identified that fully explains this compound's bioactivities.

OBJECTIVES

This thesis project has been divided into three main blocks. In a first chapter, we intended to explore the putative effect of Compound F on different nuclear receptors, in particular on the glucocorticoid receptor, as a possible mechanism of action of some of its unexplained bioactivities. Therefore, the following objectives were established:

- Screening of the activity of Compound F on different nuclear receptors, especially on steroid receptors, and preliminary characterization of its selectivity.
- Primary characterization of the effects of other ABCs on the same targets, especially of Compound F's metabolite Compound F3.
- Characterization of a possible interaction between Compound F and the GR.
- Initial characterization of the regulation of GR function by Compound F.

In a second block, inside Chapter 2, and given Compound F's described antitumor activities, we intended to study its potential as a drug for the treatment of hematologic cancers. In this case, the following aims were settled:

- Determination of Compound F's cytotoxicity on hematologic cell lines and comparison with other ABCs.
- Characterization of Compound F's general effects on the cell cycle of hematologic cell lines.
- Screening of the combined cytotoxic effects of Compound F and standard-of-care drugs on hematologic cell lines.

In the last section, again inside Chapter 2, the aim was to obtain preliminary data on the *in vivo* administration of F. This data is essential to proceed to the evaluation of F efficacy in animal models of hematologic cancers. Consequently, the following goals were established:

- Development of an aqueous formulation of Compound F to allow intravenous delivery and enhanced bioavailability.
- Preliminary pharmacokinetic and toxicology studies of the developed formulation in mice.

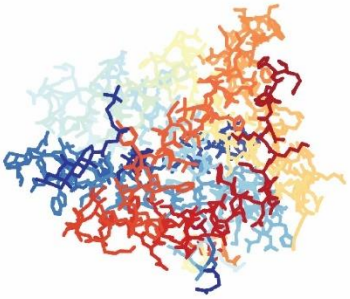

CHAPTER 1

ASSESSMENT OF COMPOUND F MODULATION OF NUCLEAR RECEPTORS: A FOCUS ON GR

Introduction

Materials and methods

Results

Discussion

INTRODUCTION

THE NUCLEAR RECEPTOR SUPERFAMILY

Nuclear receptors (NRs) comprise a large family of TRFs and several of its members are ligand-regulated by lipid-soluble (hydrophobic) molecules. They directly regulate transcription of genes that control a wide variety of biological processes, including cell proliferation, development, metabolism, stress response, inflammation and reproduction. Apart from functioning as TRFs in the nucleus, many of them also have non-genomic effects within the cytoplasm (1,2).

The regulation of NRs is highly complex and far from being understood. While ligands allosterically control the interactions of NRs with coactivators and corepressors (3), NRs are also influenced by post-translational modifications (PTMs). Consequently, their gene regulation is cell-type and context dependent. Furthermore, a complex network of interactions between NRs exists, as they usually govern similar regulatory cascades and cross-react with their cognate DNA binding sites. This broad transcriptional regulatory network is thought to determine physiological processes dependent on the anatomical site and circadian rhythm. As they are involved in many metabolic and developmental processes (see Figure 1), their dysregulation has been associated to numerous human diseases, including cancer, asthma and diabetes (2,4,5). At the same time, they represent one of the most successful drug targets for multiple indications, such as hypertension or cardiovascular diseases. Current developments are focused on small molecules that selectively modulate NR activities, trying to minimize or overcome their side effects, mostly due to ligand-binding promiscuity to other related NR members.

In humans, there are 48 members of the NR superfamily, which are classified in four subtypes based on their general mode of action (1). Type I receptors are found mainly in the cytoplasm until ligand binding occurs. Then, they generally undergo homodimerization and translocate to the nucleus, where they bind to DNA sequences termed hormone response elements (HREs). Type II receptors, such as the retinoic acid receptor, reside in the nucleus and generally form heterodimers with the retinoid X receptor (RXR). In the absence of ligand, they commonly repress transcription, while in the presence of ligand they activate it. Type III receptors function similarly, but they bind to HRE direct repeats. Type IV receptors bind to DNA and act as monomers.

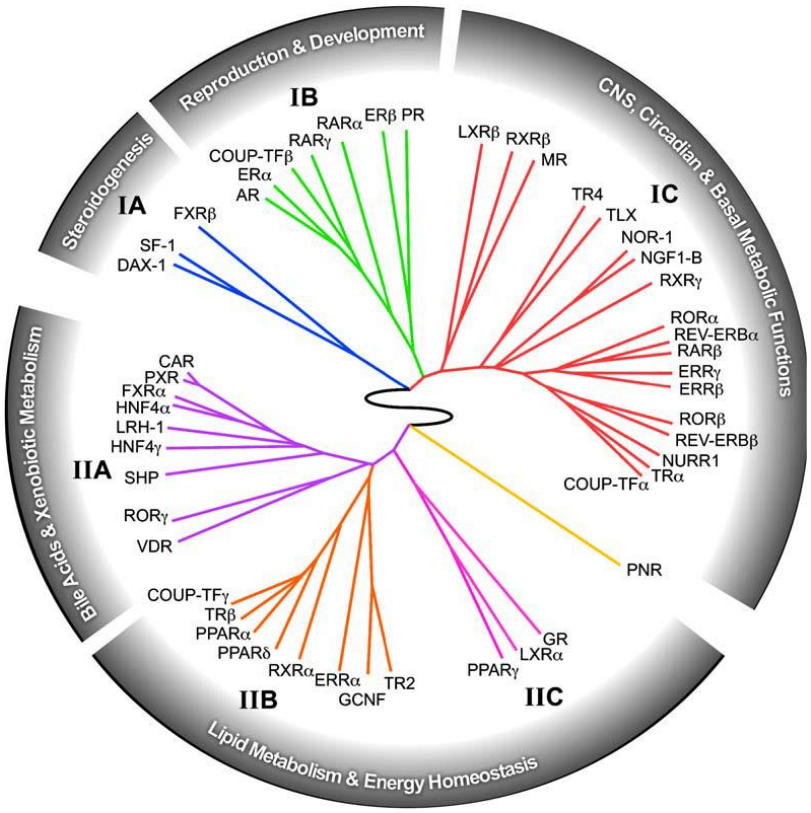

Figure 1. Functional classification of the NR superfamily. The clustering of NRs is made according to tissue expression distribution profiles, receptor function and physiology. Obtained from (5).

The NR superfamily is also classified according to their sequence homology in 7 subfamilies (6). Among them, steroid receptors constitute subfamily 3 and are one of the most studied subfamilies. It is composed by two groups: estrogen receptors (ERs) (group A) and oxosteroid receptors (group C). ERs (α and β), whose main natural ligand is the hormone estradiol or E2, play important roles in sex maturation and gestation. They are known to be altered in most breast cancer subtypes and have also been related to obesity (7). Group C comprises glucocorticoid receptor (GR), mineralocorticoid receptor (MR), progesterone receptor (PR) and androgen receptor (AR). Their main endogenous ligands are cortisol, aldosterone, progesterone and testosterone respectively. While PR and AR also have pivotal roles in development and sex maturation, MR regulates ionic and water transport. These NR are related to different diseases and so represent druggable targets: PR antagonists have been developed to induce abortion (i.e. mifepristone), AR antagonists are used in the treatment of prostate cancer (i.e. Enzalutamide) and MR antagonists are antihypertensives (i.e. aldosterone). The GR receptor, which regulates metabolism and immune response, will be discussed more in detail below.

All 7 subfamilies of NRs share a common modular structure, comprising a highly variable amino-terminal domain (NTD), where transactivation regions are found; a central conserved

DNA-binding domain (DBD); a nuclear localization signal (NLS) situated in a hinge region; and a fairly conserved carboxy-terminal ligand-binding domain (LBD) (1,2).

ABCs and NRs

ABCs are found among most living organisms. They are either synthesized by them or incorporated through the diet. In land plants and vertebrates ABCs can be cleaved to produce compounds with regulator roles.

They have long proved to confer several health benefits. Among the different proposed mechanisms of action, the interaction with TRFs, notably with members of the NR superfamily, are of particular interest for their potent applications. Nowadays, there is only preliminary evidence of functional interactions between ABCs and NR signaling.

Due to their hydrophobic nature, ABCs easily transverse the cell membrane. There, they would predictably be able bind to TRFs of the NR superfamily, which usually have lipophilic ligands.

THE GLUCOCORTICOID RECEPTOR

The glucocorticoid receptor (GR) is encoded by the NR subfamily 3 group C member 1 (NR3C1) gene, located on chromosome 5 (5q31) and is expressed ubiquitously in vertebrate cells. It belongs to type I receptors and it controls key processes involved in development, metabolism, stress response and inflammation (8). Native GR ligands are endogenous steroid hormones, such as cortisol, but numerous synthetic glucocorticoids (GCs) have been developed over the years.

Structure of the glucocorticoid receptor

As mentioned before, NRs from group 3C (GR, MR, PR and AR) share a common domain structure that consists of an NTD, a DBD and a LBD situated at the carboxyl terminal region. The DNA-binding domain is linked to the LBD by a hinge region, which contains an NLS (Figure 2). The DBD contains residues that enable both base-specific and nonspecific contacts with the DNA, as well as an important subdomain for GR dimerization (8).

Within these domains there are three important regulatory regions: activation function domain 1 (AF1) or τ1, transactivating domain 2 or τ2 and activation function domain 2 (AF2).

While the AF1 is situated in the NTD, τ2 and AF2 are located on each end of the LBD (Figure 2) (8). Despite the DBD and LBD are highly conserved between group 3C receptors; the NTD, including AF1, is more divergent in sequence and size. Differences are accentuated by alternative splicing and translational start sites that produce multiple isoforms of each NR3C family member.

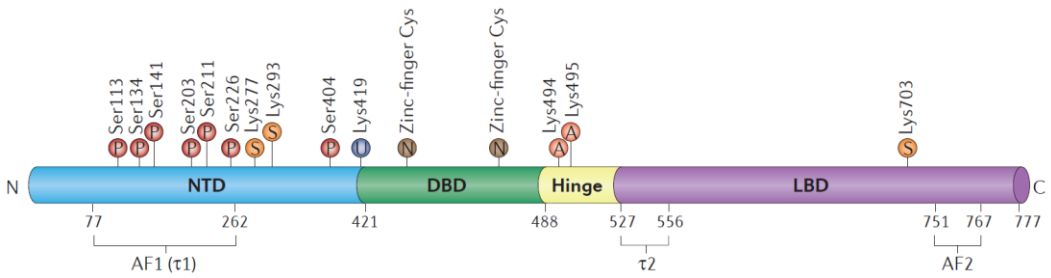

***Figure 2. GR domain structure and PTMs**. It consists of amino-terminal domain (NTD), DNA-binding domain (DBD), hinge region and ligand-binding domain (LBD). Transcription regulation segments, indicated below the scheme, include activation function domain 1 (AF1, τ1), tau2 (τ2) and AF2. Major reported sites of GR post-translational modifications are mapped over each domain. They include phosphorylation (P), sumoylation (S), ubiquitylation (U), acetylation (A) and nitrosylation (N). Obtained from* (8).

GR isoforms

Two main GR isoforms (GRα and GRβ) are generated by alternative splicing of the GR gene, which only differ in the C-terminus (Figure 3a). GRα is the most common isoform and has been extensively studied. GRβ, on the other hand, resides in the nucleus and does not regulate GC-responsive genes. Although it has not been reported to bind to any GC agonist, it binds mifepristone, which actively regulates transcription (9,10). It has recently been implicated in inflammatory diseases (11,12). Moreover, it is thought that GRβ could act as a dominant negative inhibitor of GRα by different mechanisms: competition for DNA binding, competition for coregulators or formation of inactive heterodimers (13,14). Three more minority isoforms generated by splicing have been described: GRγ, GR-A and GR-P. They are less well-characterized but present reduced activity compared to GRα, thus they have been associated with glucocorticoid insensitivity (15,16).

GRα also undergoes alternative translation initiation, generating eight additional isoforms of GR that are distinguished only by the length of their N-terminus (GRα-A, GRα-B, GRα-C1, GRα-C2, GRα-C3, GRα-D1, GRα-D2, αnd GRα- D3) (Figure 3b). They differ in their activity and

are thought to regulate GR signaling based on their relative availability in a given cell or a tissue type (17). Similarly, GRβ may also generate eight β isoforms (14). An added mechanism for generating diversity in GR protein expression is the alternative promoter usage (18).

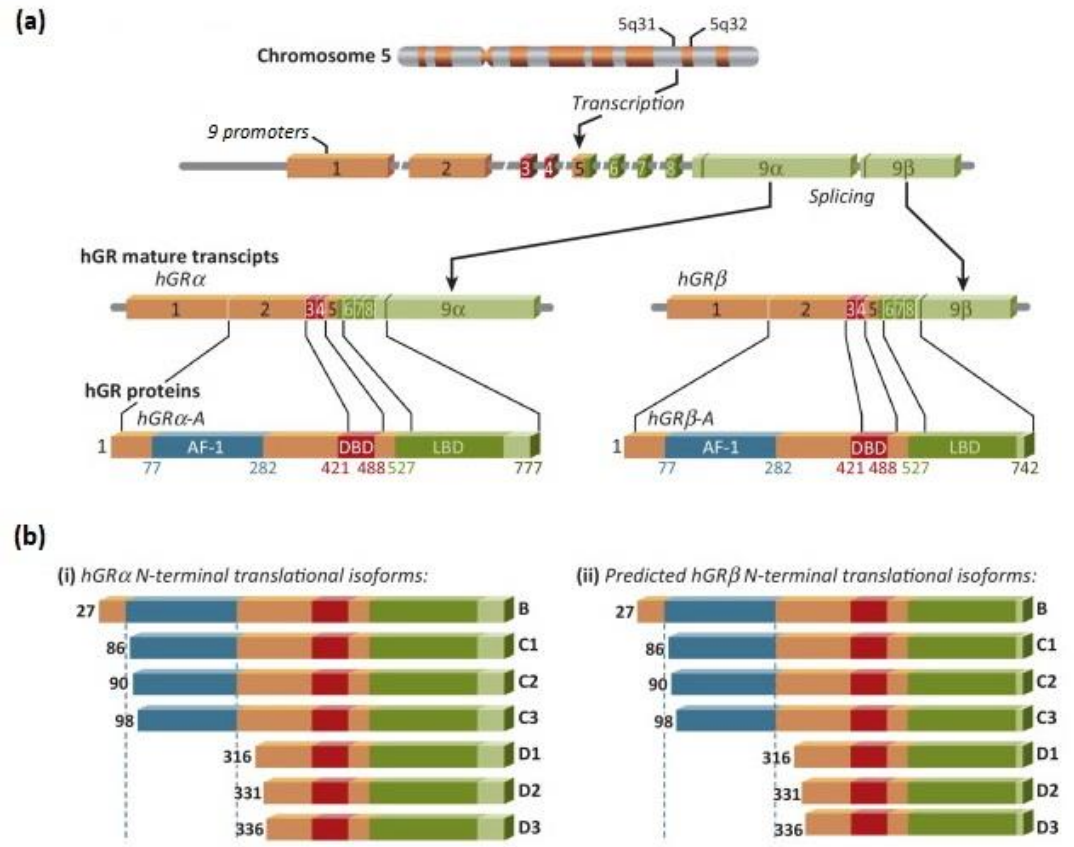

Figure 3. Alternative processing of the GR gene, located on chromosome 5q31–32. (a) *GR undergoes alternative splicing to yield multiple functionally distinct isoforms. The main isoforms GRα and GRβ are depicted, which differ only in the C-terminus. GR contains nine exons: exon 1 corresponds to the 5' untranslated region and contains 9 different transcription initiation sites; and exons 2–9 constitute the protein-coding region. (b) Alternative translation initiation of GRa generates eight additional isoforms with truncated N-terminus. GRβ is predicted to also generate the same isoforms. Modified from* (19) .

GR function and regulation

Classical GR pathway

In the absence of ligand (also referred to as Apo-GR), the receptor resides in the cytosol in a monomeric state. It is associated to molecular chaperone complexes, mainly the Hsp90/Hsp70 system, and other accessory proteins that promote ligand binding, like Hop and p23 cochaperones and immunophilins (8,20–23). As in Figure 4, upon ligand binding the GR undergoes a conformational change that exposes nuclear-localization sequences within the hinge and LBD region. This process allows the recruitment of immunophilin FKBP52, through which the complex binds to dynein. This motor protein transports the whole complex along the cytoskeleton to the nucleus, where it enters by importin-dependent facilitated diffusion (22–26). Once there, GR dissociates from the complex and develops its TRF function, activating or repressing glucocorticoid-responsive genes.

Specifically, GR associates with glucocorticoid response elements (GREs) in the genome and nucleates the assembly of transcription regulatory complexes that comprise the GR, other TRFs and coregulatory factors (Figure 4) (overviewed in Table 2). The occupancy of GREs has been observed *in vivo* by different techniques. There does not seem to be a proximity relationship between GRE and promoters of genes regulated by glucocorticoids. However, most GR-occupied regions appear to be at a distance of 10-100 kb from glucocorticoid-responsive genes (27). Some gene looping mechanisms have been proposed to explain the GRE-promoter interaction, but the complex dynamics of the interaction are still not fully understood. At the same time, many classes of GR-DNA interactions have been described (8,25). The best characterized is through the GR-binding sequence (GBS) present in GREs. It consists of two AGAACA repeats separated by a spacer of three-base pair length. GR binding to this canonical sequence is achieved as a dimer, given that in this conformation, interactions between two DBDs are stabilized. These interactions act in a positive cooperativity, promoting at the same time GR-DNA interaction (Figure 4a). LBD-LBD interactions have also been proposed to participate in this dimerization, although it has not been well demonstrated yet (28). Recent reports suggest that GR dimers, upon DNA binding, would trigger receptor oligomerization and GR would mainly function as a tetramer (29,30). The second interaction involves inverted-repeat GBS (IR-GBS), which contain the repeated motif CTCC$(N)_{0\text{-}2}$GGCGA separated by one-base-pair spacer. GR binds to opposite sides of these sequences in a head-to-tail fashion (Figure 4l). Although structural studies have shown this assembly, where the two monomers are not in direct contact; it is also true that a negative cooperativity has been observed. Thus, it is believed that GR acts on IR-GBSs as a monomer, hindering the binding of another monomer to the opposite side. This feature contrasts deeply with the cooperative binding seen in Figure 4a and is exclusive of GR, no other members of the NR3C family are able to bind to IR-GBSs. Other possible GR-DNA interactions involve different TRFs. GR can bind to DNA in cooperation with other TRFs

(Figure 4b and f) or through interacting with other TRFs (Figure 4c, d, h and i). In the first type, GR binds to GBS half sites, although the exact structure has not been characterized. No particular TRF's motifs have been proved to be enriched around GBSs. In the latter, indirect DNA binding is known as tethering. Known examples of this interaction are the TRFs AP-1 and NFκB (31,32). GR is also able to regulate transcription as a monomer by binding to GRE half-sites (Figure 4e and k) and to repress expression by competition (Figure 4g and m) or kidnapping of TRFs (Figure 4j) (33–36).

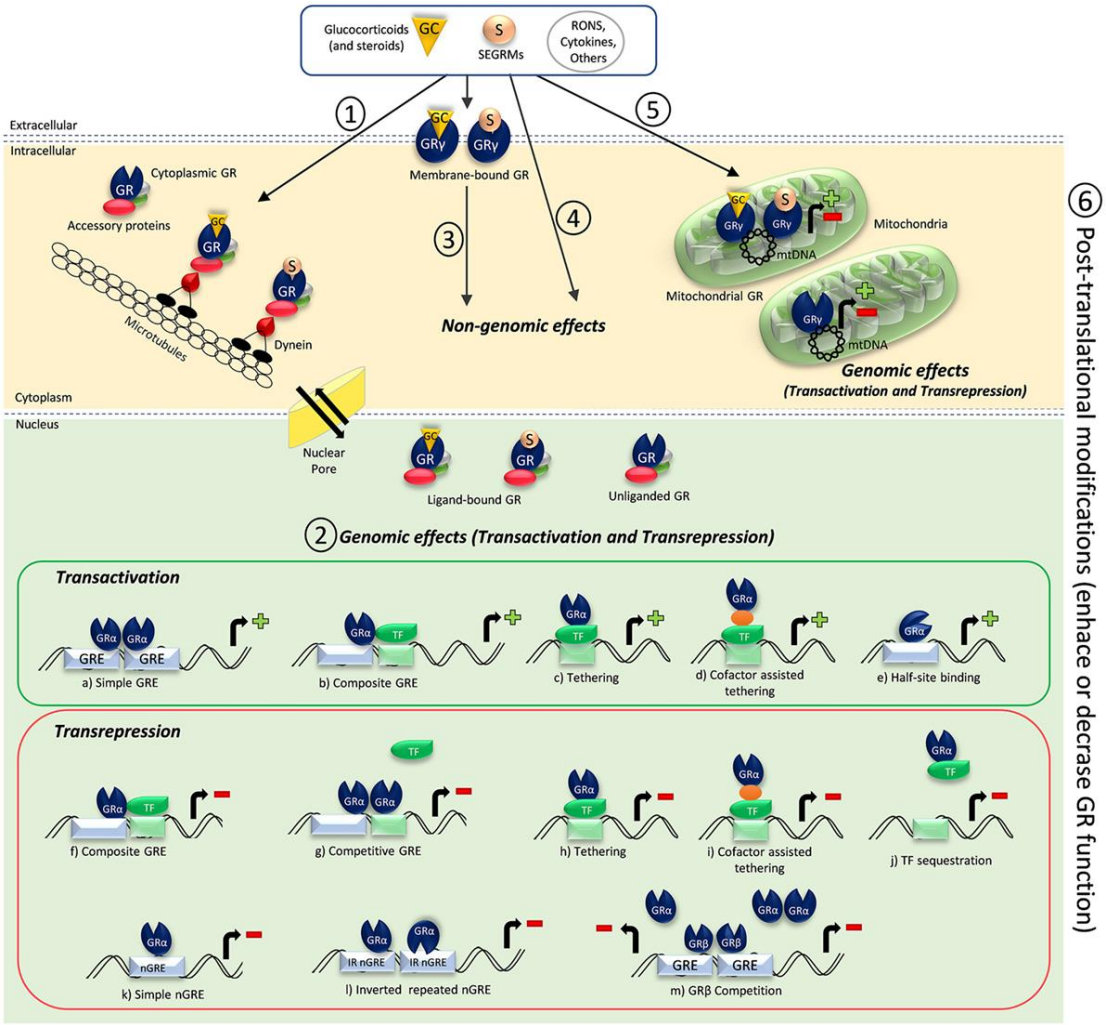

Figure 4. Overview of GR mechanisms of action and regulation. (1) A ligand (GC or SEGRAM) interacts with monomeric GR in the cytoplasm and dissociates the receptor from the chaperone complexes. Conformational changes in the GR allow nuclear transport along microtubules. Within the nucleus, the GR recruits other TRFs and coregulators to different GREs to activate or repress transcription of specific target genes. Dissociated chaperones and GR constantly shuttle between the nucleus and the cytoplasm through the nuclear pore. ROS, some cytokines and other substances, and conditions like shear stress can induce unliganded GR nuclear translocation. (2) Types of GR–genome interactions.

(a) GR homodimers binding to GRE. The DBDs from each monomer interact to allow dimerization. Recently, tetrameric structures have also been described. (b, f) GR can function in conjunction with other TRFs. In this case, GR binds to GBS half sites. (c, d, h, i) GR can indirectly bind to DNA through directly or indirectly interacting with other TRFs (tethering). In this case, it is not clear whether GR bind as a monomer or dimer. (e) Monomeric GR half-site binding. (g) GR homodimers can compete for an overlapping binding site. (j) Sequestration of a DNA-bound TRF. (k) Direct binding of monomeric GR onto a negative GRE (nGRE). (l) Two GR monomers bound to opposite sides of the DNA of an IR-GBSs. Although this structure has been crystalized, it is speculated that in vivo *GR may bind as a monomer to IR-GBSs with negative cooperativity. (m) GRβ can compete with GRα for an overlapping GRE, impairing GRα binding. (3) GR ligands can bind and interact with membrane-bound GR, leading to fast non-genomic effects. (4) Steroids at high concentrations can induce non-genomic effects through GR-independent mechanisms of action. (5) GR ligands can bind to mitochondrial GR or induce the translocation of cytoplasmic GR to mitochondria. GR can regulate transcription in mitochondrial DNA, which appears to be important to regulate mitochondrial functions and energy metabolism. (6) Posttranslational modifications modulate GR activation and function in all stages. Obtained from* (25).

GR regulates a wide range of gene networks in highly context-dependent manner. There are GR target genes specific for cell lines that can be controlled by different mechanisms (activated or repressed). It is hypothesized that the regulatory complex that assembles upon GR-DNA interaction depends on the context, as depicted in Figure 4. This theory is supported by the fact that multiple protein interaction domains have been detected along the GR by mutating specific residues. This regulation mechanism would confer specificity to GREs while enabling plasticity. Those characteristics would be achieved through different allosteric effectors: the physiological and pharmacological context provides a set of ligands and PTMs; DNA sequences imply gene-specific context; and the expression of different TRFs at different levels confers cell-specific context (8). Firstly, GRE spacer sequences and sequences flanking the GBS affect GR conformation. They are thought to act as allosteric effectors on GR and to extend the conformational change from the DBD into the NTD and LBD, and even into the dimer or tetramer partners. These changes can favor and stabilize dimerization or induce negative cooperativity, ultimately affecting transcription regulation (37). This is also the case for composites GREs, where GR acts together with other TRFs. Their contact could cause allosteric effects that modulated GR activity. Additionally, GR-GRE occupancy can be influenced by the presence of other TRFs. GR conformation state is not only specific to the DNA sequence or TRF partner, but it also depends on the ligand (38). The crystal structure of the LBD in complex with different ligands revealed that they do not completely fill the binding pocket, leaving space for potential interactions with different molecules. It is the case of cortisol and dexamethasone (DEX), for instance (39). Moreover, conformation changes depending on the ligand denote once more the complex regulation of the receptor.

Even ligand dose modifications can influence chaperone affinity, DNA binding or regulatory transcription complex recruitment and composition.

GR post-translational modifications

Next regulatory stage of GR functioning are PTMs. The receptor can be modified by different PTMs at distinct sites, as shown in Figure 2. The main known ones have been summarized in Table 1.

Table 1. Main studied post-translational modifications on GR and their characteristics.

PTM	Characteristics
Acetylation	▪ Acetylation reduces GR-DNA binding and transcription and has been shown to be important for circadian rhythm maintenance and repression of NFκB regulated genes (40). ▪ Lys494 and Lys 495, situated in the hinge region, are acetylated by CLOCK and BMAL1 and deacetylated by histone deacetylase 2 (HDAC2). This motif is conserved among the NR3C family, suggesting regulation of general functions (41).
Phosphorylation	▪ The GR presents seven confirmed phosphorylation sites. All of them are conserved serines present in the NTD: Ser113, Ser134, Ser141, Ser203, Ser211, Ser226 and Ser404 (42). ▪ The GR maintains a basal phosphorylation level (42). ▪ A range of kinases from several pathways phosphorylate *in vitro* the different sites: CDKs, MAPKs, JNKs and GSK-3 (43). ▪ GR phosphorylations are related to context-dependent effects. For instance: o Ser211 phosphorylation causes increased GR-DNA recruitment (44). o Ser203 is phosphorylated upon ligand binding and avoids GR nuclear translocation. It also appears to allow the PTM in Ser226, which increases nuclear export (45,46). o Ser211, Ser203 and Ser226 are comprised in the AF1 and are predicted to affect cofactor interactions by changing GR exposed surfaces (45,46).
Ubiquitylation	▪ Ubiquitylation of lysine residues targets the protein for proteasomal degradation (47). ▪ Ubiquitylation of Lys419 causes GR nuclear export and degradation (48).

Sumoylation	▪ Lys 277, Lys293 and Lys703 can be sumoylated with context-dependent functions. ▪ Lys293 has been particularly linked to repression of both IR-GBS-regulated genes, such as inflammatory genes; and AP-1 and NFκB tethering sites. It acts by promoting the recruitment of repressive regulatory complexes and assisting in weak GR-DNA interactions. Oppositely, it does not seem to affect genes controlled by canonical GBSs (49).
Nitrosylation	▪ Four cysteine residues in each zinc finger domain are susceptible of covalently binding nitric oxide to their thiol group. Nitrosylation causes the release of bound zinc and the inhibition of ligand binding (50). ▪ As happens to other NRs, it is hypothesized that nitrosylation could inhibit DNA binding and dimerization (51).

GR coregulators

The GR heterocomplex includes many coregulators that confer structural or functional changes upon the receptor, therefore modulating transcription. More than 300 coactivators and/or corepressors have been identified and grouped in 5 main functional classes (Table 2). Their presence is cell-dependent and so they are part of the context-specific regulation of the GR (8).

The most well-studied interaction domain of coregulators is AF2 (Figure 2). There, most coregulators bind to NR boxes or corepressor NR boxes, both composed of highly conserved motifs (52,53). Coregulators can also bind to the more disordered AF1 domain, stabilizing it, or to τ2 domain (54).

Non-genomic effects of the GR

The classical mechanism of action of GR comprises the regulation of gene expression. However, increasing evidence suggests that it also acts via rapid, nongenomic mechanisms, which also vary depending on the tissue (Figure 4).

Firstly, membrane bound GRs (mGRs) have been identified that act like G-protein coupled receptors (55–57). Secondly, GR has been found in mitochondria, along with GRE sequences in mitochondrial DNA (58–60). GR translocation from cytoplasm to mitochondria has also been detected in T cells (61,62). Lastly, protein-protein interactions between active GR and different kinases, such as ERK, c-Jun or phosphoinositol-3 kinase, have been reported (63,64). Interestingly, those effects are not antagonized by mifepristone.

Nongenomic effects have long been exploited in clinical therapy, even if they have just started to be studied. For instance, GCs inhibitory effects on neutrophil degranulation, phagocytosis and the generation of reactive oxygen species (ROS) are thought to be mediated by this mechanisms (65,66). Other therapeutic effects mediated by nongenomic mechanisms include GC vascular protective effect and anti-inflammatory actions in allergic and asthma reactions (67–70).

Table 2. Functional classes of coregulators (coactivators and corepressors) reported to interact with GR. *Adapted from* (8).

Functional class	Examples	Outcome
Structural and enzyme-interacting	p160 SRC family (SRC 1-3)	Transcription activation and structural stability (71,72). At least SRC-2 can also repress gene expression.
	Mediator	Recruitment of transcriptional machinery and enzymatic activities (73).
	HIC-5	Recruitment of transcriptional machinery and mediator in a gene-dependent way (74).
	COCOA	Synergy with p160 (75).
	CCAR1	Recruitment of mediator and p160.
Chromatin remodeling	BRG1 and BRM	ATPases that relieve the repressive state of chromatin context-specifically (76).
Methyltransferases	CARM1	Transcription activation of SRC-2-dependent genes (77).
	Lys methyltransferase G9a	Transcription activation and repression (78).
Histone acetyltransferase	CBP/p300	Cell-dependent transcription activation or repression (79).
	PCAF	Recruitment of transcriptional machinery (80).
Histone deacetylase	NCoR, SMRT	Transcription repression (49,81,82).

Ligand-independent GR activation

Several evidences support that unliganded GR can undergo activation, translocation and expression regulation (Figure 4) (83). Conditions as elevated pH or temperature, shear stress or exposure to different substances (sodium arsenite, dinitrophenol or TNFα) have proven to activate GR in the absence of ligand and both transactivation and transrepression

activities have been described (84–88). Interestingly, ligand-independent dimerization and activation has been reported to take place in cells containing high levels of receptor. In this case, it also enhances ligand binding and potentiates its effect (88). Although the mechanism of ligand-independent activation is still not completely understood, it has been suggested that phosphorylation at Ser211 and Ser134 could be involved (42,89). Some ligand independent effects have been proposed to function through nongenomic mechanisms (90).

GR ligands

Agonists

Cortisol is the endogenous glucocorticoid in humans, though numerous synthetic GCs have been developed. This steroid hormone is produced in the adrenal cortex following a circadian rhythm and is regulated by the hypothalamic-pituitary-adrenal (HPA) axis. It regulates a wide range of processes by modulating gene expression via GR. Cortisol has various metabolic effects, for example the promotion of gluconeogenesis and increase in the catabolism of lipids and proteins. It also exerts regulatory effects upon the cardiovascular and musculoskeletal system, although its main influence is the suppression of the immune system. Finally, it regulates glucocorticoid production by a negative feedback and controls the circadian rhythm (91).

The first reported synthetic GCs date back to 1950s, although cortisone had already been used to treat rheumatoid arthritis (92). Glucocorticoid therapy is used nowadays mainly in immunosuppression and anti-inflammation (91). GCs are used as immunosuppressants to treat autoimmune diseases, such as hemolytic anemia or idiopathic thrombocytopenic purpura; hypersensitivities (allergies) and to prevent organ transplant rejection. As anti-inflammatory agents, they are indicated in many inflammatory diseases, such as rheumatoid arthritis, asthma or inflammatory bowel disease, but also in less severe conditions, as topical inflammations. Apart from that, glucocorticoids constitute the hormone replacement therapy in case of adrenal failure. Finally, they are also used in cancer treatment: in combination with cytotoxic drugs in leukemia, due to their lymphocyte reduction properties; and to reduce side effects caused by cytotoxic drugs.

Antagonists

To date, no glucocorticoid antagonist has been approved for clinical use in humans, although it has many potential applications. Disorders in the HPA axis (including stress) affect the production of glucocorticoids and have mild to severe health effects. Up-regulation of cortisol, such as in Cushing's syndrome or diseases of the adrenal gland (e.g. carcinomas), can have a major impact on the immune system, mainly by the suppression of response to infection or injury. It is also related to osteoporosis, muscle wasting, raised intracranial pressure, hypertension, glaucoma, wound healing impairment and diurnal rhythm

alterations (91,93–96). Importantly, GCs have been related to hyperglycemia, diabetes and obesity (93,94,96). Links between cortisol upregulation and cognitive disorders, such as depression, psychosis or Alzheimer, have also been reported (94,97–100). Cortisol has been used as a marker for cancer survival (101–104). Psoriasis, acne and atopic dermatitis, among other skin diseases, are caused or exacerbated by cortisol production (105,106). This hormone is also the basis for the development of a broad array of gastrointestinal disorders (107).

Nowadays, an excess in endogenous glucocorticoids is mainly treated with drugs that inhibit cortisol's biosynthetic pathway. However, they have multiple adverse effects. An alternative treatment for cortisol upregulation is mifepristone. It is a potent antagonist of PR, but also of GR, although activity as a partial agonist has also been described (108). While it has been investigated for the treatment of several of the mentioned conditions (109–111), it is only approved by the FDA for the treatment of Cushing's syndrome and hyperglycemia associated with endogenous glucocorticoid excess (96,108,112–114). However, due to its interaction with PR it causes several side effects (108,109). Other antagonist have also been evaluated but none has been approved yet (97,115).

Selective glucocorticoid modulators

Most recent studies in the field have centered their efforts in finding glucocorticoid modulators with minimal side effects. Specifically, selective glucocorticoid receptor agonists and modulators (SEGRAMs) are under development (94,116–122). They seek to display an improved therapeutic index by only acting via specific GR mechanisms. It is largely assumed that most anti-inflammatory effects of the GCs are mediated by transrepression mechanisms, while side effects are principally associated to transactivation. Although this assumption has proven to be too simplistic, several compounds (both steroidal and non-steroidal) have been described that selectively induce transrepression and only partially transactivation, and that display reduced systemic side effects (116,119,123–126). In fact, two SEGRAMs are currently on clinical trials. Fosdagrocorat has just successfully ended phase II for the treatment of rheumatoid arthritis and mapracorat is in different studies for the treatment of inflammatory skin and ocular disorders (127,128). The effect of SEGRAMs on GR non-genomic pathways has just started to be investigated, as well as GR-protein surface modulators, SEGRAM combinatorial approaches or their effects on GR splice variants. For instance, conjugation of SEGRAMs to glycine or albumin gives larger structures that are incapable of crossing the cell membrane but can act through mGRs (66,129). Tissue specific delivery systems for SEGRAMs is another open research line (116,123).

Compound F bioactivities and glucocorticoids

Although there is no current evidence of a direct interaction between F and glucocorticoid receptor (GR), several of its bioactivities might correspond to those of a GR modulator. These activities are briefly discussed in Table 3 and Table 4.

Apart from F, other ABCs have also been described to have effects comparable to a GR modulator. Compound A, for instance, is used in cosmetics for fat reduction and has been studied in relation to anxiety and the reduction of cataract formation induced by glucocorticoids. Compound L and Compound Z cause an increase in the synthesis of hyaluronic acid, contrarily to the skin atrophy caused by GCs. A lot of ABCs have been applied in skin treatments and have even been proposed to be used as immunosuppressors for the treatment of autoimmune diseases.

Table 3. F effects comparable to a GR agonist.

Activity	Description
Anti-tumor	There are numerous studies on the antitumor and cancer preventive effects of F. In cancer, GCs are mainly used in the treatment of leukemia. In this area, F has shown cytotoxic activity against several cell lines.
Anti-inflammation	Both GCs and F are known to inhibit several inflammation mediators, as TNFα, IL-6, IL-1β, COX-2 or nitric oxide (NO).
Anti-angiogenesis	F suppresses the differentiation of endothelial progenitor cells, avoiding new blood vessel formation. GCs also have anti-angiogenic properties through the down-regulation of VEGF, but not by affecting endothelial cells' viability, migration or proliferation.

Table 4. F effects comparable to a GR antagonist.

Activity	Description
Anti-diabetes and anti-obesity	GCs modulate the expression of adipocytokines related to insulin resistance and obesity. They downregulate adiponectin, while F upregulates it. F improves insulin signaling, decreases blood glucose and insulin levels in diabetic mice. However, GCs and F downregulate IL-6, MCP-1 and TNFα.

	GCs induce triglycerides accumulation in the liver and upregulation of fatty acid synthase, while F has opposite effects, including an increase in fatty acids oxidation.
Skin pigmentation	F inhibits tyrosinase activity and melanogenesis, whereas GCs stimulate it.
Bone protection	F suppresses osteoclastogenesis by inhibiting differentiation and inducing apoptosis in osteoclasts but has no effects on osteoblasts. Therefore, it prevents bone diseases as osteoporosis and rheumatoid arthritis. Although GCs are critical importance for bone homeostasis, they directly and indirectly cause bone loss. GCs inhibit bone formation by suppressing osteoblast proliferation and increasing osteoclast activity.
Brain protection	GC are known to accelerate the development of Alzheimer's disease by promoting β-amyloid fibrils. On the contrary, F has been shown to reduce the formation of those fibrils and oligomers.

MATERIALS AND METHODS

EXTRACTION AND PURIFICATION OF ABCs

ABCs were extracted from different microalgae species and purified following proprietary methods. Unless specifically stated, final purity was determined to be above 97% by HPLC-PDA.

NR-TRANSACTIVATION TR-FRET ASSAYS

SelectScreen™ Cell-based Nuclear Profiling Service by ThermoFisher®, based on GeneBLAzer™ technology, was used. The activation and inhibition of the expression driven by a NR was followed by Time-resolved fluorescence resonance energy transfer (TR-FRET), as in Figure 6. In the case of GR and according to SelectScreen™ protocol, GR-UAS-bla HEK 293T cells were thawed and resuspended in DMEM, phenol red free media, containing 2% CD-treated FBS, 0.1 mM NEAA, 1 mM Sodium Pyruvate and 100 U/mL/100 µg/mL Penicillin/Streptomycin; to a concentration of 625,000 cells/mL. RU-486 was used as a reference inhibitor and dexamethasone as reference agonist. Cell-free wells and wells without treatment were also included in the assay as background and no activation controls, respectively. 4 µL of a 10X serial dilution in DMSO of RU-486 (starting concentration 10 nM) or F (starting concentration 100 µM) were added to appropriate wells of a TC-Treated assay plate. 32 µL of cell suspension was added to the wells and pre-incubated at 37ºC and 5% CO2 in a humidified incubator for 30 minutes. 4 µL of 10X dexamethasone at the pre-determined EC80 concentration was added to wells containing the control antagonist or F. After 16-24 hours incubation, 8 µL of 1 µM LiveBLAzer™ FRET B/G substrate Loading Solution was added to each well and the plate was incubated for 2 hours at room temperature and read on a fluorescence plate reader.

To study other NRs, some changes in the protocol were applied. For androgen receptor, AR-UAS-bla GripTite™ 293 cells were resuspended to a concentration of 312,500 cells/mL. R1881 (metribolone) was the control agonist, while cyproterone acetate was the control inhibitor (starting concentration 3.16 nM). For mineralocorticoid receptor, MR-UAS-bla HEK 293T cells were seed at 781,250 cells/mL in a poly-D-Lysine assay plate. Spironolactone was used as reference antagonist at starting concentration 1 µM and aldosterone as agonist stimuli. For progesterone receptor, PR-UAS-bla HEK 293T cells were resuspended to 468,750 cells/mL. RU-486 (starting concentration 100 nM) was used as control antagonist and R5020 (promegestone) as agonist. For ERα, the cell line ER-alpha-UAS-bla GripTite™ 293 was plated at 625,000 cells/mL. 17-beta-estradiol and 4-hydroxytamoxifen were used as control agonist

and antagonist, respectively. For ERβ, the cell line ER-beta-UAS-bla GripTite™ 293 was resuspended at 625,000 cells/mL. 17-beta-estradiol and mifepristone were used as control agonist and antagonist, respectively. For ERRα, the cell line ERR-alpha-UAS-bla HEK 293T was plated at 625,000 cells/mL. XCT790 was applied as reference antagonist. For PPARγ, PPAR-gamma-UAS-bla HEK 293H cells were resuspended to 937,500 cells/mL in a poly-D-Lysine assay plate. T0070907 was assay's reference antagonist, at starting concentration 1 µM. Receptor induction was performed with rosiglitazone. For RXRα and RXRβ, the cell line RXR-alpha-UAS-bla HEK 293T or RXR-beta-UAS-bla HEK 293T was plated at 312,500 cells/mL. While the control agonist used was 9-cis retinoic acid, this assay does not have an antagonist control. For RARα, the cell line RAR-alpha-UAS-bla HEK 293T was plated at 312,500 cells/mL. ATRA and Ro-41-5253 were added as control agonist and antagonist, respectively. For RARβ and RARγ, the cell line RAR-beta-UAS-bla HEK 293T or RAR-gamma-UAS-bla HEK 293T were thawed at 312,500 cells/mL. The reference agonist used was ATRA and the control antagonist was AGN193109.

GR AND PXR COMPETITIVE BINDING TR-FRET ASSAYS

To study F binding to GR, SelectScreen™ Nuclear Receptor Profiling Service offered by ThermoFisher® was used. A Competitive Binding Assay based on LanthaScreen™ technology was carried out. In this assay, binding is detected by displacement of a fluorescent ligand, which results in a loss of FRET signal, as shown in Figure 11.

A 10-point titration curve of 3-fold serial dilutions (starting at 10 µM) was performed. According to manufacturer's protocol, between 4 µL and 160 nL of 100X F in DMSO plus 3.84 µL assay buffer (TR-FRET Coregulator Buffer K, GR stabilizing peptide, 5 mM DTT) were added to a black 384-well plate. After that, wells were supplemented with 8 µL of 2X GR/Antibody mixture and 4 µL of 4X tracer to a final concentration of 1080 nM of GR, 2 nM of Tb-anti-GST and 5 nM of GS1. Plate was incubated for 60 minutes at room temperature and read on a fluorescence plate reader. To establish minimum emission ratio, control wells without F were included. A known inhibitor control curve (dexamethasone) was also carried out to set maximum emission ratio.

To assess F binding to PXR the protocol described above was applied with the following exception: assay was performed in TR-FRET PXR (SXR) Assay Buffer, 5 mM DTT with final concentrations of 5 nM of PXR, 10 nM of Tb-anti-GST and 40 nM of Green fluorescent PXR tracer. SR-12813 was included as a known inhibitor in the control.

NR-COREGULATOR INTERACTION TR-FRET ASSAY

A coregulator assay recruitment or displacement was carried out by ThermoFisher SelectScreen™ service, as in Figure 13.

To study putative agonistic interactions, 10-point titration curves of 3-fold serial dilutions (starting at 10 µM) were performed. According to SelectScreen™ protocol, between 4 µL and 160 nL of 100X F in DMSO plus 3.84 µL assay buffer containing 5 mM DTT were added to a black 384-well plate. To study putative antagonistic interactions, assay buffer was replaced for a receptor's agonist at a pre-determined EC80 concentration (Table 5). This reference activator and a reference inhibitor were also included in the assay as control agonist and antagonist, respectively (Table 5). After that, wells were supplemented with 8 µL of 2X NR/Antibody mixture and 4 µL of 4X coregulator peptide to final concentrations listed in Table 5. Plate was incubated for 2-4 hours at room temperature and read on a fluorescence plate reader.

Table 5. Parameters in LanthaScreen™ Coregulator Assays for the different NRs studied.

NR group	NR	NR (nM)	Tb-anti-GST (nM)	Coregulator peptide	Known activator	Known inhibitor
1B	RARα	3.5	5	D22 (50 nM)	ATRA	-
	RARβ	2.5	5	SRC2-2 (125 nM)	ATRA	AGN193109
	RARγ	3	5	PGC1a (250 nM)	ATRA	-
1C	PPARγ	5	5	TRAP220/DRIP2 (125 nM)	GW1929	GW9662
2B	RXRα	10	5	PGC1a (500 nM)	9-cis-RA	-
	RXRβ	6	2	D22 (350 nM)	9-cis-RA	-
3B	ERRα	5	5	PGC1a (500 nM)	-	XCT790
3C	GR	540	5	SRC1-4 (300nM)	MF	RU-486

INDUCTION OF MMTV PROMOTER ACTIVITY (TR-FRET ASSAY)

SelectScreen™ CellSensor service by ThermoFisher® was used. In this assay, HeLa cells transfected with an MMTV-*bla* construct were used. The MMTV promoter contains a GRE, where the GR is known to bind and to activate gene expression. The expression of the *bla* reporter gene allowed to evaluate the effect of F on receptor's transactivation activity, as in Figure 21.

According to SelectScreen™ protocol, MMTV-bla HeLa cells were thawed and resuspended in OPTI-MEM assay media containing 0.5% dialyzed Fetal Bovine Serum (FBS), 0.1 mM Non-Essential Amino Acid (NEAA), 1 mM Sodium Pyruvate and 100 U/mL/100 µg/mL Penicillin/Streptomycin; to a concentration of 156,250 cells/mL. 32 µL of cell suspension was added to each well of a 384-well TC-Treated assay plate. Cells were incubated for 16-24 hours at 37ºC and 5% CO_2 in a humidified incubator. RU-486 was used as reference inhibitor. 4 µL of a 10X serial dilution in DMSO of RU-486 (starting concentration 100 nM) or the tested compound F (starting concentration 100 µM) were added to appropriate wells and pre-incubated for 30 minutes. 4 µL of 10X control activator dexamethasone at a pre-determined EC80 concentration was added and the plate was incubated for 5 hours. Cell-free wells and wells without treatment were also included in the assay as background and no activation (no act.) controls, respectively. Finally, 8 µL of the LiveBLAzer™ FRET B/G substrate Loading Solution was added to each well. After 2 hours of incubation at room temperature, the plate was read on a fluorescence plate reader.

TR-FRET DATA TREATMENT

Fluorescence values from FRET assays were corrected for background fluorescence and used to calculate the emission ratio (ER). In cell-based assays Equation 1 was used, while in biochemical binding assays Equation 2 was applied.

Equation 1 $$ER = \frac{Coumarin\ emission\ (460\ nm)}{Fluorescein\ emission\ (530\ nm)} \quad (130)$$

Equation 2 $$ER = \frac{Fluorescein\ emission\ (520\ nm)}{Terbium\ emission\ (495\ nm)} \quad (131)$$

For each compound concentration, either the activation (act.), inhibition or ligand displacement (disp.) percentage was obtained, according to the following formulas:

Equation 3 $$\%\ activation = \frac{ER_{compound} - ER_{no\ act.}}{ER_{100\%\ act.} - ER_{no\ act.}} \times 100 (130)$$

Equation 4 $$\%\ inhibition = \left(1 - \frac{ER_{compound} - ER_{no\ act.}}{ER_{EC80\ act.} - ER_{no\ act.}}\right) \times 100 \quad (130)$$

Equation 5 $$\%\ displacement = \frac{ER_{no\ disp.} - ER_{compound}}{ER_{no\ disp.} - ER_{100\%\ disp.}} \times 100 \quad (132)$$

Then, dose-response curves were fit to the following sigmoidal dose-response model using XLfit from IDBS (model number 205).

Equation 6 $$y = A + \frac{B-A}{1+\left(\frac{C}{x}\right)^{d}}$$

A is the minimum inhibition value (bottom plateau); B is the maximum inhibition value (top plateau); C is the determined IC50 for the compound; and D is the slope factor. The IC50 value corresponds to the relative IC50, i.e. the concentration of compound giving half the maximal inhibition observed.

Using ER values from controls, the Z'-factor was also calculated to assess cells responsiveness in each assay.

SURFACE PLASMON RESONANCE

Surface plasmon resonance (SPR) allows to measure molecular interactions in real time. To study the interaction between two molecules, one partner (called ligand) is attached to the surface of a sensor chip and the other (the analyte) is passed over in a continuous flow of sample solution. The changes in the concentration of analyte, as it binds to or dissociates from the surface, cause changes in refractive index within about 150 nm from the sensor surface. The detection of this deviation is the surface plasmon resonance event. The SPR response is directly proportional to the change in mass concentration close to the surface, and thus, allows to monitor molecular interactions and measure interaction kinetics and affinity.

SPR assays were performed by the Structural Biology of Human Nuclear Receptors Group at the Institute of Biomedicine of the University of Barcelona (IBUB).

GR expression and purification

Recombinant expression of the full-length GR results in a highly unstable protein. To enhance expression and stability, the ancestral variant AncGR2 LBD (GenBank accession number EF631976.1) is used in the SPR assays. It was phylogenetically inferred and is considered a precursor of vertebrate GR. Although it contains several mutations, ligand affinity is not affected (133).

AncGR2 LBD was cloned into a pMALCH10T vector and fused to a maltose-binding protein (MBP) with a hexahistidine tag and a tobacco etch virus (TEV) restriction site (Figure 5). The plasmid was transformed into the *E. coli* strain BL21(pLysS), which was grown in 4L LB cultures at 37°C until the sample reached an optical density at 600 nm of 1. Induction of protein expression was achieved by adding 1 mM IPTG and 50 μM dexamethasone. After

that cells were grown for 4-5 hours at 32°C and then lysed by sonication in a buffer containing 20 mM Tris-HCl (pH 7.4), 300 mM NaCl, 25 mM imidazole, and 10% glycerol. The receptor was expressed in the absence or presence of dexamethasone.

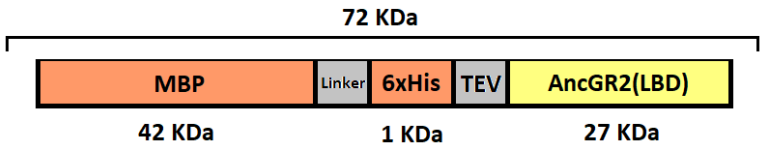

Figure 5. Construct used for expressing AncGR2(LBD).

Fusion protein was purified by the Structural Biology of Human Nuclear Receptors Group of IBUB following a proprietary method. Briefly, it was firstly purified affinity chromatography with HisTrap FF media (GE Healthcare). MBP tag removal was performed by means of TEV protease cleavage followed by an additional chromatographic step. Resulting protein was dialyzed and concentrated before immobilization into sensor chips.

Sensor surface preparation

The purified receptor was immobilized in CM5 S-series chips (GE Healthcare). These sensor chips consist in a dextran matrix functionalized with carboxyl groups, where the capturing molecule (AncGR2(LBD), denominated ligand) is covalently bound.

CM5 chips were first washed with water and immobilization buffer (0.1M Hepes, 1.5M NaCl, 30mM EDTA, 0.5% Tween20). Carboxyl groups were activated for amine coupling with a mixture of 75µL of EDC 0.2M and 75µL NHS 50mM for each channel. Resulting reactive succinimide esters were used for ligand binding, as they react spontaneously with primary amine groups on proteins. Immobilization of apo-AncGR2(LBD) and AncGR2(LBD) bound to dexamethasone was carried out in two different channels. In the first case, 0.8 mg/mL of receptor in acetate buffer at pH 5 were injected until 2056'9 RUs. Ethanolamine, used to deactivate excess reactive groups, was injected afterwards and channel was stabilized at 1880 RUs. In the second case, the receptor bound to dexamethasone was injected at 0.4 mg/mL in the same conditions until 2200 RUs. Deactivation was performed and response was stabilized at 1569 RUs.

Binding detection

Surface plasmon resonance was performed in a T200 Biacore (GE Healthcare). Analytes (dexamethasone and F) were injected at 60 µL/min in running buffer (containing Hepes,

Li_2SO_4, DTT and tween) with a maximum of 5% DMSO. Serial two-fold dilutions of the analytes were tested, starting at 250 µM. Three separate runs with different conditions were performed for each channel (Table 6).

Table 6. Tested run conditions in the surface plasmon resonance.

	Contact time (s)	Dissociation time (s)
Run 1	60.1	180.5
Run 2	90.1	180.5
Run 3	90.1	240.5

Affinity and kinetics analysis

The concentration of complex formed is measured in Response Units (RU) using the Biacore T200 control software. The measurements over a range of analyte concentrations allow to measure affinity and kinetic interaction parameters. In this case, data treatment was performed in Biacore T200 evaluation softwares (Scrubber and Biaval).

Kinetic parameters (association and dissociation rate constants) are usually obtained by fitting the sensogram data according to the 1:1 Langmuir model between analyte and ligand GR. Interaction kinetics could only be determined in one assay. In this case, response measurements as a function of time were plotted for each tested analyte concentration and resulting data was fit to the following model:

Equation 7 $$\frac{dR}{dt} = k_a \times C \times (R_{max} - R) - k_d \times R \quad (134)$$

k_a is the association rate constant ($M^{-1}s^{-1}$); C is the analyte concentration (M); R_{max} is the response at the maximum analyte binding capacity (RU); R is the response (RU); and k_d is the dissociation rate constant (s^{-1}). Closeness of fit was evaluated by the chi-square value. The significance of the obtained parameters was indicated by the standard error (T-value) and the U-value.

The affinity constant K_D reflects the strength of the binding, but not the rate, and can be derived either from the kinetic constants (Equation 8) or from binding analysis at steady state. As kinetics could not be determined in most assays, steady-state affinity equations were mainly used. Response measurements against analyte concentration in each run were fit to the model in Equation 9 and affinity was determined by Equation 10. Closeness of fit was evaluated by the chi-square value.

Equation 8 $$K_D = \frac{k_d}{k_a} \quad (134)$$

Equation 9 $$R_{eq} = \frac{K_A \cdot C R max}{K_A \cdot C + 1} \quad (134)$$

Equation 10 $$K_D = \frac{1}{K_A} \quad (134)$$

R_{eq} is the equilibrium response level (RU); C_{Rmax} is the analyte concentration at maximal response (M); C is the analyte concentration (M); K_A is the equilibrium association constant (M^{-1}); and K_D is the equilibrium dissociation constant or, simply, affinity constant (M).

GFP-GR TRANSLOCATION ASSAY

A GR nuclear translocation assay was performed by Innoprot, using HEK293 cells that stably express human full-length GR tagged with tGFP in the N-terminus. HEK293 tGFP-hGR cell line was thawed and maintained in DMEM supplemented with 10% FBS at 37ºC in a humidified 5% CO2 atmosphere. 20000 cells per well were plated in coated 96-well plates and incubated overnight.

F was assayed in agonist mode: cells were treated for 1h or overnight with ½ log dilution series of the tested compound, at a starting concentration of 10 or 32 µM. Dexamethasone at 100 nM was used as a control agonist. Nuclei were then stained with Hoechst at 5 µg/ml for 30 min at 37ºC. Fluorescence redistribution was analyzed in "BD Pathway 855" High-Content Bioimager from BD Biosciences with a 20X objective. A total of 9 pictures (1h incubation) or 4 pictures (overnight incubation) per well were taken, where green fluorescence intensity in the nucleus area (Hoechst stained) was measured. Nuclei were counted as a measure of cell number.

In antagonist mode, cells were treated with ½ log dilution series of F at a starting concentration of 32 µM. Geldanamycin (1 µg/ml) was included as control antagonist. After 15 minutes incubation with the compounds, dexamethasone 100 nM was added and incubated for 1 hour. Nuclei staining and fluorescence imaging was carried out as described above. This time 9 pictures of each well were taken.

NATIVE GR STUDIES IN HaCat CELLS

Cell culture

Native GR translocation and expression/degradation was studied in HaCat keratinocytes, provided by the Biomed division at Leitat Technological Center. 10^6 cells per well were seeded in 6-well plates and incubated in cortisol-free DMEM, supplemented with 10% FBS at 37ºC, 5% CO_2 and 90% humidity. After 24 hours, F was added to appropriate wells at the desired concentration and incubated for 1 hour. Then, dexamethasone was added and the plate was incubated for 1, 5 or 24 hours before trypsinization and cell harvesting by

centrifugation. Cells were washed with PBS to get rid of media remains and divided in two tubes to perform technical replicates. Protein extracts were obtained the same day to avoid cell freezing.

Protein extraction

To obtain total protein extracts, cell pellets were resuspended in 100 µL of Extraction Buffer (50 mM Tris pH8, 1mM EDTA, 1% Triton X-100, 0.2% SDS, 150 mM NaCl, 1% protease inhibitor (P9599, Sigma)). Samples were incubated on ice for 1 hour with periodical vortexing. After that, tubes were centrifuged at 15000G for 10 min to pellet the insoluble fraction. The resulting supernatants were quantified by Bradford method (B6916, Sigma) and immediately stored at -20ºC.

Nuclear and cytoplasmic protein extracts were obtained following the subsequent protocol. Cell pellets were gently resuspended in 100 µL of Cytoplasmic Extract (CE) Buffer: 10 mM HEPES, 60 mM KCl, 1 mM EDTA, 0.075% (v/v) Triton X-100, 1mM DTT, 1% protease inhibitor (P9599, Sigma), pH 7.6. Samples were incubated on ice for 3 min and span at 200G for 4 min, after which the supernatant containing the CE was removed to a clean tube. Pelleted nuclei were then resuspended and washed with 100 µL of CE buffer without detergent. Nuclei were span as before and 60 µL of Nuclear Extract (NE) buffer were added. NE buffer contained 20 mM Tris HCl, 420 mM NaCl, 1.5 mM $MgCl_2$, 0.2 mM EDTA, 1% protease inhibitor (P9599, Sigma) and 25% (v/v) glycerol and was adjusted to pH 8.0. Preparations were incubated on ice for 10 min with regular vortexing. Finally, all samples were centrifuged at 15000G for 10 min to pellet any remaining nuclei. The resulting supernatants were quantified by Bradford method (B6916, Sigma) and immediately stored at -20ºC.

Western blotting

Samples were denatured at 95ºC for 5 min in presence of laemmli sample buffer (60 mM tris pH 6.8, 2% SDS, 10% glycerol, 200mM DTT, bromophenol blue). Preparations were loaded into denaturing SDS-PAGE (Any kD™ Mini-PROTEAN® TGX™ Precast Protein Gels, BioRad) and ran at 200 V for 50 min. PageRuler™ Plus Pre-stained Protein Ladder (26619, Thermo Fisher) was also loaded. Transference to nitrocellulose membranes (1704159-Trans-Blot® Turbo™ Midi Nitrocellulose Transfer Packs, BioRad) was performed with Trans-Blot® Turbo™ Transfer System (BioRad) for 30 min at 25V. Blots were blocked in PBS containing 5% non-fat dry milk for 1h at room temperature (RT) and incubated with primary antibodies diluted in PBX (1x PBS pH 7.4, 0.1% Tween-20) with 5% dry milk at 4°C overnight. Antibody dilutions were as follows: mouse monoclonal anti-GR (1:200) clone G-5 (sc-

393232, Santa Cruz), polyclonal rabbit anti-tubulin beta-2A chain (TUBB2A) (1:3000) (PA025320LA01HU, Cusabio) and polyclonal rabbit anti-histone H1.0 (1:2000) (GTX114462, Genetex). Membranes were washed twice in PBX for 10min before incubation with secondary antibodies for 1h at RT. IRDye® 800CW conjugated goat anti-mouse-IgG (1:7000) (926-32210, Li-Cor) and IRDye® 680RD conjugated goat anti-rabbit-IgG (1:7000) (926-68071, Li-Cor) were used. Blots were washed as described above and processed for infrared fluorescence detection using Odyssey® IR 9120 imaging system. Obtained images were quantified using Image Studio™ software. GR fluorescence signal was divided per its corresponding tubulin signal (CE) or histone signal (NE) and was then normalized to control condition.

EXPRESSION ANALYSIS IN MOUSE MACROPHAGES

The expression of different inflammatory genes was analyzed in bone marrow-derived mouse macrophages. Experiments were performed at the Nuclear Receptor Research Group at the Department of Cell Biology, Physiology and Immunology (Universitat de Barcelona).

C57BL/6 male mice (8-12 week old) were obtained from Envigo and maintained under specific pathogen-free conditions. All the protocols requiring animal manipulation have been approved by the ethical committee from Barcelona Science Park (PCB). For each experiment, bone marrows were obtained from the femurs of two mice. Hematopoietic stem cells were extracted from bone marrow and differentiated by seeding them on polystyrene plates in DMEM containing L-glutamine (Gibco) and supplemented with 20% heat-inactivated FBS (Biosera), 30% L-cell (medium enriched in M-CSF) and 1% Penicillin/Streptomycin (Gibco) and left to grow for 6-7 days at 37ºC and 5% CO_2 to allow macrophage differentiation. L-cell conditioned medium was obtained as the supernatant of proliferating L929 cells (ATCC).

After differentiation, bone marrow-derived macrophages were collected by scraping. $3x10^6$ cells/plate were transferred to 60 mm plates and incubated for 6 hours, after which media was changed for DMEM supplemented with 2% FBS (resting media). Plates were left for 16 h in resting conditions before cells were treated with different concentrations of F (10-fold dilutions from 10 nM to 1 µM), dexamethasone (10 nM and 1 µM), a combination or vehicle (DMSO) for 2 h. Then, cells were stimulated with LPS (10 ng/ml) (L4516, Sigma) or PMA (100 ng/ml) (P1585, Sigma) for 2h.

At the end of the incubation with the different compounds, cells were washed in cold PBS and lysed using Trizol (93289, Sigma). Total RNA was extracted by phase separation using chloroform and isopropanol precipitation. RNA pellets were washed in 75% ethanol and resuspended in H_2O-mQ (RNase free). For cDNA synthesis, 1 µg of RNA was subjected to

reverse transcription using M-MLV Reverse Transcriptase RNase H Minus Point Mutant (Promega), a PCR nucleotide mix (Promega) and oligo(dT)$_{15}$ primers (Sigma).

mRNA determinations in technical triplicates were achieved by quantitative real-time PCR (qPCR) using the Power SYBR Green Reagent Kit (Applied biosystems, Foster City, CA) following the manufacturer's recommendations. Sequences of the primers used are detailed in Table 7. Real-time monitoring of PCR amplification was performed using the CF384 Real Time PCR Detection System (Bio-Rad) and the CF Manager Software with the following settings: 95ºC (10min) - [95ºC (30s) – 60ºC (30s) – 72ºC (30s)] x 35 cycles. Finally, data was expressed as relative mRNA levels normalized to ribosomal L14 expression. An additional normalization was performed to allow comparison between experiments.

For each gene, the intensity of each experiment (ie) was obtained by calculating the mean value between the expression levels in the basal state (vehicle-treated cells) and in the positive control cells (LPS-treated cells). In the case of Gilz and Mkp1, sample treated with dexamethasone was considered the positive control. With the ie values, the mean intensity value of all experiments (im) was then calculated. The intensities of each experiment were normalized by im (im/ie). After that, the expression values of all the samples in that experiment were multiplied by the resulting normalization factor (im/ie). In the case of the study of TNFα induction upon exposure to PMA, gene expression was normalized to the positive control cells (PMA-treated cells) to calculate the percentage of repression.

Table 7. Primers used in the qPCR for the determination of mRNA levels in macrophages.

Gene	Forward primer	Reverse primer
Cox2	5´-ATTCTTTGCCCAGCACTTCA-3´	5´-GGGATACACCTCTCCACCAA-3´
Gilz	5'-TGTGGTGGCCCTAGACAAC-3'	5'-GTCTTCAGGAGGGTGTTCTCG-3'
Il1b	5´-TGGGCCTCAAAGGAAAGAAT-3´	5´-CAGGCTTGTGCTCTGCTTGT-3´
Il6	5´-CCAGAGATACAAAGAAATGATGG-3´	5´-ACTCCAGAAGACCAGAGGAAAT-3´
Il12b	5'-GGAAGCACGGCAGCAGAATA-3'	5'-AACTTGAGGGAGAAGTAGGAATGG-3'
L14	5'-TCCCAGGCTGTTAACGCGGT-3'	5'-GCGCTGGCTGAATGCTCTG-3'
Mkp1	5'-CTCCACTCAAGTCTTCTTTCTCC	5'-TAGGCACTGCCCAGGTAC-3'
Nos2	5´-GCCACCAACAATGGCAACA-3´	5´-CGTACCGGATGAGCTGTGAATT-3´
Tnfa	5'-CCAGACCCTCACACTCAGATC-3'	5'-CACTTGGTGGTTTGCTACGAC-3'

Cox2, cyclooxygenase 2; Gilz, glucocorticoid-induced leucine zipper protein; IL1b, interleukin 1 beta; Il6, interleukin 6; Il12, interleukin 12; L14, ribosomal gene L14, Mkp1, mitogen-activated protein kinase phosphatase 1; Nos2, nitric oxide synthase 2; Tnfa, tumor necrosis factor alpha.

IL8 DETERMINATION IN MONOCYTES

IL8 secretion was studied in THP-1 monocytes, provided by the Biomed division at Leitat Technological Center. $6x10^4$ cells per well were seeded in 1mL of medium in 6-well plates. After 24 hours, compounds diluted in 1 mL of media were added to appropriate wells at the desired concentrations and incubated for 1h. Assayed concentrations were: 10nM dexamethasone, 5 nM mifepristone and 0.1-10 µM F. Coincubations of products were performed by preincubating F or mifepristone for 30 minutes. IL8 secretion was induced either by adding LPS (L4516, Sigma) at 10ug/mL and incubating for 24h, or by adding 10 ng/mL of PMA (P1585, Sigma) and incubating overnight. Cell supernatants were centrifuged at 13000 rpm and 4ºC for 10 min to discard any debris and stored at -80ºC.

IL8 determination in the supernatants was carried out with a commercial ELISA kit (DY208, R&D Systems) and following manufacturer's instructions. Briefly, a 96-well white microplate was coated overnight with 100 µL of the capture antibody. Plate was washed three times with wash buffer and blocked with 300 µL of blocking buffer 1h at RT. 100 µL of supernatants diluted 100-fold were added and incubated for 2h at RT. Provided standards were also diluted and incubated likewise. After repeating the washing step, the plate was incubated with detection antibody for 2h and with streptavidin-HRP solution for 20 additional minutes. At last, plate was revealed with a chemiluminescent substrate solution (ELLUF0100, Millipore) and read in a Synergy H1M (Biotek). The standard curve was used to quantify IL8 in samples. Background signal from non-stimulated cells was subtracted and cells treated incubated only with PMA were considered as maximal IL8 secretion.

TNFα DETERMINATION IN MONOCYTES

TNFα secretion was studied in THP-1 monocytes, provided by the Biomed division at Leitat Technological Center. 20000 cells per well were seeded in 100 µL of medium in 96-well plates. After 24 hours, F nanoparticles or dexamethasone were added to appropriate wells at the desired concentrations, ranging from 0-0.4 µM. Then, TNFα secretion was induced by adding 50 ng/mL Phorbol 12-mysistate 13-acetate (PMA) (P1585, Sigma) and incubating for 24h. Cell supernatants were centrifuged at 13000 rpm and 4ºC for 10 min to discard any debris and stored at -20ºC.

A second assay was performed where dexamethasone was added at increasing concentrations and coincubated with a constant concentration of F: 100 nM or 1 nM.

TNFα determination in the supernatants was carried out with a commercial ELISA kit (KHC3011, Invitrogen) and following manufacturer's instructions. Briefly, samples and provided standards were diluted and incubated for 2 hours in the functionalized plate. A

biotinylated anti-TNFα antibody was then added and kept for 1 hour, after which a solution of streptavidin-HRP was applied for 30 minutes. The ELISA was developed with a chromogenic HRP substrate and stopped with an acidic solution. The plate was read at 450 nm and the standard curve was used to quantify TNFα in samples. Background signal from non-stimulated cells was subtracted and cells treated only with PMA were considered as maximal TNFα secretion.

TNFα DETERMINATION IN MACROPHAGES

Bone marrow-derived macrophages were obtained from C57BL/6 male mice as described previously. $2x10^6$ cells per well were seeded in 2 mL of medium in 6-well plates. After 24 hours, F (alone or in coincubation with dexamethasone) was added to appropriate wells in DMSO at the desired concentrations (ten-fold dilutions starting from 1 µM). After 1h, TNFα secretion was induced by adding 100 ng/mL of PMA (P1585, Sigma) and incubated for 24h. Cell supernatants were centrifuged at 13000 rpm and 4ºC for 10 min to discard any debris and stored at -80ºC for further analysis.

TNFα determination in the supernatants was carried out with a commercial ELISA kit (DY410, R&D Systems) and following manufacturer's instructions. Briefly, a 96-well white microplate was coated overnight with 100 µL of the capture antibody. Plate was washed three times with wash buffer and blocked with 300 µL of reagent diluent 1h at RT. After washing again, 100 µL of supernatants diluted 2-fold were added and incubated for 2h at RT. Provided standards were also diluted and incubated likewise. After repeating the washing step, the plate was incubated with detection antibody for 2h and with streptavidin-HRP solution for 20 additional minutes. At last, plate was revealed with a chemiluminescent substrate solution (ELLUF0100, Millipore) and read in a Synergy H1M (Biotek). The standard curve was used to quantify TNFα in samples. Background signal from non-stimulated cells was subtracted and cells treated only with PMA were considered as maximal TNFα secretion.

STATISTICAL ANALYSIS

Data analysis was performed using GraphPad Prism 7 software. Statistical significance among two groups was calculated by running unpaired t-tests (two-tailed, 95% confidence intervals). In analysis of more than 3 groups, it was calculated by applying a one-way ANOVA followed by multiple comparisons tests: Dunnett's test, when comparing a control mean with the other group means; or Tukey test, when comparing every mean with every other mean.

RESULTS

INFLUENCE OF ABCS ON NRs TRANSCRIPTIONAL ACTIVITY

NRs are a family of ligand-regulated TRFs that share a common structure. They are promising therapeutic targets given the wide variety of processes they control, including development, reproduction, and metabolism. In fact, their dysregulation can contribute to numerous diseases, such as cancer, diabetes, and infertility.

ABCs have structural differences that confer them different properties, but they also have many common roles. They have been proposed to act by different mechanisms of action, among which the interaction with NRs is of particular interest, although currently there is only preliminary evidence.

We decided to screen the effect of different ABCs on a panel of NRs, to determine if these compounds induced a modulation of the transcriptional activity of the receptors. At the same time, we attempted to determine if this characteristic was intrinsic to all ABCs, or on the contrary, to identify which structural features confer them different activities related to NRs. A group of ABCs was selected based on their abundance in nature and availability. Selected ABCs included Compound A, Compound B, Compound F, Compound L, Compound N and Compound F4 (F4). F is present in many diets mainly in the form of algae. It is supposedly metabolized to F2 by intestinal or pancreatic cells, which is later converted to F3 in the liver. Therefore, after oral ingestion, very little F is absorbed, while the presence of F3 in plasma and tissues is predominant in rodents. It has been reported that many of F bioactivities are retained in these metabolites. In this way, the metabolites F2 and F3 were also included in the assays. The study of all compounds is crucial to determine the possible effects of F ingestion in the organism.

The screened NRs included steroid receptors, retinoid receptors and PPARγ. They were selected based on both literature and assay availability. Studies were performed with division arrested HEK 293T cells transfected to stably express a fusion protein consisting in the GAL4 TRF DBD and the NR LBD. HEK 293T cells have also been stably transfected with a construct containing the beta-lactamase (*bla*) cDNA under transcriptional control of an Upstream Activator Sequence (UAS). This sequence is activated by GAL4(DBD). As depicted in Figure 6, upon agonist binding, the GAL4(DBD)-NR(LBD), binds to the UAS, which controls transcription of the reporter *bla*. Cells are then loaded with a substrate that allows to follow the activation and inhibition of the fusion protein by FRET, as well as to measure cell viability.

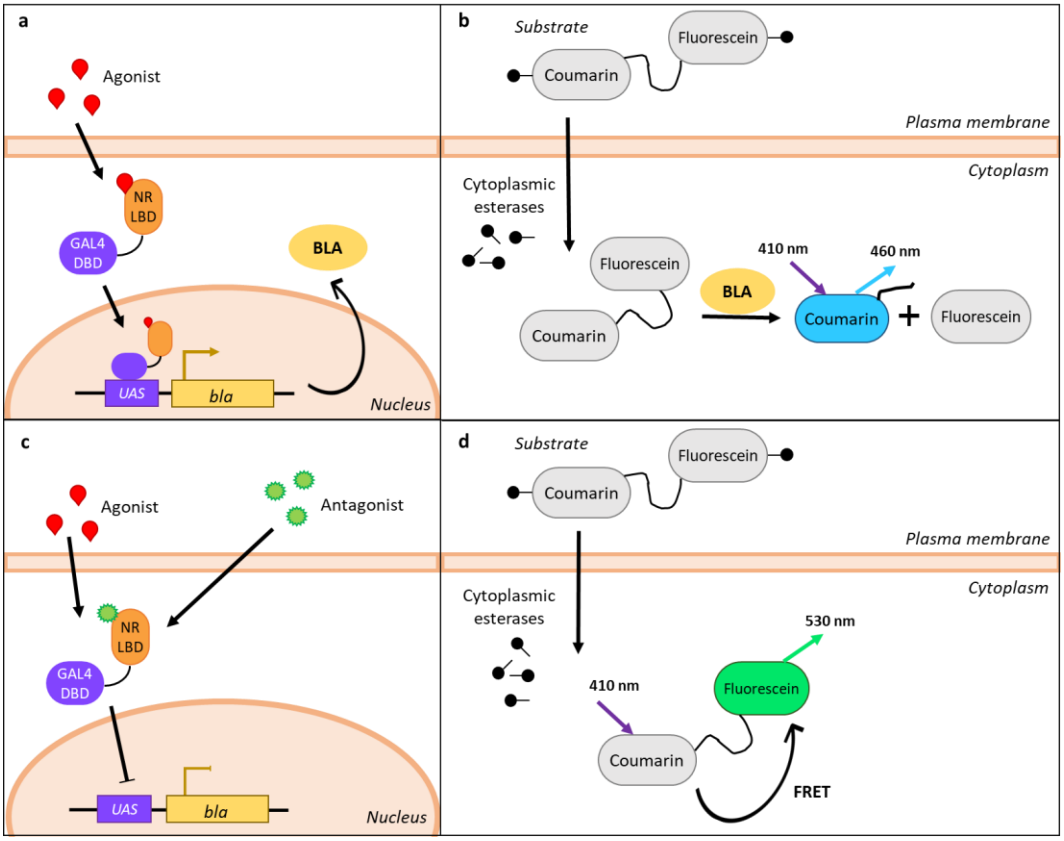

Figure 6. Fluorescent detection of GAL4(DBD)-NR(LBD) transcriptional activity. (a-b) Upon incubation with an agonist, the fusion protein GAL4(DBD)-NR(LBD) is activated and induces bla *expression. Cells are loaded with a fluorescent bla-substrate containing coumarin and fluorescein. When it enters the cell, cleavage by endogenous cytoplasmic esterases traps it within the cytosol, allowing to monitor cell viability. In the presence of Bla, the substrate is cleaved, which disrupts energy transfer and shifts the emission peak to 460 nm. (c-d) In the absence of NR activation or upon incubation with an antagonist, there is little* bla *expression. In this case, the substrate molecule remains intact. Coumarin excitation results in FRET to fluorescein, which is detected by a fluorescence emission peak at 530 nm. The resulting coumarin: fluorescein ratio is used to quantify the activation of the fusion receptor, while raw fluorescein fluorescence allows to monitor cell viability.*

Transactivation inhibition on subfamily NR3

The subfamily of estrogen receptor-like NRs is composed by 3 groups. Oxosteroid receptors (group NR3C) comprise 4 different receptors with high sequence and structural homology. They also share many coregulators, such as SRC1. The other steroid receptors are the estrogen receptors and estrogen-related receptors (ERRs), belonging to groups NR3A and B respectively. It is common that molecules that have been found to interact with one steroid receptor also affect other NRs with variable affinities. Accordingly, we investigated the effect of various ABCs on the transactivation of many receptors of the subfamily 3.

In a first assay, GR response was evaluated. Transfected HEK293T cells responded to dexamethasone stimulation with the activation of the reporter gene and the consequent FRET disruption, as intended. Upon additional incubation with F, a concentration-dependent decrease in reporter expression was detected in two independent assays. The concentration of compound at which the middle inhibition value was attained (relative IC50) was determined from Hill analysis of the curve to be 1.02 μM, 650 times lower than the potency shown by mifepristone. Maximal inhibition achieved was around 50% (Figure 7a and Table 8).

Compound N, F4 and Compound L presented similar behaviors, reaching around 80% of maximal response (Figure 7a and Table 8). Surprisingly, F metabolites F3 and F2 showed similar antagonism, displaying higher efficacy than its precursor. Oppositely, Compound B and Compound A showed no antagonist effects on GR (Figure 7b and Table 8).

In order to compare the potency of the different compounds, their estimated IC50 was divided by the IC50 of the reference compound mifepristone, used as a control in each assay. The resulting normalized value was designated as Competition Factor (CF). As detailed in Table 8, potency of most of the compounds was lower than F's. F4 and Compound L showed the steepest dose-response curves, with CFs above 6 and so, the lowest potencies. Compound N and F2 exhibited a CF of 1.4 and 3, respectively. Interestingly, F3 presented the highest potency with a CF of 0.49.

In a second assay, the androgen receptor was studied with the same procedure. Among the tested compounds, F3 and Compound L achieved the highest responses: 102% and 83% inhibition, respectively (Figure 7c and Table 9). In fact, it represented the highest inhibition among the oxosteroid receptors. Compound N showed a comparable response to F, with a 44% and 35% of inhibition. In the cases of F3 and F2, the maximum dose could not be tested due to cell toxicity. As experienced with GR, Compound A and Compound B presented no antagonist activity on AR (Figure 7d and Table 9).

Compound potency, in terms of IC50, could only be determined for F3 and Compound L (Table 9). It appears that the former, with an IC50 of 1.18 μM was the most active compound on AR. It showed an only 100 times lower IC50 than the synthetic compound cyproterone acetate, which also indicated a higher potency for AR than for GR (IC50 2.07 μM).

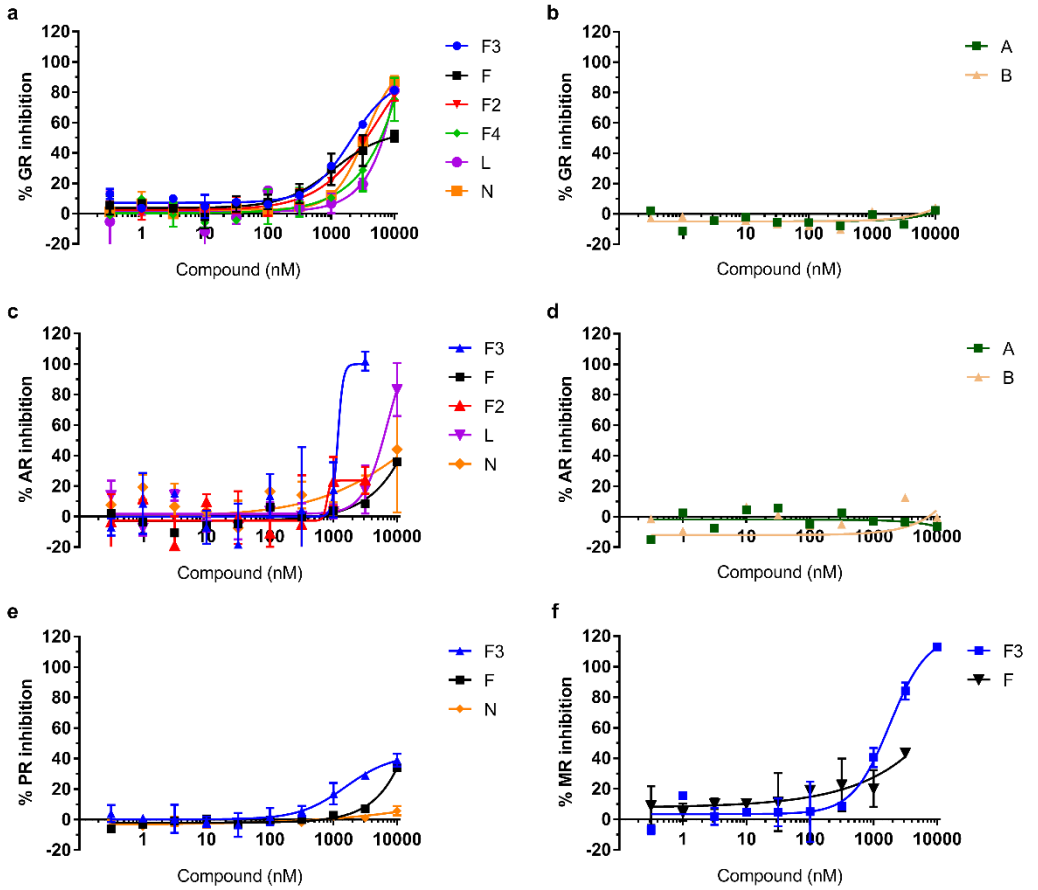

Figure 7. Inhibition curves of different ABCs on NR3C. *Cells expressing GAL4(DBD)-NR(LBD) were coincubated with increasing concentrations of different ABCs and a corresponding reference agonist at its EC80. The activation of the reporter gene* bla *was detected by TR-FRET. (a) Some ABCs antagonize dexamethasone stimulation of GR(LBD). (b) Compound A and Compound B are unable to antagonize dexamethasone stimulation of GR(LBD). (c) Some ABCs antagonize metribolone stimulation of AR(LBD). (d) Compound A and Compound B are unable to antagonize metribolone stimulation of AR(LBD). (e) F3 and F slightly antagonize promegestone stimulation of PR(LBD), whereas NX does not. (f) F3 and F antagonize aldosterone stimulation of MR(LBD). Error bars indicate standard deviation from two biological replicates.*

Table 8. Estimated parameters for the GR inhibition curves of different ABCs. *Potency and efficacy values of the antagonist effect on GR transactivation were determined for several compounds by the expression of a reporter gene. Competition factor (CF) is expressed as: IC50 test compound (µM)/ IC50 reference compound (nM). Efficacy is expressed as the receptor inhibition percentage at the ABC maximal tested concentration (10 µM).*

			Curve parameters			Control parameters	
	CF	% efficacy	IC50	Hillslope	R^2	Z'	RU-486 IC50
F3	0.49	81	2.07 µM	1.35	0.99	0.85	1.98 nM
A	-	2	>10 µM	9.85	0.24	0.77	0.84 nM
B	-	4	>10 µM	1.82	0.41	0.77	0.84 nM
F (rep 1)	0.72	53	0.755 µM	1.06	0.95	0.54	1.05 nM
F (rep 2)	0.61	49	1.28 µM	1.45	0.99	0.93	2.09 nM
F2	3.00	78	5.94 µM	0.92	0.99	0.85	1.98 nM
F4	6.36	75	5.34 µM	1.61	0.96	0.77	0.84 nM
L	6.77	81	5.69 µM	2.51	0.93	0.77	0.84 nM
N	1.40	87	3.45 µM	1.78	0.99	0.69	2.46 nM

The next studied receptor was PR. No variation in reporter gene expression was detected upon incubation with Compound N, although cells responded satisfactorily to agonist stimulation (Figure 7e and Table 10). Oppositely, F3 did inhibit PR transactivation to 39%, reaching similar efficacy as F. Apparently, F3 potency was higher than F's, despite it could not be estimated due to lack of data at higher concentrations.

PR inhibition can be directly compared to GR inhibition, as they use the same control antagonist with similar sensitivity. In the case of F, the antagonism on PR showed comparable Hillslope but much higher IC50 (although not exactly determined), meaning lower compound potency in PR than in GR.

The activity of the last oxosteroid receptor, the mineralocorticoid receptor, was only evaluated upon incubation with F and its derivative F3. The latter completely inhibited MR activity at the highest tested concentration (Figure 7f and Table 11). The estimated IC50 was 1.8 µM, indicating a similar potency than for GR (IC50 2.07 µM). Although F maximum dose could not be tested due to cell toxicity and so, no proper curve could be modelled, it presented lower potency and efficacy than F3. F partially blocked the transcriptional activity of MR, similarly to what was seen with GR, indicating comparable potency and efficacy. It appears that F acts as a partial antagonist in those receptors, as well as in AR and PR.

Table 9. Estimated parameters for the AR inhibition curves of different ABCs. *Potency and efficacy values of the inhibition of transactivation were determined for AR by the expression of the LBD fused to GAL4 and using a reporter gene. Competition factor (CF) is expressed as: IC50 test compound (µM)/ IC50 reference compound (nM). Efficacy is expressed as the receptor inhibition percentage at the ABC maximal tested concentration (10 µM unless stated).*

			Curve parameters			Control parameters	
	CF	% efficacy	IC50	Hillslope	R^2	Z'	CPA IC50
F3	0.016	102*	1.18 µM	9.65	0.91	0.41	72.0 nM
A	-	0	>10 µM	0.10	0.14	0.59	58.0 nM
B	-	0	>10 µM	0.10	0.00	0.59	58.0 nM
F	-	36	>10 µM	1.15	0.87	0.73	49.3 nM
F2	-	24*	>3.16 µM	16.66	0.60	0.41	72.0 nM
L	0.098	83	7.06 µM	2.29	0.92	0.59	72.3 nM
N	-	44	>10 µM	1.32	0.70	0.59	72.3 nM

CPA, cyproterone acetate.

** maximum tested concentration 3.16 µM.*

Table 10. Estimated parameters for PR inhibition curves of different ABCs. *Potency and efficacy values of the inhibition of transactivation were determined for PR by the expression of a reporter gene. Competition factor (CF) is expressed as: IC50 test compound (µM)/ IC50 reference compound (nM). Efficacy is expressed as the receptor inhibition percentage at the ABC maximal tested concentration (10 µM).*

			Curve parameters			Control parameters	
	CF	% efficacy	IC50	Hillslope	R^2	Z'	RU-486 IC50
F3	-	39	>10 µM	0.60	0.96	0.75	0.35 nM
F	-	34	>10 µM	1.36	0.97	0.93	1.71 nM
N	-	6	>10 µM	0.06	0.76	0.93	1.71 nM

RU-486, mifepristone.

Table 11. Estimated parameters for the antagonist effect of different ABCs on MR. *Potency and efficacy values of the inhibition of transactivation were determined for MR by the expression of a reporter gene. Competition factor (CF) is expressed as: IC50 test compound (µM)/ IC50 reference compound (nM). Efficacy is expressed as the receptor inhibition percentage at the ABC maximal tested concentration (10 µM unless stated).*

			Curve parameters			Control parameters	
	CF	% efficacy	IC50	Hillslope	R^2	Z'	SC-9420 IC50
F3	0.210	113	1.80 µM	1.47	0.98	0.76	8.56 nM
F	-	44*	>3.16 µM	0.56	0.89	0.60	4.65 nM

SC-9420, spironolactone.
** maximum al tested concentration 3.16 µM.*

NR3 receptors also include the estrogen receptors and estrogen-related receptors (groups NR3A and B). The inhibition of transactivation in these subfamilies was quite high for F, ranging from 67 to 75% (Figure 8 and Table 12). Obtained dose-response curves allowed to calculate the IC50 in all cases: ERα, 5.55 µM; ERβ, 5.55 µM; and ERRα, 1.89 µM. Surprisingly, the potency in ERRα was comparable to GR inhibition. Compound F3 antagonized ERα in a comparable way as PR, with a corresponding efficacy of 45%.

ERβ data can be compared to GR in terms of CF, as they use the same control antagonist, although with quite different sensitivity. The antagonism on ERβ showed comparable slope but a much lower competition factor than GR, probably due to a much lower sensitivity for the reference compound mifepristone. In terms of IC50, however, F would have lower potency in ERβ.

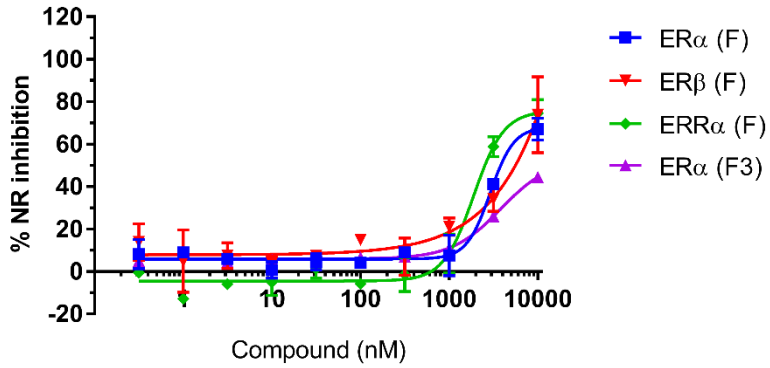

Figure 8. F and F3 inhibition curves of ERs and ERRs. *Compound F and Compound F3 antagonize the stimulation of different estrogen and estrogen-related receptors in UAS-bla HEK 293T cells. Cells expressing GAL4(DBD)-NR(LBD) were coincubated with increasing concentrations of a ABC and a reference NR agonist at its EC80 (except for the constitutively active ERRα). The activation of the reporter gene bla was detected by TR-FRET. Error bars indicate standard deviation from two biological replicates.*

Table 12. Estimated parameters for the antagonist effect of F and F3 on NR3A and NR3B. *Potency and efficacy values of the inhibition of transactivation were determined estrogen and estrogen-related receptors by the expression of a reporter gene. Competition factor (CF) is expressed as: IC50 test compound (µM)/ IC50 reference compound (nM). Efficacy is expressed as the receptor inhibition percentage at the ABC maximal tested concentration (10 µM).*

			Curve parameters			Control parameters	
	CF	Efficacy	IC50	Hillslope	R^2	Z'	Control IC50
ERα (F)	1.04	67	5.55 µM	1,29	0,97	0,82	4-OHT 5.33 nM
ERβ (F)	0.03	74	5.53 µM	1,41	0,96	0,75	RU-486 167 nM
ERRα (F)	0.01	75	1.89 µM	2,55	0,98	0,61	XCT790 334 nM
ERα (F3)	>0.893	45	>10 µM	0.95	0.98	0.68	4-OHT 11.2 nM

4-OHT, 4-hydroxytamoxifen; RU-486, mifepristone.

Transactivation inhibition on retinoid receptors

Retinoid X and retinoic acid receptors are the endogenous receptors for retinoids, which naturally derive from ABCs. Different ABCs and derivatives have been shown to interact with the retinoid-related receptors, both as agonists and antagonists. Therefore, F's effect on those groups was evaluated. The activation of a chimeric receptor containing the LBD of a retinoid receptor was followed by the expression of a reporter gene.

F completely antagonized RXRα activation at the highest tested concentration, with an estimated IC50 of 3.59 µM (Figure 9 and Table 13). In the other assays, the highest concentration could not be tested due to cytotoxicity problems. However, F showed a similar inhibition tendency on RXRβ and RARγ. On the other hand, no inhibition of the transactivation was observed on RARα and RARβ.

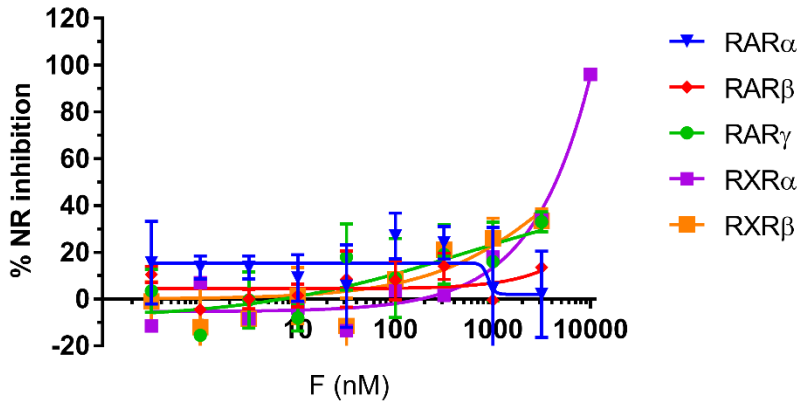

Figure 9. F inhibition curves of retinoid receptors. *F antagonizes the stimulation of RXRα and partially of RXRβ and RARγ. Cells expressing GAL4(DBD)-NR(LBD) were coincubated with increasing concentrations of F and a reference agonist at its EC80. The activation of the reporter gene bla was followed by TR-FRET to determine the transactivation inhibition. Error bars indicate standard deviation from two biological replicates.*

Table 13. Estimated parameters for the antagonist effect of F on retinoid receptors. *Potency and efficacy values of the inhibition of transactivation were determined for NR1B and NR2B by the expression of a reporter gene. Competition factor (CF) is expressed as: IC50 test compound (µM)/ IC50 reference compound (nM). Efficacy is expressed as the receptor inhibition percentage at the ABC maximal tested concentration (10 µM unless stated).*

			Curve parameters			Control parameters	
	CF	Efficacy	IC50	Hillslope	R^2	Z'	Control IC50
RARα	>2.65	8*	>10 µM	1.00	0.15	0.74	Ro-41-5253 3.78 nM
RARβ	>1.50	14*	>3.16 µM	0.27	0.70	0.66	AGN193109 2.10 nM
RARγ	>5.06	33*	>3.16 µM	0.42	0.86	0.45	AGN193109 0.624 nM
RXRα	-	96	3.59 µM	1.89	0.94	0.47	-
RXRβ	-	34*	>3.16 µM	0.10	0.40	0.55	-

** maximum al tested concentration 3.16 µM.*

PPARγ inhibition

It is known that GR activation, which has been shown to be affected by several ABCs, is involved in effects induced by other NR subfamilies, such as PPAR. Interestingly, Compound A has been described to directly interact with PPARα and PPARγ. PPARγ plays an important role in adipogenesis and glucose metabolism, and has been related to diseases such as diabetes, obesity or cancer. Some ABCs, and in particular F, have been described to increase lipolysis and to have protective effects against those diseases. Consequently, PPARγ transactivation was studied upon incubation with ABCs. In this case, only F and F3 were evaluated. As before, transfected HEK293T cells were incubated with the compound and receptor activation was followed by TR-FRET.

For F, the inhibition response obtained at maximum tested concentration was 46% (Figure 10). As before, cytotoxicity above 3 µM was observed. F potency in this receptor (IC50 2.5 µM) was about half its potency on GR (Figure 7a and Table 14). F3 inhibition of PPARγ was up to 62% and presented the lowest potency among all receptors evaluated with this ABC, with an IC50 of 7.85 µM. Although the achieved inhibition is comparable for both compounds, F potency was quite higher.

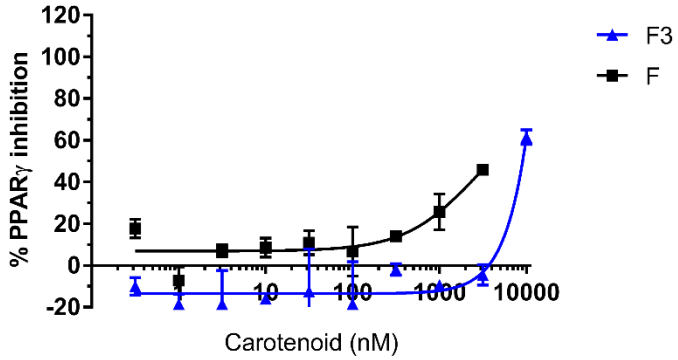

Figure 10. PPARγ inhibition curves. *F and F3 antagonize the stimulation of PPARγ, as determined by TR-FRET. Cells expressing GAL4(DBD)-PPARγ(LBD) were coincubated with increasing concentrations of a ABC and rosiglitazone (reference agonist) at its EC80. The activation of the reporter gene bla was detected. Error bars indicate standard deviation from two biological replicates.*

Table 14. Estimated parameters for the PPARγ inhibition curves of different ABCs. *Potency and efficacy values of the inhibition of transactivation were determined for PPARγ by the expression of the LBD fused to GAL4 and using a reporter gene. Competition factor (CF) is expressed as: IC50 test compound (μM)/ IC50 reference compound (nM). Efficacy is expressed as the receptor inhibition percentage at the ABC maximal tested concentration (10 μM unless stated).*

			Curve parameters			Control parameters	
	CF	% efficacy	IC50	Hillslope	R^2	Z'	T0070907 IC50
F3	2.62	62	7.85 μM	2.71	0.95	0.5	3.00 nM
F	2.34	46*	2.50 μM	1.07	0.81	0.76	1.07 nM

** maximum tested concentration 3.16 μM.*

COMPOUND F COMPETITIVE BINDING TO GR AND PXR

Among all screened ABCs in the transcriptional inhibition assays, F was selected to continue studying the interaction with NRs. The first approach was to assess if the ABC competed with the ligand for the steroid pocket in the LBD. It was tested in GR and Pregnane X Receptor (PXR) by a biochemical competitive binding assay. In this assay, a modified GR(LBD) with a Glutathione S-transferase (GST) tag is indirectly labeled with a terbium-labeled anti-GST antibody. Green fluorescent GS1, an engineered GR ligand, is bound to the receptor and binding is followed by TR-FRET. Competitive ligand binding to GR is detected by tracer displacement, which results in a loss of FRET signal, as shown in Figure 11.

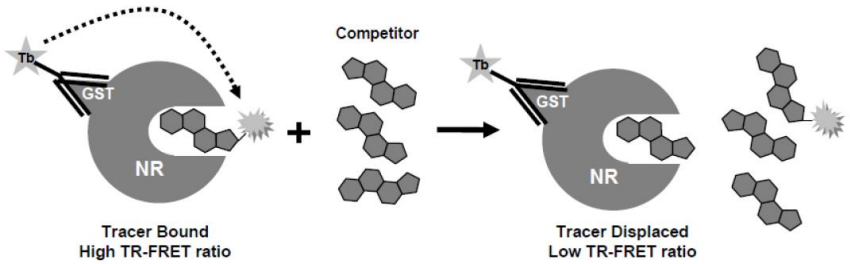

***Figure 11. Layout of the competitive binding TR-FRET assay**. A terbium-labeled anti-GST antibody indirectly labels GR by binding to its GST tag. When a fluorescent ligand (tracer) is bound to the receptor, energy transfer from the antibody to the tracer occurs, and a high TR-FRET ratio is observed. Competitive ligand binding to the GR is detected by a test compound's ability to displace the tracer from the GR, which results in a loss of FRET signal between the antibody and the tracer. Obtained from* (132).

At the highest tested concentration, 16% displacement of the labelled ligand GS1 was obtained in GR. The resulting binding curve is depicted in Figure 12 and its parameters are listed in Table 15. Despite showing a concentration-dependent pattern, assay variability was high and values from -20 to 20% binding are generally considered to be within the range of noise for this assay. Therefore, the ABC was unable to significantly displace GS1 (with a K_d of 2nM) from steroid's pocket.

PXR belongs to the NR1I family. Our results showed that F was able to bind and compete with a PXR agonist with an estimated IC50 of 7.23 µM. It reached an efficacy of 63% (Table 15 and Figure 12).

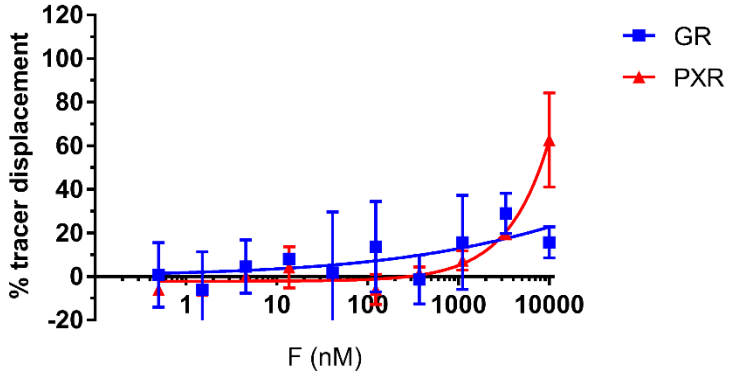

Figure 12. GR and PXR ligand displacement by F. *The displacement of a fluorescent tracer by competitive binding to PXR or GR LBD was determined by TR-FRET upon F incubation. In PXR, F was able to displace the artificial ligand from the receptor in a concentration-dependent manner. Error bars indicate standard deviation from two replicates.*

Table 15. Estimated parameters of GR and PXR ligand displacement by F. *Potency and efficacy values were obtained from biochemical competitive binding assays. Competition factor (CF) is expressed as IC50 test compound (µM)/ IC50 reference compound (nM). Efficacy is expressed as the tracer displacement percentage at the ABC maximal tested concentration (10 µM).*

			Curve parameters			Control parameters	
	CF	Efficacy	IC50	Hillslope	R^2	Z'	Control IC50
GR	-	16	>10 µM	0.17	0.56	0.60	Dexamethasone 4.09 nM
PXR	0.083	63	7.23 µM	1.57	0.97	0.70	SR-12813 87.25 nM

COMPOUND F INFLUENCE ON NRs–COREGULATOR INTERACTION

The next step in evaluating the interaction between F and NRs was to assess its effect on coregulator peptide recruitment or displacement. In this assay, both competitive binding and ability to recruit or displace a coactivator were assessed. Essentially, agonist binding to a NR causes a conformational change in the LBD, resulting in higher affinity for a fluorescein-coregulator peptide (see Table 5 for the corresponding coregulators). This peptide mimics the receptor binding motif of native coactivators. Recruitment of the peptide is followed by TR-FRET, as in Figure 13. On the contrary, antagonist binding displaces the agonist and reverses the conformational change, thus disrupting fluorescence resonance. Selection of NR to test was based on availability of the already studied receptors in the transactivation assays.

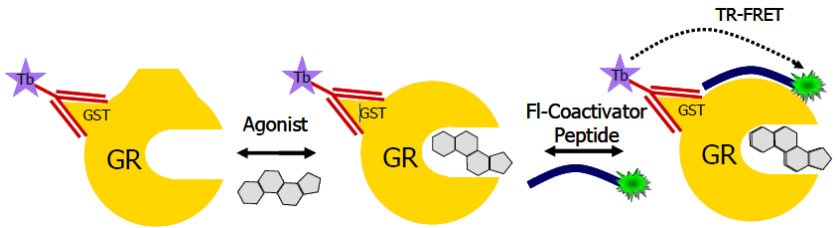

Figure 13. Layout of the GR-coregulator interaction TR-FRET assay*. A terbium-labeled anti-GST antibody indirectly labels GR(LBD) by binding to its GST tag. Upon ligand binding, the receptor undergoes a conformational change that results in an increased affinity for coactivator labelled peptides. Energy transfer from the antibody to the peptide occurs and a high TR-FRET ratio is observed. Competitive antagonist binding to the GR displaces the peptide, which results in a loss of FRET signal. Obtained from* (131).

Firstly, F was incubated with the labelled receptor and peptide to study if it could act as an agonist. However, the compound was unable to exert any significant effect on any of the tested receptors and to promote peptide recruitment (Figure 14a). In a second experiment, antagonism was assessed by adding a reference agonist to the incubation. When competing with an agonist, F could not displace it and cause the release of the coactivator peptide (Figure 14b). Obtained parameters are summed up in Table 16.

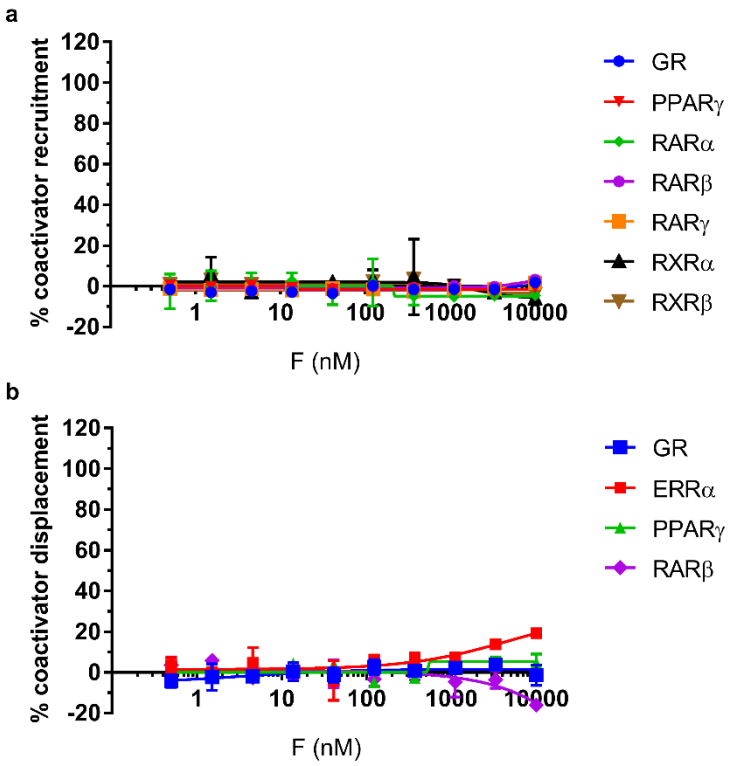

Figure 14. F effects on NR-coactivator interaction. *(a) F was unable to recruit a coregulator peptide in tested NRs when assayed in agonist mode. The ABC was incubated at increasing concentrations with a mixture of tagged NR(LBD) and fluorescent coregulator. Peptide recruitment was determined by TR-FRET. (b) F was unable to release the corresponding coregulator peptide from tested NRs when assayed in antagonist mode. The ABC was incubated at increasing concentrations with an agonist at its EC80, the tagged NR(LBD) and a fluorescent coregulator. Peptide displacement was determined by TR-FRET. All error bars indicate standard deviation from two replicates.*

Table 16. Estimated parameters for the effect of F on NR-coactivator interaction. *Potency and efficacy values were obtained from biochemical coregulator binding assays. Efficacy is expressed as the receptor inhibition percentage at the ABC maximal tested concentration (10 µM).*

			Curve parameters			Control parameters	
Assay	NR	% efficacy	EC50	Hillslope	R^2	Z'	Control EC50
Coactivator recruitment	GR	2	>10 µM	1.26	0.57	0.69	MF 2.51 nM
	PPARγ	0	>10 µM	-22.31	0.63	0.71	GW1929 6.47 nM
	RARα	0	>10 µM	-46.03	0.58	0.62	ATRA 1.89 nM
	RARβ	3	>10 µM	1.37	0.83	0.87	ATRA 6.79 nM
	RARγ	2	>10 µM	7.27	0.86	0.72	ATRA 5.86 nM
	RXRα	0	>10 µM	-1.96	0.58	0.51	9-cis-RA 69.8 nM
	RXRβ	0	>10 µM	-3.49	0.64	0.72	9-cis-RA 167 nM
Coactivator displacement	GR	0	>10 µM	-0.08	0.54	0.84	RU-486 125 nM
	ERRα	19	>10 µM	0.49	0.83	0.66	XCT790 6.95 nM
	PPARγ	5	>10 µM	79.45	0.44	0.81	GW9662 139 nM
	RARβ	0	>10 µM	-0.69	0.77	0.88	AGN193109 47.7 nM

ATRA, all-trans retinoic acid; EC50, half maximal effective concentration; MF, mometasone furoate; RA, retinoic acid; RU-486, mifepristone.

BINDING AFFINITY OF COMPOUND F AND COMPOUND F3 TO AR AND GR

As previously described, F was able to antagonize *in vitro* several NRs. Among those, GR was antagonized with the highest potency, although it did not achieve maximal response. Its metabolite F3 showed higher antagonistic activity on GR, but also on AR. In addition, GR modulators have many potential applications. Glucocorticoid receptor agonists' clinical use is highly extended due to their immunosuppressive and anti-inflammatory activities. However, they present a broad range of adverse effects, and no antagonist has yet been approved to treat those effects, as well as to treat endogenous GCs dysregulation. Anti-androgenic compounds are clinically used for the treatment of hyperandrogenism, prostatic cancer and benign prostatic hypertrophies. Androgen antagonists are also in clinical trials for the treatment of breast cancer and spinal and bulbar muscular atrophy (135), while in cosmetics they are used to reduce alopecia, hirsutism and acne. The current anti-androgenic compounds are associated to numerous side-effects, such as osteoporosis and hepatotoxicity (136). For that reasons, we chose to further study F and F3 interaction with GR and AR.

Both ABCs antagonized GR and AR transactivation in an effect mediated by the LBD, but showed no displacement of the ligand or effect on coregulators and so the mechanism remained unclear. Modulation of the GR complex can be achieved by multiple ways, including interaction with the receptor or its coregulators. In this section, the possibility of a direct interaction with the receptor was studied. Apart from the steroid pocket, there are at least two regulatory regions were the ABC could bind, τ2 and AF2 (8). In order to determine whether a direct binding to GR occurred, a more sensitive approach was needed, and surface plasmon resonance assays were performed. SPR allows to study the interaction between two molecules. The changes in the concentration of analyte, as it binds to or dissociates from the ligand, are measured in response units (RU) and allow to measure interaction kinetics and affinity.

Compound F binding to GR

To study the interaction between GR and F by SPR, the ancestral variant of the receptor AncGR2 was immobilized into a sensor chip, both in the apo form and bound to dexamethasone. Then, F binding was detected in three different runs (Table 6). Dexamethasone was also analyzed as a reference.

A first exploratory run was performed with short contact and dissociation times and resulted in unclear results, probably due to compound aggregation. In a second run the contact time was extended to 90 seconds and duplicates were performed. It resulted in the curves of maximal RU against compound concentration represented in Figure 16a and c. F did not bind to the Apo-receptor. However, binding to the dexamethasone-bound form was observed, although the obtained curve did not reach saturation. Higher concentrations of the compound could not be tested due to compound precipitation. Data could be suitably fitted to the mentioned model and a K_D of 6.90×10^{-4}M was obtained (Table 17). In the same experiment, dexamethasone was included as a positive control (Figure 15a and b). The resulting dissociation constant was 8.90×10^{-5}M for apo-AncGR2 and 1.61×10^{-4}M for DEX-AncGR2. Therefore, dexamethasone showed higher affinity for the unbound receptor, as expected. The affinity for the liganded form was comparable to F's.

In a third SPR run, the dissociation time was extended to allow proper washing and avoid aggregations. Duplicates were run consecutively to avoid baseline clusters. Results from the last run were confirmed: F interacted with dexamethasone-bound receptor, but not with the apo form, as seen in Figure 16b and d. In the first case, the calculated K_D was 1.33×10^{-5} M.

In all cases data fitting using kinetics model failed, as the interaction was too fast to obtain the rate constants.

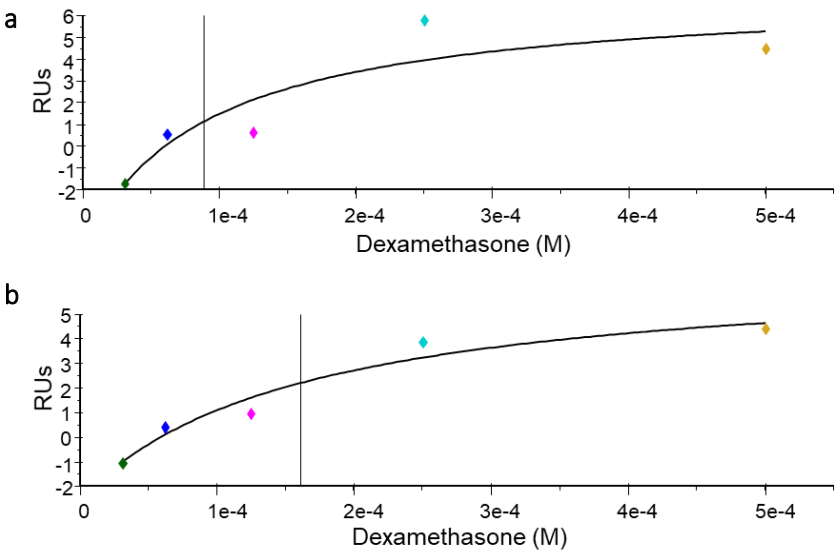

Figure 15. Dexamethasone binding to AncGR2(LBD). *Response at binding equilibrium has been plotted against analyte concentration. (a) and (b) correspond to control analysis of receptor interaction with dexamethasone (apo-AncGR2 and DEX-AncGR2 respectively). DEX interacts with higher affinity to the unbound receptor.*

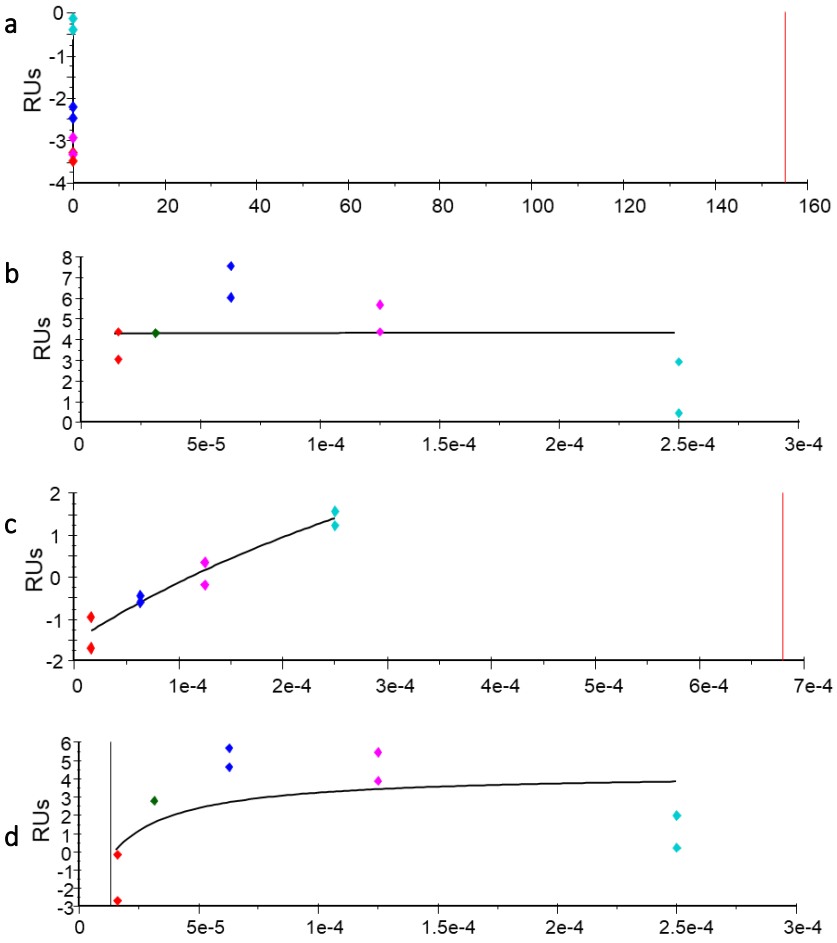

Figure 16. F binding to AncGR2(LBD). Response at binding equilibrium has been plotted against analyte concentration. (a) and (b) correspond to two consecutive analysis of F binding to apo-AncGR2 (runs 2 and 3 respectively). No interaction between the two molecules can be seen. (c) and (d) represent two analyses of F binding to DEX-AncGR2 (run 2 and 3 respectively). In this case, there is binding to the receptor and data can be modelled to a 1:1 Langmuir model.

Compound F binding to AR

In this case, AR(LBD) bound to dihydrotestosterone (DHT) was immobilized into a sensor chip and F binding was detected in two different runs performed in duplicate (Table 6). Dexamethasone was also analyzed as a reference compound.

F interacted with DHT-bound receptor following a 1:1 Langmuir model, with a K_D of 2.63×10^{-4}M and 1.61×10^{-6} M in two different runs (Figure 17 and Table 17). In the same experiment, dexamethasone was included as a positive control and the resulting dissociation constant was 1.01×10^{-4} M, similar to F.

In both cases interaction was too fast to obtain the rate constants, so data could not be analyzed in terms of binding kinetics.

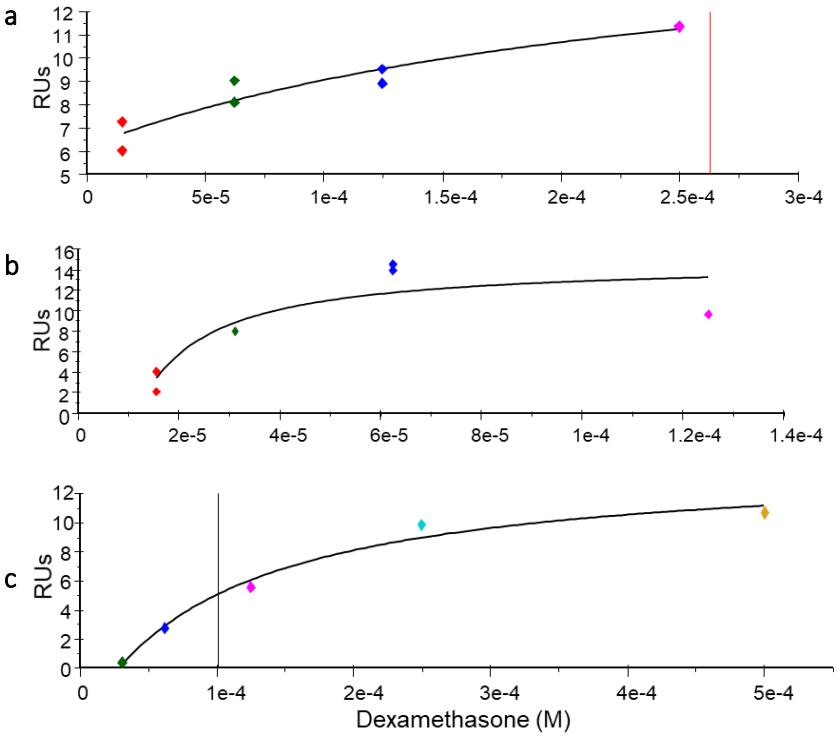

Figure 17. F and dexamethasone binding to AR(LBD). Response at binding equilibrium has been plotted against analyte concentration. (a) and (b) correspond to two consecutive analysis of F binding to DHT-AR (runs 2 and 3 respectively). (c) corresponds to control analysis of receptor interaction with dexamethasone. In all cases binding can be modelled to a 1:1 Langmuir model.

Table 17. SPR-derived parameters of F-GR and F-AR binding. K_D was estimated at steady state following a 1:1 Langmuir model of interaction. Rmax represents the theorical maximal RUs.

		Apo-AncGR2(LBD)		DEX-AncGR2(LBD)		DHT-AR(LBD)	
		K_D (M)	Rmax (RU)	K_D (M)	Rmax (RU)	K_D (M)	Rmax (RU)
DEX	Run 2	8.90E-05	11.82	1.61E-04	9.46	1.01E-04	18.11
F	Run 2	117.2	1.42E+06	6.90E-04	10.95	2.63E-04	10.35
	Run 3	2.47E-07	2.33	1.33E-05	9.08	1.61E-06	122.70

DEX, dexamethasone.

Compound F3 binding to GR

As stated above, F3 has been shown to antagonize both GR and AR transactivation with high potency. To determine whether a direct binding to the receptors occurred, surface plasmon resonance assays were performed. The ancestral variant of the receptor AncGR2 was immobilized again into a sensor chip, both in the apo form and bound to dexamethasone.

F3 interacted with both forms of AncGR2: the Apo-receptor and the dexamethasone-bound receptor; although the obtained curve in the first case did not reach saturation (Figure 18).

Data could be suitably fitted to a 1:1 Langmuir model and an average K_D of 1.52×10^{-4}M and 2×10^{-6}M were respectively obtained (Table 18). As F, F3 also showed higher affinity and response for the dexamethasone-bound receptor. Surprisingly, this affinity was higher than dexamethasone (1.61×10^{-4}M, Table 17).

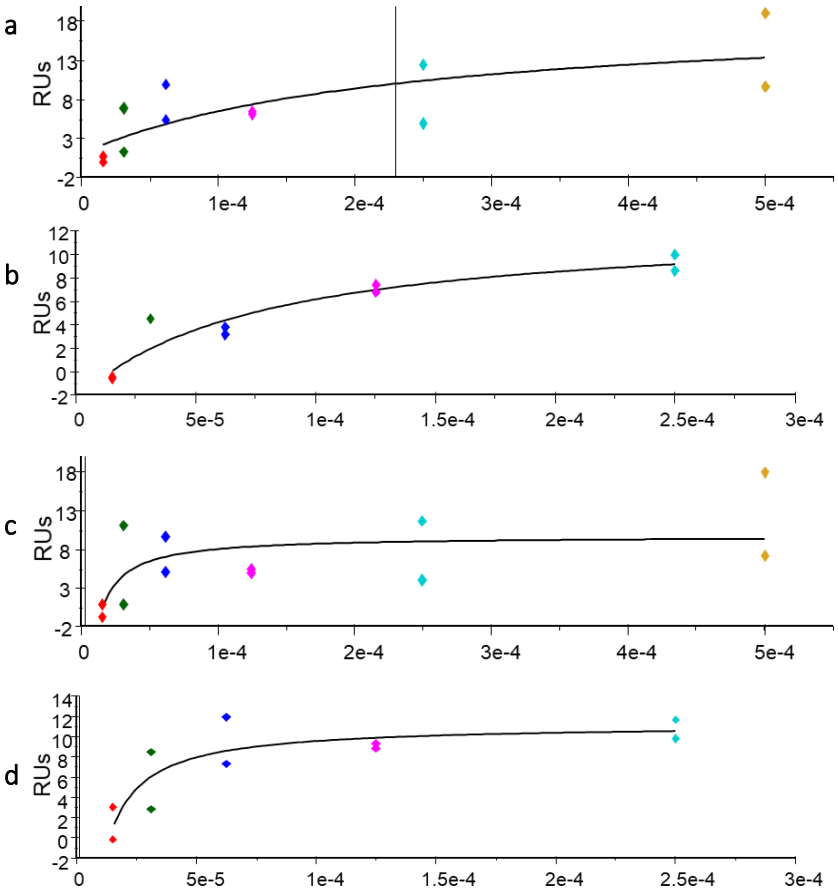

Figure 18. F3 binding to AncGR2(LBD). Response at binding equilibrium has been plotted against F3 concentration. (a) and (b) correspond to two consecutive SPR analysis of F3 binding to apo-AncGR2 (runs 2 and 3 respectively). (c) and (d) represent two analyses of F3 binding to DEX-AncGR2 (run 2 and 3 respectively). In all cases F3 binds to the receptor and data can be modelled to a 1:1 Langmuir model.

Compound F3 binding to AR

As before, AR(LBD) bound to dihydrotestosterone (DHT) was immobilized and F3 binding was detected in duplicates and in two different runs (Table 6).

F3 also interacted with DHT-AR(LBD) with an average K_D of 5.13×10^{-5}M (Figure 19a and b and Table 18), comparable to F and higher than dexamethasone. In this case, the kinetic parameters of the interaction could be obtained (Figure 19c and Table 18). Estimated k_a was $332.3\ M^{-1}s^{-1}$ and k_d $0.0298\ s^{-1}$. The calculated K_D resulted then in $8.995 \times 10^{-5}M$, which is the same range as the value obtained with the analysis at steady state.

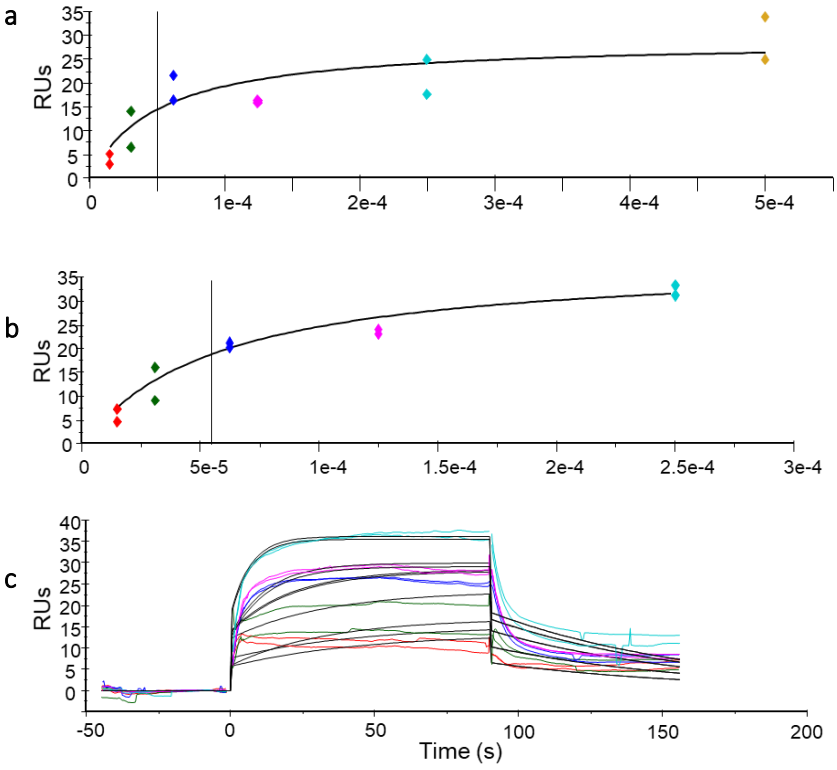

Figure 19. F3 binding to AR(LBD). *(a) and (b) correspond to two consecutive analysis of F3 binding to DHT-AR (runs 2 and 3 respectively). Response at binding equilibrium has been plotted against analyte concentration. In both cases F3 binds to the receptor and data can be modelled to a 1:1 Langmuir model to obtain the binding affinity. (c) Sensograms of the different concentrations of F3 tested for the determination of association and dissociation rate constants in run 3.*

Table 18. SPR-derived parameters of F3-GR and F3-AR binding. *K_D was estimated at steady state following a 1:1 Langmuir model of interaction (unless stated otherwise). Rmax represents the theorical maximal RUs.*

	Apo-AncGR2(LBD)		DEX-AncGR2(LBD)		DHT-AR(LBD)	
	K_D (M)	Rmax (RU)	K_D (M)	Rmax (RU)	K_D (M)	Rmax (RU)
Run 2	2.29E-04	17.82	2.76E-06	61.54	4.86E-05	31.83
Run 3	7.45E-05	15.27	1.24E-06	133.70	5.40E-05	41.32
					8.995E-05*	22.78*

** Values derived from kinetic measurements*

INHIBITION OF MMTV PROMOTER ACTIVITY BY COMPOUND F

At this point, both F and F3 have been shown to interact with the LBD of AR and GR. They could also inhibit gene transactivation mediated by both receptors, among other NRs. In this case, the effect was also driven by the LBD. We decided to focus on the interaction between F and GR for its potential applications. In this way, we studied the effects of the ABC on the full-length receptor to assess if the observed interaction could take place between F and the native GR. In this assay, HeLa cells transfected with an MMTV-*bla* construct were used. The construct consisted in the *bla* reporter gene under the control of the MMTV promoter, which contains a GRE. The activation and inhibition of the GC pathway was followed by TR-FRET, as depicted in Figure 21.

Cells stimulated with dexamethasone and in the presence of F showed a decrease in reporter expression. This decrease was dependent on F concentration, reaching an 86% inhibition at the maximum tested concentration (Figure 20). The half-effective concentration (relative IC50), determined from Hill analysis of the curve, was estimated to be 4.85 µM. In terms of potency, it resulted to have 2000 times lower potency than the reference compound mifepristone (RU-486), which showed an IC50 of 2.42 nM. Therefore, the obtained competition factor (IC50 test compound (µM)/ IC50 reference compound (nM)) was 2.

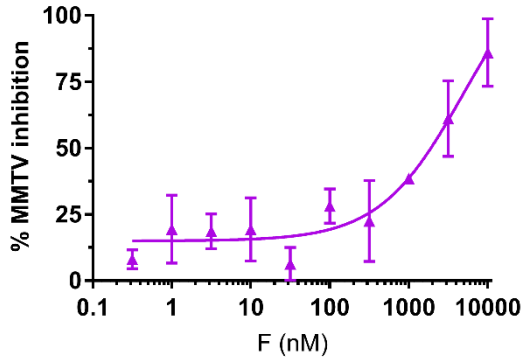

Figure 20. Inhibition of MMTV promoter transactivation caused by Compound F. *F antagonizes dexamethasone stimulation of MMTV-bla HeLa cells, as determined by TR-FRET. Cells were incubated with increasing concentrations of F and dexamethasone at its EC80, and the activation of the reporter gene* bla *was detected. Resulting curve presented a hillslope of 0.82 and a R^2 of 0.95. Error bars indicate standard deviation from two biological replicates.*

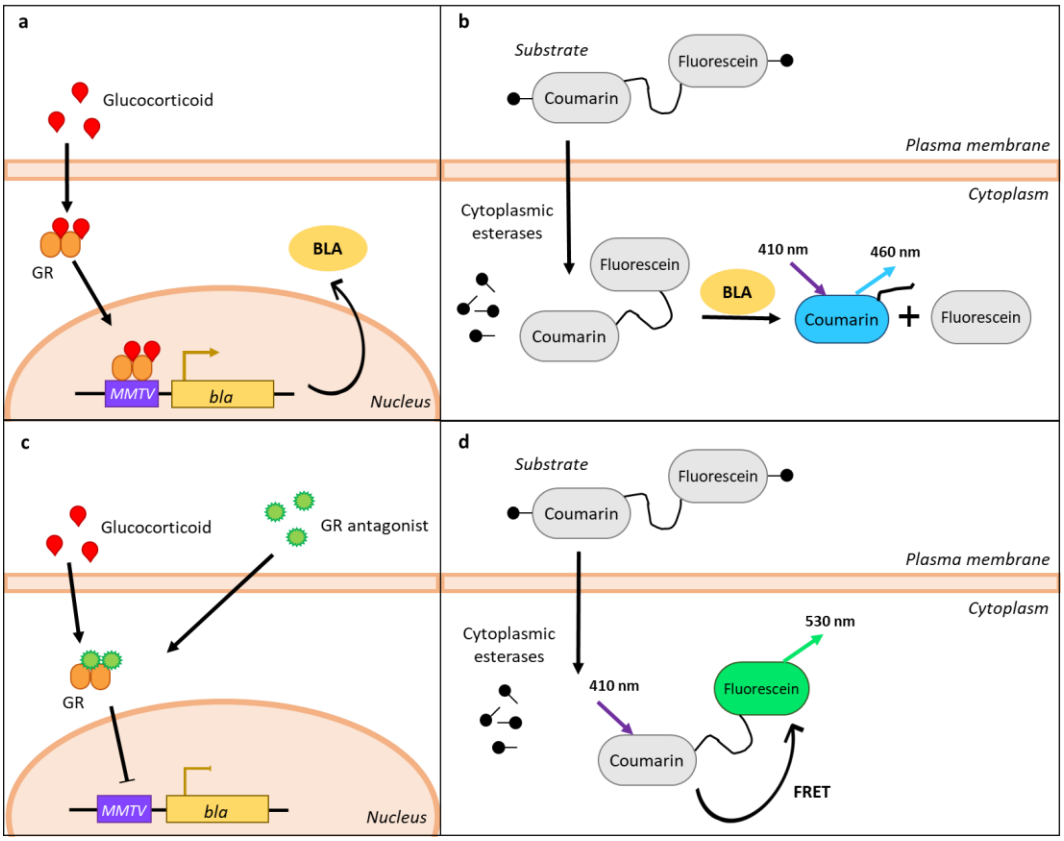

Figure 21. Fluorescent detection of MMTV promoter activity. *(a-b) Upon incubation with a GR agonist, the receptor is activated and induces* bla *expression. Cells are loaded with a fluorescent bla-substrate containing coumarin and fluorescein. When it enters the cell, cleavage by endogenous cytoplasmic esterases traps it within the cytosol, allowing to monitor cell viability. In the presence of Bla, the substrate is cleaved, which disrupts energy transfer and shifts the emission peak to 460 nm. (c-d) In the absence of GR activation or upon incubation with an antagonist, there is little* bla *expression. In this case, the substrate molecule remains intact. Coumarin excitation results in FRET to fluorescein, which is detected by a fluorescence emission peak at 530 nm. The resulting coumarin: fluorescein ratio is used to quantify GC pathway activation, while raw fluorescein fluorescence allows to monitor cell viability.*

COMPOUND F INFLUENCE ON GR-MEDIATED REGULATION OF INFLAMMATION

F has been described to have important anti-inflammatory effects that could be related to a modulation of NRs, in particular to GR. We studied the effect of the ABC on the expression and secretion of several inflammatory genes and mediators particularly related to GR, as markers of receptor's activity.

Expression of GC-transactivated anti-inflammatory genes

We evaluated the effect of F on the induction of the genes glucocorticoid-induced leucine zipper (*Gilz*) and Mitogen-activated protein kinase phosphatase 1 (*Mkp1*) in bone-marrow derived mouse macrophages. *Gilz* regulates T cell activation, differentiation and apoptosis. It interacts with other TRFs to inhibit the expression of pro-inflammatory genes (137). The *Mkp1* gene is an inducible nuclear phosphatase that regulates p38 MAPK and JNK, suppressing inflammation (138). Both genes are induced by GCs and have important roles in mediating their anti-inflammatory actions. Therefore, they are interesting biomarkers of GR activity, as well as of inflammation. Their expression was studied in mouse macrophages extracted from the bone marrow. qPCR was used to evaluate expression levels of both genes after incubation with F, dexamethasone (reference GC) or their combination.

Incubation with dexamethasone alone caused the transactivation of both genes after 2h of treatment (Figure 22), as it has been extensively described. In contrast, F had no effect on the expression of *Gilz* and *Mkp1*. No variations in mRNA levels in comparison to basal state were detected. Moreover, no significant differences were measured between incubation with the GC alone or in coincubation with F. Therefore, at the tested concentration it did not antagonize the induction of *Gilz* and *Mkp1* caused by dexamethasone.

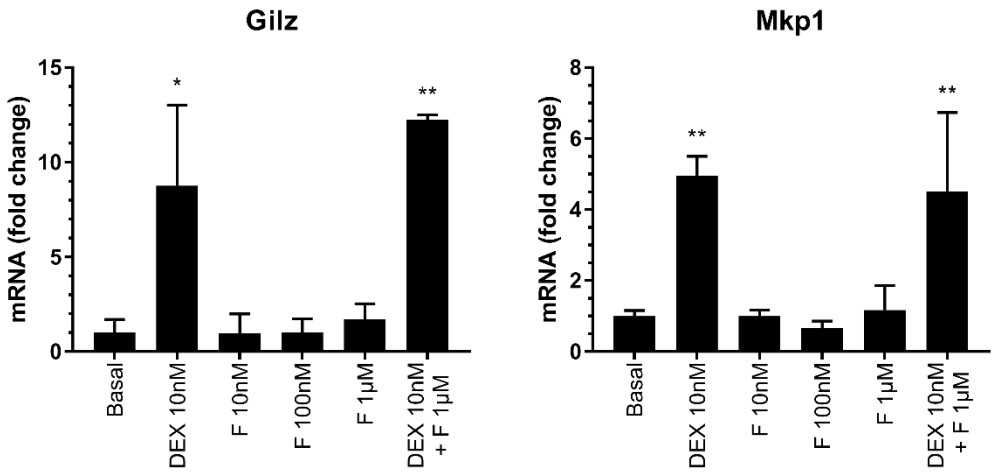

Figure 22. Induction of the anti-inflammatory genes Gilz ***and*** Mkp1 ***in macrophages.*** *Bone marrow-derived macrophages were incubated with dexamethasone (DEX), Compound F (F) and a combination of the compounds. Analysis of* Gilz *and* Mkp1 *expression was performed by qPCR. F did not induce the expression of the anti-inflammatory genes and did not avoid the induction caused by DEX. Values are mean±SD of triplicates (basal, DEX, F 1 µM) or duplicates (rest of the samples) and are normalized as described in page 105. * significant difference from control with a* p value *< 0.05. ** significant difference from control with a* p value *< 0.01.*

Effect on LPS-induced inflammation

Lipopolysaccharides (LPS) are large molecules composed by lipids and polysaccharides that are found in the outer membrane of Gram-negative bacteria. LPS are generally recognized by Toll-like receptors of immune cells, as part of the host's response to infection. It triggers the secretion of pro-inflammatory cytokines, nitric oxide and eicosanoids. In particular, LPS initiate an inflammatory response by inducing NF-κB activation via several signal transduction pathways. In this case, we focused on the analysis of inflammatory genes related with GR transrepression activity.

IL8 secretion

The neutrophil chemotactic factor (IL8 or CXCL8) is a chemokine secreted mainly by macrophages. Its primary function is to attract neutrophils and granulocytes to the site of injury and stimulate phagocytosis. It also promotes angiogenesis, and thus is an important factor in cancers. We evaluated the secretion of IL8 in THP1 monocytes by immunodetection after LPS stimulation.

Unstimulated THP1 monocytes secreted no detectable levels of IL8 and incubation with F or dexamethasone did not induce the cytokine (data not shown). Upon stimulation of inflammation with LPS, IL8 secretion was induced. However, none of the tested treatments repressed the secretion of the cytokine. Coincubation of mifepristone, a reference GC antagonist, and dexamethasone, resulted in upregulation of IL8. Although dexamethasone alone did not inhibit IL8 significantly, results of the addition of an antagonist probably indicate that some repression was taking place. On the other hand, coincubation of F with dexamethasone or mifepristone showed no variations compared to control.

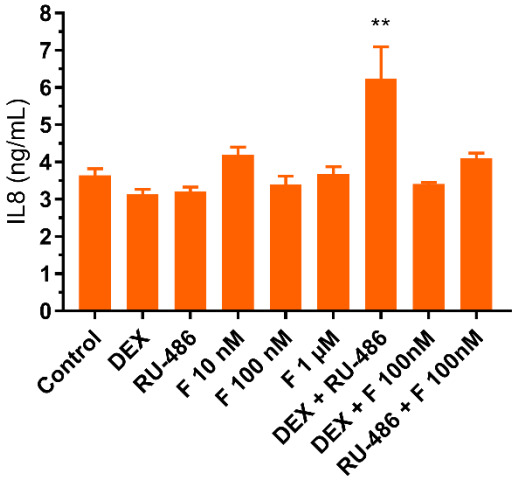

Figure 23. IL8 secretion of LPS-stimulated monocytes after treatment with F. *THP1 cells were incubated with Compound F (F), 10 nM dexamethasone (DEX), 5 nM mifepristone (RU-486) and combinations thereof. After preincubation for 1h cells were stimulated with LPS for 24h. F did not affect IL8 secretion under tested conditions. Values are mean±SD from 3 technical replicates. ** significant difference from control with a* p value *< 0.01.*

Expression of GC-transrepressed inflammatory genes

The expression of several pro-inflammatory genes that are known to be transrepressed by GR was studied by qPCR in mouse macrophages after stimulation with LPS. Studied genes included the pro-inflammatory cytokines *IL1β*, *IL6*, *IL12* and *Tnfα*; *Cox2* and Nitric oxide synthase 2 (*Nos2*). *Cox2* codifies for the enzyme responsible for the formation of prostanoids, which are mediators of inflammatory reactions and *Nos2* is responsible of the synthesis of nitric oxide, an important mediator of vasodilatation.

Cells were incubated with F or dexamethasone, which was used as a glucocorticoid of reference. In the absence of LPS stimulation, no induction of inflammation was observed, as expected: neither F nor dexamethasone upregulated the studied genes (data not shown).

When macrophages were stimulated with LPS, all studied genes were considerably induced. Upon incubation with dexamethasone, a decrease in the expression was observed, despite

it was not significant (Figure 24). F did not repress mRNA levels of the selected inflammatory genes.

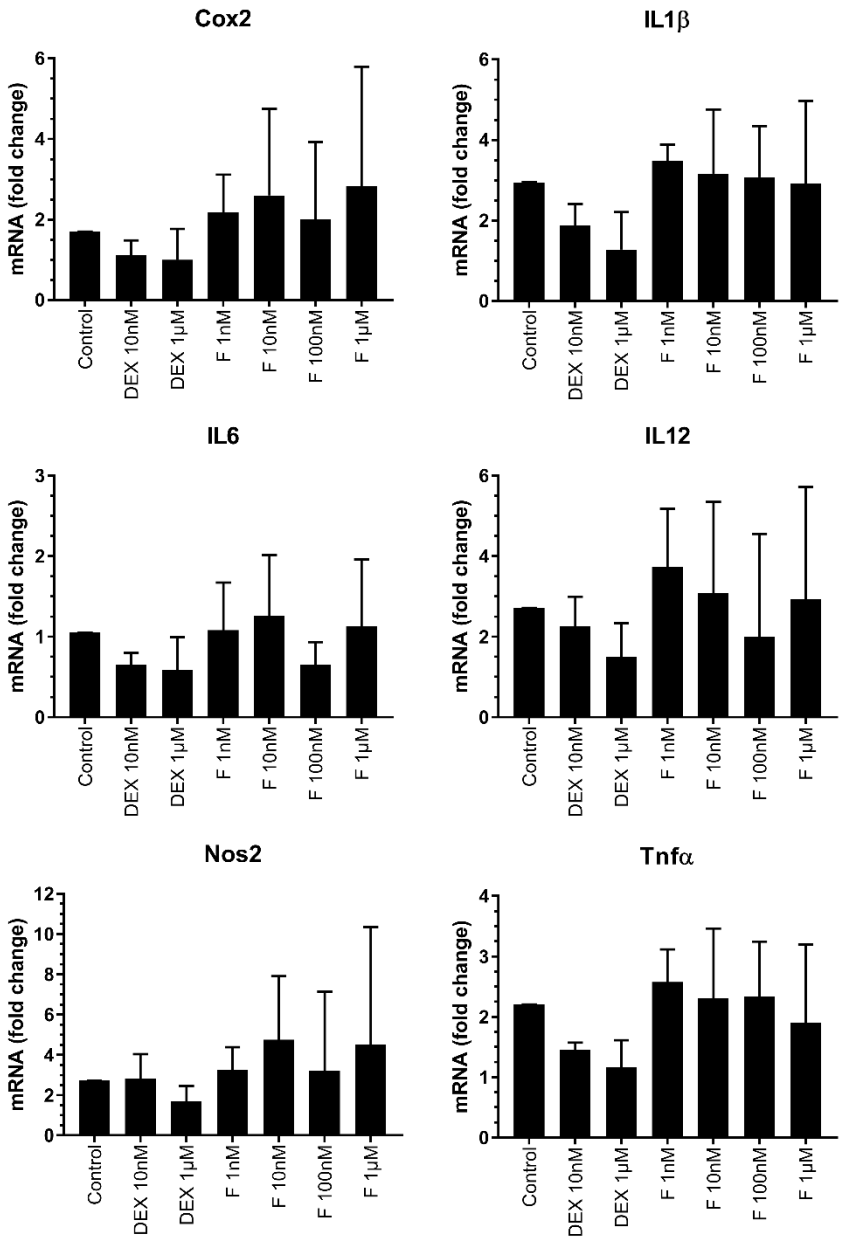

Figure 24. Effect of F on LPS-induced inflammation in macrophages. *Bone marrow-derived macrophages were incubated with dexamethasone (DEX) or Compound F (F) for 2h and then stimulated with LPS for 2h. Gene expression analysis of several GC-transrepressed genes was performed by qPCR. F did not inhibit the expression of the pro-inflammatory genes. The reference GC DEX did not have significant effects either. Values are mean±SD of triplicates and are normalized as described in page 105.*

Effect on PMA-induced inflammation

Phorbol 12-myristate 13-acetate (PMA), a phorbol diester, is an activator of Protein kinase C (PKC). This family of serine/threonine kinases play critical roles in the regulation of cell activation, differentiation, proliferation and death. They are importantly related to hematopoietic and immune responses and have potent tumor promoter effects. PKCs can either associate with receptors on the cell surface of immune cells and activate downstream signal transduction cascades or be activated by second messengers. In this case, they participate in Ca^{2+} signaling pathways (139). PMA is a common inflammatory stimulus and it is known to trigger the secretion of several cytokines, among them IL8 and TNFα.

IL8 secretion

The secretion of IL8 was studied in THP1 monocytes upon the incubation with F. Dexamethasone was used again as a reference anti-inflammatory compound. Previous studies showed that while stimulation with LPS induced IL8 secretion, it was not properly suppressed by dexamethasone. In consequence, stimulation with PMA was performed.

Unstimulated cells showed no secretion of the chemokine under all tested conditions (data not shown). No IL8 was detected upon incubation with F, dexamethasone, mifepristone or their combinations. Therefore, F did not induce IL8 secretion in resting monocytes.

Dexamethasone at 10nM reduced PMA-stimulated IL8 secretion by 75% (Figure 25). Surprisingly, the GC antagonist mifepristone also reduced around 20% of IL8. Incubation with F alone between 0.1 and 3 µM had no effect on the cytokine secretion. However, at 10 µM, it increased secretion by 36%, probably due to its cytotoxic effects at high concentrations in this monocytic cell line (as described before).

Mifepristone, included as a GC antagonist control, slightly antagonized dexamethasone IL8 reduction (Figure 25). Coincubations with dexamethasone at 10nM and F between 0.1 and 3 µM again showed no variation in comparison to dexamethasone alone. At 10 µM of F, once more an increase in IL8 secretion was observed, probably due to cell death and release of intracellular IL8. In the light of the results, further combinations with mifepristone and F were not carried out.

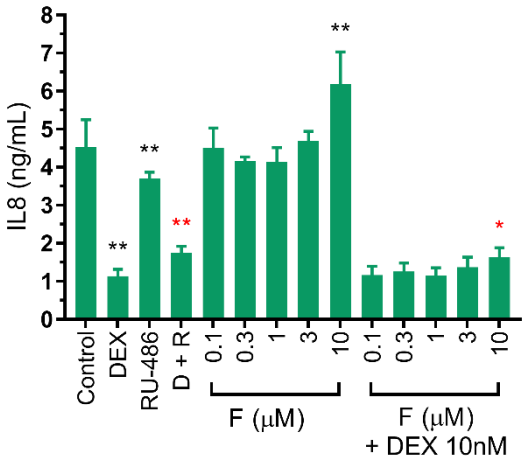

Figure 25. IL8 secretion of PMA-stimulated monocytes after treatment with F. *THP1 cells were incubated with Compound F (F), 10 nM dexamethasone (DEX), 5 nM mifepristone (RU-486) and combinations thereof. After preincubation for 1h cells were stimulated with PMA ON. F induced IL8 secretion only at cytotoxic concentrations. Values are mean±SD from 2 biological and 6 technical replicates. D+R, dexamethasone and RU-486. * significant difference from control (black) or DEX (red) with a* p value *< 0.05. ** significant difference from control (black) or DEX (red) with a* p value *< 0.01.*

TNFα expression and secretion

TNFα is a major pro-inflammatory cytokine involved in many processes, including inflammation, immune responses and development. It is a major driver of acute inflammation and plays a key role in some oncogenic processes and in autoimmune diseases, such as rheumatoid arthritis and Crohn disease (140). Its secretion was first studied in THP-1 monocytes stimulated with PMA and dose-response curves were obtained for F, dexamethasone and their combination.

Dexamethasone is a known inhibitor of TNFα expression both at transcriptional and translational levels (141–145). Accordingly, it strongly inhibited PMA-induced TNFα secretion with an IC50 in the range of 1.28 nM, reaching a maximal reduction of 23% of the control secretion (Figure 26 and Table 19). F presented an unusually different behavior, inhibiting cytokine upregulation but not dose-dependently. F reduced TNFα in the supernatant to around 60% of initial secretion (Figure 26 and Table 19).

Dexamethasone was then combined with 1 and 100 nM of F to explore possible interactions. A negative interaction was observed in both cases. Below 2 nM of dexamethasone the effect of F seemed to predominate, causing an almost constant inhibition. On the other hand, above this concentration no difference was observed between the effect of the combination or dexamethasone alone. Therefore, maximal efficacy was maintained at around 20% of control secretion, whereas potency slightly decreased (see IC50s in Table 19).

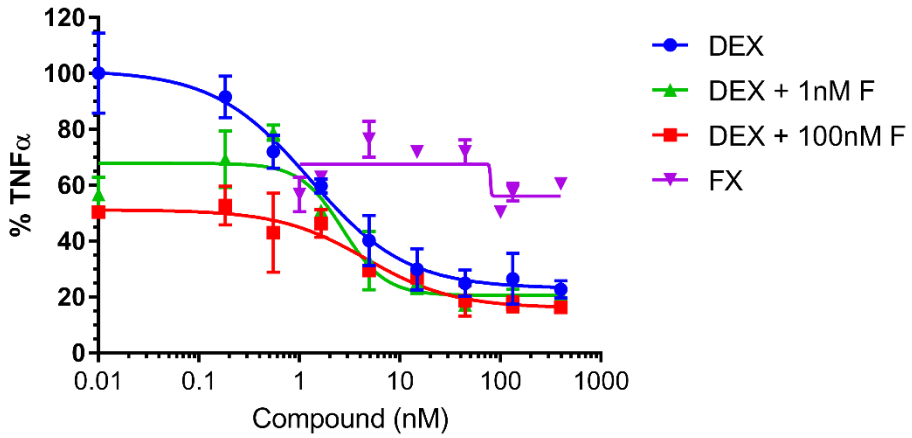

Figure 26. TNFα secretion in monocytes after treatment with PMA, DEX and F. F reduced the production of TNFα but not in a concentration-dependent manner. In combination with dexamethasone, maximal efficacy is maintained, whereas minimal efficacy improves. Values are mean±SD from two biological replicates, except for DEX that includes 4 replicates. DEX, dexamethasone; F, Compound F.

Table 19. Estimated parameters for inhibition curves of TNFα secretion. Potency and efficacy values of the effect of F and dexamethasone on TNFα secretion were determined by incubation in monocytes stimulated with PMA. Efficacy is expressed as the maximum and minimum secretion percentage.

	Minimum efficacy (%)	Maximum efficacy (%)	IC50 (nM)	Hillslope	R^2 value	Z' factor
DEX	101.10	22.98	1.276	0.907	0.941	0.969
DEX + 100 nM F	51.13	16.03	4.636	0.998	0.882	0.546
DEX + 1 nM F	67.82	20.50	2.702	2.044	0.892	0.546
F	67.47	56.07	~ 79.63	~ 86.38	0.394	0.969

~ approximate values due to an inadequate fit to the model or insufficient data.
DEX, dexamethasone; F, Compound F

The inhibition of TNFα secretion was further assessed in mouse primary macrophages obtained from bone marrow. In this case, both the presence of the secreted cytokine in the supernatant and its mRNA expression levels were evaluated.

First, inhibition of *Tnfα* expression was studied by qPCR. Dexamethasone at 10nM strongly inhibited PMA-induced *Tnfα* transcription, supposedly by transrepression via NF-κB and AP-

1 (142). F had no effect on *Tnfα* transcription, neither alone or in combination with dexamethasone (Figure 27). However, when TNFα secretion was analyzed by ELISA, similar results as with monocytes were obtained. In this case, a significant average inhibition around 30% of secretion was reported for F, which was not dose-dependent. Dexamethasone alone also inhibited protein secretion, according to the observed transcription inhibition. When F was coincubated with a constant concentration of dexamethasone, TNFα presence was further reduced to undetectable levels.

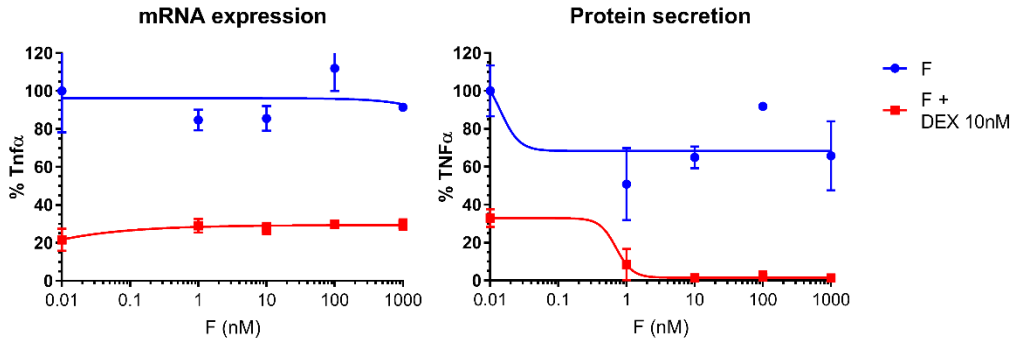

Figure 27. TNFα expression and secretion in macrophages after treatment with PMA, DEX and F. *F post-transcriptionally reduced the production of TNFα but not in a concentration-dependent manner. In combination with dexamethasone the same behavior was observed. Values are mean±SD from three technical replicates, except for controls that include two biological replicates, and are normalized to the corresponding control. DEX, dexamethasone; F, Compound F.*

EFFECT OF COMPOUND F ON GR NUCLEAR TRANSLOCATION

Effect on GFP-GR translocation

We have shown that F is able to interact with GR, but its effects on its modulation are not clear yet. Next, we wanted to evaluate whether F affects the nuclear translocation of the receptor. It is the case for passive GR antagonists, which inhibit GR transcriptional activity by competing with agonists and reducing receptor translocation. To study this, an immunofluorescence assay with a HEK293 line expressing the GFP-GR fusion protein was designed. GFP fluorescence allowed to monitor the nuclear translocation process and quantify receptor's distribution inside the cell.

Initially, HEK293 tGFP-hGR cells were incubated with dexamethasone or F for 1 or 16h. Compared to cells treated with vehicle (DMSO), dexamethasone incubation significantly increased nuclear location of GR in a time dependent manner. DMSO alone caused a slight rise in translocation in relation to non-treated cells after 1h. However, treatment with F resulted in no effects on cell's basal state (Figure 28a and Figure 29a-f). Compound toxicity was evaluated based on nuclei count and was not affected by any treatment (Figure 28b).

As the ABC was not able to induce translocation, a second assay was performed to disguise if it could prevent it. Geldanamycin, a known Hsp90 inhibitor, was used as a control for translocation inhibition. In this case, overnight incubation was not possible due to known geldanamycin toxicity at longer expositions.

Pre-treatment with geldanamycin completely avoided GR translocation induced by dexamethasone after 1h. Still, F could not prevent GFP-GR translocation at tested concentrations (Figure 28c and Figure 29g-i). Even if some F concentrations seem to slightly induce fluorescent receptor redistribution into the nucleus (0.32, 3.2 and 10 µM), they are considered not relevant, as there is no dose-dependence and variation is extremely small. In this case, more replicates could help to strengthen the statistical analysis.

Coincubation of dexamethasone and the compound presented toxicity at the highest concentrations. Although values are not significant when compared to the basal state, there is indeed a significant difference between the treatment at low and high F doses (0.32 µM vs. 32 µM). No toxicity was observed in dexamethasone and geldanamycin controls (Figure 28d).

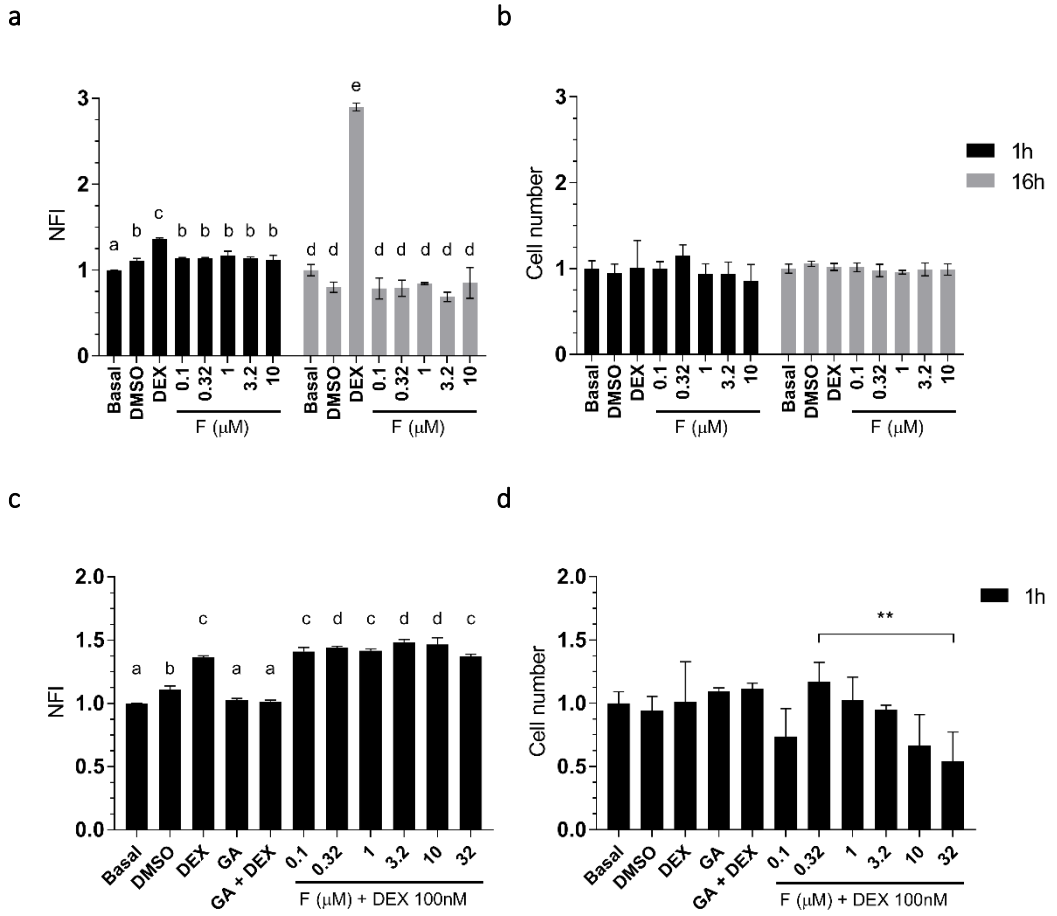

*Figure 28. Quantification of F effect on GFP-GR nuclear translocation. (a) Relative fold increase of GR nuclear translocation in HEK293 tGFP-hGR cells after 1h and overnight treatment with dexamethasone (DEX) or Compound F (F). Nuclear fluorescence intensity (NFI) has been normalized to non-treated cells (Basal). (b) Nuclei number quantification of (a), normalized to non-treated cells. No cell mortality was observed in the assay. (c) Relative fold increase of GR nuclear translocation in HEK293 tGFP-hGR cells after the treatment with dexamethasone (DEX), geldanamycin (GA) and combinations with Compound F (F) for 1h. Nuclear fluorescence intensity (NFI) has been normalized to non-treated cells (Basal). (d) Nuclei number quantification of (c), normalized to non-treated cells. All data points represent the average and standard deviation of a single experiment performed by triplicate. Letters above bars indicate clusters of significance with p<0.01. ** p value < 0.01.*

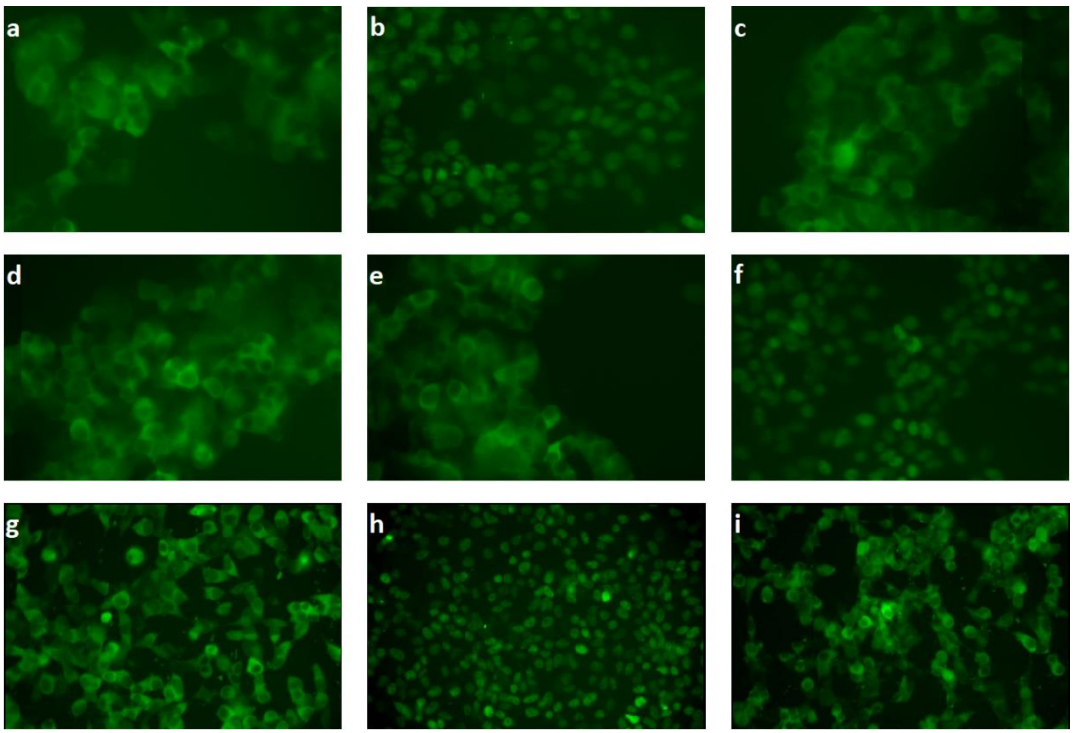

Figure 29. Effect of F on GFP-GR nuclear translocation. *Representative fluorescence microscopy images at 20x of the translocation assay corresponding to: (a) DMSO 1h, (b) dexamethasone 1h, (c) geldanamycin 1h, (d) geldanamycin + dexamethasone 1h, (e) Compound F 1h, (f) Compound F + dexamethasone 1h, (g) DMSO 16h, (h) dexamethasone 16h and (i) Compound F 16h. GFP-GR is mostly present in the cytosol in all the images, except for b, f and h, where fluorescence has migrated to the nuclei.*

Effect on native GR translocation

As F effects on GR nuclear translocation needed validation, a new assay based on the detection of native receptor translocation was designed. HaCat cells were incubated with the compound at different time points and GR location was studied by compartmental cell extraction and western blotting. In all cases, histone presence in the cytoplasmic extract, as well as tubulin presence in the nuclear extract, were assessed in order to validate the extraction procedures. No measurable cytoplasmic tubulin was detected in nuclear extracts and vice versa. Both biomarkers were also used to normalize GR signal in their corresponding extracts.

Firstly, HaCat cells' responsiveness to glucocorticoids was tested and keratinocytes were incubated with different concentrations of dexamethasone. After 1h incubation, GR nuclear translocation increased with dexamethasone concentration, indicating GR sensitivity. As seen in Figure 30a-d, the amount of GR detected in the cytoplasm decreased, while it increased in nuclei. No difference was observed between 100 nM and 500 nM dexamethasone, probably indicating that the fraction of GR available for translocation (around 75% of cytoplasmic GR) had been already transferred to nucleus, thus reaching saturation. Coincubation with different concentrations of F and dexamethasone at 100 nM did not show any changes in GR translocation at 1h (Figure 30a-d).

When tested at different time points, dexamethasone 100 nM was able to mobilize the receptor after 1, 5 and 24h incubation. F could not prevent dexamethasone-induced receptor translocation at any time points. It had no effect on its own either, as receptor quantification after F incubation in both cytoplasmic and nuclear extracts was comparable to basal state (Figure 30e-h). Despite variability in nuclear extracts was too high to give significant differences, values obtained from cytoplasmic extracts were consistent.

When data from GR isoforms α and β was analyzed separately (not shown), very similar results were obtained, which indicates parallel dynamics of translocation of both isoforms to the nucleus. GR translocation was also primarily assessed in the THP1 cell line. However, GR expression could barely be detected by the present methods (data not shown), which could be related to its described glucocorticoid resistance (146). Therefore, no further tests were performed.

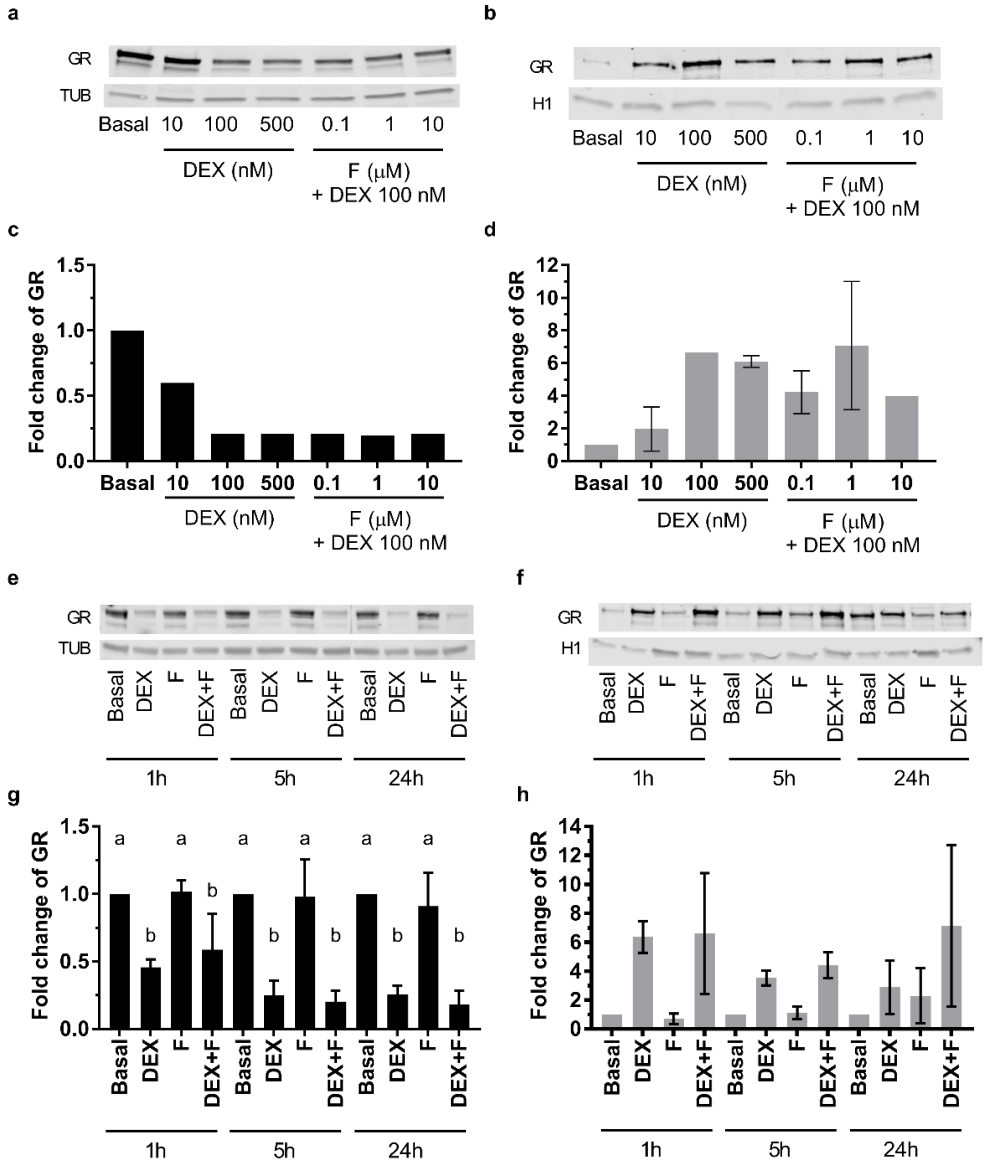

Figure 30. Effect of F on GR nuclear translocation in HaCat cells. *HaCat keratinocytes were incubated with dexamethasone (DEX) and Compound F (F) to study native GR translocation. Cytoplasmic (a) and nuclear (b) extracts were obtained after incubation with different concentrations of the compounds and analyzed by western blotting. Relative quantification of the western blotting was performed for cytoplasmic (c) and nuclear GR (d). Cytoplasmic (e) and nuclear (f) extracts of HaCat cells were also obtained after incubation with 100nM dexamethasone and/or 1μM Compound F at different time points. Relative quantification of the western blotting was performed for cytoplasmic (g) and nuclear GR (h). In western blotting, specific bands appeared at 95KDa (GR alpha), 90KDa (GR beta), 50 KDa (TUBB2A) and 30 KDa (H1.0). In relative quantifications, the sum of GR fluorescence signal from α and β isoforms has been corrected by tubulin signal (cytoplasm extracts) or histone signal (nuclear extract) and normalized to corresponding control (Basal) to obtain the fold change. Error bars indicate standard deviation from two biological replicates (b), or two biological and two technique replicates (g and h). Letters above bars indicate clusters of significance with $p<0.05$.*

MODULATION OF GR EXPRESSION AND DEGRADATION BY COMPOUND F

Another possible GR regulation pathway involves receptor expression and stability modulation. To study it, different concentrations of dexamethasone and F were applied to HaCat keratinocytes and cell extraction was carried out at different time points.

After 1 and 5 hours of incubation, dexamethasone at tested concentrations had no effect in the total amount of GR detected. Coincubation with different concentrations of F did not show significant effects either (Figure 31a).

After 24h of culture exposure to dexamethasone, a decrease in total GR was detected, probably caused by proteasome degradation (47). GR down-regulation was also observed in coincubation with the ABC, despite this alone did not affect GR after long-term exposure (Figure 31b). Accordingly, cytoplasmic and nuclear extracts (Figure 30g and h) obtained after 24h dexamethasone incubation also showed lower GR presence in both compartments than shorter incubations.

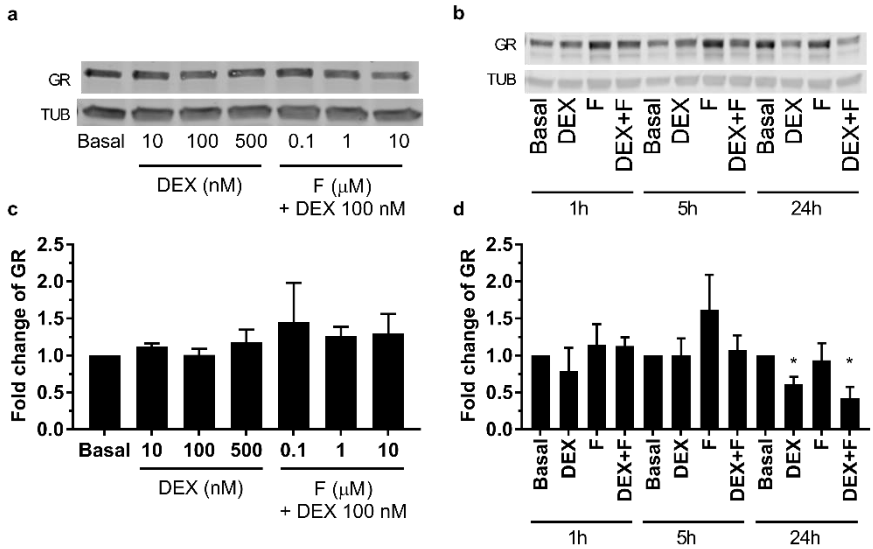

Figure 31. Effect of F on GR expression in HaCat cells. *HaCat keratinocytes were incubated with dexamethasone (DEX) and Compound F (F) at different concentrations and times to study GR expression and stability. (a) Whole cell extracts were obtained after incubation with different concentrations of the compounds and analyzed by western blotting. (b) Whole cell extracts of HaCat cells incubated with 100nM dexamethasone and/or 1μM F at different time points were analyzed by western blotting. (c) Relative quantification of total GR in (a). (d) Relative quantification of total GR in (b). In western blotting, specific bands appeared at 95KDa (GR alpha), 90KDa (GR beta) and 50 KDa (TUBB2A). The sum of GR fluorescence signal from α and β isoforms has been corrected by tubulin signal and normalized to corresponding control (Basal) to obtain the fold change. Error bars indicate standard deviation from two biological and two technique replicates. * p value < 0.05.*

DISCUSSION

ABCs have many common bioactivities and share a common scaffold. In particular F has been described to have many effects on human health and is considered to have considerable potential in such applications. However, to date there is no satisfactory description of its mechanism or mechanisms of action that explains these bioactivities. Modulation of NRs has been proposed as a possible mechanism of action, which would be possible thanks to its lipophilicity. Nevertheless, to date there is only preliminary evidence that supports this interaction. Several ABCs and their derivatives have been shown to interact with retinoid receptors, AR or PPAR or to modulate their expression. In fact, F has also been suggested to interact with RAR based on its effects on endothelin-1, despite it has not been directly tested. Apart from that, F was described to inhibit the interaction between PXR and the coregulator SRC1, common in many NRs. Additionally, some of the described F bioactivities could correlate with a GR modulator. For instance, F presents anti-leukemia, anti-inflammatory and anti-angiogenesis properties, just as a glucocorticoid agonist. At the same time, F has been shown to reduce insulin resistance and obesity, as well as skin pigmentation, and has been reported to protect against osteoporosis and Alzheimer, which could be antagonistic activities against GR. In fact, it is improbable that all these properties are related to a single mechanism of action. A broad spectrum of molecular targets would better explain its biological activity spectra. In this chapter we have studied the putative interaction with NRs, especially with GR, as a possible mechanism of action for at least some of F bioactivities.

Considering the high degree of homology among some NR domains, it was hypothesized that ABCs, and in particular F, could influence more than one NR. In fact, many NRs have overlapping ligand binding specificities. It is the case of cortisol, which binds equally to both GR and MR. MRs also have equivalent high affinity for aldosterone and progesterone. Despite many steroids can fit into the binding pocket of other NRs, mostly they are unable to form all necessary contacts to yield a transcriptionally active receptor conformation. Moreover, the NR superfamily share many coregulators, which don't bind to the ligand's binding pocket. It is the case of the mentioned coactivators SRC1 and FKBP52. To study these putative interactions, a screening of the activity of selected ABCs on a panel of NRs was performed by assessing their effects on the transcriptional activity of NRs.

Firstly, the effects of F on steroid receptors was analyzed. Despite many IC50 values were not obtained, the sigmoidal curves suggest similar potency and response in GR and MR, and lower for AR and PR. However, SPR assays performed later indicated similar affinity for both GR and AR. Potency was also lower for ERs, although they displayed higher responses.

Precisely, ER modulators have interesting applications, as they have long been used in the treatment of breast cancer, among other cancer types. Remarkably, many ABCs have already been described to act on breast cancer cell lines. Altogether, F displayed similar behavior as other glucocorticoid modulators, antagonizing GR with higher potency and similar response than other 3-ketosteroid receptors (NR3C). For instance, commercially available glucocorticoids are known to bind to PR with different affinities, which have been suggested to be proportional to their lipophobicity. Even endogenous ligands as progesterone and aldosterone show certain affinity for GR, although they may trigger different or no response. These results are consistent with an effect mediated by NR(LBD), given that it is a highly conserved domain and the region of interaction of many common coregulators.

The next analyzed compound was F3, as it is the main metabolite found in rodents after F ingestion. Similarly to its precursor, F3 has been shown to possess interesting bioactivities: cytotoxic activity against leukemia cell lines and attenuation of adipogenesis. Overall, F3 proved to be a more potent compound than F in transactivation inhibition of steroid receptors. While the antagonism for PR was similar in both compounds, the metabolite displayed preferences for AR, but also strong inhibition of GR and MR. On the other hand, F showed to be more active in ERs. Interaction between F3 and GR and between F3 and AR was confirmed to have similar affinity by SPR. As in the transactivation assays, F3 bound with higher affinity to NRs than F. Surprisingly, it presented a dissociation constant in the same order than dexamethasone for the Apo-GR.

After analyzing the results for F3, the study was extended to other ABCs. Surprisingly, different ABCs showed similar behaviors to F in avoiding GR transactivation. Although almost all tested compounds showed higher efficacy than F, in terms of potency only F3 was superior. In both cases, receptor inhibition starts around 300 nM. F2 also presented similar efficacy. The fact that both F and its metabolites have proven to be highly active, if confirmed, could be advantageous from a pharmacological point of view.

The evaluated ABCs have also shown to have variable affinities for AR. For instance, Compound L antagonized AR with similar potency and efficacy than GR. Interestingly, anti-androgenic compounds are clinically used for the treatment of hyperandrogenism, prostatic cancer and benign prostatic hypertrophies. In fact, a group of ABCs (Compound N and F among them) has been reported to have effects on the proliferation of prostatic cancer cell lines, as well as downregulating AR signaling and reducing prostate cancer risk, while being considered safe. Indeed, Compound Y has been directly related to AR activity. ABCs have also been studied for the treatment of hyperplasia. Interestingly, this activity was not found in all ABCs, which would confirm that their structure determines receptor selectivity. Androgen antagonists are also in clinical trials for the treatment of breast cancer and spinal

and bulbar muscular atrophy. As already mentioned, ABCs are thought to have potential in the treatment of breast cancer. In cosmetics, AR antagonists are used to reduce alopecia, hirsutism and acne. However, the current anti-androgenic compounds are associated to numerous side-effects, the most severe being osteoporosis and hepatotoxicity. ABCs, on the contrary, have been recently shown to prevent osteoporosis and other inflammation conditions, which would make them an interesting AR antagonist candidate.

Aside from focusing on F, another interesting compound that should be further studied is Compound N. It presented around 80% efficacy in GR antagonism under the assayed conditions and only a slightly higher competition factor than F. Both compounds showed the lowest response and potency on AR, meaning higher selectivity for GR. Additionally, Compound N proved not to interact with PR. Although we have not evaluated the activity of Compound N metabolites, its bioconversion to neochrome stereoisomers has been briefly described both *in vivo* and *in vitro.* Said compounds have also shown to retain interesting bioactivities from its precursor, such as cytotoxicity in prostate cancer cells. It is then an interesting alternative molecule to consider for further development.

Oppositely, Compound B and Compound A showed no evidence of antagonism in neither GR nor AR, although they have been described to interact with different NRs. In the case of Compound A, it has been reported to interact with PPARα and PPARγ, while it seems not to act on LXR. Compound B is a precursor of the retinoid family of molecules, which have both agonist and antagonist activities on RAR and RXR, but has also been related to PXR and ERs. Although the particularly low solubility of Compound B and Compound A may have affected the results of the *in vitro* assays, it is equally possible that specific ABCs or their metabolites may have direct distinct metabolic effects mediated by different NRs. In this way, it is not clear whether GR or AR antagonism is an intrinsic characteristic of ABCs or ABCs. It would be interesting to evaluate more ABCs in order to establish whether NR antagonism is present among this group. Nonetheless, even if Compound B or Compound A proved to be effective, their use would be clearly limited by their aqueous insolubility. As described later in Chapter 2, this problem can be greatly reduced by using a nanoparticle formulation, although it has proved not to work for Compound A.

After steroid receptors, we considered that another interesting family of NRs to study were retinoid receptors (RAR and RXR). Derivatives of Compound B are their ligands, but also other ABCs, as products from Compound Y have proven to activate those receptors. Interestingly, other derivatives have shown antagonist activity. It has been previously suggested that F could antagonize RAR activity as an explanation for the observed upregulation of endothelin-1. However, our results suggested that F did not inhibit the transcriptional activity of RARα or RARβ. On the contrary, we observed that it completely antagonized the activity of the RXRα *in vitro*. The effects on RARγ and RXRβ seemed to follow

a similar inhibition pattern, although it could not be determined due to cell toxicity. RXRs dimerize not only with RARs, but also with other NRs from subfamily 1, including PPAR, LXR, FR, PXR, TR and VDR. In case that this interaction was confirmed *in vivo*, it could indicate a simultaneous regulation of multiple pathways, adding more complexity to the network of interactions observed between ABCs and NRs.

The last screened NR was PPARγ. F also antagonized it, although it belongs to a less related NR group. PPARγ is crucial regulator of fatty acid and glucose metabolism, but also contributes to the anti-inflammatory response. Its alteration has been related to obesity, diabetes, atherosclerosis and cancer. Precisely, F is known to prevent the accumulation of fat and white adipose tissue by increasing lipolysis and oxidation of fatty acids. F effects are indeed similar to the phenotype observed in PPARγ knock-out mice. Moreover, F has been described to modulate PPARα and PPARγ expression, which reinforces the theory of a putative interaction with these receptors. In this case, it is not the first ABC described to have this effect: Compound A has been studied in relation to PPARα and PPARγ. However, in our studies Compound A did not avoid GR nor AR transactivation. Hence, it is possible that their structural differences confer them some selectivity for NRs. PPARγ regulation is also very complex and can involve other NRs. Indeed, PPARγ forms a heterodimer with RXRα to regulate the transcription of target genes. As our results suggest that F also antagonizes RXRα, described effects of F could be a mixture of both actions, as well as one inhibition could potentiate effects on the other receptor. Apart from that, a functional cross-talk between the pathways of GR and different PPAR isoforms has been reported. Mainly additional effects of their agonists on inflammation and apoptosis have been studied, but other interesting properties have come up too. For instance, mifepristone is able to antagonize PPARγ activation, although the mechanism has not been characterized. Moreover, both receptors can physically interact to produce a differential transcriptional regulation. Our data adds one more stage in this cross-talk regulation, as we present a molecule capable of inhibiting both receptors.

In the light of the previous results, F and its metabolite F3 were selected to further study the interaction with NRs. The decision was not only based on the interesting properties that they had shown on different NRs, but also on F's abundance in nature and available references. The inhibition of several NRs could be interpreted as off-target events and hence a possible source of side effects, but new applications may also arise for F and for other ABCs form this novel described interactions. Most NRs share a similar biological niche, and a dual action on different NRs could reinforce a unique final activity. However, a major focus in the current discovery of drugs targeting NRs is identifying drugs with reduced side effects. This can be achieved not only by improving selectivity, but also by selective modulation of the NR of interest. Therefore, more information on the modulation of each receptor by ABCs needs to be gathered to define their potential uses.

Based on the results obtained with the assays performed with chimeric receptors, the effect of F on NRs was probably mediated by the receptor's LBD, as it was able to inhibit transcription in the absence of the DBD. Given that the transfected construct for the fusion protein was not under control of the native promoter, results could not be attributed to changes in receptor expression either. In the case of GR, this fact was later confirmed by western blot analysis of the native receptor. Even though the modulation of other regulators involving NRs signaling pathways could not be discarded at this point, we decided to explore the possibility of a competitive interaction with NR ligands. Firstly, it was performed by a biochemical competitive binding assay, which was carried out with GR and PXR. In this assay, competition for the binding pocket, situated in the LBD, was directly assessed.

In the case of the PXR, competitive binding assay seemed to confirm published data that describes how F decreases PXR-SRC1 coactivator binding and so, attenuates PXR transcriptional activity. PXR main function is to act as a sensor for toxic chemicals and metabolites and enhance their elimination, subsequently it has no physiological known ligands. As a result, it possesses the largest known binding pocket among NRs, which allows the interaction with a broad spectrum of molecules (including some steroids). Considering the promiscuity of the receptor and its structural singularities, F interaction with PXR may not be related to the inhibition of other NRs. However, it gives a hint of a possible metabolism route for the ABC.

In contrast, in the case of GR, no significant interaction was detected, which suggests that the inhibitory effect seen in previous assays would not be mediated by a competitive interaction with the steroid pocket in the LBD. Apart from this direct biochemical competitive binding assay, other assays were designed to F2low the interaction of some NRs with a coregulator upon exposure to F. In these assays, the recruitment or displacement of a coactivator was detected by TR-FRET. Almost all NR tested before in the transactivation activity assessment were again analyzed. However, F had no effect in the interaction with any coregulator, indicating again that probably it does not act in competition with the ligand. SPR confirmed the interaction between F and GR in the ligand-bound form of the receptor. Despite binding affinity was comparable to that of dexamethasone, no binding to the Apo-receptor was detected. Consequently, it is reasonable to assume that F binds non-competitively to the LBD and only upon agonist presence, probably acting as a modulator. In fact, some protein surface modulators have already been described for the GR, as well as putative interaction channels.

The next step to study F site of interaction and to confirm the previous hypothesis is to obtain the crystal structure of GR in complex with dexamethasone and F. For the moment, different crystals have been obtained for both AR and GR by the Structural Biology of Human

Nuclear Receptors Group at IBUB. However, receptor's copurification with F has not been determined and data from crystals' diffraction is pending evaluation.

After that, we focused on the evaluation of the effect of F on the GR, due to the potential applications of new GR modulators. For instance, GCs are widely used in immunosuppression and anti-inflammation. Initially, F was able to partially block the transcriptional activity of the ligand-bound fusion protein GAL4(DBD)-GR(LBD) transfected to HEK293 cells. It also showed binding to GR LBD in the SPR assay. The interaction was then confirmed with the full-length receptor by transfecting a reporter gene containing the MMTV promoter to HeLa cells. Under the tested conditions, F dose-dependently antagonized the response to GC stimuli. These results suggest that F inhibits the transactivation activity also on native GR, although with lower potency than synthetic compounds. Differences in antagonism efficacy and potency detected with the previous assay can be attributed to different assay sensitivities. For instance, F showed lower efficacy (51% vs 86%) but higher potency (CF of 0.67 vs 2) in the chimeric receptor compared to the MMTV activity assay. The similar slope of the curves could indicate that the ABC may have the same affinity for both receptors, despite possible conformational differences of the LBD between the native receptor and the fusion protein.

The next step was to assess the biological relevance of the detected interaction between F and GR in a native environment. F has been described to have important anti-inflammatory effects that could be attributed to a modulation of NRs and, specifically, to GR regulation. Therefore, we studied the influence of the ABC on the expression and secretion of GR-regulated inflammatory mediators. Contrarily to what had been observed in the past assays, F was not able to antagonize the transcription of the GR-transactivated genes *Gilz* and *Mkp1* on mouse macrophages. Neither did it down-regulate the expression of *Tnfα*, *IL-1β*, *IL-6*, *IL-12*, *Cox-2* and *Nos2* on the same cells, after induction of inflammation with LPS. Despite that, it has been reported that F is able to reduce *Cox-2* expression and *Tnfα*, *IL1β* and *IL6* expression and release in LPS stimulated murine RAW 264.7 macrophages. In those reports, cells were treated for 24h with high concentrations of the ABC (up to 60 μM), which we have found to be toxic (see Chapter 2). Moreover, RAW 264.7 macrophages are an immortalized line, whereas in this case we have worked with primary cultures. Extending incubation times from 2h to 24h would be something to consider in order to confirm the results.

In further analyses, F did not alter IL8 secretion neither after LPS nor after PMA stimulation on human monocytes, although in these assays the incubation times were longer. F did not antagonize dexamethasone inhibition of IL8 secretion either. At high concentrations (10 μM), F caused an increase in levels of the cytokine, which could be due to cell death and release of intracellular IL8. Notably, we had previously detected low levels of GR expression

in THP1 monocytes by western blotting. Since F is thought to be less active than dexamethasone and other synthetic ligands, as seen in the previous assays, it could require higher levels of receptor to exert a significant effect.

The last studied inflammation mediator was TNFα. Its expression and secretion were analyzed both in mouse macrophages and human monocytes after induction with PMA. *Tnfα* transcription is promoted by a complex of TRFs, among which NFκB and AP-1 are found. Since no GRE has been detected in the *Tnfα* gene, it is thought that GCs antagonize its transcription via competition with other TRFs. GILZ is also known to mediate the downregulation of TNFα triggered by GCs. On the other hand, GCs also inhibit TNFα post-transcriptionally: *Tnfα* mRNA is stabilized when cells are stimulated by inflammatory mediators and GCs reverse this effect, resulting in rapid degradation of the messenger. Accordingly, in our assays dexamethasone antagonized the increase in TNFα expression and secretion, without affecting the expression in the absence of inflammatory stimuli. The percentage of inhibition was similar at mRNA and protein levels, although we expected to see an accumulated decrease in the secreted protein. It probably indicated a saturated effect of dexamethasone. On the contrary, F downregulated the secretion of the cytokine, but did not change its transcription rate. It differs again from reported anti-inflammatory activities of F, were a downregulation of both transcription and secretion is described, despite other assays report only an inhibition of secretion. The observed inhibition was consistent in mouse macrophages and human monocytes: it was not dose-dependent but formed a plateau around 35%. Surprisingly, in combination with dexamethasone, it further repressed TNFα secretion, although it is not clear whether the combined effects were additive or slightly antagonic. Since TNFα seemed not to be repressed transcriptionally or post-transcriptionally, F activity would not be comparable either to a GC in terms of GR gene transrepression. Therefore, F would not act as a classical GR ligand, but as a modulator. Another possible level of regulation of TNFα is its proteolytic cleavage. Initially, it is expressed as a transmembrane protein (also active), which is then cleaved by the metalloprotease TNFα-converting-enzyme (TACE) to be secreted. Intracellular and membrane TNFα should hence be measured in assayed cells, to determine if repression takes place at the translational or secretion level. The former downregulation could be attributed to GR non-genomic mechanisms, given that GCs are known to drive rapid anti-inflammatory effects in macrophages. For instance, diverse kinase pathways, such as JNK and p38/SAPK2 or MAPK/ERK, have been reported to be involved in the regulation of *Tnfα* mRNA transport and translation. Those pathways are blocked by GCs in several cell types, affecting TNFα expression and secretion. On the other hand, the modulation of TNFα secretion could imply the regulation of TACE.

Another circumstance that should be further investigated is that anti-inflammatory effects of F are not mediated by GR, particularly considering that affinity of F for the Apo-GR was

found to be very low in comparison with that for the ligand-bound receptor. The modulation of another NR, or several of them, could be involved. For instance, VDR response elements have been detected in the promoter of *Tnfα*. Since VDR dimerizes with RAR or RXR, ligands of those receptors have proven able to down-regulate TNFα in macrophages, although they show a reduction its mRNA content too. TNFα suppression could also be mediated by alternative pathways. We have preliminary results that suggest a possible inhibition of protein kinase C (PKC) by F. This theory is supported by the partial inhibition of the Nuclear factor of activated T-cells (NFAT) by F that we have recently observed, although it still needs validation. Furthermore, F has been reported to regulate intracellular calcium levels. It would explain why better results were obtained with PMA than with LPS stimuli, in spite that dexamethasone also showed higher activity after PMA stimuli. In this way, the anti-inflammatory effect would probably be independent of the observed GR transcriptional antagonism. In combination with dexamethasone, for example, F GR-independent inhibition of TNFα would be observed at low dexamethasone levels. At some interval, it could even antagonize the GC (between 0.2-2 nM in Figure 26). At high GC concentrations (above 2 nM in Figure 26), conversely, dexamethasone effects would be predominant and F would not add extra inhibition. It would particularly be consistent with an inhibition of the secretion of the cytokine: if dexamethasone largely inhibits TNFα expression at high concentrations (above 2 nM in our assays), no inhibition of the secretion is needed.

Lastly, to define the modulatory effect of F on GR, expression arrays could be carried out. Changes in the expression profile upon F incubation in comparison to basal state, as well as upon coincubation with a GR agonist, could help determine if GR-regulated genes are affected and how. Expression studies should also be carried out in GR knock out models or upon F combination with a GR antagonist, to find out whether the observed effects are mediated by the receptor. At present, endogenous tyrosine aminotransferase activity in HepG2 is being measured as an additional GR transactivation indicator.

Although F's effects on GC-regulated inflammation were not clear, we decided to further characterize the interaction of the ABC with GR, by exploring the mechanism by which it antagonized the receptor in the transcription assays. There are many described processes that lead to a decrease of GR activity. One of the most common mechanisms, which was indeed firstly analyzed, is the blockage of nuclear translocation. In the absence of ligand, GR resides in the cytoplasm associated to a chaperone complex. Upon ligand binding, the complex is linked to dynein, which rapidly transports it to the nucleus along microtubules. Active antagonists, such mifepristone, don't interfere in this process but sterically block coactivator recruitment. The result is that GR translocates in an inactive form. On the contrary, passive or competitive GR antagonists minimize receptor translocation so it cannot access DNA and so, reduce transcription regulation. It is the case of steroidal antiandrogen cyproterone acetate and many synthetic compounds. Interaction with other targets can also

affect translocation. For instance, geldanamycin inhibits ATP binding to Hsp90, avoiding the high affinity binding state it creates on GR. Thus, neither ligand binding nor receptor translocation can take place. Dynein or tubulin inhibitors also affect directly GR transport to the nucleus. Other compounds contribute to a reduced glucocorticoid responsiveness by kidnapping or causing abnormalities in other proteins from the GR heterocomplex, such as hsp70, hsp40, Hop, p23, immunophilins, and importins. For instance, expression alterations of the cochaperone Trp2 or immunophilin FKBP52 minimize GR translocation. Lastly, phosphorylation of the receptor modulates its translocation. For instance, phosphorylation at Ser203 and Ser226 indicates the predominant presence of the receptor in the cytoplasm, whereas phosphorylation at Ser211 denotes increased nuclear import. Nevertheless, when we explored the effects of F on receptor translocation to the nucleus, F did not affect GR transport under any tested conditions. Therefore, all possible mechanisms previously suggested could be discarded. Firstly, F did not induce neither inhibit nuclear translocation of GFP-GR in HEK293 cells. To avoid that an altered conformation of the fusion protein had affected the results, nuclear translocation of the native GR in HaCat was assessed. Again, receptor location was not affected by F, neither in the presence or absence of dexamethasone. In contrast, it has been previously reported that F may inhibit Hsp90 function in primary effusion lymphoma cells: while it did not affect the level of Hsp90, it caused the depletion of several Hsp90 client proteins, which was inhibited by a proteasome inhibitor. In this case, similarly to what has been described for geldanamycin, nuclear translocation inhibition should have been observed. Interestingly, maximal receptor translocation was observed to be around 75% of cytoplasmic GR and isoforms α and β seemed to have equivalent dynamics in terms of translocation, contrarily to what has been previously described. As the mobility of GR is cell-dependent and highly dependent of ligand affinity, it could differ from what has been described for other cell types. At present, studies of receptor translocation to mitochondria, a process that has been described in T cells, are being carried out to study how F affects this non-genomic mechanism.

Another of the main factors affecting GR activity that we studied is the modulation of receptor expression and degradation. Although the regulation of GR is extremely complex and it is not completely understood, it is known that its levels are dynamic and cell-type-dependent. In fact, the level of receptor protein determines the scope of the response, and subsequently many ligands induce GR downregulation at both mRNA and protein levels. Accordingly, we observed that upon long-term exposure to dexamethasone, GR was down-regulated, which is described to be a proteasome-dependent process. However, F had no effect alone or in coincubation with dexamethasone on GR levels in HaCat cells. In effect, it could not prevent dexamethasone GR-downregulation. In contrast, it has been described to modulate the expression of other NRs, as PPARα and PPARγ.

Although no changes in GR levels have been detected, it does not necessarily translate into an identical GR activation state, as different PTMs can alter receptor affinity for its ligand or for DNA. As an example, F has been described to inhibit the phosphorylation of ERK, while dexamethasone induces its activity. At the same time, ERK is thought to phosphorylate GR Ser203, which in the nucleus attenuates receptor's transcriptional activity. F could also induce different modifications on the receptor critical for cofactor interactions, such as acetylation or sumoylation. Other PTMS, such as nitrosylation have been related to a reduced binding affinity to ligands and can be indirectly promoted by altering the NO intracellular system. Therefore, it would be relevant to study GR activation state more in-depth upon F incubation, in order to establish the overall effect of the ABC. A first approach could be based on determining phosphorylation at Ser211, which is a known marker of receptor activation.

Another described mechanism of GR inhibition is to induce glucocorticoid resistance. Although F has been shown to modulate GR activity *in vitro* after short time incubations, as well as to directly interact with the receptor, it is still possible that it acts by multiple mechanisms and should be considered in further studies. For example, the pattern of GR isoforms expression can alter its activity. GRβ, apart from having intrinsic transcriptional activity, has been described to function as an inhibitor of GRα. Despite that the mechanism remains unclear, current hypothesis include competition for GRE binding, for coregulators or the formation of inactive GRα/GRβ heterodimers. GRγ also presents lower activity than GRα. In addition to isoforms generated by splicing, many isoforms with different activity profiles can be generated by alternative translation initiation. Even though it would not be the main mechanism of GR activity modulation, the alteration of the expression pattern cannot be dismissed. Nevertheless, it is difficult to study, as it is time and cell-dependent and the function of each isoforms is still not well-defined. In the same way, GR activity can be decreased by upregulation of other TRFs that interact with it. It would be the case of AP-1 or NF -KB, whose activation should also be assessed. Yet another interesting approach would be to measure the intracellular level of glucocorticoids. Insufficient levels can lead to the denominated multidrug resistance (MDR), which has been proposed to be a cause of glucocorticoid resistance in inflammatory diseases. In particular, the drug efflux pump P-glycoprotein or MDR1, a member of the ATP-binding cassette transporters, is known to pump glucocorticoids out of the intracellular space. The increased efflux of steroids is then the origin of insufficient ligand availability for GR. Interestingly, ABCs have been linked to the inhibition and downregulation of these transporters. In fact, they are substrates for MDR1 and so have been proposed to function as chemosensitizers. However, this event would cause an intracellular raise in glucocorticoid concentration and an increased response, contrarily to what we have observed.

Taking everything into consideration, F did not antagonize GR transactivation via translocation inhibition or changes in intracellular receptor level. As it seems to bind only to ligand-bound receptor in a non-competitive way, it probably acts as a negative coregulator. Whether it induces PTMs or simply performs an allosteric modulation of the receptor is not clear. In the latter case, F could induce changes in the exposure of protein surfaces that facilitate the assembly of repressive regulatory complexes or that reduce the receptor coactivator recruitment potential. Remarkably, there are experimental evidences that indicate that F inhibits the interaction between PXR and its co-activator SRC1, which is shared with other NRs as GR and possesses intrinsic histone acetyltransferase activity. Accordingly, other reports maintain that ER inhibition by Compound Y and Compound B is not affected by an overexpression of SRC coactivators. By inhibiting coactivator binding, ABCs would reduce NR transactivation, but not impede translocation. This might be mediated a conformational change in the receptor that would not allow further interaction with SRC, even if its overexpressed. However, when we studied SRC1-GR interaction by a TR-FRET assay no inhibition was observed. It is possible that this inhibition is restricted to some NRs. Considering the low aqueous solubility of the ABC, it would be interesting to perform the FRET assay in a cell environment by co-transfecting both proteins to confirm the results. Aside from obstructing receptor interaction with cofactors, F could also hinder GR oligomerization. Although the main known dimerization domain is situated in the DBD, conformational changes in the LBD caused by coregulators can affect dimer formation and so, avoid dimer-driven transcription. Putative dimerization surfaces among the LBD are also under study. Interestingly, the inhibition of dimerization prevents GR binding to tandem GREs, but does not avoid transrepression and GR monomeric activity, including some non-genomic mechanisms. Hence, it would be interesting to study the effect of the ABC binding on receptor dynamics. Firstly, crystallography will allow to evaluate if F interacts with the mentioned dimerization domains. If the region of interaction is identified, mutations within it could also be useful to define which effects of F are mediated by GR. Secondly, the expression profile of GR dimerization-defective mutants could be compared to the profile induced by F upon the wild type GR. Dimerization can also be studied using mutants in the NL1. These modified receptors can be cotransfected with the wild type GR to evaluate nuclear translocation, as it only takes place in case of dimerization. Co-immunoprecipitation or FRET assays could also be convenient to assess changes in GR interaction with other TRFs. Interaction between F and membrane-bound GRs could also be assessed by this method. However, to date we have not been able to tag F. Finally, chromatin immunoprecipitation would be useful in evaluating alterations in the affinity of the receptor for DNA and define changes in binding regions.

In conclusion, we have shown that F antagonizes *in vitro* the transcriptional activity of the GR, probably acting as a negative coregulator that preferentially binds to ligand-bound GR. However, as anti-inflammatory it seems either to not act through the classical GR pathway or to preferentially act through other mechanisms of action. Nevertheless, interaction with GR could be responsible of, at least, some of the bioactivities that have been already described for this ABC. Furthermore, other interesting compounds with that characteristics have been also identified. F3, a F metabolite, presents higher potency and efficacy in receptor antagonism, as well as interesting antagonism on the AR. Compound N, on the other side, possesses higher selectivity for GR in front of PR. Interaction with GR and AR have been studied more in depth, although further characterization is needed. Antagonism of other receptors, such as ERs, has just been initially assessed but would be of high interest for biomedical applications.

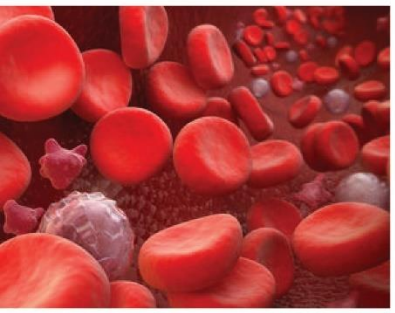

CHAPTER 2

EVALUATION OF COMPOUND F ACTIVITY ON CELL MODELS OF HEMATOLOGIC MALIGNANCIES

Introduction

Materials and methods

Results

Discussion

INTRODUCTION

HEMATOLOGIC MALIGNANCIES

Hematologic malignancies (HMs) are a wide group of highly variable cancers derived from the blood, bone marrow and lymphatic system (147). They are especially prevalent in children, where they are the most common form of childhood cancer (147).

Classification

HMs can be subdivided in three main groups and several subtypes, based on the origin of the disease and cell types involved (Figure 33) (147). HMs involve the dysregulation of multiple signaling pathways and several recurrent genetic abnormalities have been identified among the different types (148).

Hematopoietic stem cells originate all cell blood types in the process of hematopoiesis. In a first step, they differentiate in the bone marrow into myeloid or lymphoid progenitor cells (Figure 32). Cancers that derive from both lineages of bone marrow cells are known as leukemia, the first main group of HMs (Figure 33). Four subtypes of leukemia have been described depending on the cell type affected and its degree of differentiation: [1] acute lymphoblastic leukemia (ALL), [2] acute myeloid leukemia (AML), [3] chronic lymphoid leukemia (CLL) and [4] chronic myeloid leukemia (CML) (147,149). Acute malignancies involve highly undifferentiated cells and tend to be more aggressive, while chronic disorders originate from the dysregulation of mature cells. In lymphoid leukemias, lymphoid precursors suffer abnormal proliferation and differentiation, instead of originating B and T lymphocytes and natural killer cells (Figure 32). ALL is the most common leukemia among children and affects bone marrow, blood and extramedullary sites. It has been described that 85% of ALL arise from the B cell lineage (150). CLL the commonest leukemia in western countries and typically occurs in elderly patients. It is characterized by the accumulation of monoclonal CD5 positive B cells in blood, bone marrow and lymphocytic tissue (151,152). On the other hand, myeloid leukemias are characterized by the abnormal proliferation and differentiation of a clonal population of myeloid progenitors, which normally would differentiate into granulocytes, monocytes, mast cells, erythrocytes and thrombocytes (Figure 32). In AML, abnormal myeloid blasts are found in the bone marrow, peripheral blood and can infiltrate other organs. It is a highly heterogeneous disease and is the most common leukemia in adults (153,154). *Per contra*, CML involves a disorder in clonal haemopoietic stem cells. Abnormal myeloid cells can be found in the bone marrow, blood and spleen. Its incidence, mainly among adults, is lower than AML and has a better

prognosis. Almost all CML cases are characterized by a translocation between the long arms of chromosomes 9 and 22, which results in the juxtaposition of the human analogue of the Abelson murine leukemia viral oncogene homolog 1 (Abl1) oncogene from chromosome 9 with the Breakpoint cluster region protein (Bcr) housekeeping gene on chromosome 22, also called Philadelphia translocation (155). Abl1 encodes a tyrosine kinase that regulates cell proliferation, loss of stromal adhesion, and resistance to apoptosis (147). The resulting fusion protein BCR-ABL1 leads to uncontrolled signaling and the apparition of CML (155). Importantly, it can be used both as a biomarker for diagnosis and a drug target in disease treatment.

The second main group of HMs are lymphomas, which involve aberrations in the proliferation of mature lymphoid cells in the lymph nodes, mainly of B cells (Figure 33). Hodgkin's lymphoma (HL) is an uncommon B-cell lymphoid malignancy typical of either early or late adulthood. It is characterized by the presence of giant cells (Hodgkin and Reed-Sternberg cells) in spleen and lymph nodes (156). Other lymphomas, known as non-Hodgkin lymphomas (NHL), include follicular lymphoma (FL) and diffuse large B cell lymphoma (DLBCL). This wide spectrum of illnesses arises from lymphocytes at various stages of development. FL is the second most frequent non-Hodgkin lymphoma, occurring also mostly in late adulthood. In this case, germinal center B cells infiltrate into several lymph nodes, typically cervical, axillary, inguinal and femoral nodes; but bone marrow can also be involved (157). DLBCL is the most common lymphoma in adults, although it affects a broad age range, and it is biologically and clinically heterogeneous. It is characterized by large B cells with vesicular nuclei, prominent nucleoli, basophilic cytoplasm and a usually high proliferation rate that can be found in nodal or extra nodal sites (158).

The third group of HMs is multiple myeloma (MM) (Figure 33). Its incidence is mainly among elderly patients, being rare under the age of 40 years. It consists on a malignant proliferation of a single clone of plasma cells that results in monoclonal immunoglobulin production, probably due to an abnormal plasma cell response to antigenic stimulation. Those cells infiltrate both in bone marrow and extramedullary sites (159).

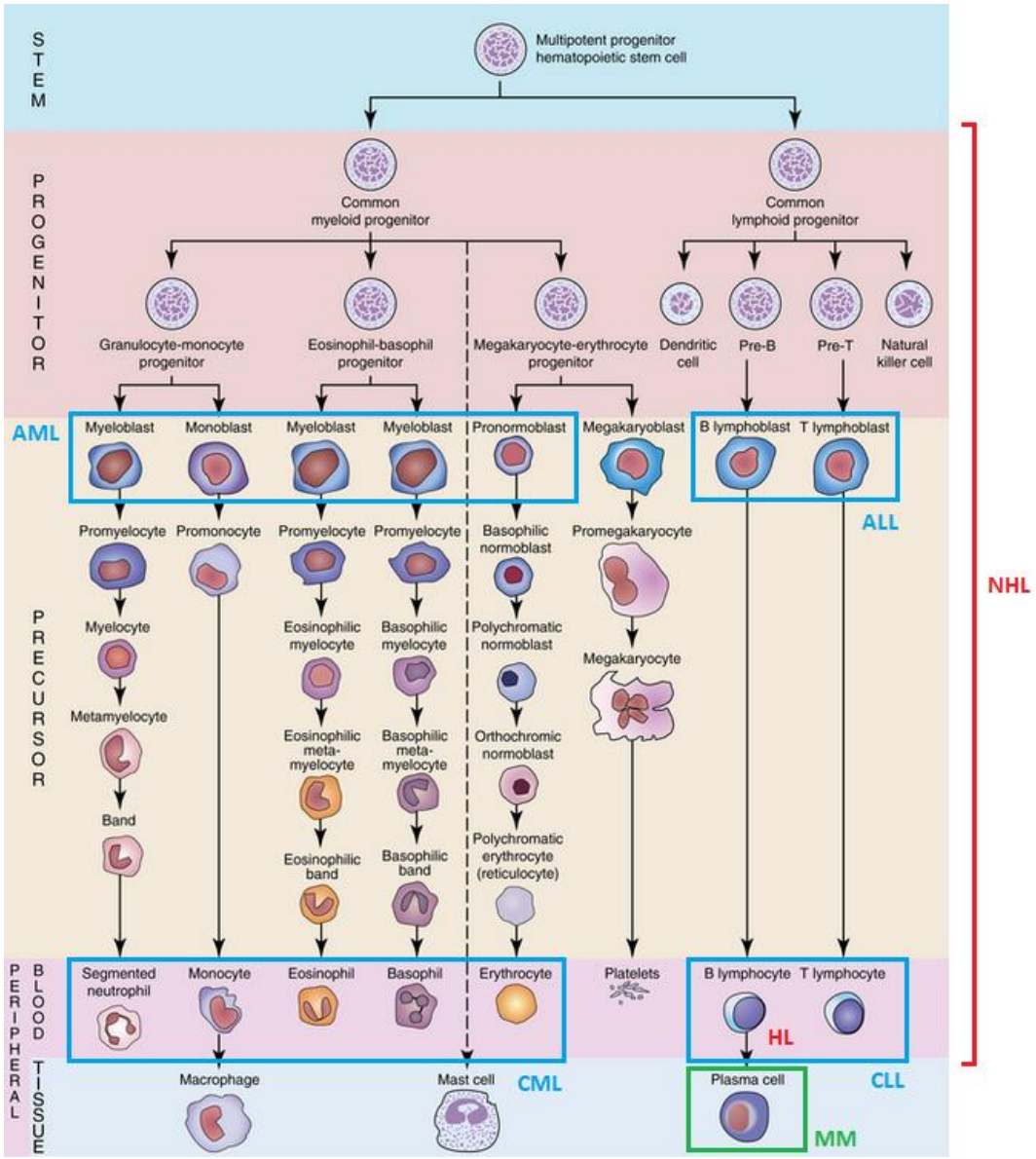

Figure 32. Overview of hematopoiesis and cell types affected by HMs. *A pluripotential hematopoietic stem cell differentiates into a common myeloid or common lymphoid progenitor in response to cytokine signaling. The lymphoid progenitor further proliferates and differentiates into T, B or natural killer cells. The myeloid progenitor proliferates and differentiates into granulocyte, monocyte, erythrocyte, and megakaryocyte lineages. Those different lineages are affected by different types of HMs. Acute leukemia derives from the proliferation of undifferentiated myeloblasts (AML) or lymphoblasts (ALL), whereas chronic leukemia affects mature granulocytes (CML) or lymphocytes (CLL). Lymphomas generally derive from B lymphocytes at various stages of development. In multiple myeloma, the clonal proliferation of plasma cells takes place. Modified from* (160).

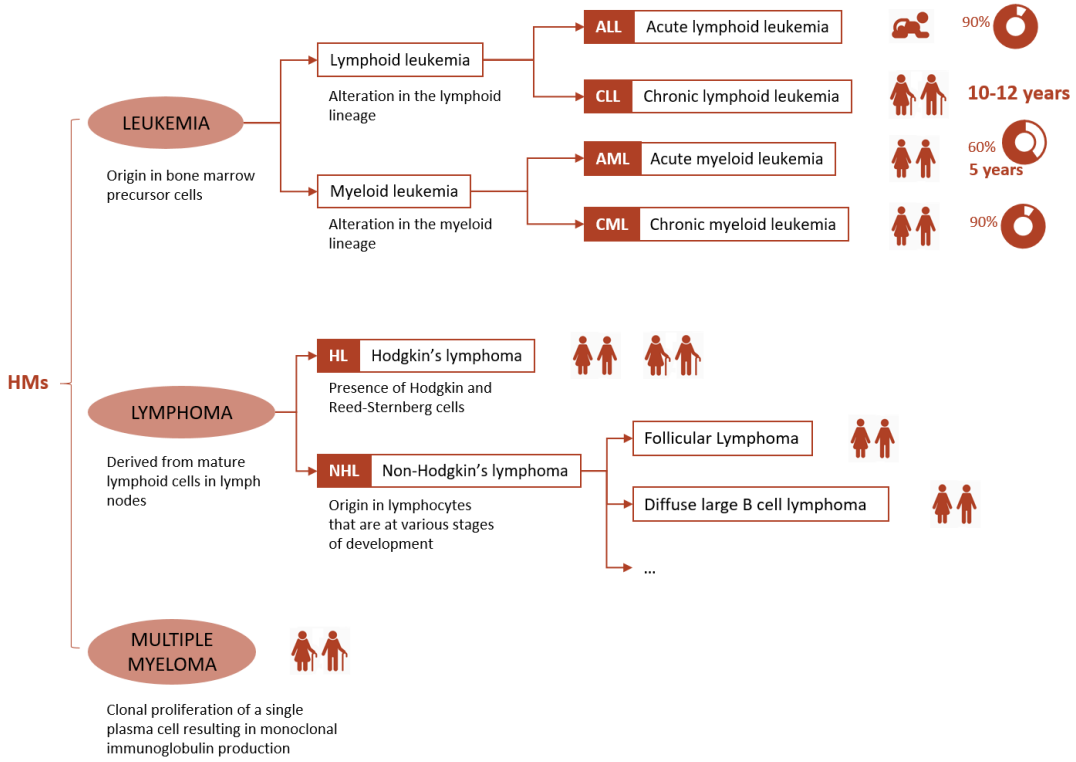

Figure 33. General classification of HMs based on the origin of the disease and cell types involved. Pictograms denote the incidence and survival rates of each disease when available, as published by (161) .

Current drugs and treatments

As HMs are a collection of highly variable disorders, treatments are also specific of the type and stage of the disease. Apart from that, HMs affect multiple tissues: bone marrow, lymph nodes, spleen, peripheral blood and even the liver (147). It is highly challenging for a drug to be effective in multiple tissues, and subsequently it is common to combine different treatments. Most common treatment strategies are bone marrow transplantation, chemotherapy and radiotherapy (147,162,163).

Bone marrow cell transplantation offers durable remissions of the disease but requires a previous destruction of the patient's hematopoietic system by cytotoxic drugs or radiation (147,163). Autologous stem cells transplantations are based on the re-infusion of the patient's healthy stem cells, previously collected. In contrast, in allogeneic stem cell transplantations, transplanted cells derive from a matched healthy donor. These treatments are associated with risks of relapse or graft-versus-host disease apparition, respectively (163).

Radiotherapy consists on the administration of ionized radiation to the region of the malignant neoplasm, with the consequent trigger of DNA damage to cells. It has limited application due to the diffuse distribution of abnormal cells in HMs. It also causes damage to the surrounding healthy tissue (162).

There are multiple chemotherapy treatments available for hematologic disorders, including cytotoxic drugs and immunomodulators. A summary of current drugs can be found in Table 20. They are often applied in combination or together with radiation. Thanks to the increasing information available on the regulatory mechanisms and pathways of hematologic cells, targeted approaches can be developed, such as deacetylase inhibitors, proteasome inhibitors or tyrosine kinase inhibitors. For instance, imatinib was the first kinase inhibitor used. It targets ABL1 and represented a great improvement in the treatment of CML (147). Nowadays, a third generation of kinase inhibitors is available, and some even target multiple kinases (164,165). Apart from kinase inhibitors, current efforts are centered also on inhibitors of the B cell receptor signaling and regulators of apoptosis (147,166). Hematopoietic cells possess a stringent control of apoptosis due to their high turnover (149). In most malignancies it is dysregulated, resulting in uncontrolled proliferation and accumulation. In addition, resistance to apoptosis is a common cause of treatment failure. Therefore, pro-apoptotic and anti-apoptotic proteins are being studied as potential targets. Bcl-2 and surviving are among those factors (147).

Immunotherapy has recently raised as a common treatment option for HMs (167). It has been reflected in this year's Nobel Prize in Physiology or Medicine, awarded to James P. Allison and Tasuku Honjo. The latter, described how the blockage of Programmed cell death 1 (PD-1) antigen in the surface of T cells promoted T-cell activation and proliferation, leading to the elimination of tumorous cells (168). PD-1, which is upregulated in many tumors, has been shown to act as a mechanism of immune evasion. Nivolumab and Pembrolizumab target PD-1 and have been approved for the treatment of HL, among other cancers (169). Other active immunotherapy strategies have also been tested. They intend to stimulate the patient's immune system to produce an antitumor effect, resulting in a long-lasting response (170). Bispecific antibodies, either conjugated to drugs or that only establish a physical connection between two epitopes are an example. Blinatumomab activates T cells by bringing them closer to B malignant cells and is approved for the treatment of ALL (171). Chimeric antigen receptor (CAR) T-cell therapy is also based on the usage of antibodies. In this case, T cells isolated from a patient are modified to recognize the target tumor cells via CAR and then reinfused into the patient (172). The delivery of therapeutic compounds by CAR T-cells is also being evaluated. On the other side, passive immunotherapy strategies have also been developed. They consist on the direct administration of cytokines, antibodies or immune cells to the patient to initiate an antitumor action (170). Most extended strategies involve monoclonal antibodies designed to recognize specific antigens in the

surface of the malignant cell population. After binding, abnormal cells are killed by direct cytotoxic effects, complement mediated lysis or antibody dependent cytolytic effects by NK cells (147). The first approved antibody was rituximab, which binds to the antigen CD20 (173). Similar antibodies with higher efficacies have been developed since then (174). Other antibodies are been used with the same target for the delivery of cytotoxic agents or radioisotopes, such as ibritumomab (175). Other antibodies have been targeted to VEGF or VEGF receptor with the aim of angiogenesis inhibition (176).

Table 20. Current available treatments for hematologic malignancies. *Classification is based on their primary mechanism of action. Obtained from* (147).

Category	Drug	Indication
Antitumor antibiotics	Bleomycin	HL, NHL
	Daunorubicin	AML, ALL
	Doxorubicin	AML, ALL, HL, NHL
	Idarubicin	AML
	Mitoxantrone	AML, NHL
	Azacitidine	CML
Antimetabolites	Cladribine	CLL
	Clofarabine	AML, ALL
	Cytarabine	AML, ALL, HL, NHL
	Decitabine	AML
	Fludarabine	CLL, NHL
	Hydroxyurea	CML
	Mercaptopurine	ALL
	Methotrexate	AML, ALL, CLL, CML, HL, NHL
	Pralatrexate	NHL
	Thioguanine	AML, ALL, CML
Biphosphonates*	Pamidronate	MM
	Zoledronic acid	MM
Cell-maturing agents	Arsenic trioxide	AML
	Tretinoin	AML
DNA-damaging drugs	Bendamustin	CLL, HL, NHL
	Busulfan	AML, ALL, CLL, CML, HL, NHL
	Carboplatin	HL, NHL
	Carmustine	MM, HL, NHL

	Chlorambucil	CML, NHL
	Cisplatin	AML, ALL, CLL, CML, HL, NHL
	Cyclophosphamide	AML, ALL, CLL, CML, HL, NHL
	Dacarbazine	HL
	Ifosfamide	HL, NHL
	Lomustine	HL
	Mechlorethamine	CLL, CML
	Melphalan	MM
	Nelabrine	ALL, NHL
	Procarbazine	HL
DNA-repair enzyme inhibitors	Etoposide	AML, ALL, CLL, CML, HL, NHL
	Teniposide	ALL
GCs	Dexamethasone	MM
	Methylpresinolone	ALL
	Prednisone	ALL, HL, NHL, MM
Histone deacetylase inhibitors	Belinostat	NHL
	Panabinostat	MM
	Romidepsin	NHL
	Vorinostat	NHL
Immune Modulators	Lenalidomide	MM
	Pomalidomide	MM
	Thalidomide	MM
Mitotic inhibitors	Paclitaxel	ALL
	Vinblastine	HL
	Vincristine	ALL, HL, NHL
Monoclonal antibodies	Alemtuzumab	CLL, NDL
	Blinatumomab	ALL
	Brentuximab vedotin	HL, NHL
	Daratumumab	MM
	Gemtuzumab ozogamicin	AML
	Ibritumomab	NHL
	Obinutuzumab	CLL
	Ofatumumab	CLL
	Rituximab	AML, ALL, CLL, CML, HL, NHL
	Tositumomab	FNHL
Phosphoinositide 3-kinase inhibitors	Idelalisib	CLL, NHL

Proteasome inhibitors	Bortezomib	MM, NHL
	Carfilzomib	MM
	Ixaomib	MM
Tyrosine kinase inhibitors	Bosutinib	CML
	Dasatinib	ALL, CML
	Ibrutinib	CLL
	Imatinib mesylate	ALL, CML
	Nilotinib	CML
	Omacetaxine mepesuccinate	CML
	Ponatinib	CML

ALL, acute lymphoid leukemia; AML, acute myeloid leukemia; CLL, chronic lymphoid leukemia; CML, chronic myeloid leukemia; FNHL, follicular non-Hodgkin lymphoma; HL, Hodgkin's lymphoma; MM, multiple myeloma.
**Biphosphonates are used as supportive care.*

Most mentioned current drugs to treat HMs are characterized by a lack of specificity and short biological half-life, which translates into the need of high and frequent doses. Consequently, they present multiple off-target adverse effects. Novel drug delivery systems of existing drugs are necessary to reduce their adverse effects and to increase their half-lives (147). The development of nanoformulations for the treatment of HMs has experimented a recent outbreak (147). Those formulations tend to accumulate at inflammation sites, which display a phenotype of increased angiogenesis and infiltration of immune cells. Interestingly, they also accumulate in organs of the mononuclear phagocytic systems, such as live, spleen and bone marrow; which are the main targets for the treatment of HMs (147).

Currently, four liposomal formulations are approved for clinical use. They consist on vesicles of one or more phospholipid bilayers, which include different cytotoxic agents: doxorubicin, daunorubicin, vincristine or a combination of cytarabine and daunorubicin (177–180). Many more liposomal formulations are under clinical trials (147). Notably, a liposomal encapsulation of dexamethasone is in phase I/IIa for the treatment of MM (181). Pegylated polymeric nanoparticles (NPs) of dexamethasone are also in pre-clinical stages for ALL treatment (182).

Other polymer-based nanomedicines are also under development (147). Among those, protein NPs stand out, which consist on polymeric protein delivery nanosystems between 1 and 100 nm in size. In the case of HMs, it is interesting that they do not exceed 60 nm, as it

is the size of pores in the blood capillaries that lead to the bone marrow. Hence, smaller particles can penetrate and distribute into bone marrow interstitial space, which also tends to attract nanoformulations due to its inflammatory phenotype in HMs (183,184). Moreover, smaller particle sizes contribute to an increased circulation time and a reduced interaction with plasma proteins. Negatively charged particles and liposomes also contribute to improved delivery and accumulation in the bone marrow (185). At present, two albumin-based NPs containing cytotoxic drugs are under clinical trials: Abraxane® and ABI-011. Abraxane® is a albumin-paclitaxel conjugate, an antimitotic agent that prevents cell division by stabilizing microtubules. It is in phase II for the treatment of lymphomas and MM (186,187). ABI-011 consists on albumin NPs loaded with a thiocolchicine dimer that displays both tubulin and topoisomerase I inhibitory activities. It completed phase I for the treatment of lymphomas (188).

NR ligands in the treatment of HMs

Many NRs regulate cell differentiation, proliferation and death (1,5). Therefore, their ligands and regulators could play an important role in the treatment of several cancers (1,189). In the specific case of hematologic malignancies, GCs and all-trans retinoic acid (ATRA) are first-line drugs in determinate malignancies (190,191). Other ligands are also being studied.

GCs have long been used in the treatment of hematopoietic malignancies of the lymphoid lineage, as they induce cell apoptosis in lymphoid cells (191–193). Although the signaling pathways have not been completely characterized, they are known to transactivate pro-apoptotic genes as Bim and down-regulate survival cytokines via transrepression of AP-1 and NF-κB-mediated transcription (191,192). GCs are used in the treatment of ALL, CLL, MM, HL and NHL, sometimes as adjuvant therapy to chemotherapy (147).

Acute promyelocytic leukemia (APL) is a subtype of AML characterized by a reciprocal translocation involving RARα. In 95% of the cases, the RARα gene in chromosome 17 is translocated with the promyelocytic leukemia gene (PML) on chromosome 15 t(15;17)(q24;q21). The dysregulation of this NR results in enhanced transcription blockage in granulocytes, which accumulate as immature cells called promyelocytes (Figure 32). Treatment with ATRA induces terminal differentiation of leukemic promyelocytes into mature granulocytes, which can lead to complete remission of the disease. Nowadays it is administered in combination with arsenic trioxide (190).

PPARγ is another NR investigated in cancer, as it modulates gene networks involved in cell growth, differentiation and apoptosis. In fact, higher PPARγ expression has been observed in AML and some of its ligands have been shown to inhibit growth of malignant cells (194–

199). Differentiation therapy, similarly to what is done in PML with ATRA, has also been tested (200).

VDR has also been found to be overexpressed in CLL and HL, but not in Burkitt's lymphoma (201–203). Calcitriol, the active form of vitamin D, bind to VDR, which heterodimerizes with RXR. It has been described to inhibit proliferation, induce apoptosis, decrease angiogenesis and sensitize cells to chemotherapy. In fact, calcitriol and its analogs have been explored in Phase I and Phase II clinical trials for multiple cancers (204). In hematologic disorders, vitamin D has been shown to induce differentiation and inhibit proliferation in AML cells, as well as inhibit growth of malignant B cell progenitors from ALL (201,202,205–207).

The NR4A subfamily of NRs includes 3 orphan receptors: Nerve Growth factor IB (NGFIB), NR related 1 (NURR1) and Neuron-derived orphan receptor 1 (NOR1). They have been proposed to function ligand-independently, but also diverse synthetic molecules have been described to interact with different regions of NR4A (208–210). Besides, NR4A1 and NR4A2 can also function as heterodimers with RXR (209). In spite of not having a described endogenous ligand, they have proved to be regulators of hematopoiesis, including hematopoietic stem cell maintenance, T lymphocyte development and function and monocyte and macrophage maturation and inflammation (210). They also function as tumor suppressors of both myeloid and lymphoid malignancies (211–213). Therefore, their regulation could lead to the development of new treatment strategies for hematologic malignancies.

Furthermore, the dysregulation of many NR corepressor complexes has been related to cancer (214–218). Targeting corepressors in a context-specific manner has become a new research approach. It is the case of NR corepressor (NCoR) and silencing mediator for retinoid and thyroid hormone receptors (SMRT). In mentioned PML, those factors are the responsible of the enhanced transrepression of RARα: they exhibit a higher binding affinity for the receptor and are not released by physiological doses of ATRA (214,215). The disruption of corepressor interaction restores RARα sensitivity (216). The family of ETO proteins are other studied corepressors (217). They bind to the NCoR/SMRT complexes and also promote transcription repression. There is a subtype of AML caused by a t(8;21) translocation that originates a AML1-ETO fusion protein. AML1 is a hematopoietic TRF that upon fusion with ETO recruits NCoR/SMRT, leading to gene silencing and promoting leukemia (217,218).

COMPOUND F EFFECTS ON HMs

F and its metabolites have been studied as potential treatments for several cancers, including HMs. In fact, intakes of different ABCs have been associated with a significant reduced risk of NHL.

Formulation of Compound F for *in vivo* administration

F is a quite nonpolar molecule, resulting in a very low solubility in water. Nevertheless, it is soluble in organic solvents and oils, such as ethanol or soybean oil. This property limits the formulation of F, as well as the administration route. Most of the *in vivo* assays that have been carried out with F have delivered the compound orally and solubilized in lipoid vehicles. Although the presence of fatty acids has been shown to increase F absorption, its bioavailability is still very low. When ingested, F oral absorption is minimal, as it is supposedly metabolized to F2 by intestinal or pancreatic cells, which is later converted to F3 in the liver. While it is true that these metabolites have shown similar beneficial properties to F, it is also interesting to increase F solubility, which influences drug effectiveness and stability independently of the administration route. At the same time, to date F has proven to be safe and non-toxic in *in vivo* administration. With the aim of enabling the usage of F as a nutraceutical or pharmaceutical product, several formulations have been developed.

Many lipid-based formulations have been studied for ABC delivery, mostly for oral administration. The first non-lipid formulations studied were cyclodextrin inclusion complexes, where the hydrophobic ABCs are incorporated inside the ring structure of cyclodextrins. The association of ABCs with sugars has been shown to decrease their lipophilicity, therefore increasing their aqueous solubility. These preparations are obtained by simple addition and mixing and display an improved absorption. However, ABC concentrations in solution are very low and require the administration of extremely high volumes. Nanodispersions, obtained by solvent diffusion process, have also been tested. They consist on colloidal dispersions of single particles in the presence of surfactants or polymers.

ABCs have also been encapsulated in different polymers. Firstly, they have been included in nanogels. In this case, inert materials (chitosan, sodium tripolyphosphate and glycolipids) protect and isolate the compound from the environment. Several methodologies have been developed to produce these formulations. Interestingly, they are in the nano-range scale and can be manipulated for controlled delivery. At last, encapsulation of ABCs in protein matrixes has been evaluated. The association of ABCs with proteins, as well as with sugar, enhances their aqueous solubility. Interestingly, current pharmaceutical compositions used for cancer treatment are albumin-based, as Abraxane® (187,219).

Among all mentioned formulations, none displays a preparation technique that combines low complexity, low costs and low energy consumption, which hinders commercial production feasibility. Although some of them have shown bioavailability and stability enhancements, most technologies are on an early research state.

MATERIALS AND METHODS

EXTRACTION AND PURIFICATION OF ABCs

F was extracted and purified following proprietary methods to >95% purity by NMR analysis and >99% purity by HPLC (450 nm). F3 and F2 were chemically derived from F following proprietary methods to a final purity above 97% by HPLC-PDA.

IN VITRO ASSAYS

Cell viability assay: IC50 determinations

Cell viability was determined by an MTT assay. It is based on the reduction of MTT (3-(4,5-Dimethylthiazol-2-yl)-2,5-Diphenyltetrazolium Bromide), to formazan crystals by mitochondrial succinate dehydrogenase. This enzyme is only active in living cells, which enables to quantify them and, therefore, determine the toxicity of added compounds.

Multiple HM cell lines were evaluated upon the addition of F and other compounds (Table 23). In all cases, 10000 cells per well were seeded in 100 µL of medium in 96-well plates. After 24 hours, compounds diluted in 100 µL of medium were added to appropriate wells. Seriated dilutions of the compounds were performed to allow IC50 determination. Controls of 0% and 100% viability were included by adding 2.5% Triton-X100 or the vehicle alone (DMSO), respectively. After 72h, medium was replaced by PBS with 0.5 mg/mL MTT, which was kept for 3h. Then, cells were lysed for 1h at 37ºC with an aqueous extraction buffer containing 50% dimethylformamide and 15% SDS. Plate was read at 570 nm in a Multiskan Ascent spectrophotometer (Thermo).

After subtracting background (0% viability control) to all values, and considering the vehicle control as the maximum viability, compound potency was determined by GraphPad Prism 7 software. Briefly, data was normalized and modelled to a four-parameter dose-response curve with variable slope, as seen in Equation 11. Potency is expressed in terms of relative IC50: concentration of compound giving half the maximal toxicity observed.

Equation 11

$$y = A + \frac{B-A}{1+\left(\frac{C}{x}\right)^{d}}$$

$\mathbf{A}$ is the minimum inhibition value (bottom plateau); $\mathbf{B}$ is the maximum inhibition value (top plateau); $\mathbf{C}$ is the determined IC50 for the compound; and $\mathbf{D}$ is the slope factor. The IC50 value corresponds to the relative IC50, i.e. the concentration of compound giving half the maximal inhibition observed.

In combination analysis, the Chou-Talalay method was used to calculate the combination index (CI), as seen in the following equation:

Equation 12 $$CI = \frac{[A]}{IC50\ A} + \frac{IC50\ (A+B)}{IC50\ B} \quad (220)$$

A and B are the tested compounds, first tested separately and then in combination, where A is added at a constant concentration.

Apoptosis, cytotoxicity and viability assay

Viability, cytotoxicity and apoptosis were assayed in MV-4-11 cell line with the commercial kit ApoTox-Glo™ Triplex Assay (G6320, Promega). It measures the activity of two proteases and caspase 3/7 activity. The first protease is a marker of cell viability, as it only functional in viable cells. The kit contains a peptide, fluorogenic and cell-permeant substrate (glycyl-phenylalanyl- aminofluorocoumarin; GF-AFC) that enters to intact cells, where it is cleaved by the mentioned protease. Peptide cleavage generates a fluorescent signal proportional to the amount of living cells. The second measured protease is a marker of cytotoxicity. In this case, the kit contains a peptide, fluorogenic and cell-impermeant substrate (bis-alanylalanyl-phenylalanyl-rhodamine 110; bis-AAF-R110). This protease is released from cells upon the loss of membrane integrity, where it cleaves this substrate. Products AFC and R110 can be detected simultaneously without spectra interference. At last, the kit contains a luminogenic caspase-3/7 substrate contained in a specific reagent for caspase activity, luciferase activity and cell lysis. Cell cultures can be lysed by adding this reagent and, at the same time, caspase activity is measured by the cleavage of the substrate, which gives a luminescent signal.

Briefly, 104 MV-4-11 cells per well were seeded per condition in 96-well plates. Twenty-four hours later, increasing concentrations of F were added to appropriate wells. Staurosporine was added to positive control wells. Cells were incubated for 6, 24, 48, 72, 96 and 120h with F and 6h with staurosporine. After that, 20 µL of Viability/Cytotoxicity Reagent were added and incubated for 30 minutes at 37°C. Then, plate was read in a fluorescent plate reader (Cytation 5, BioTek) at 400/505 nm (viability) and 485/520 nm (cytotoxicity). After data acquirement 100µL of Caspase-Glo® 3/7 reagent were added to each well and the plate was incubated again for 30 minutes at 37°C. Finally, plate was read in a luminescence reader (Cytation 5, BioTek).

After background subtraction, data was normalized by the highest mean in each data set. Untreated cells were considered as maximal viability.

Cell cycle analysis by flow cytometry

To study the effect of F on monocytes' cell cycle, $5x10^4$ THP-1 cells were seeded in 6-well plates and incubated for 24, 48 or 72h hours in the presence or absence of 1.3 µM of F. Cells were then harvested, washed twice in flow cytometry buffer (PBS, 1% BSA, 0.1% NaN3) and stained with propidium iodide. Data was acquired on a FACS Gallios (Beckman Coulter) and analyzed with FlowJo software. Percentages of cells in the G0/G1, S and G2/M phases were determined. DAPI was used to select viable cells.

COMPOUND F FORMULATION IN ALBUMIN NANOPARTICLES

Nanoparticles preparation

To prepare albumin-ABC NPs, the desolvation method described by Zhou et al. was adapted (221). Different amounts of BSA (A1933, Sigma) or HSA (A3782, Sigma) were dissolved in 1 volume unit of deionized water to get solutions at 1, 2.5, 5, 10 and 20 mg/mL. At the same time, F was dissolved in ethanol at 1 mg per ¼ volume units by sonication. For the preparation of control NPs, ethanol alone and 5mg/mL BSA were used. The ABC solution was added dropwise and slowly to the protein solution, under nitrogen atmosphere, while stirring at 1500 rpm on a magnetic stirrer. The resulting solution was stirred at room temperature for 10 additional minutes. Afterwards, ethanol was completely removed from the NP solution, either in a speed vacuum or in a rotary evaporator. The solution was concentrated 4.25 times to a final theoretical F concentration of 5 mM. Finally, the NP solution was filtered through a 0.22 µm PES membrane filter and immediately stored in the dark at 4ºC, -20ºC or at room temperature (20-25ºC). Some samples were freeze-dried or vacuum-dried and stored at -20˚C. All NPs were stored protected from light. The preparation protocol was successfully scaled-up to 10 mL of final volume.

Nanoparticle analysis and characterization

Compound F quantification

F concentration was determined by HPLC-PDA (1100 series Agilent Technologies, Waldbronn, Germany). NPs in solution were diluted 1/20 in acetone and stirred on an orbital shaker at 200 rpm for 5 min, after which tubes were centrifuged 3 min at 13000 rpm. Supernatant was recovered by decantation and used for HPLC analysis. Freeze-dried samples were resuspended in the original volume with deionized water before applying the previous protocol. Separations were performed by a proprietary method.

Stability of the ABC in the nanoparticles was also assessed by HPLC analysis. Measures from 4 different batches were taken periodically for up to 4 months after preparation.

Dynamic light scattering analysis

Particle size distribution and Z-potential were measured by dynamic light scattering (DLS) at the Smart NanoBioDevices Research Group of IBEC. Nanoparticle samples were diluted 1/10 or 1/20 in H_2O-mQ and measured using a Möbiuζ, equipment (Wyatt Technologies) and a Möbiuζ Dip Cell (Wyatt Technologies).

IN VIVO EXPERIMENTATION

Animal experimentation was performed in collaboration with the Biomed division of Leitat Technological Center.

Animal models

In vivo assays were performed with immunocompetent mice from the strain Hsd:ICR (CD-1) (females, 6-7 weeks old from ENVIGO), selected on the extensive historical background data available for this species. Animals were housed under sterile conditions at a constant temperature of 20-22ºC and relative humidity (45-65%) under daily cycles of light / darkness (12 hours). Manipulation was performed in laminar flow hood and sterilized water and food were available *ad libitum*.

The procedure involving experimental animals was approved by the "Ethical Committee of Animal Experimentation" of the animal facility plate at Science Park of Barcelona (Platform of Applied Research in Animal Laboratory). Once approved by the Institutional ethical committee, this procedure was additionally approved by the ethical committee of the Catalonian authorities according to the Catalonian and Spanish regulatory laws and guidelines governing experimental animal care. Along the procedures, continuous supervision and animal control was also established to monitor animals' degree of suffering and if there was the need to sacrifice them, according to the defined end point criteria described by the United Kingdom Coordinating Committee of Cancer Research (UKCCCR), by the Canadian Council on Animal Care (1998), by the Institute for Laboratory Research Journal (2000), by the Conference 22-25 November 1998 Zeist (The Netherlands) and by the Guidelines for the welfare and use of animals in cancer research (2010). The euthanasia method applied was by CO_2 saturated atmosphere.

Repeated dose toxicity study

Drug administration and sample collection

To assess the maximum tolerated dose of the developed F nanoparticle formulation, F-BSA NPs were diluted in water and dispensed intravenously at variable doses (Table 21). Administration was performed at 5 mL/kg once per day for a total of five days. A control group with untreated animals was also included. Doses higher than 30 mg/kg could not be administered due to technical constraints, as the highest F concentration tested in the formulation until the moment was 6.6 mg/mL (10 mM).

Animal weight was monitored daily before administration. The end point criterion was established at a mean group weight loss equal or above 15%. Additionally, any individual mouse with a loss of 20% would have been sacrificed. Body weight loss was calculated according to the initial animal weight.

At the end of the experiment, different samples were collected for further analysis. Blood was collected by intracardiac puncture on recipients containing 5 µL of 0.5 M EDTA. Different organs were also removed, weighted and frozen for further analysis: liver, kidneys, brain, heart, pancreas and bone marrow.

Table 21. Treatment groups in the repeated dose toxicity assay.

Group	Number of animals	Dosage (mg/kg)
1	3	1
2	3	2.5
3	3	5
4	3	10
5	3	20
6	3	30
7 (control)	2	-

Analysis of blood samples

Blood samples were analyzed at PCB-PRBB Animal Facility. Complete hematology profiles were obtained with Abacus JuniorVet (Diatron) and compared to the reference ranges provided by the equipment. Glucose, cholesterol, triglyceride acids, complement component 3 and 4, C-reactive protein, albumin, creatinine, aspartate aminotransferase, alanine aminotransferase and bilirubin were determined by Spinlab 100 analyzer (Spinreact), by means of absorption spectrometry and immunoturbidimetry. Biochemical parameters were compared to the reference values provided by Envigo. In this case, the first

and third quartiles of a normal distribution were calculated for the mean values provided and considered the limits.

UPLC-MS/MS analytical method

Brains and pancreas from groups 6 and 7 were processed and analyzed at Draconis Pharma S.L. for the presence of F3. Briefly, tissues were homogenized with water at 1:2 w/w ratio. 300 µL of tissue homogenate extracted with ethyl acetate containing an internal standard (0.5 µM F4). Blank samples and calibration standards were equally processed. After extraction, samples were filtered through a Captiva ND Lipids (Agilent Technologies) to remove phospholipids. Filtrates were evaporated under nitrogen at RT and stored for further analysis. Evaporated samples were resuspended in a mixture of 4:1 of acetonitrile and H_2O and transferred to a 1 mL injection plate. F3 was quantified by UPLC-MS/MS methods. The equipment used for the analysis was an ACQUITY Ultra Performance LC (Waters) coupled to an API 3200 (AB Sciex, USA) with an electrospray ionization source (ESI). Chromatographic separations were performed by a proprietary method.

Pharmacokinetic studies

The pharmacokinetic parameters of F and F-BSA NPs were studied in intravenous and in oral administration routes.

Drug administration and sample collection

For the intravenous administration, F was dissolved at 2 mg/mL in 40% polyethylene glycol (PEG), 40% dimethylacetamide (DMA) and 20% H_2O and sterile-filtered. Toxicity of the vehicle had been previously assessed. F-BSA NPs were diluted in water to the same concentration and sterilized by filtration.

For the oral administration, F was dissolved at 2 mg/mL in oil, specifically in Caprylic/capric triglyceride (Myritol®-318, BASF), and sterilized by filtration. F-BSA NPs were diluted in water to the same concentration and sterile-filtered.

Animals were weighted before the assay to determine the appropriate dispensing volume at 5 mL/kg. Formulations were administered once, intravenously or intragastrically, at a subtoxic dose of 10 mg/kg. Blood was collected at different time points, as stated in Table 22. It was extracted either through the facial vein or by intracardiac puncture (end points), on recipients containing 5 µL of 0.5 M EDTA.

Table 22. Treatment groups in the intravenous and oral kinetics assay.

Group	Number of animals	Blood extraction
1	3	5 min, 8h
2	3	15 min, 24h
3	3	30 min, 48h
4	3	1h
5	3	2h
6	3	4h

HPLC-MS/MS analytical method

Blood samples were centrifuged at 5000 rpm for 10 minutes to obtain plasma. Either 50 or 100 µL of plasma were extracted twice with 500 µL of ethyl acetate. The organic phase was separated and evaporated under a nitrogen atmosphere. A standard curve was created by diluting known concentrations of the reference compounds in mouse plasma (P9275, Sigma) and following the previous extraction procedure. Samples were stored at -20ºC and protected from light until further analysis.

Evaporated samples were resuspended in 100 µL of a mixture 1:1 of acetonitrile and H_2O. F and its metabolites (F2 and F3) were quantified by HPLC-MS/MS methods. The equipment used for the analysis was a 1260 series HPLC (Agilent Technologies, Waldbronn, Germany) coupled to a 4000 QTRAP spectrometer (AB Sciex, USA) with an ESI. Chromatographic separations were performed by a proprietary method.

Determination of pharmacokinetic parameters

Firstly, background signal was subtracted from peak areas obtained with the HPLC-MS/MS analysis. Standard curves of known concentrations of the reference compounds were then used to quantify the amount of F and its metabolites in each sample.

Further data analysis was performed using GraphPad Prism 7 software. F elimination after an intravenous bolus injection was fit to a bicompartmental model (exponential two-phase decay model), as stated in Equation 13. Data from the oral administration route included an absorption-predominant phase followed by an elimination-predominant phase. In this case, the model used was Equation 14. The same model was used to fit the formation and elimination processes of the metabolites in both administration routes.

Equation 13 $$C = A \times e^{-k_a \times t} + B \times e^{-k_b \times t} \quad (91,222)$$

Equation 14. $$C = \frac{C_0 \times k_{abs}}{k_{abs} - k_{el}} \times (e^{-k_{el} \times (t - t_0)} - e^{-k_{abs} \times (t - t_0)}) \quad (222,223)$$

In the two compartment model in Equation 13, A is the initial concentration of the fast phase (M); k_a is the elimination rate constant of the fast phase (s^{-1}); B is the initial concentration of the slow phase (M); and k_b is the elimination rate constant of the slow phase (s^{-1}).

Similarly, in the model stated in Equation 14, C_0 is the initial concentration (M); k_{abs} is the absorption or formation rate constant (s^{-1}); k_{el} is the elimination rate constant (s^{-1}); and t_0 is the lag time before the absorption or formation process (s).

STATISTICAL ANALYSIS

Data analysis was performed using GraphPad Prism 7 software. Statistical significance among two groups was calculated by running unpaired t-tests (two-tailed, 95% confidence intervals). In analysis of more than 3 groups, it was calculated by applying a one-way ANOVA followed by multiple comparisons tests: Dunnett's test, when comparing a control mean with the other group means; or Tukey test, when comparing every mean with every other mean.

RESULTS

CYTOTOXICITY EVALUATION OF COMPOUND F ON HM CELL LINES

Assessment of the cytotoxic activity of Compound F on different HM cell lines

It has been reported that F has cytotoxic effects on several hematologic cell lines but there is no consensus on the active concentration range. We wanted to confirm the cytotoxic activity of F on hematologic cell lines and, at the same time, to study whether the cytotoxic concentration depended on the type of HM. For that purpose, we screened a handful of available HM cell lines by a cell viability assay (MTT assay) at 72h. Moreover, GCs are often used in the treatment of HMs due to their pro-apoptotic function in lymphocytes (191–193). Therefore, we assayed also the cytotoxicity of dexamethasone in the same cell lines, as a GC of reference.

Table 23. Characteristics of tested HM cell lines.

	Cell type	Disease	Origin	Patient (age/gender)
THP1	Monocyte	AML	PB	1/M
TF-1	Erythroblast	Erythroleukemia (AML)	BM	35/M
HL-60	Promyeloblast	APL (AML)	PB	35/F
K562	Lymphoblast	CML	PE	53/F
CCRF-CEM	T Lymphoblast	ALL	PB	4/F
MV-4-11	Macrophage	Biphenotypic B myelomonocytic leukemia (AML+ALL)	PB	10/M
Ramos	B lymphocyte	Burkitt's lymphoma (NHL)	AF	3/M
U937	Lymphocyte	Histiocytic Lymphoma (NHL)	PE	27/M
MM1S	B lymphoblast	IgA λ myeloma (MM)	PB	42/F

AF, Ascitic fluid; BM, bone marrow; PE, Pleural effusion; PB, peripheral blood.

A total of 9 HM cell line were evaluated (Table 23). Among them, there were 6 leukemia cell lines: 3 AML lines, a CML line, an ALL line and a biphenotypic AML and ALL line. Lymphoma cell lines were also tested, in particular two types of NHL. At last, one MM line was evaluated. Results are depicted in Figure 34, Figure 35 and Figure 36 and in Table 24 and Table 25.

Four cell lines were clearly sensitive to dexamethasone treatment (Figure 34): TF-1 (AML), CCFR-CEM (ALL), MV-4-11 (biphenotypic AML+ALL) and MM1s (MM). Among them, maximal estimated cytotoxicity was in CCFR-CEM cells. All IC50s at 72h were in the nM range (Table 24). When these lines were treated with F, higher maximal toxicities were achieved in all cases. However, estimated IC50s at 72h were in the µM range (Table 25).

The remaining lines showed certain resistance to the treatment with dexamethasone, as observed in Figure 35 and Figure 36a. However, F displayed cytotoxicity again in the low µM range at 72h. Furthermore, maximal achieved toxicity was 100% in all cell lines except for K562. MV-4-11 was the cell line with highest sensitivity to F (Table 25).

In general, F exerted a cytotoxic effect on all leukemia and lymphoma cell lines with IC50 values at 72h ranging from 1-4 µM. The myeloma cell line tested was also sensitive to F but showed a higher IC50.

Table 24. Estimated parameters for the cytotoxicity curves of dexamethasone on HM cell lines.

	Max cytotoxicity (%)	IC50 (µM)	IC50 Std. Error	R^2
TF-1	58	0.002	0.000	0.91
CCFR-CEM	81	0.015	0.005	0.98
MV-411	69	1.06	1.77	0.86
MM1S	53	0.003	0.001	0.93
HL60	54	95.37	162.10	0.88
K562	-	-	-	-
Ramos	47	0.51	1.63	0.81
U937	-	-	-	-
THP1	19	0.13	0.11	0.62

MV-4-11 curve was modelled to a sigmoidal dose-response curve but showed high error due to lack of data points at low and high concentrations. HL-60 and Ramos also lacked data at high concentrations and K562 and U937 could not be modelled with existing data.
IC50, half maximal effective concentration; Max, maximal; Std, standard.

Table 25. Estimated parameters for the cytotoxicity curves of F on HM cell lines.

	Max cytotoxicity (%)	IC50 (µM)	IC50 Std. Error	R^2
TF-1	71	1.91	1.83	0.85
CCFR-CEM	-	-	-	-
MV-4-11	91	1.19	0.07	0.99
MM1S	95	11.42	2.21	0.99
HL60	99	3.52	0.23	0.99
K562	66	1.56	0.27	0.95
Ramos	94	7.48	0.46	1.00
U937	98	3.93	0.47	0.97
THP1	96	3.71	0.37	0.99

CCFR-CEM curve could not be properly modelled to a sigmoidal dose-response curve. TF-1 curve lacked data at high concentrations and so showed a high standard error of the estimated IC50.
IC50, half maximal effective concentration; Max, maximal; Std, standard.

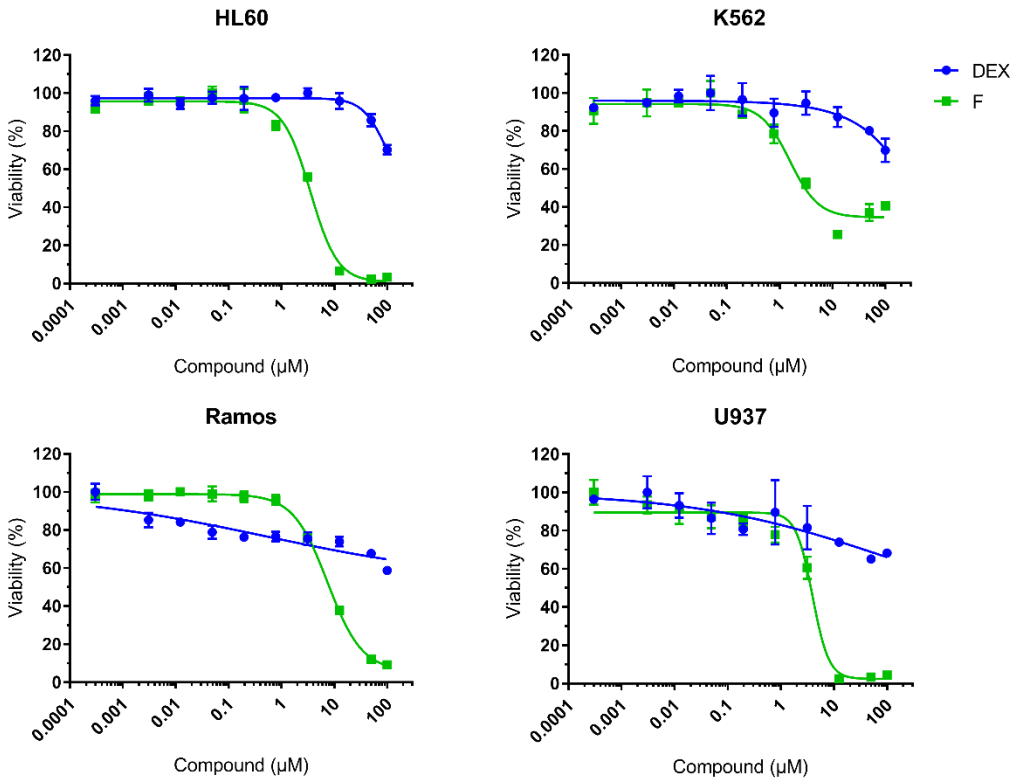

Figure 34. F and DEX reduce cell viability of several HM cell lines: TF-1 (AML), CCFR-CEM (ALL), MV-4-11 (biphenotypic AML+ALL) and MM1s (MM). *Cell cultures were incubated with increasing concentrations of DEX or F for 72h and cytotoxicity was then evaluated by MTT assay. Parameters from obtained curves are enlisted in Table 24 and Table 25.*

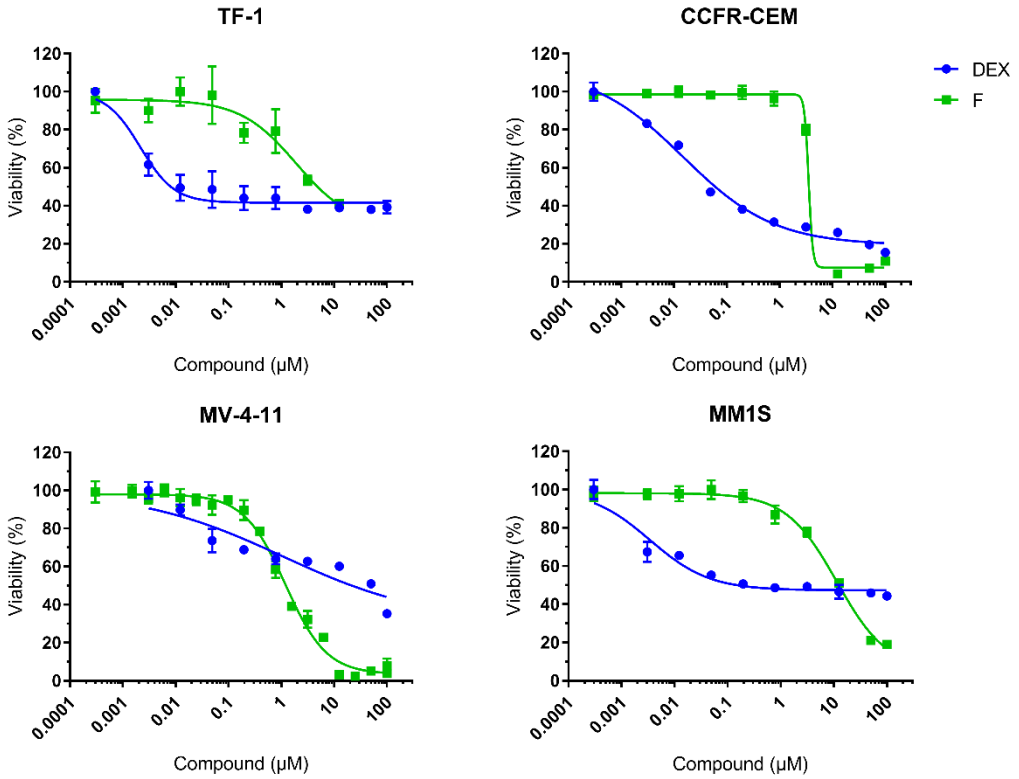

Figure 35. F reduces cell viability of several HM cell lines with higher efficacy than DEX: HL-60 (AML), K562 (CML), Ramos (NHL) and U937 (NHL). *Cell cultures were incubated with increasing concentrations of DEX or F for 72h and cytotoxicity was then evaluated by MTT assay. Parameters from obtained curves are enlisted in Table 24 and Table 25.*

Comparison with the cytotoxicity of other ABCs on THP1

THP1 cell line showed no sensitivity to treatment with dexamethasone but could be inhibited by F. Different ABCs were then assayed in this cell line, to explore the possible differential effects of the different structures related to F.

F metabolites F3 and F2 displayed maximal toxicity and similar IC50 values (Figure 36b and Table 26). Compound L was estimated to reduce cell viability by 34%, although at quite reasonable concentrations. Compound B and Compound A displayed no cell mortality at the tested concentrations, while Compound N only had activity at the highest concentration (Figure 36c). In this case, it is not clear whether it is a specific cytotoxic effect.

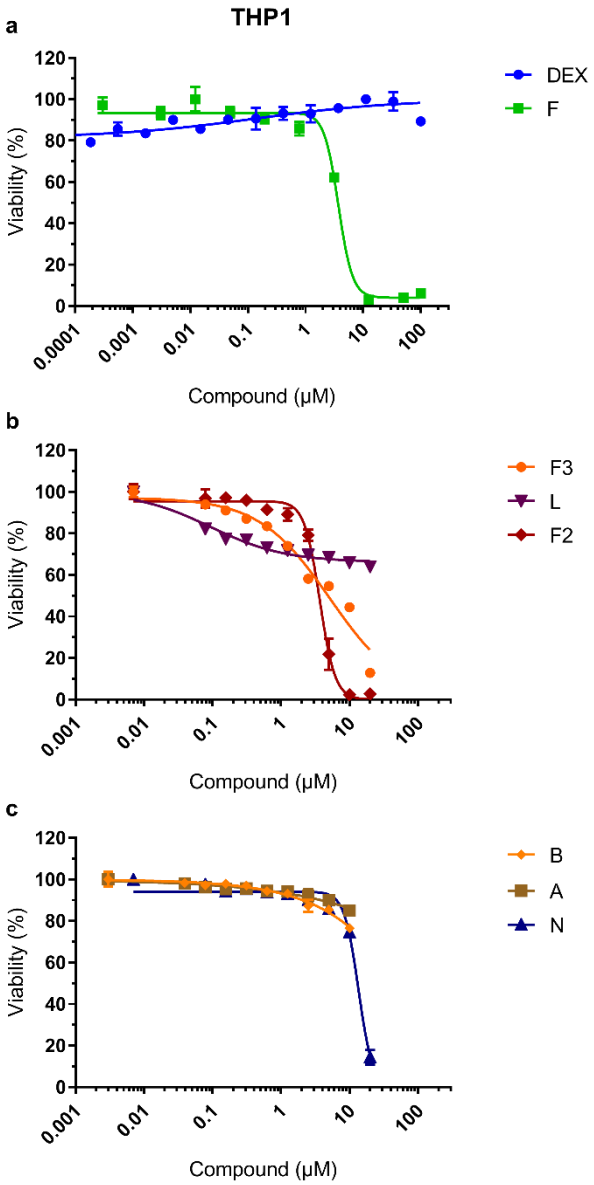

Figure 36. Some ABCs reduce cell viability of THP1 with higher efficacy than DEX. (a) Effect of dexamethasone (DEX) and F. (b) Effect of F3, Compound L and F2. (c) Effect of Compound B, Compound A and Compound N. A THP1 culture was incubated with increasing concentrations of the different compounds for 72h. Cytotoxicity was then evaluated by MTT assay. Parameters from obtained curves are enlisted in Table 26.

Table 26. Estimated parameters for the cytotoxicity curves of different ABCs on THP1 cell line.

	Max cytotoxicity (%)	IC50 (µM)	IC50 Std. Error	R^2
F3	100	5.19	0.56	0.96
N	100	13.50	0.37	0.98
F2	100	3.68	0.11	0.99
L	34	0.09	0.02	0.94

Cytotoxic activity of Compound F in combination therapy

Besides the intrinsic antitumoral activity of F, it has also been reported to enhance the cytotoxic effect of some chemotherapy drugs. Synergistic antitumoral activities are always of high interest for clinical applications. Combination therapies also help decrease the adverse effects of cytotoxic drugs by reducing its dosage. We explored the combined cytotoxic effects of F and different first-line drugs in the treatment of HMs and other cancers. Two cell lines were selected for that purpose. First, combinations on MV-4-11 were evaluated, as F had shown maximal cytotoxic activity with the lowest IC50 at 72h in this line (Table 25). Among the remaining tested lines, THP1 was selected as another model of AML. Interestingly, it also displayed high sensibility for F.

Cytarabine (Cyt) is a nucleoside analog that also inhibits polymerase, causing S-phase arrest. It is used in the treatment of AML, ALL, CML and NHL. Both selected cell lines, MV-4-11 and THP1, were highly sensitive to the compound, with estimated IC50 at 72h in the nM range (Table 27). The drug was incubated with different concentrations of F in MV-4-11, which lowered the IC50 (Figure 37a and Table 27). Interaction was further analyzed by the Chou-Talalay method (220). Resulting isobolograms can be found in Figure 38a. The combination of all tested concentrations of F (except 0.3 µM) showed an additive effect with Cyt in a wide concentration range (IC25 and IC50). However, antagonistic interactions were detected in the IC75 range. F's metabolite F3 was also tested in combination with Cyt and similar results were obtained (Figure 37b and Table 27). Interestingly, F3 alone showed a higher potency than its precursor and the same happened when combined with Cyt. In this case, all combinations proved to be additive or slightly synergistic in the IC25 and IC50 range, while they were fairly at low concentrations (Figure 38b). At last, Cyt was coincubated with two concentrations of F in THP1 cells (Figure 37c and Table 27). In this case, the obtained IC50 at 72h was higher than for cCyt alone, although the combination showed higher efficacy at low Cyt doses. Antagonist effect was confirmed by the isobolograms (Figure 38c).

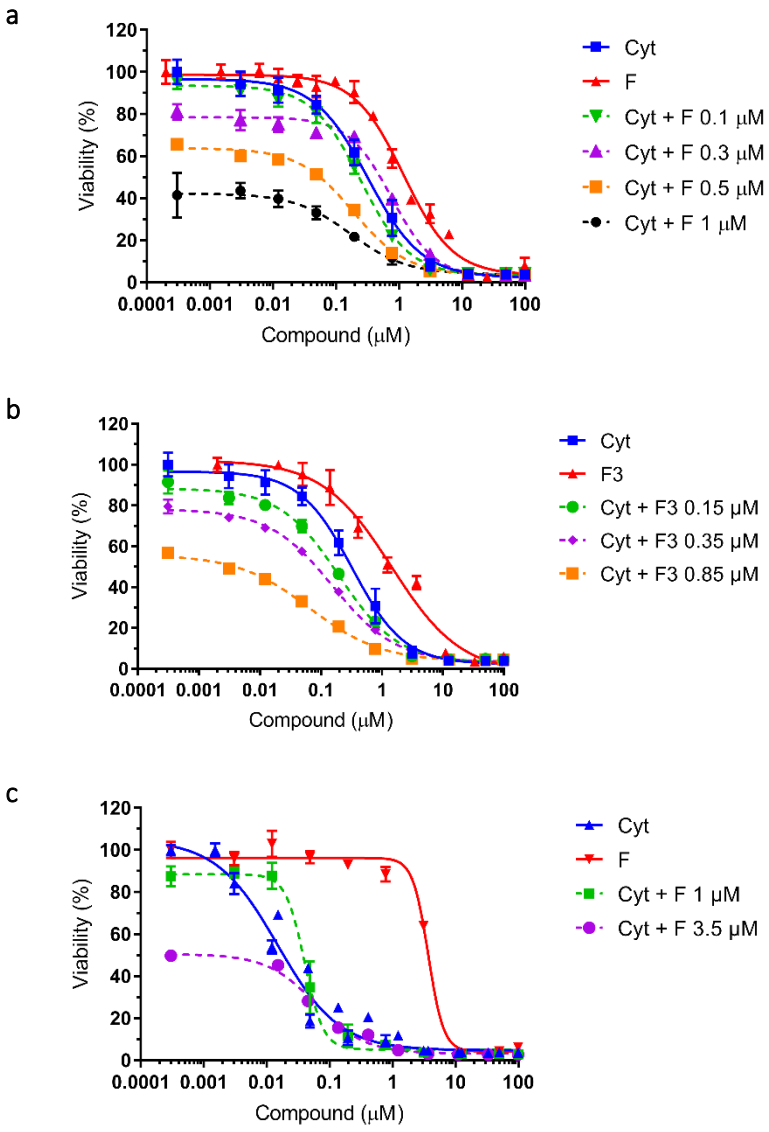

Figure 37. Cytotoxic activity of F and its metabolite F3 in combination with cytarabine. Cells were incubated with Cyt and different concentrations of F or F3 for 72h, after which an MTT assay was carried out. (a) Combination of F and Cyt in MV-4-11 showed increased cytotoxic effects (dotted lines). (b) Combination of F3 and Cyt in MV-4-11 showed increased cytotoxic effects (dotted lines). (c) Combination of F and Cyt in THP1 showed increased cytotoxic effects only at low Cyt concentrations.

Table 27. Estimated parameters for the cytotoxicity curves of the combination of cytarabine with F or F3 in two cell lines.

	MV-4-11			THP1		
	IC50 (µM)	IC50 Std. Error	R^2	IC50 (µM)	IC50 Std. Error	R^2
F	1.19	0.07	0.99	3.71	0.37	0.99
F3	1.45	0.27	0.98	-	-	-
Cytarabine	0.32	0.02	0.98	0.01	0.00	0.97
Cyt + F 3.5 µM	-	-	-	0.06	0.00	0.99
Cyt + F 1 µM	0.17	0.04	0.91	0.04	0.00	0.98
Cyt + F 0.5 µM	0.19	0.01	0.99	-	-	-
Cyt + F 0.3 µM	0.76	0.06	0.99	-	-	-
Cyt + F 0.1 µM	0.25	0.02	0.99	-	-	-
Cyt + F3 0.85 µM	0.07	0.01	1.00	-	-	-
Cyt + F3 0.35 µM	0.16	0.01	1.00	-	-	-
Cyt + F3 0.15 µM	0.20	0.02	0.99	-	-	-

Cyt, cytarabine; IC50, half maximal effective concentration; Std, standard.

Other cytotoxic drugs of common clinical use were also tested in combination with F in MV-4-11 cells. Daunorubicin (DR) is a cytotoxic drug specifically aimed at the treatment of HMs. It is approved for AML, ALL and CML. Its activity is mediated both by DNA intercalation and topoisomerase II inhibition. Methotrexate (MTX) is an inhibitor of dihydrofolate reductase (DHFR) that leads to the blockage of DNA synthesis. Its use is approved for several cancers, ALL and NHL among them. Lenalidomide (LLD), a derivative of thalidomide, is applied in MM treatment. It is an antiangiogenic and immunomodulatory compound, although it acts by different mechanisms. The combination of the three mentioned drugs with 0.5 µM of F showed a slight reduction in the estimated IC50 at 72h in MV-4-11 cells (Figure 39 and Table 28). However, when analyzed by the Chou-Talalay method, slight to moderate antagonism was detected (Table 29). The same happened with the combination with gemcitabine (GCB) and 5-fluorouracil (5FU). In this case, GCB, a nucleoside analog, is used in different cancer treatments. It causes apoptosis specifically in S-phase. The pyrimidine analog 5FU is also applied to treat many cancers.

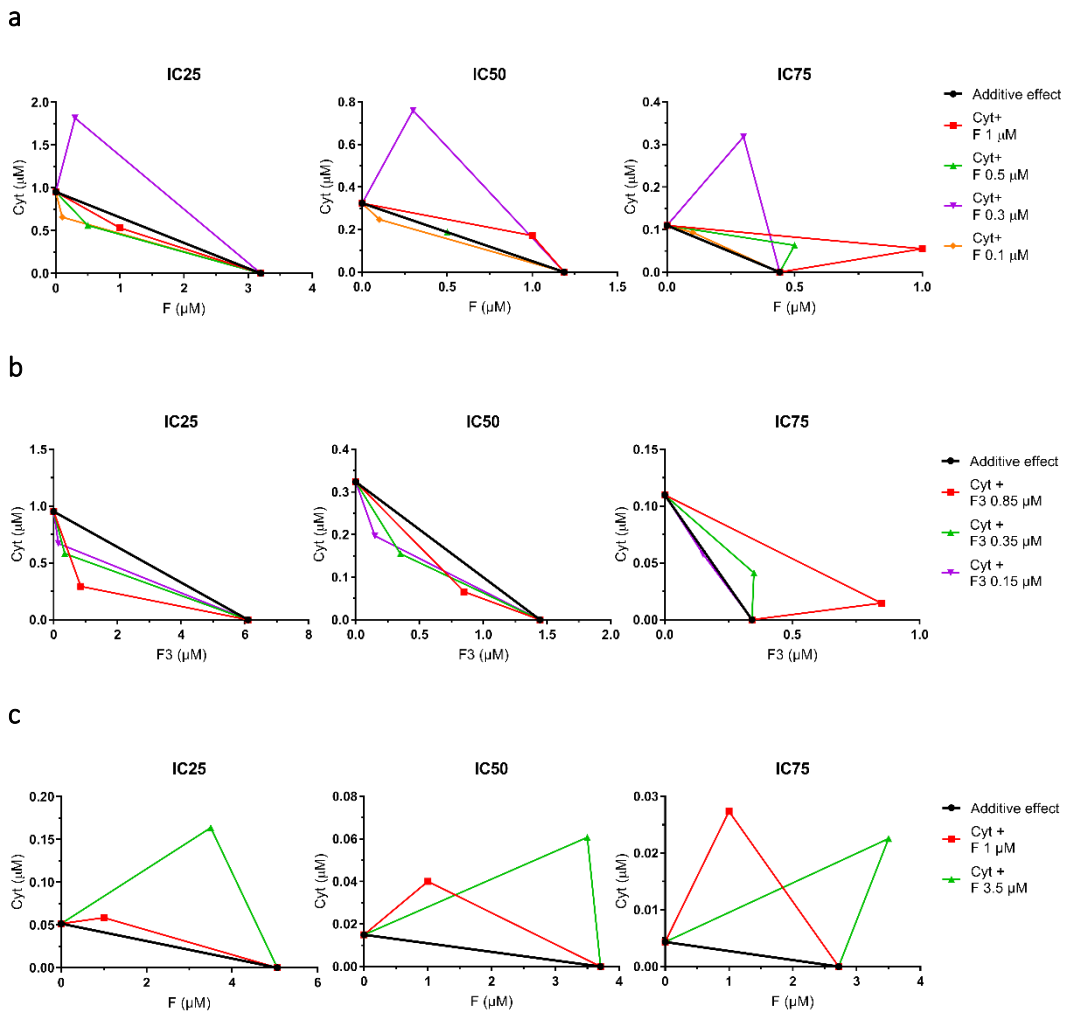

Figure 38. Isobologram analysis of the interaction of cytarabine with F or F3. *IC25, IC50 and IC75 concentrations of F or F3 are plotted on the x-axes, while cytarabine (Cyt) concentrations are on the y-axes. The black line connecting these two points represents the line of additivity. Points located below the line indicate synergy, whereas points situated above denote antagonism. (a) Cyt and F show mostly additive effects on MV-4-11. (b) Cyt and F3 show additive and synergistic effects on MV-4-11. (c) Cyt and F show mostly antagonistic effects on THP1.*

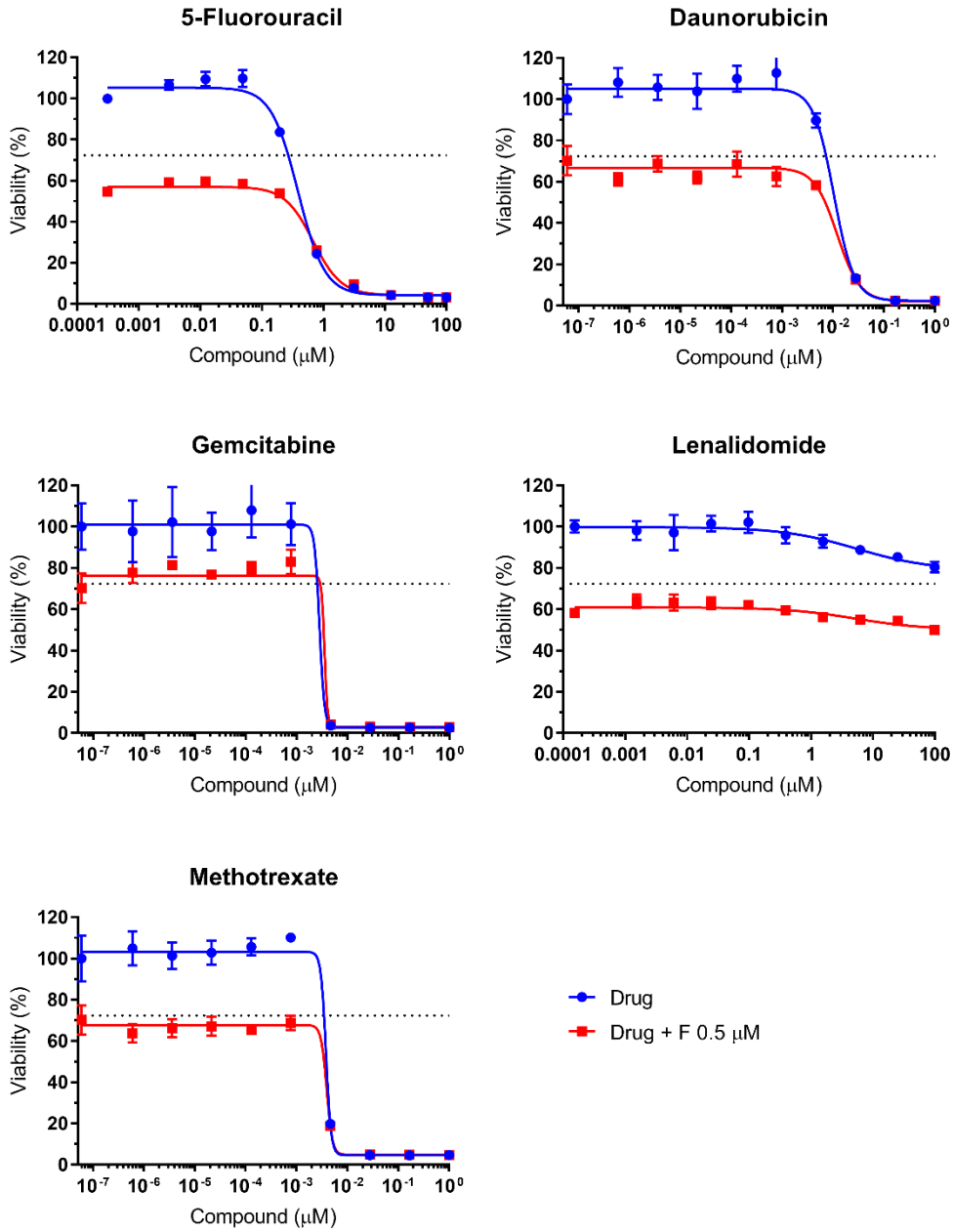

Figure 39. Cytotoxic activity of F in combination with different cytotoxic drugs in MV-4-11 cells. Cells were incubated with drugs and 0.5 μM of F for 72h, after which an MTT assay was carried out. Dotted line indicates the effect of 0.5 μM of F on cell viability.

Table 28. Estimated parameters for the cytotoxicity curves of the combination of different cytotoxic drugs with 0.5µM F in MV-4-11 cells.

	IC50 (µM)	IC50 Std. Error	R^2
F	1.188	0.070	0.99
LLD	5.443	5.706	0.75
LLD + F 0.5 µM	5.208	6.719	0.60
DR	0.0104	0.0013	0.98
DR + F 0.5 µM	0.0121	0.0019	0.96
5FU	0.386	0.022	0.99
5FU + F 0.5 µM	0.680	0.041	0.99

Gemcitabine and methotrexate could not be properly modelled into a sigmoidal dose-response curve due to lack of data points.
5FU, 5-fluorouracil; DR, daunorubicin; LLD, lenalidomide; IC50, half maximal effective concentration; Std, standard.

Table 29. Combination indexes (CI) of the interaction of different cytotoxic drugs with 0.5 µM F on MV-4-11. Values are interpreted as follows: <1 synergism, >1 antagonism, and =1 additive effect.

	5FU	DR	GCB	LLD	MTX
IC25	2.23	1.65	1.59	1.30	1.48
IC50	2.18	1.58	1.68	1.38	1.45
IC75	2.13	1.52	1.68	1.47	1.39

For the determination of GCB and MTX CIs approximate IC values were used.
5FU, 5-fluorouracil; DR, daunorubicin; GCB, gemcitabine; LLD, lenalidomide; MTX, methotrexate.

Three additional compounds that are NR ligands were evaluated in combination with F: ATRA, calcipotriol (CaPT) and rosiglitazone (RGZ). Although ATRA is not a cytotoxic drug, it is used in the treatment of APL, due to the specific translocation involving RARα that causes this leukemia (190). CaPT is a synthetic derivative of calcitriol, the active form of vitamin D that binds to VDR. It is in clinical trials for the treatment of multiple cancers and it is known to inhibit proliferation of HM cell lines (201,202,204–207). The latter, RGZ, is a PPARγ agonist that has been shown to induce apoptosis in AML, CML and CLL cells (196–199).

Both ATRA and CaPT compounds alone showed high cytotoxicity. Their curve could not be properly modelled and therefore no IC50 has been obtained and no synergy analysis was possible. In view of that, the combination curve was performed with a constant concentration of the compounds added to increasing concentrations of F. As observed in Figure 40, cytotoxicity at low F concentrations was higher than observed with F alone but similar to the values obtained with ATRA or CaPT alone. In two combinations the obtained IC50 at 72h was slightly lower in comparison with F (Table 30).

RGZ alone presented low cytotoxicity on MV-4-11, with an IC50 around 45 µM at 72h (Table 30). The combination with 0.5 µM of F reduced the estimated IC50 to 32.58 µM. After analyzing these data with the Chou-Talalay method, the following CI were obtained: 1.12 (IC25), 1.15 (IC50) and 1.17 (IC75); indicating additive effects between both compounds.

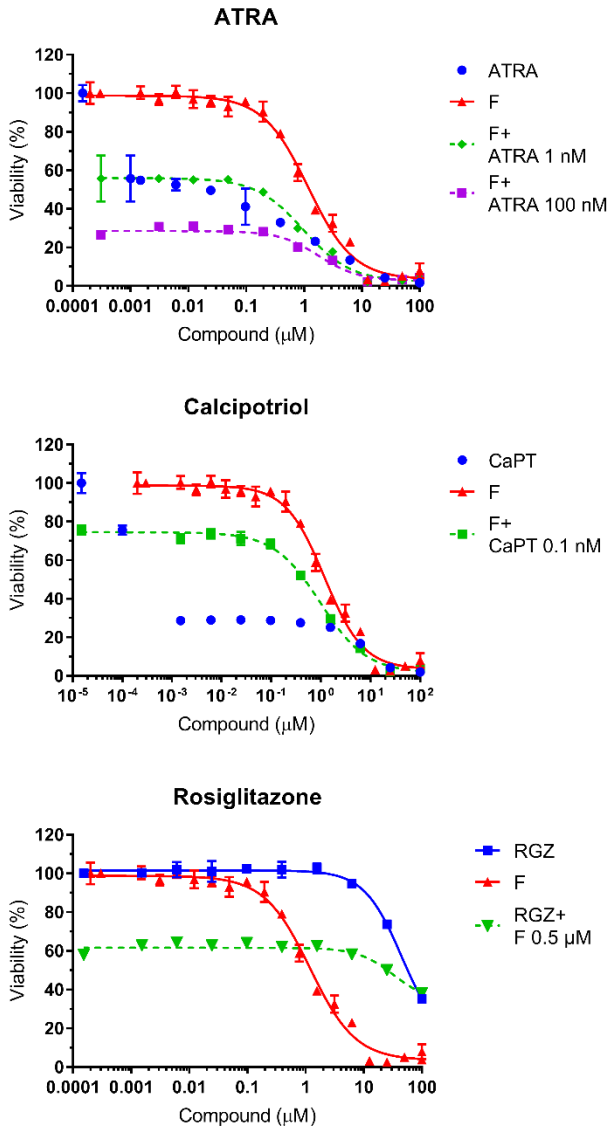

Figure 40. Cytotoxic activity of F in combination with ATRA, calcipotriol and rosiglitazone in MV-4-11 cells. Cells were incubated with F and different concentrations of the compounds for 72h, after which an MTT assay was carried out. Combinations of F and the compounds showed increased cytotoxic effects at low concentrations but variable IC50s.

Table 30. Estimated parameters for the cytotoxicity curves of the combination of F with NR ligands drugs in MV-4-11 cells.

	IC50 (μM)	IC50 Std. Error	R^2
F	1.188	0.070	0.99
F + CaPT 0.1 nM	0.975	0.084	0.99
F + ATRA 100 nM	1.791	0.297	0.96
F + ATRA 1 nM	0.980	0.242	0.93
RGZ	44.920	14.30	0.98
RGZ + 0.5 μM F	32.580	15.99	0.88

All-trans retinoic acid (ATRA) and Calcipotriol (CaPT) could not be properly modelled into a sigmoidal dose-response curve due to lack of data points. IC50, half maximal effective concentration; RGZ, rosiglitazone; Std, standard.

INDUCTION OF APOPTOSIS BY COMPOUND F

After examining the effects of F on cell viability of HM cell lines, we wanted to examine whether cell death was driven by apoptosis, as it has been extensively described. For that purpose, cell viability, cytotoxicity and apoptosis were simultaneously measured in MV-4-11 cells incubated with increasing concentrations of F at different time points. Different fluorescent substrates were used: one cell-permeant substrate sensible to intracellular protease cleavage (viability marker); one cell-impermeant substrate cleaved by free proteases released from death cells (cytotoxicity marker); and one substrate sensible to cleavage by caspase 3/7 (apoptosis marker). Staurosporine, an alkaloid known to induce apoptosis, was included as a positive control.

As expected, viability and cytotoxicity signals were inversely proportional. In general, caspase 3/7 activity was detected in all incubation times (Figure 41), although the peak was not well-defined. It might indicate that cell death was mediated by the sequential activation of caspases, which leads to apoptosis. Compared to staurosporine, that rapidly induced apoptosis (Figure 42), F effects were quite slower and did not allow to establish proper cytotoxicity and apoptosis curves. At short incubation times (6h), a decrease in viability was already detected, although only at the highest tested concentrations. Similarly, cytotoxicity and apoptosis only occurred upon 100 µM of F. After 24h, the observed effects had shifted to lower concentrations. Notably, at 100 µM no viable cells remained, and the viability decline was concomitant to a substantially reduced detection of apoptosis and cytotoxicity. Altogether, it indicates a quick cell death probably attributed to necrosis or to a non-regulated process of cell death. At longer incubation times, effects were detected even at lower concentrations. The obtained viability curves at 48h, 72h, 96h and 120h were similar and the estimated IC50 value stabilized around 4 µM (Figure 43). Apoptosis and cytotoxicity also started to be observed at lower concentrations. Interestingly, after 72h and at concentrations above 10 µM of F, cell viability was minimal, as did cytotoxicity and apoptotic signaling. From 72h, the reduction in viability started at slightly lower concentrations than the increase in cytotoxicity. These unpair events are typically attributed to compounds that cause cell cycle arrest and alterations in cell division, without affecting cell integrity. Although it has been reported that F induces arrest at G0/G1 phase, further investigation was needed.

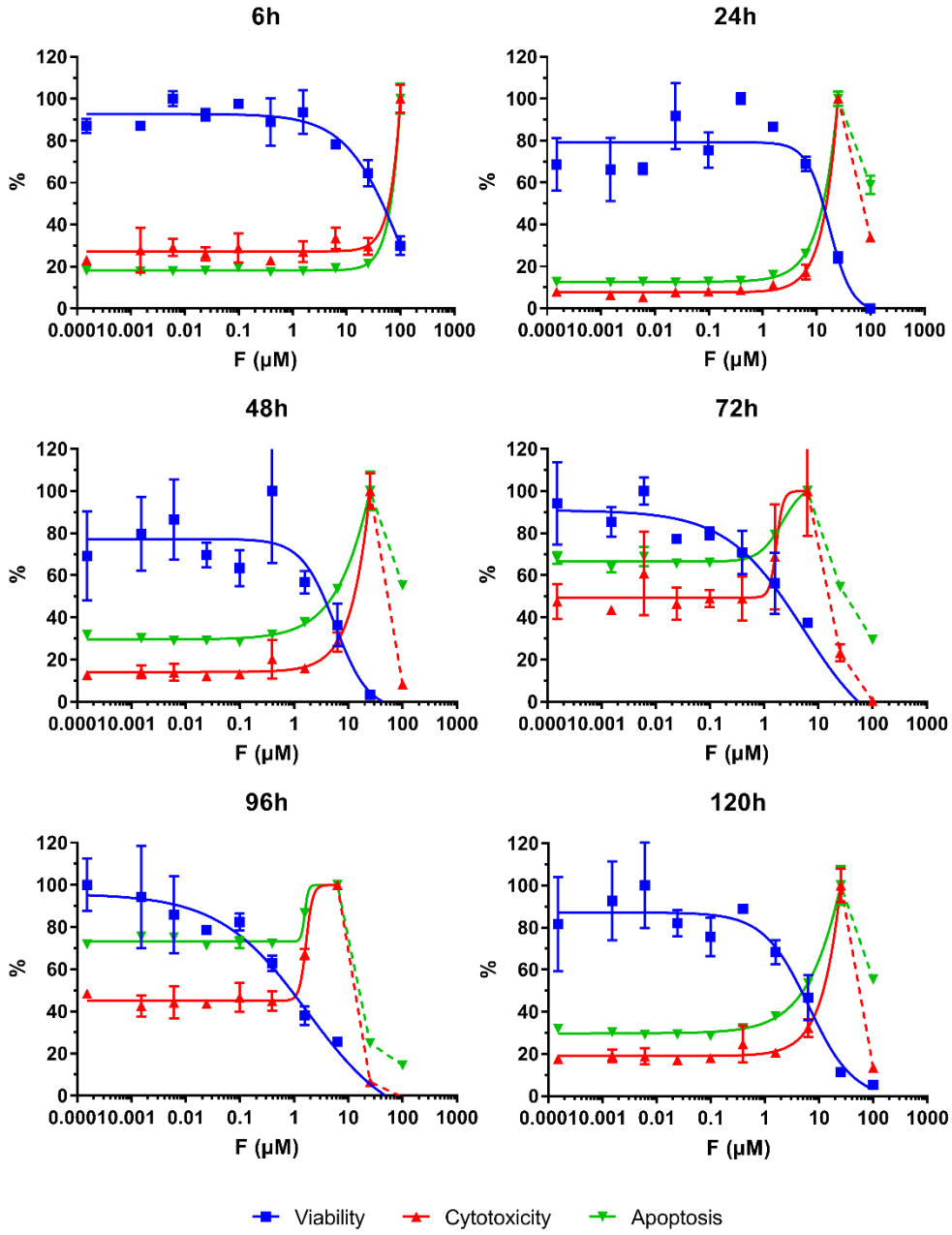

Figure 41. Viability, cytotoxicity and apoptosis curves of MV-4-11 treated with F for different periods of time. Cells were incubated for 6h, 24h, 48h, 72h, 96h or 120h with F at increasing concentrations. After each interval, viability, cytotoxicity and apoptosis were assessed by measuring the cleavage of fluorescence substrates. Values are normalized by the highest mean in each data set. Mean values ±SD from two replicates are plotted.

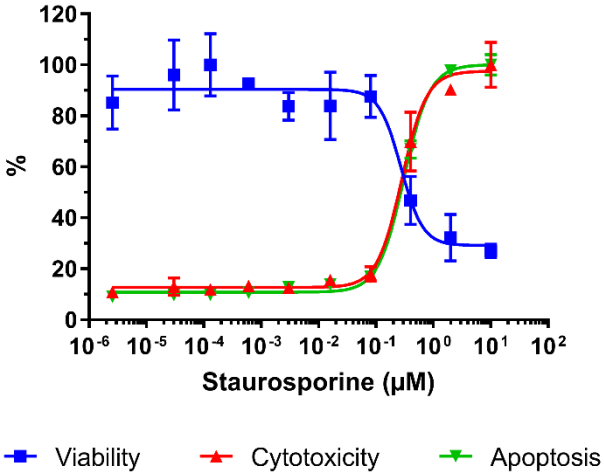

Figure 42. Viability, cytotoxicity and apoptosis curves of MV-4-11 treated with staurosporine. *Cells were incubated for 6h with staurosporine at increasing concentrations as a positive control of apoptosis induction. Then, viability, cytotoxicity and apoptosis were assessed by measuring the cleavage of fluorescence substrates. Mean values ±SD from two replicates are plotted.*

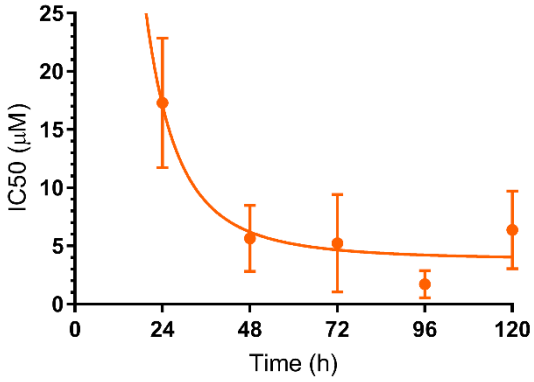

Figure 43. Evolution of estimated IC50 of F on MV-4-11 over time. *Relative IC50s were estimated from viability assays performed with F at different time points (Figure 41).*

EFFECT OF COMPOUND F ON MONOCYTES' CELL CYCLE

F has been described to have a cytotoxic effect in many cancerous cell lines mediated by a cell cycle arrest. Moreover, previous results showed a delay between the decline in viability and the apparition of a cytotoxicity marker, reinforcing the theory of cell cycle arrest. To study it, the influence of the incubation with the ABC on monocytes cycle was analyzed by flow cytometry at different time points. At the same time, cell viability and cell count were determined.

Control cells progressed normally through cell cycle, mainly experiencing cell division between 24 and 48h (Figure 44 and Figure 45a-c). The number of cells in S and G2/M phases experienced a decrease between those time points, while the number of cells in G0/G1 phase increased, indicating that cells that were preparing for mitosis have already divided. Accordingly, total cell number doubled in this interval, while viability was kept at its maximum. At 72h a new round of cell division is preparing, and so, the phase profile was similar to 24h.

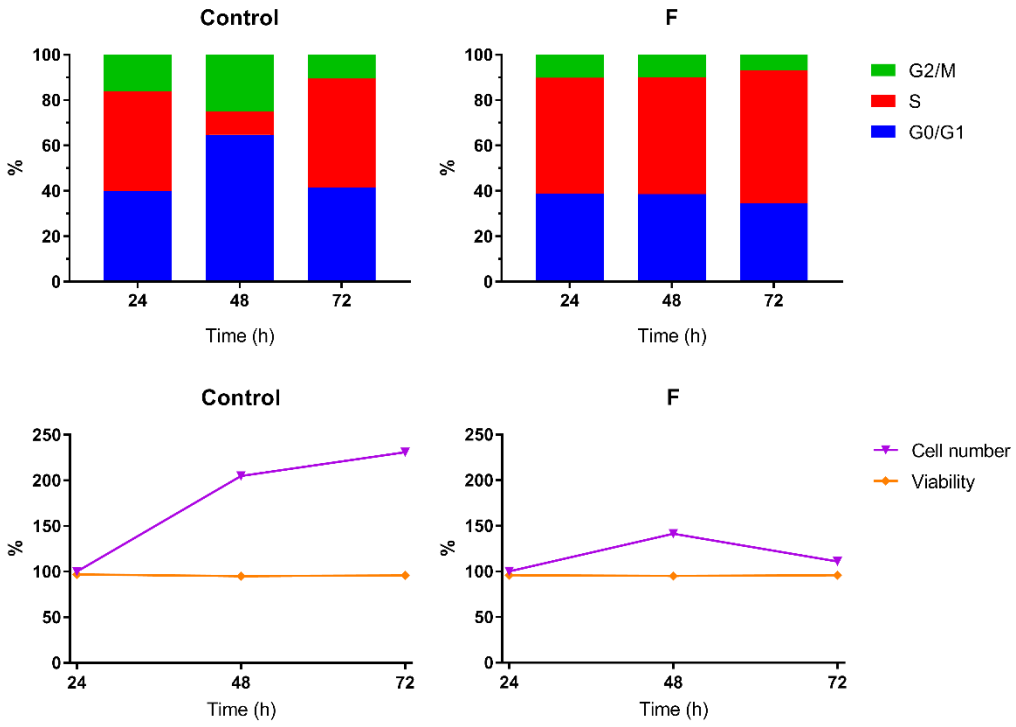

Figure 44. Influence of F on THP1 cell cycle. *Cells incubated with and without F at 1.3 µM were analyzed by flow cytometry to determine the percentage of cells in each phase of the cell cycle, as well as the total number of cells and their viability. THP1 cells were arrested at S phase after 48 hours, while no toxicity was observed*

Cells incubated with F showed no changes compared to control after 24h. However, cell cycle did not progress as in control, and at 48h the percentage of cells undergoing each phase remained the same as at 24h. After 72h of incubation, a slight increase in the percentage of cells in S phase was observed, pointing to a cell cycle arrest at S phase. In accordance with that, total cell number did not double between 24 and 48h as in control: only about 50% of cells were able to divide. Furthermore, at 72h the number of cells declined to initial values, although cell viability was maximal. Contrarily to what has been reported in several occasions, no arrest at G0/G1 phase was observed.

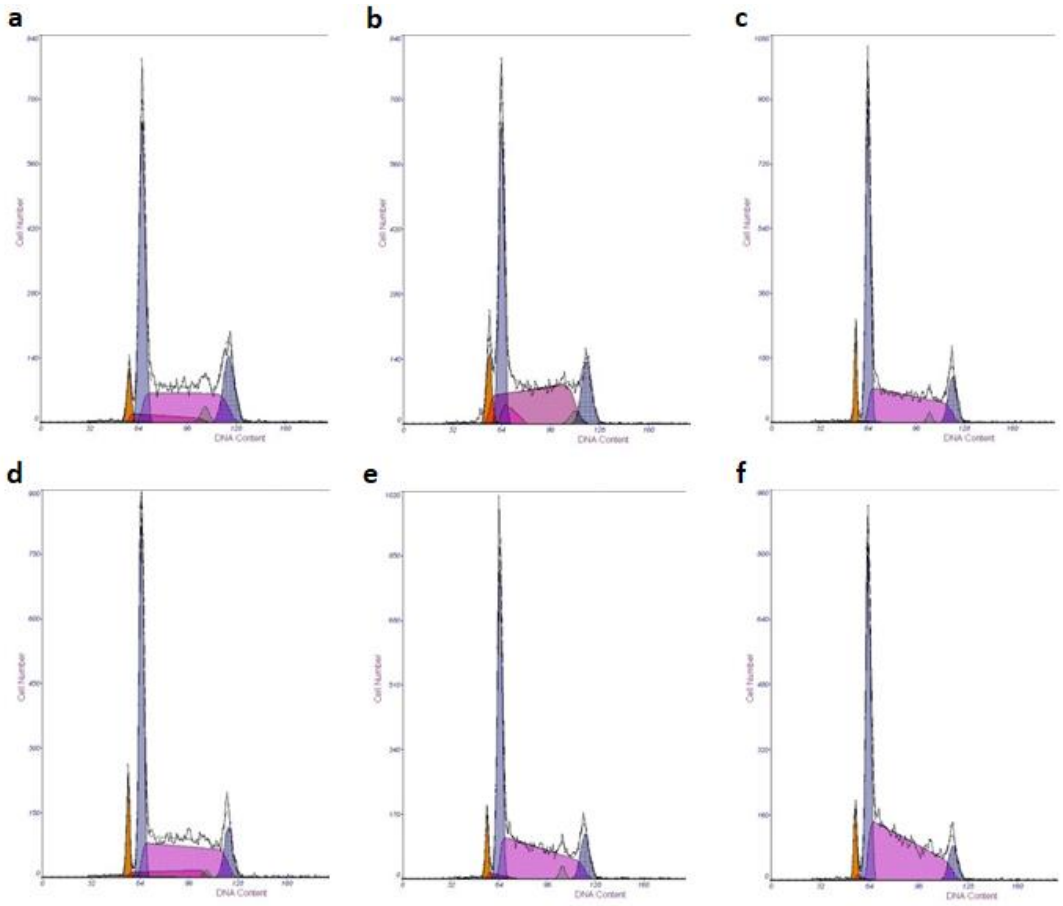

Figure 45. Cell cycle analysis by flow cytometry of the incubation of THP1 with F. *Cell size and DNA content was used to determine the number of cells at each phase of the cell cycle. THP1 control cells at 24, 48 and 72h (a, b and c) were compared to cells treated with F after 24, 48 and 72 h (d, e and f). Cell cycle arrest at S phase is observed after 48 hours.*

COMPOUND F FORMULATION IN ALBUMIN NANOPARTICLES

ABCs are highly hydrophobic molecules and their use in health applications is clearly limited by their low aqueous solubility. Therefore, there is a need for the development of specific formulations to ensure their stability and enhance their bioavailability. Accordingly, an ABC aqueous composition based on albumin NPs, which have been extensively studied, was developed.

Nanoparticles characterization and scalability

First, a protocol for the preparation of ABC-albumin NPs was designed by adapting the desolvation method described by Zhou et al. (221). Initially bovine serum albumin (BSA) was used. A range of weight to weight (w/w) F:BSA ratios was tested to study nanoparticle formation: 1:1, 1:2.5, 1:5, 1:10 and 1:20. Control NPs that contained only BSA (at a concentration equivalent to 1:5 ratio) were also included in the assay. F concentration was measured by HPLC methods. The different preparations were also characterized by DLS.

DLS uses molecular light diffraction to measure particle hydrodynamic diameter in a suspension. This measure is a reflection of the particle and its ion coating, since it is based on the diffusion of the particle. The mean particle diameter (MPD) can then be obtained, as well as the polydispersity index (PDI). The PDI is a measure of uniformity of sizes of particles in the sample. Monodisperse preparations possess low PDI values, whereas PDIs above 0.7 indicate high polydispersity, i.e. a broad distribution of sizes in solution (224). Another important parameter for the characterization of the NPs is the Z-potential. It is the electric potential at the surface of a sphere and is derived from the electrophoretic mobility of a particle. Charged NPs possess an oppositely charged layer of counterions around them (Stern layer), surrounded by another less densely charged layer. When the particle diffuses, those layers move along with the molecule, creating a slipping plane (Figure 46). Z potential is used as an indicator of the stability of a colloidal system, in terms of prediction of aggregate formation (225). High absolute values of Z-potential indicate particle repulsion and, thus, low tendency to aggregate.

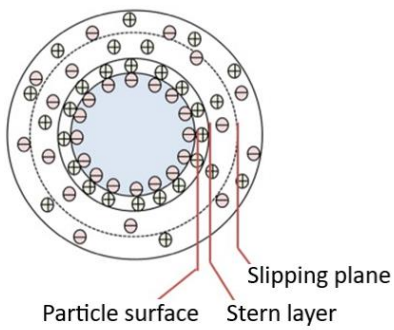

Figure 46. Scheme of the electrical double layer on the surface of a negatively-charged particle. *A slipping plane forms in the interface between the particle with its ion cloud and the solvent. Zeta-potential is the electrokinetic potential at this slipping or shearing plane. Modified from* (225).

F initial incorporation in the NPs was equivalent in all tested ratios, as seen in Figure 47a. However, when NPs were filtered, more than 50% of the ABC was lost in the lowest ratios (Figure 47a), presumably due to the formation of large aggregates that were discarded with the filtration step. Filtered NPs of 1:1 ratio also showed the largest MPD (162.7±0.8 nm), while they presented one of the lowest Z-potential absolute values (-149.1±4.3 mV), indicating good stability in this buffer (Figure 47b-d). In terms of colloid stability and aggregation, Z-potentials below -30mV are generally considered to indicate high stability (225). Similarly, NPs prepared at 1:20 w/w ratio had a Z-potential comparable to that of the control sample (-28.8±2.9 mV and -45.2±34 mV respectively). Curiously, they showed a biphasic distribution of particles size, with two clusters of NPs around 60 and 120 nm (Figure 47b). The resulting MPD was larger than intermediate ratios (94.1±20.7 nm). Their great size variability also translated in 32% particle dispersity, which is considered a fairly polydisperse sample (Figure 47c and d).

Based on the previous results, NPs with a ratio of 1:5 and 1:10 were considered to have the most interesting characteristics for clinical applications. They both showed an MPD of 63 nm with very low size dispersity (5 and 9% respectively) and a Z-potential below -370 mV (Figure 47b-d), which predicts a low aggregation rate. A homogenous size distribution, as well as a small diameter, is critical for *in vivo* administration. The entrapment of F in the NPs was comparable in both cases, as they retained above 80% of the initially added ABC, even after filtration (Figure 47a). At this point, we decided to continue with the 1:5 w/w ratio NPs, based on the lower protein concentration.

The selected NPs were also compared to control NPs prepared without the compound. This sample showed the broadest size distribution observed, with values ranging from the size of free albumin (1-10 nm) to large aggregates (larger than 100 nm) (Figure 47b). Mean measured diameter was 32.1±20.5 nm, about half the size of the F-BSA NPs. Probably, higher protein aggregation takes place in the presence of F, i.e. its entrapment in BSA during the formation of NPs contributes to the formation of larger aggregates. In general, loaded NPs possess higher size uniformity and absolute Z-potential than the control, which could also indicate higher stability, particularly in terms of aggregation (Figure 47c and d).

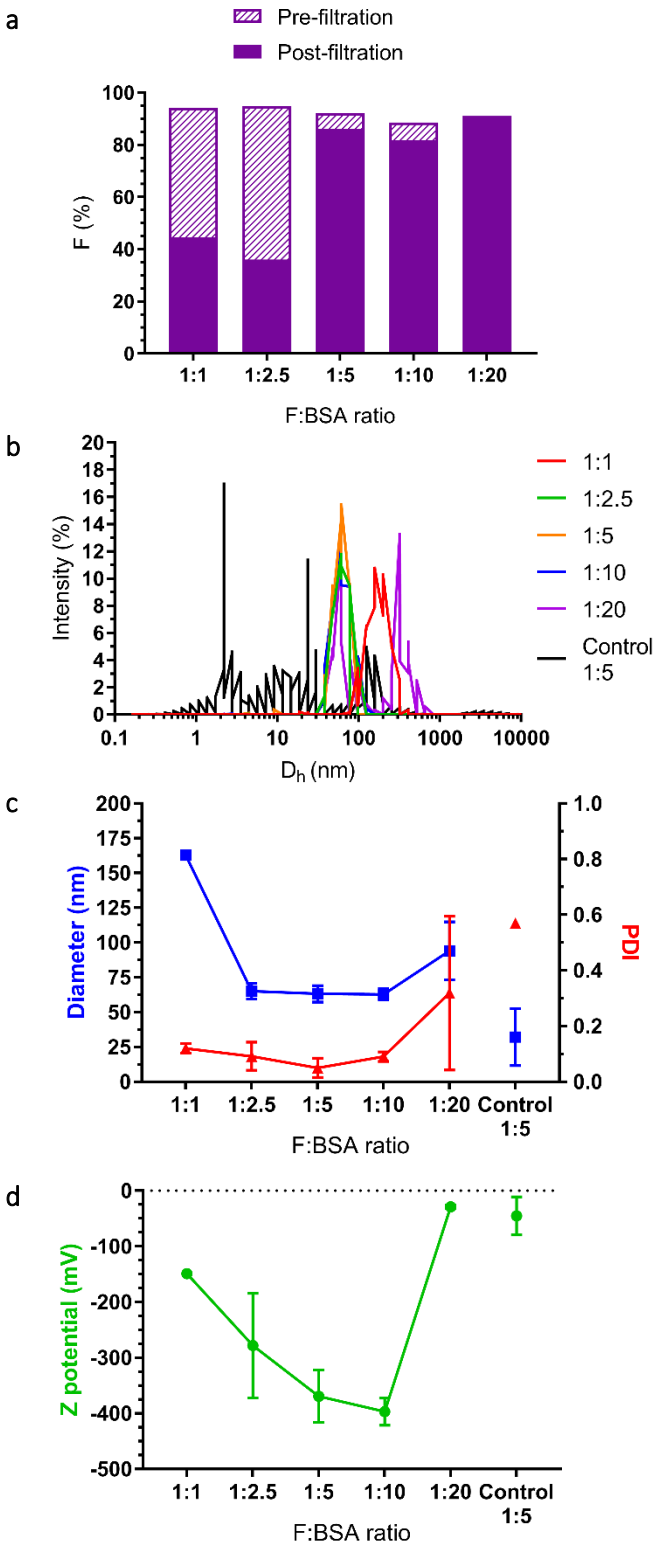

Figure 47. Characterization of F-BSA NPs prepared at different w/w ratios. *(a) F incorporation into NPs (pre-filtration) and retention after filtration through a 0.22 µm-pore-sized filter (post-filtration). Low w/w ratio NPs show a tendency to form aggregates that are eliminated during the filtration step. Quantification was performed by HPLC analysis and is expressed as a percentage of maximum theoretical concentration. (b) Particle size distribution of a representative sample of the different tested w/w ratios. Hydrodynamic diameters (D_h) were measured by DLS after NP filtration. Ratios 1:2.5, 1:5 and 1:10 show a similar distribution, while 1:1 presents a displaced peak towards higher sizes and 1:20 displays a biphasic distribution. A broad size distribution, including free albumin, is observed in the control sample. (c) Mean particle diameter (MPD) (left axis, blue) and polydispersity index (PDI) (right axis, red) were measured by DLS after NP filtration. Low w/w ratio NPs have substantially higher diameters, while high w/w ratio NPs present higher variability and polydispersity. In contrast, control NPs have small diameters with high dispersity. (d) Z potential was measured after NP filtration by DLS. 1:5 and 1:10 ratios possess the lowest Z-potential, meaning higher stability of the colloidal system. Measures represent mean±SD from two technical replicates. Control NPs were prepared without F at a BSA concentration equivalent to the 1:5 ratio.*

New independently prepared samples with the 1:5 ratio were characterized to study batch consistency and protocol scalability. Figure 48 summarizes the measurements performed. From 12 different batches, average particle diameter obtained was 65.7±8.1 nm, with only 9% of polydispersity and a mean Z-potential of -335.9±40.4 mV, predicting low risk of aggregation. F incorporation in the filtered NPs was 80.6±10.2 % of the initially added ABC. The main difference observed between this final NP preparation and batches measured before the last filtration step was, precisely, F quantification. Presumably, larger aggregates are eliminated during this process, which reduces the ABC content. Accordingly, MPD slightly decreased, along with polydispersity and Z-potential (Figure 48). The NP preparation protocol was successfully scaled up to final volumes of 10 mL.

After characterizing the F-BSA NPs obtained with the implemented desolvation protocol, an initial test was conducted to substitute BSA with HSA, which would ensure human treatment compatibility. This approach gave NPs of an MPD of 40.79 nm and high size uniformity (PDI 0.09). A Z-potential of -216.4 mV indicated extremely high stability of the colloidal system. In this case, the incorporation of the ABC in the final filtered sample was of only 58%, which was not satisfactory.

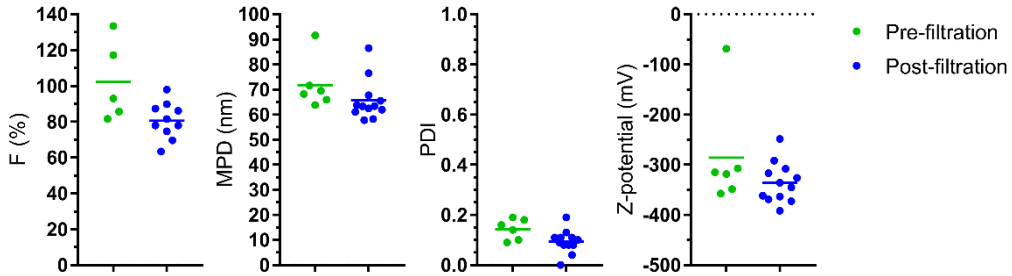

Figure 48. Characterization of different batches of F-BSA NPs at 1:5 w/w ratio*. Different batches were analyzed by DLS and HPLC before and after the final filtration step. Scattered dots represent measures from each batch and the line indicates their mean. MPD, Mean particle diameter; PDI, Polydispersity index.*

Stability of Compound F-albumin nanoparticles

Preliminary studies of NP stability were conducted by taking periodical measures of F concentration of 4 different batches stored at different temperatures. Additionally, samples from each batch were dried in the speed-vacuum and also stored in the same conditions for stability evaluation.

The NPs stored at 4ºC and frozen at -20ºC showed a similar degradation pattern. Most samples retained about 70% of the initial F after 4 months (Figure 49). Apparently, batches kept at room temperature (RT) similarly preserved the ABC, although with higher variability (Figure 49). However, NP precipitation was observed after between 1 and 2 months, meaning that the formulation was not stable.

Dried samples stored at -20ºC presented similar stability to liquid ones kept at the same temperature, except for batch 2 (Figure 49). On the contrary, only 30% of F remained in dried samples at 4ºC after 3 months. As predicted, at room temperature, stability of the ABC was even poorer: only around 15% of F persisted after 3 months (Figure 49). Significantly higher ABC degradation in the powdered formula is probably due to oxidation caused by larger air contact surfaces.

Even though a powder formula would be the preferred option to ensure albumin stability, F stability needs to be improved, as seen above. On the other hand, solutions to be used within 2 months can be stored in the liquid form at 4ºC.

Although NP size distribution changes over time were not evaluated in these batches, particle size stability was preliminary assessed mainly in dried NPs. It was evaluated in 4 different batches, among which 2 samples had undergone freeze-drying (FD) and one had been vacuum-dried (VD) (Figure 50). Dried were stored at -20ºC and resuspended just before the analysis. These batches were compared to a sample kept in a liquid form at 4ºC. In this way, by means of DLS, the effect of drying in the NPs could be roughly studied.

MPD was kept constant for 100 days in batch 5 (FD). Nevertheless, a tendency to aggregate and form larger particles was observed in the other dried batches, as well as in the liquid control (Figure 50). Polydispersity index was constant and below 0.20 in most samples, even in batches that experimented changes in size, indicating a uniform size distribution. Further studies need to be conducted to assess if the increase in the diameter is reproduced and whether it depends on the drying technique or the initial MPD. In batches 3 (VD) and 6 (FD), Z-potential experimented a decline and then seemed to stabilize, while in batch 5 (FD) it increased (Figure 50). Batch 7 (4ºC) experimented an increase followed by a decline in Z-potential, concurring with the slight increase in MPD. Despite this increase, the solubility of the NPs was not compromised, as it did not exceed -30mV, indicating high stability.

In all cases, extended stability studies need to be conducted with different storage conditions to confirm previous results.

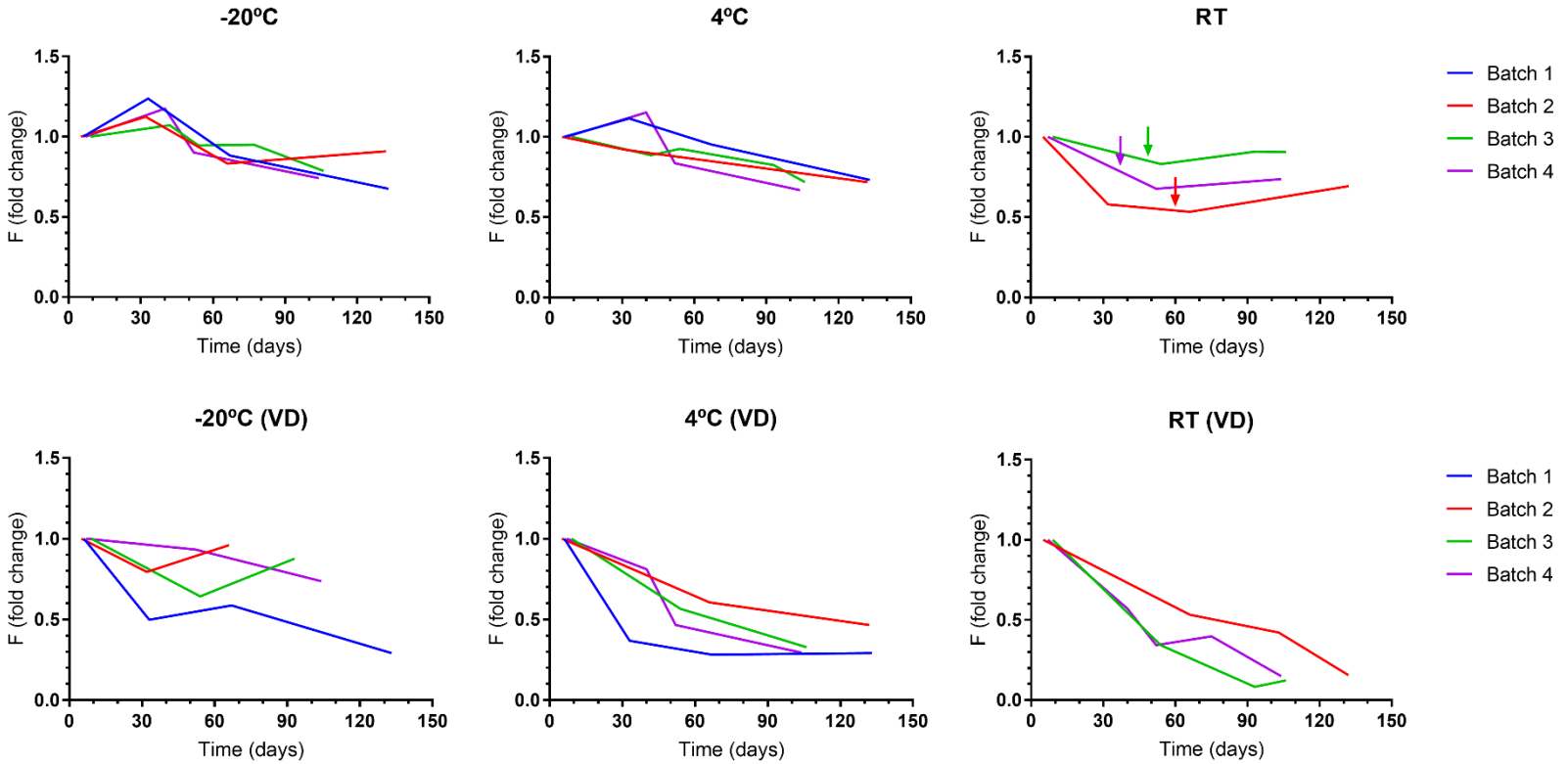

Figure 49. Stability of F in different batches of F-BSA nanoparticles at 1:5 w/w ratio. *ABC degradation was higher in dried samples compared to liquid ones and under all tested store temperatures, probably due to oxidation caused by air contact. At room temperature (RT), NPs precipitation after 1-2 months was observed (indicated by arrows), which suggests unsuitable conservation of the formulation. F quantification was obtained by chromatographic methods and values are normalized to initial batch concentration. FD, freeze-dried; PDI, Polydispersity Index; VD, vacuum-dried.*

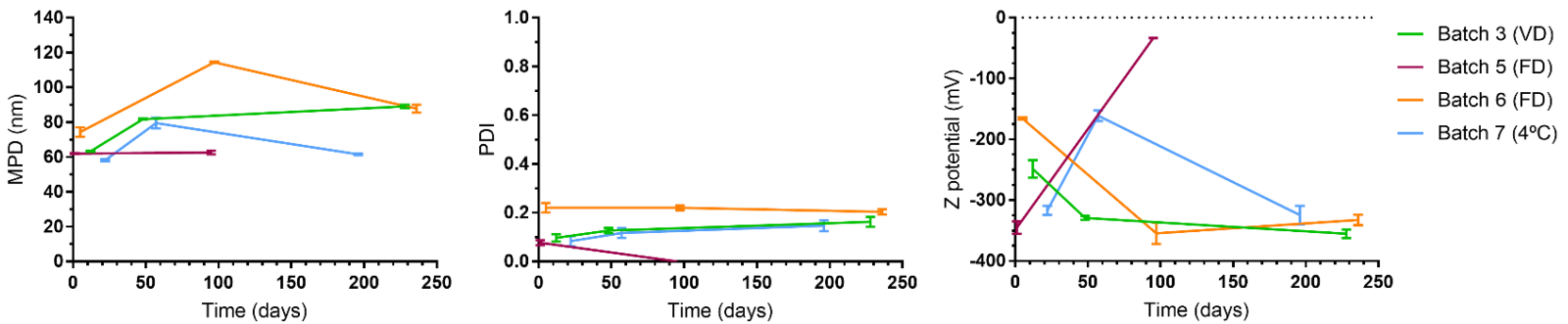

Figure 50. Stability of DLS parameters in different batches of F-BSA nanoparticles at 1:5 w/w ratio. *NPs were characterized by DLS at different time points. Storage conditions included different drying processes and a liquid control at 4ºC. Mean particle size diameter increased in two batches, while size dispersity was low in all samples and Z-potential was kept negative. Error bars indicate statistical deviation from 3 measures. FD, freeze-dried; PDI, Polydispersity Index; VD, vacuum-dried.*

REPEATED DOSE TOXICITY STUDY OF F-BSA NPs

The formulation of F in albumin NPs enabled to overcome the solubility problems of the compound and, thus, could simplify its delivery. However, the potential toxicological effects of the formulation needed to be assessed. Therefore, a repeated dose toxicity (RDT) study was designed. F-BSA NPs were administered intravenously and daily for up to 5 days to immunocompetent mice at doses permitted by technical constraints.

Maximum tolerated dose (MTD) assessment

No toxic effects were observed based on data obtained along the assay. There was no apparent incidence on the behavior or body weight (Figure 51) of the animals during this period. Despite petechias were not detected, a slight accumulation of the product was observed along the vein of the tail, where the product was administered. This accumulation was more obvious in groups 5 and 6, treated with the higher doses.

It appears that F-BSA NPs are well-tolerated at the dose range tested and under the defined administration pattern. Although the MTD could not be determined, the no-observed adverse effect level (NOAEL) was established at 30 mg/kg/day.

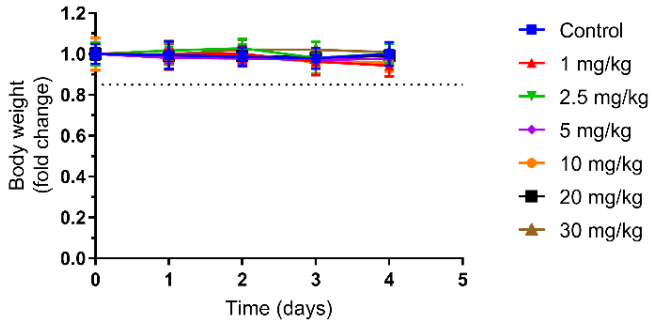

Figure 51. Progression of body weights along the RDT study. *No significant changes in body weight were observed. Data represents the mean±SD weight of each treatment group, normalized by the initial weight. The dotted line indicates the end criterion.*

Hematologic profiles

Blood samples from all animals were analyzed for changes in the hematology profile at the end of the RDT assay with Abacus JuniorVet (Diatron) (Table 31 and Table 32).

No major changes were noticed among red cell population (RBC) (Figure 52a), but there was a significant decrease in platelet count (PLT) in almost all experimental groups when compared to control animals (Figure 52b). Lowest values were still within the normal range (provided by the animal facility), while control animals were above normal limits. However, the reduction was markedly dose-dependent.

In general, the white cell population was the most affected. With increasing dosage, a redistribution of this population was detected: granulocytes presence increased in detriment of lymphocytes (Figure 52c), which caused the global white blood cell (WBC) count to drop.

In particular, the major affected population were the lymphocytes (LYM). Although a dose-dependent decrease is observed at the highest doses, only in group 6 (30 mg/kg) the reduction was significant (Figure 52d). Most values, including the control, were above the normal range. Despite that, the percentage of WBC that LYM represented was around the lower normal limit in all cases and significantly lower than in control group, except for group 1 (1 mg/kg). Hence, LYM were clearly displaced towards granulocytes (GRA).

Granulocyte count includes neutrophils, part of eosinophils, basophils and mast cells. It generally increased in treatment groups, being significantly higher and above normal threshold in groups 2, 4 and 6 (Figure 52f). GRA percentage also increased in most groups but was kept within normal range.

A widespread proliferation in medium size cell population of white cells (MID), which include monocytes and part of eosinophils, was also identified (Figure 52e). Although it was not statistically significant, it was indeed around the upper normality limit.

Overall, treatment with F-BSA NPs for five days produced a dose-dependent decrease of platelet count, as well as lymphocytic count. Granulocytes and monocytes, on the contrary, slightly increase but no correlation with the dose was observed.

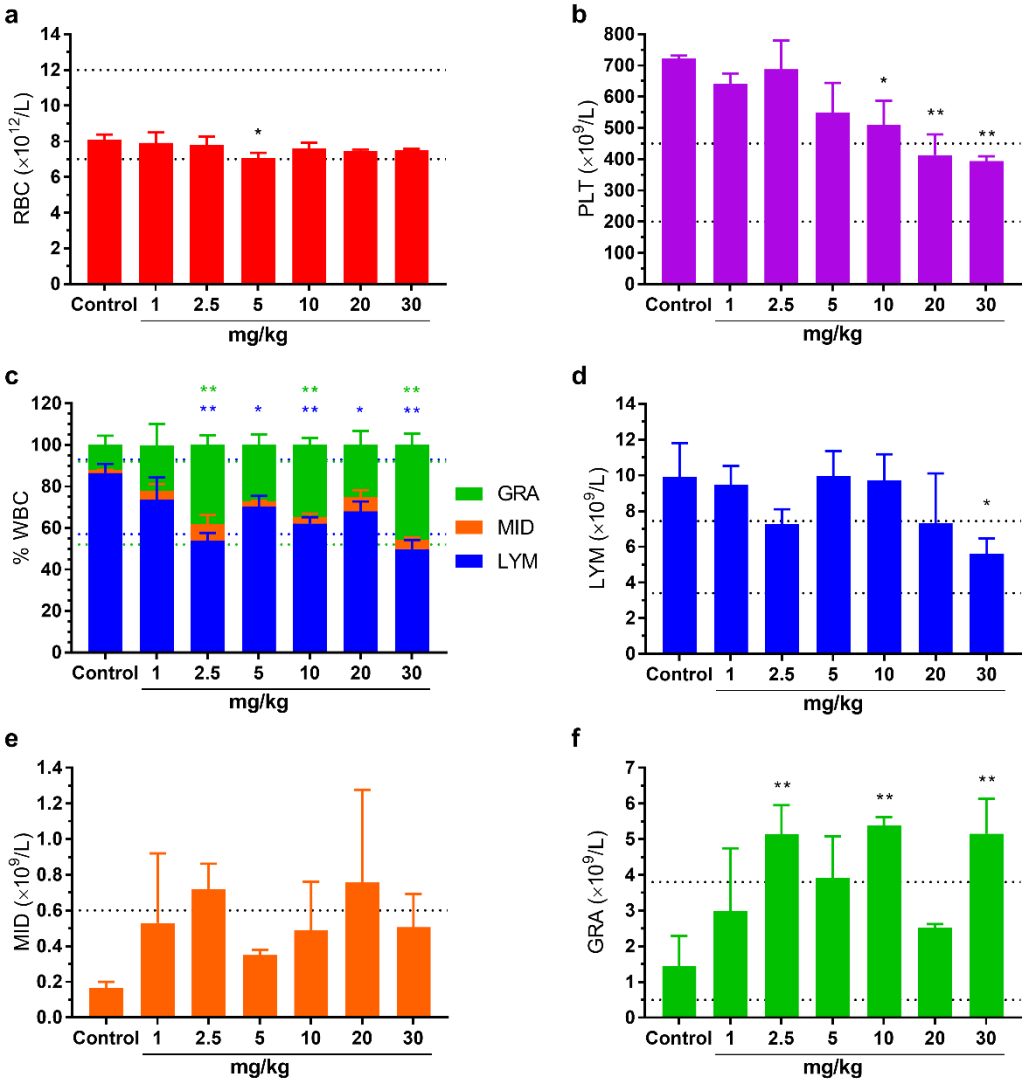

*Figure 52. Findings in the hematologic profiles of mice after the RDT study: (a) red blood cell count (RBC); (b) platelet count (PLT); (c) percentage distribution of white blood cells (WBC); (d) lymphocytes count (LYM); (e) medium size cells count (MID); (f) granulocytes count (GRA). Granulocytes include neutrophils, part of eosinophils, basophils and mast cells. Medium size cells include monocytes and part of eosinophils. Dotted lines indicate normal range values provided by Diatron. Values represent mean±SD of 3 animals (treatment groups) or 2 animals (control group). * significant difference from control with a* p value *< 0.05. ** significant difference from control with a* p value *< 0.01.*

Table 31. Hematologic profiles of mice at the end of the RDT study. Measures are average values for each treatment group. Corresponding standard deviations are stated in Table 32. Numbers in italics indicate out of normal range values; in red, significant difference from control animals with p-value<0.05; and in bold, values that fulfil both criteria.

	Parameter	Units	Limit	Group						
				1 mg/kg	2,5 mg/kg	5 mg/kg	10 mg/kg	20 mg/kg	30 mg/kg	Control
White cells	WBC	$x10^9/L$	[6-15]	13,0	13,6	14,2	*15,6*	10,6	11,3	11,5
	LYM	$x10^9/L$	[3,4-7,44]	*9,5*	7,3	*10,0*	*9,7*	7,3	5,6	*9,9*
	MID	$x10^9/L$	[0-0,6]	0,5	*1,2*	0,4	0,5	*0,8*	0,5	0,2
	GRA	$x10^9/L$	[0,5-3,8]	3,0	***5,1***	*3,9*	***5,4***	2,5	***5,2***	1,4
	LYM%	%	[57-93]	73,6	***53,8***	70,3	62,2	68,1	***49,8***	86,6
	MID%	%	[0-7]	4,2	*8,2*	2,5	3,1	6,7	4,5	1,4
	GRA%	%	[8-48]	22,2	38,0	27,2	34,7	25,2	45,7	12,0
Red cells	RBC	$x10^{12}/L$	[7-12]	7,9	7,8	7,1	7,6	7,5	7,5	8,1
	HGB	g/dL	[12,2-16,2]	13,2	13,3	*12,2*	12,8	12,2	12,3	13,3
	HCT	%	[35-45]	43,1	44,9	38,1	42,5	39,8	39,3	44,5
	MCV	fL	[45-55]	54,4	*57,6*	53,7	*55,8*	53,5	52,3	55,0
	MCH	pg	[11,1-12,7]	*16,6*	*17,0*	*17,2*	*16,8*	*16,4*	*16,3*	*16,4*
	MCHC	g/dL	[22,3-32]	30,7	29,5	32,2	30,1	30,7	31,4	29,8
	RDWsd	fL		40,4	42,7	40,6	42,2	41,9	40,6	42,6
	RDWcv	%		18,4	18,3	18,8	18,7	19,4	19,4	19,1
Platelets	PLT	$x10^9/L$	[200-450]	*642,0*	*688,2*	*549,1*	***510,1***	413,7	394,1	*723,0*
	PCT	%		0,4	0,4	0,3	0,3	0,2	0,2	0,4
	MPV	fL		5,5	5,6	5,5	5,4	5,5	5,7	5,7
	PDWsd	fL		5,5	5,8	5,5	5,3	5,7	5,9	5,9
	PDWcv	%		30,0	30,5	30,0	29,5	30,3	30,9	30,9

WBC, total white blood cell count; LYM, lymphocytes count; MID, medium size cells count; GRA, granulocytes count; RBC, red blood cell count; HGB, hemoglobin; HCT, hematocrit; MCV, mean corpuscular volume; MCH, mean corpuscular hemoglobin; MCHC, mean corpuscular hemoglobin concentration; RDW, red cell distribution width; PLT, platelet count; PCT, platelet percentage; MPV, mean platelet volume; PDW, platelet distribution width; sd, standard deviation; cv, coefficient of variation.

Table 32. Standard deviations of average measures in Table 31.

Parameter	1 mg/kg	2,5 mg/kg	5 mg/kg	10 mg/kg	20 mg/kg	30 mg/kg	Control
WBC	1,90	2,02	2,30	1,59	3,25	1,59	2,78
LYM	1,05	0,84	1,41	1,45	2,80	0,87	1,90
MID	0,39	0,77	0,03	0,27	0,52	0,18	0,04
GRA	1,75	0,82	1,17	0,25	0,09	0,97	0,85
LYM%	10,74	3,82	5,15	3,09	4,81	4,41	4,38
MID%	3,41	4,30	0,40	1,64	3,47	1,27	0,06
GRA%	10,15	4,72	5,14	3,40	6,71	5,57	4,45
RBC	0,58	0,47	0,28	0,31	0,09	0,08	0,28
HGB	7,13	9,94	5,43	4,69	4,97	4,88	9,61
HCT	4,15	2,31	4,39	1,69	0,98	3,26	0,12
MCV	2,44	0,88	4,94	1,69	0,79	4,80	2,04
MCH	0,34	0,40	0,19	0,44	0,55	0,71	0,62
MCHC	15,84	6,93	32,61	1,42	12,48	32,17	22,45
RDWsd	0,91	0,45	3,41	0,78	0,45	4,69	2,76
RDWcv	0,45	0,28	0,45	0,20	0,31	0,33	0,56
PLT	32,96	91,94	95,23	77,74	66,28	15,85	8,77
PCT	0,01	0,04	0,06	0,04	0,04	0,02	0,01
MPV	0,11	0,12	0,09	0,10	0,29	0,05	0,16
PDWsd	0,13	0,13	0,45	0,12	0,54	0,33	0,46
PDWcv	0,31	0,30	1,10	0,33	1,32	0,77	1,07

Biochemical analysis

Plasma samples were analyzed for different biochemical blood parameters. Due to limitations in sample volume available, some biomarkers could only be analyzed in group 6. In this case, results could only be compared to reference values provided by the mice breeder and not to control group.

Results indicate that general metabolism of the mice was affected by the administration of F-BSA NPs (Figure 53a). Glucose in blood was slightly reduced in all treatment groups, although not significantly. This is often observed in toxicology studies 24h after dosing (226). More importantly, a dose-dependent lipid mobilization was observed. Cholesterol increased from group 2 and was above reference limits for most groups. Inversely, triglyceride acids

decreased with growing dosage, achieving a reduction of more than 50% compared to the control, indicating increased lipolysis.

To evaluate immune system activity, the only available biomarker is the complement component 3 (C3) (Figure 53b). In this case, although a slight C3 reduction with dosage is perceived, no significant differences were detected with the control. C4 and C-reactive protein were also measured in groups 1-5 and in the control group, but they were absent in all samples, indicating that no major infection or inflammatory processes existed.

Some hepatoxicity indicators were altered at the highest administered dose (Figure 53d). Aspartate aminotransferase (AST) and alanine aminotransferase (ALT) catalyze the transfer of amino groups from alanine to α-ketoglutarate, and between aspartate and glutamate, respectively. In case of liver or muscle injury, damaged hepatocytes leak those enzymes to plasma (227). Both markers were among the normal limits and the AST/ALT ratio was 2.38±0.52. On the contrary, total bilirubin was especially high and above normal values, particularly, unconjugated bilirubin. It is a breakdown product of hemoglobin that derives from aged red cells. It is transported by albumin and binds to UDP-glucuronosyltransferase in hepatocytes to be excreted, becoming conjugated bilirubin (226).

Renal function was also presumably affected in group 6. Both albumin and creatinine were above the reference values (Figure 53c), suggesting renal function alterations. Albumin binds and transports insoluble molecules in blood, while creatinine is a waste product from the creatine metabolism in muscle. Both are indicators of glomerular injury (226). However, albumin cannot be considered a reliable marker, due to the albumin content in the injected formulation.

Biodistribution

Several organs were obtained and stored at the end of the RTD study. Currently, only pancreas and brains from control group and group 6 (30 mg/kg) have been analyzed for the presence of F3. Results are summarized in Table 33. As expected, no compound was detected in samples from control animals. In treated animals, the presence of F3 was detected in brains in the pmol/g range, meaning that either F or F3 were able to cross the blood brain barrier. Pancreas presented higher concentrations of the metabolite. Particularly, the animal that presented the highest F3 concentration in pancreas also showed the highest concentration in brain. However, more information is still needed about the biodistribution and accumulation of F and its metabolites.

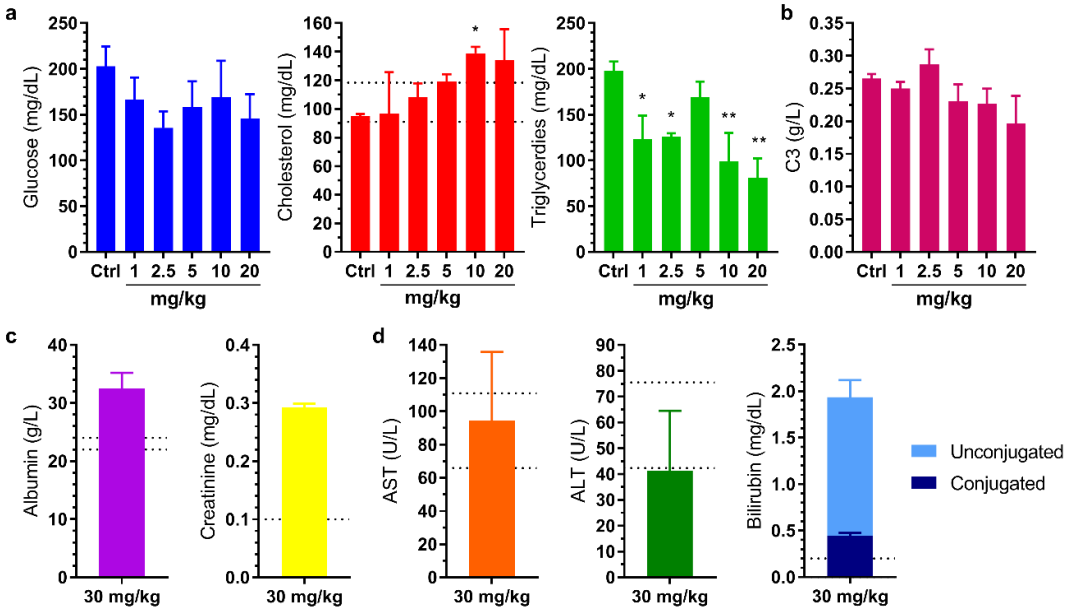

*Figure 53. Biochemical blood parameters of mice at the end of the RDT study. (a) Metabolism biomarkers. (b) Immune system biomarker. (c) Renal function indicators. (d) Hepato-biliary function indicators. Dotted lines delimit the reference range provided by Envigo. Values represent mean±SD of 3 animals (treatment groups) or 2 animals (control group). ALT, alanine aminotransferase; AST, aspartate aminotransferase; C3, complement component 3; U, units. * significant difference from control with a* p value *< 0.05. ** significant difference from control with a* p value *< 0.01.*

Table 33. Concentrations of F3 in brains and pancreas from mice subjected to the RTD study. The presence of F3 was analyzed in tissues obtained from control group and group 6 (30 mg/kg) by means of UPLC-MS/MS.

Tissue	Group	Animal	F3 (nmol/g)	Mean ± SD
Brain	Control	1	0.00	0.00 ± 0.00
	30 mg/kg	1	0.07	0.08 ± 0.02
		2	0.11	
		3	0.07	
Pancreas	Control	1	0.00	0.00 ± 0.00
	30 mg/kg	1	2.47	2.26 ± 0.54
		2	2.66	
		3	1.64	

PHARMACOKINETICS OF COMPOUND F IN MICE

The new formulation of F in NPs enhanced its water solubility and therefore has potential to simplify its delivery via administration routes alternative to oral delivery, which is the most used in published assays. We wanted to examine if this formulation displayed an advantageous pharmacokinetic profile after intravenous and oral administration, in particular when compared to F solubilized in common administration vehicles.

Firstly, F-BSA NPs and F in a tested solvent were administered intravenously at 10 mg/kg to immunocompetent mice. In a second assay, F-BSA NPs and F in oil were administered orally at the same concentration. In both cases, blood was collected at different time points (up to 48h) and plasma was analyzed for the presence of F and its metabolites F2 and F3 by HPLC-MS/MS.

After intravenous administration, F was rapidly metabolized to F2 and F3 (see the metabolic profile in Figure 54). Its half-life was only around one minute in the fast phase for both formulations. However, in the slow metabolism and elimination phase it was 2.7h for the NPs and 4.2h for the organic solvent formulation (PEG-DMA). Although both metabolites appeared almost at the same time, F2 decreased quicker and reached lower levels, probably due to its intermediate metabolite nature. Maximum concentrations achieved were around 3.7 µM of F2 at 3.3h and around 5.9 µM of F3 at 8.6h for the nanoparticulated formulation; and of the order of 4.8 µM of F2 after 5.3h and 7.9 µM of F3 at 13.4h for the organic solvent formulation. Interestingly, in both cases µM levels of F3 were still detectable after 48h of administration. Other obtained pharmacokinetic parameters are enlisted in Table 34. Although the formulation with PEG-DMA resulted in higher concentrations of compounds in plasma and longer half-lives, mice experimented necrosis in the tail due to the injection of the formulation. Solvent had been previously assessed in mice and had shown no toxic effects. Apparently, F's poor solubility in water environments caused a considerable compound precipitation in the site of administration. One of the subjects of group 3 died between 24 and 48h after the administration, presumably for the same reasons.

On the contrary, in the oral administration no toxic effects were observed along the assay. However, F was barely detectable in plasma in either cases (see the metabolic profile in Figure 55). Maximum concentrations achieved were 0.02 µM (NPs) and 0.05 µM (oil), at 0.45h and 1.81h after administration respectively. Formulation of F in Myritol® oil (caprylic/capric triglycerides) showed a delayed absorption when compared to NPs and reached higher plasmatic concentrations of metabolites. Curiously, F2 maximum concentrations were reached at the same time as after intravenous administration but were

around 5 times lower (Table 35). F3 maximum concentrations were only 3-4 times lower than in the intravenous experiment.

Bioavailability, or the fraction of F that reaches systemic circulation unchanged, has been calculated for the NP formulation, by dividing the area under the plasma concentration-time curve in the oral administration (100% bioavailability) by the intravenous administration. Resulting bioavailability is in the order of 0.0001%.

Table 34. Estimated pharmacokinetic parameters of F and its metabolites after an intravenous bolus administration. *Two different formulations of F were injected at 10 mg/kg to three CD-1 mice per condition. Plasma samples were collected periodically and analyzed by HPLC-MS/MS. F metabolism and elimination was fitted to a two-compartment model (Equation 13 in page 109). The formation and elimination processes of the metabolites were fit to Equation 14 in page 109. Values in italics indicate lack of data for an optimal fit.*

PK parameters	Units	F		F2		F3	
		NPs	PEG-DMA	NPs	PEG-DMA	NPs	PEG-DMA
C_{max}	µM	*4814*	*75599*	3.73	4.84	5.87	7.88
t_{max}	h	*0*	*0*	3.26	5.34	8.57	13.36
k_a	h^{-1}	-	-	0.943	0.364	0.309	0.048
k_{el}	h^{-1}	*0.253*	*0.166*	0.052	0.080	0.028	0.110
k_{el2}	h^{-1}	*45.480*	*31.75*	-	-	-	-
$t_{1/2}$	h	***2.74***	***4.17***	**13.43**	**8.68**	**24.92**	**6.33**
V_d	mL	*0.09*	*0.01*	103.29	61.39	61.13	13.39
CL_{tot}	mL/h	*0.024*	*0.001*	5.33	4.90	1.70	1.47
AUC	nM·h	*19.02*	*454.32*	0.09	0.09	0.27	0.31

AUC, area under the plasma concentration-time curve; CL , total body clearance; C_{max}, maximum plasma concentration; k_a, absorption rate; k_{el}, elimination rate; k_{el2}, elimination rate in the fast phase; NPs, nanoparticles; PEG-DMA, polyethilenglycol-dimethylacetamide; t_{max}, time at C_{max}; $t_{1/2}$, half-life; V_d, apparent distribution volume.

Table 35. Estimated pharmacokinetic parameters of F and its metabolites after a single-dose oral administration. *Two different formulations of F were administered at 10 mg/kg to three CD-1 mice per condition. Plasma samples were collected periodically and analyzed by HPLC-MS/MS. The absorption/formation and elimination processes of the compounds were fit to Equation 14 in page 109. Values in italics indicate lack of data for an optimal fit.*

PK parameters	Units	F		F2		F3	
		NPs	Oil	NPs	Oil	NPs	Oil
C_{max}	µM	0.02	*0.05*	0.74	0.85	1.62	*2.50*
t_{max}	h	0.45	*1.81*	3.71	5.04	7.43	*8.92*
k_a	h^{-1}	3.752	*0.553*	0.073	0.376	0.275	*0.112*
k_{el}	h^{-1}	1.158	*0.553*	0.672	0.088	0.053	*0.112*
$t_{1/2}$	h	**0.60**	***1.25***	**1.03**	**7.86**	**13.13**	***6.19***
V_d	mL	16278.06	*3385.11*	50.70	344.40	189.31	*67.15*
CL_{tot}	mL/h	18850.00	*1872.30*	34.05	30.36	9.99	*7.51*
AUC	pM·h	0.02	*0.24*	13.37	15.00	45.56	*60.59*

AUC, area under the plasma concentration-time curve; CL , total body clearance; C_{max}, maximum plasma concentration; k_a, absorption rate; k_{el}, elimination rate; k_{el2}, elimination rate in the fast phase; NPs, nanoparticles; t_{max}, time at C_{max}; $t_{1/2}$, half-life; V_d, apparent distribution volume.

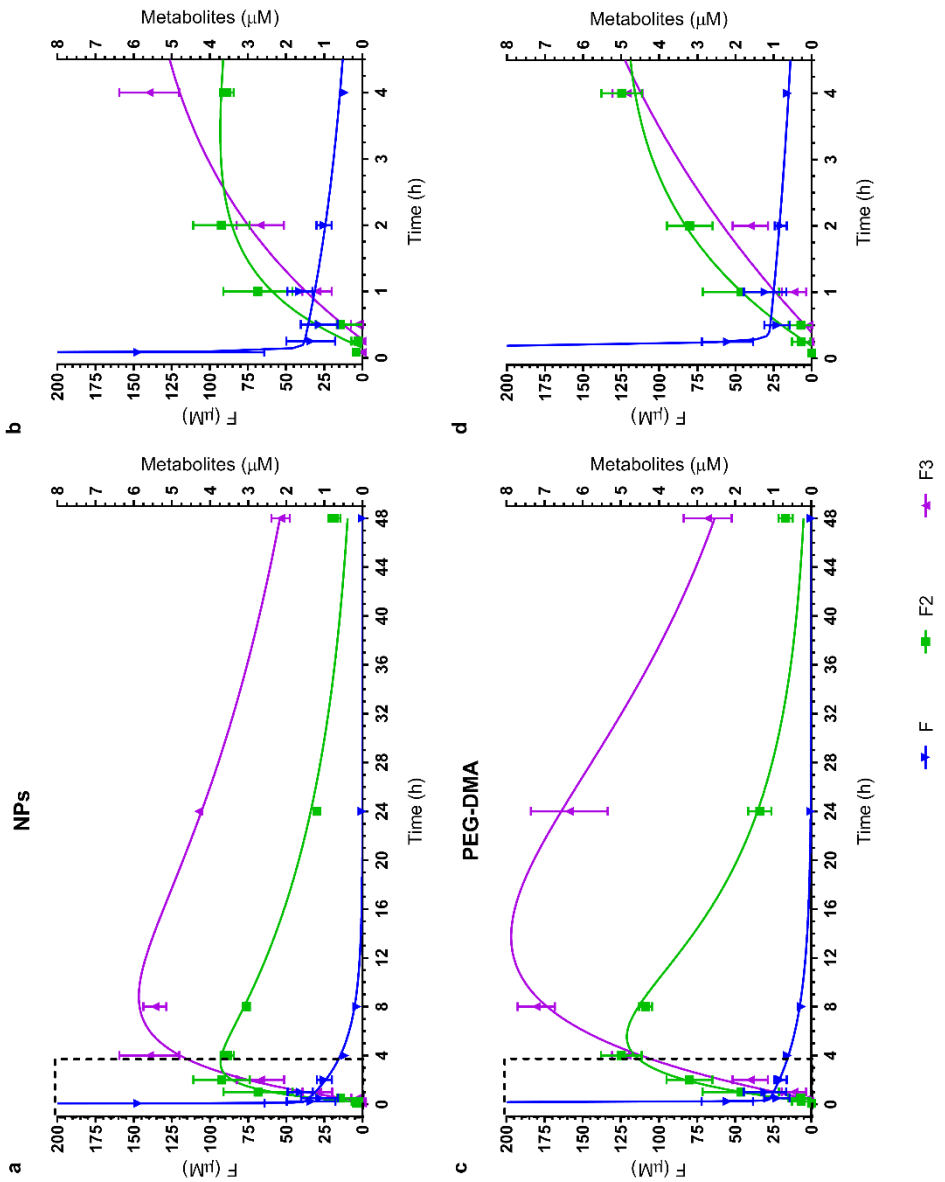

*Figure 54. **Pharmacokinetic profiles of F and its metabolites after an IV bolus administration.** Two different formulations of F were injected to CD-1 mice at 10 mg/kg. Plasma samples were collected periodically and analyzed by HPLC-MS/MS. (a) Pharmacokinetic profile of the IV administration of the nanoparticle formulation of F. (b) Amplification of the dotted region in (a). (c) Pharmacokinetic profile of the IV administration of the formulation of F in PEG-DMA. (d) Amplification of the dotted region in (c). Error bars indicate standard deviation from 3 animals or 2 animals (PEG-DMA at 48h). NPs, nanoparticles; PEG-DMA, polyethilenglycol-dimethylacetamide.*

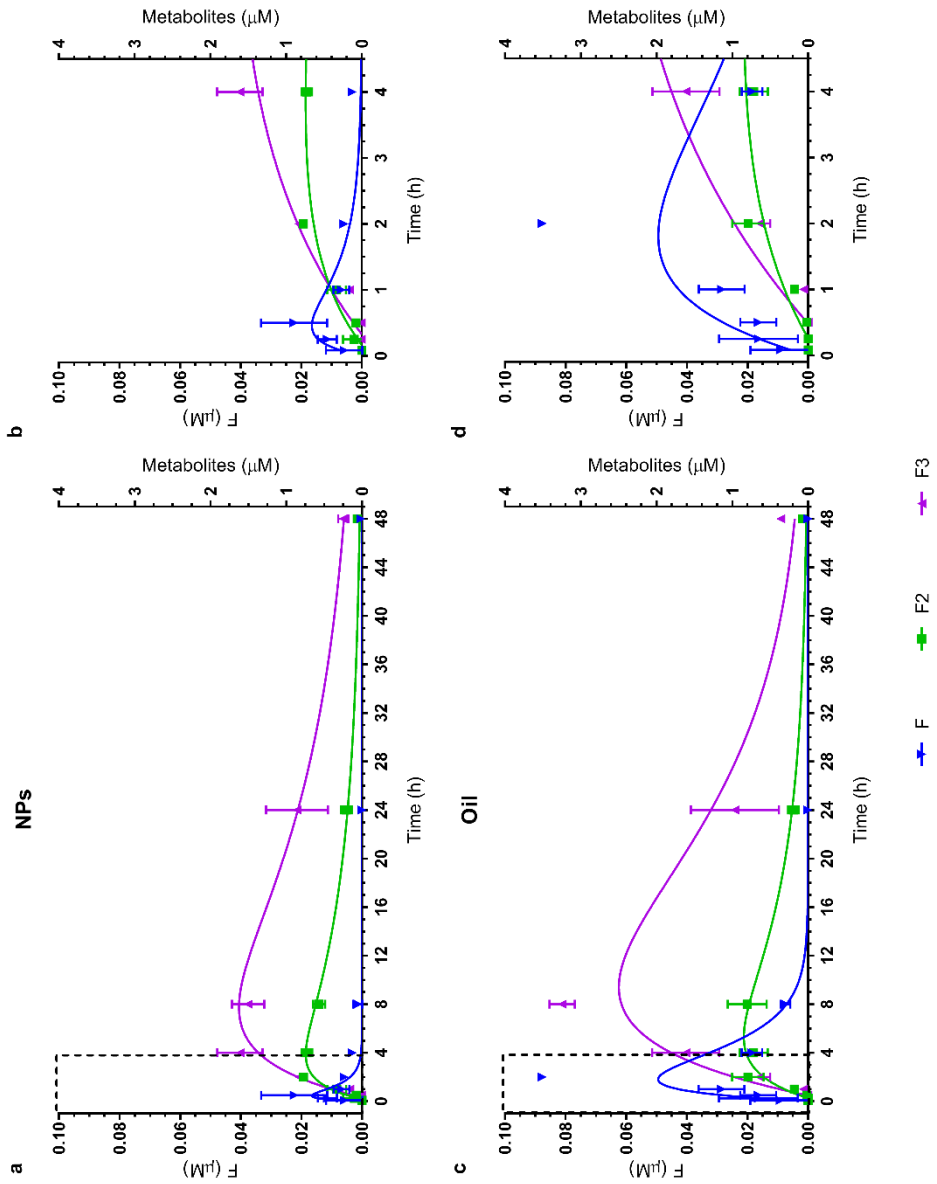

Figure 55. Pharmacokinetic profiles of F and its metabolites after oral administration. *A single dose of two different formulations of F were administered to CD-1 mice at 10 mg/kg. Plasma samples were collected periodically and analyzed by HPLC-MS/MS. (a) Pharmacokinetic profile of the oral administration of the nanoparticle formulation of F. (b) Amplification of the dotted region in (a). (c) Pharmacokinetic profile of the oral administration of the formulation of F in oil. (d) Amplification of the dotted region in (c). Error bars indicate standard deviation from 3 animals.*

DISCUSSION

F and its metabolites have been widely studied in relation to cancer treatment and prevention. Among their anticancer effects, HMs are of special interest because of the abundant literature in relation to F. They are a wide family of blood cancers with high incidence among different segments of the population. F has been described to have cytotoxic effects on both leukemia and lymphoma cell lines and has also been reported to reduce tumor growth *in vivo*. In particular, AML is the most common acute leukemia in adults and is one of the HMs with worse prognosis. In addition, F is supposed to possess many anti-inflammatory activities. Although we could only partially confirm these activities, the use of HM models have allowed us to study simultaneously both properties.

Firstly, we wanted to confirm the cytotoxic activity of F on hematologic cell lines and its dependence upon the type of HM. All tested cell lines were sensitive to the treatment with F, including the ones that presented GC resistance. In those cases, treatment with dexamethasone did not significantly induce apoptosis. As we discussed in the first chapter, there are many causes of GC insensitivity, such as the expression of low levels of GR, mutations in the receptor that alter its affinity for GC or its PTMs, or the expression of less active GR isoforms. These results might imply that the observed cell toxicity caused by F is not mediated by GR.

F showed the highest potency for the treatment of myeloid leukemia, as the lowest IC50 values were obtained for the following cell lines: MV-4-11, K562, TF-1, HL60 and THP1. Among these, the cytotoxicity on CML presented lower efficacy in comparison to AML, although only one cell line was tested. In THP1, F2 had the same effects as its precursor, while F3 presented a slightly higher IC50, confirming that both F metabolites are active. F appeared to act with the lowest potency on MM, although again more cell lines need to be assayed to confirm the results. The study of the effect of F and its metabolites on more cell lines could help to confirm if sensibility is definitely dependent on HM subtype and determine if it is influenced by any characteristic mutation.

APL is a specific subtype of AML that involves a translocation affecting RARα. Although F did not inhibit RARα *in vitro*, it showed cytotoxicity against HL60, a model of APL. It may indicate again that the induced cytotoxicity is not mediated by NRs. There are several other reports on the cytotoxicity of F on HL-60. In fact, other models of APL, such as HP50-2 and HP100, have been described to be even more sensible to F than HL-60. A research group reported an inhibition rate on HL60 at 72 h of 86.0% at 30 μM and 65.0% at 15 μM. Despite we measured cell viability by the same method, in our assays both concentrations resulted in viability inhibition above 90%. Others reported that at 12.5 μM reduced the cell viability to

around 10% after 48h of incubation, while F only achieved around 50% inhibition at that concentration. Oppositely, we described that for F at 12.5 µM and after 72h viability was approximately 10%. A research group described that F, Compound N and V reduced HL-60 viability at 5 µM after only 24h. In contrast, Compound A and Compound L only presented effects above 10 µM and 20 µM, respectively, while Compound B did no induce apoptosis in HL-60. A research group also reported very little viability reduction with Compound B in HL-60, while they calculated an IC50 for F around 12 µM after 24h. A research group reported the same effects on HTLV-1-infected T-cell lines. Accordingly, we observed that Compound L had a reduced effect on THP1, while Compound A and Compound B had no effect up to 10 µM at 72h. Noticeably, Compound A and Compound B did not inhibit GR nor AR transcriptional activity, contrarily to other ABCs. They also possess the lowest water solubility among the tested compounds. A research group confirmed that different ABCs presented different effects on malignant cells and it also depended on cell type. Interestingly, they postulate that algae extracts also had potential inhibitory effects on normal hematopoietic progenitor cells. Despite we and others have not observed this effect, it would be interesting to investigate whether it is related to the lymphocyte and platelet reduction observed in the RDT assay.

Not only F metabolites appeared to be more active in HL60, but also on PEL lines. A research group reported IC50 values in PEL lines at 24h of 2.4–3.3 and 1.1 µM for F and F2, respectively. F3 has also been proposed to have cytotoxic activity both in leukemia and lymphoma cell lines, although it has only been studied in mouse cells. Although we observed similar potencies of F, F2 and F3 on THP1, these results suggest that the activity of metabolites should be further studied.

In models of CML, as K562 or TK6, 10 µM of F has been reported to cause 25% cell death after 24h. In our assays, the estimated IC50 in K562 was 1.56 µM at 72h, although it only inhibited up to 66% cell growth. Similarly to APL, in K562 cells Compound B had low activity: only a 15% viability reduction at 10 µM and after 72h. However, Compound A at 10 µM decreased cell viability to 60% at 72h. Other reports in ALL suggest that F has an IC50 of 24.57 µM at 24h in CCRF-CEM cells, while Compound B and retinoic acid do not cause substantial cell growth, presenting IC50 values at 24h between 100-200 µM. Our assays in the same cell line roughly estimated an IC50 of 3.5 µM for F at 72h. In general, reported IC50s for F are higher than our observations. It is also true that most published studies have been performed at 24h, impeding the direct comparison of values.

Currently, there are multiple chemotherapy treatments available for hematologic disorders, including cytotoxic drugs and immunomodulators. Most of them are characterized by a lack of specificity and multiple off-target adverse effects. In contrast, F has been considered a

safe compound with no reported adverse effects after oral administration. However, effective concentrations on HM cell lines are apparently restricted to the low micromolar range. Even though there are examples of drugs that work in that range, such as the anti-estrogen tamoxifen, it could be considered that F might not have enough cytotoxic potency alone. Nevertheless, it could still have potential to be used in combined therapies. In fact, the combination of cytotoxic drugs with adjuvants that enhance their activity is a common strategy to reduce their adverse effects.

To study combined therapies we focused on MV-4-11. Although it is a macrophage cell line, it was initially established from a patient of mixed-phenotype acute leukemia, which shows features of both AML and ALL. The standard of care for AML is a combination of cytarabine with an anthracycline, whereas for ALL it is a multi-agent chemotherapy based on vincristine, corticosteroids and an anthracycline. Both treatments may also be followed by allogeneic stem cell transplantation. The aggressiveness of the treatment is sometimes intolerable for patients, mainly for elderly ones. In this way, we explored the possibility of combining F and first line cytotoxic drugs on MV-4-11: two nucleosides and one pyrimidine analog (cytarabine, gemcitabine and 5-fluorouracil), an intercalating agent (daunorubicin), a DHFR inhibitor (methotrexate) and an antiangiogenic and immunomodulatory compound (lenalidomide). In general, the observed effects were additive or slightly antagonistic at low concentrations. However, when we tested the combination of F and cytarabine in THP1 cells (model of AML) it resulted in moderate antagonism. Accordingly, THP1 were less sensitive than MV-4-11 to F.

The combination of F with some cytotoxic drugs has also been reported in literature with different outcomes. For instance, F has been combined with cisplatin, a DNA crosslinking agent, in the treatment of hepatomas. In this case, it further decreased cell proliferation via a NFκB-mediated pathway. In colon cancer, F potentiated the effect of 5FU (a pyrimidine analog), although it did not look synergistic. In the same way, in our studies F action on MV-4-11 increased the effects of 5FU and other nucleoside analogues at low concentrations, but without displaying synergy. Curiously, in breast cancer F has shown less activity than other ABCs when combined with the intercalating drug doxorubicin, although it also enhanced its effect. In our case, Compound B and Compound L had almost no effect against AML. In CML, F has been tested in combination with imatinib and doxorubicin. Although F proved to have antiproliferative effects, no differences were reported with the addition of the other drugs at their IC30. Similarly, we observed slight antagonism in the combination of F with daunorubicin, a similar anthracycline, in MV-4-11. F has also been tested as a chemosensitizer in colon adenocarcinoma. It acted synergistically with 8 cytotoxic drugs: doxorubicin (intercalating agent), vinblastine (tubulin binding), amphotericin-B (membrane pore formation), paclitaxel (tubulin binding), 5FU (pyrimidine analog), cycloheximide (translation inhibition), etoposide (topoisomerase inhibitor) and cisplatin (DNA crosslinking

agent). In this case, the effect was attributed to the inhibition of the MDR. However, we observed the contrary on MV-4-11 cells with 5FU and daunorubicin. Differences in the expression of MDR1 between the adenocarcinoma and the AML cell line might be responsible for this difference.

In summary, no synergy was observed or has been reported between F and cytotoxic drugs, although to confirm it a matrix of assays with more combinations of concentrations of the compounds should be carried out. If confirmed, it might indicate that their cytotoxic effects are mediated by very different pathways. To check it, it may be interesting to test the combination of F with other types of drugs in different cell lines, for instance with mitotic inhibitors as paclitaxel or with DNA-repair inhibitors as etoposide. Lately, a lot of efforts have been invested in developing kinase inhibitors. They could also be tested in combination with F. Furthermore, F activity has been compared to dexamethasone in several cell types, but no coincubation has been performed. The interaction between F and dexamethasone could also help to figure out whether F is modulating the GR (for instance by antagonizing dexamethasone), inducing apoptosis via the receptor or acting independently. Results from TNFα secretion suggested that there was no interaction between the two compounds. Apart from GCs, many NR ligands have shown synergistic effects with cytotoxic drugs. For example, RARα/β selective agonists have been reported to have synergistic antitumoral effects with taxol but not with other cytotoxic agents. A research group described that PPARγ ligands downregulate metallothioneins, which are involved in the resistance to platinum-based drugs such as cisplatin. Cisplatin cytotoxicity has also been reported to be increased by the PR and GR antagonist mifepristone, as it increases the intracellular accumulation of the drug. The reversion of drug resistance can also be achieved by antiandrogenic compounds. Therefore, if F modulated a NR to induce cell death, we would expect to probably see an interaction with some drug.

The fact that no synergy has been detected could also point to a non-regulated form of cell death. This would be supported by the relatively low caspase-3/7 activation detected in the apoptosis assay in MV-4-11. Moreover, the apoptotic process was slow and only from 48h were IC50 estimated values stabilized. At high concentrations (above 25 μM) the compound caused a rapid cell death. This event was represented by a decline in cell viability not paired with measurable cytotoxicity or apoptosis markers. Although it should be confirmed, it could probably be attributed to necrosis or fast-acting apoptosis. It is known that primary necrosis or catastrophic cell lysis normally takes place quickly after the addition of a toxic compound, while apoptosis proceeds over a longer period. We hypothesized that the former mechanism was taking place independently of cell type, as we have observed this behavior also with other non-hematologic cell lines. Moreover, we have experienced that concentrations above the solubility limit caused rapid cell death, probably attributed to physical damage caused by aggregates. In the case of non-regulated form of cell death,

however, we would have expected to clearly see cytotoxicity signal in absence of caspase activation, while they seemed to increase simultaneously. On the contrary, it has been extensively described that F is an apoptosis inductor. Several publications also sustain that the apoptosis induction is slow and time-dependent. Currently, replicates of the apoptosis assay are being performed to confirm or refuse the activation of the apoptotic pathway. Moreover, a protein array with varied apoptosis markers (apart from caspase 3/7) will be carried out. In the case of the confirmation of a non-regulated cell death, described antitumor effects of F may well be related to other effects in the tumor environment. For instance, the interaction of F with GR could avoid immunosuppression, which in can lead to the escape of immune detection and progression of tumor. The antitumoral effect of F could also be mediated by the described down-regulation of secreted TNFα. TNFα is known to be a regulator of apoptosis in leukemia. It is expressed by malignant cells and it is involved in cell transformation, proliferation and even in angiogenesis. Secreted and transmembrane TNFα are important mediators in the tumor microenvironment.

Despite no synergy has been observed between F and tested compounds, additive cytotoxicity could also help reduce the effective doses of the cytotoxic drugs, and therefore their side effects. Importantly, F has proved to be safe, mostly in oral administration, and we observed no major adverse effects in the intravenous RDT assay in mice. Another benefit would be an expected advantageous dose regimen of F. It might not need to be administered with high frequency, as we showed that in mice F metabolites were still detected at µM concentrations after 48h of an intravenous bolus administration. Current AML treatments with cytarabine consist on 7 days of continuous infusion, while ALL treatment includes long exposures to GCs. Although further studies are needed, reducing the administration frequency would therefore imply a reduction of side effects.

F has also been combined in literature with other substances to enhance its apoptotic effects. The PPARγ ligand troglitazone is an example. Their combination showed increased cytotoxicity on colon cancer cells, presumably in a synergistic interaction. We tested the effects of the combination of rosiglitazone, another PPARγ agonist that has been described to induce apoptosis in several HM cell lines. It resulted to have additive effects in the tested concentration range. We evaluated the combination of F with other NR ligands: ATRA (used in APL treatment) and calcipotriol (with potential applications in AML). Despite their combination indexes could not be calculated, the combination appeared to have an additivity or slightly antagonistic effect on cytotoxicity. Although they are not used in the treatment of HMs, we had previously tested the combination of F with mifepristone (PR and GR antagonist) and cyproterone acetate (AR antagonist) in THP1 monocytes. Subtoxic concentrations of both compounds did not cause any change in F cytotoxicity curve, but a wider range of concentrations should be tested to confirm the results. Preliminary results on the combination of F with the retinoid adapalene, which targets RARβ/γ, also showed no

interaction. Results were similar to the combination with ATRA, despite F displayed higher antagonism against RARγ than against RARα. Again, these data do not point to a NR-mediated apoptosis. Currently, ATRA is used in combination with arsenic trioxide for the treatment of APL. This combination is another option to be explored for F.

It has been repeatedly reported that F cytotoxicity is mediated by an induced arrest at G0/G1 phase. Interestingly, when we simultaneously measured viability and cytotoxicity induction in MV-4-11, a lapse between the reduction in the former and the appearance of the latter was observed after 72h. These slightly unpaired event is usually attributed to compounds that cause cell cycle arrest and alterations in cell division, without affecting cell integrity. In this case, antiproliferative effects would be detected for a sustained time before the detection of cytotoxicity, which implies membrane integrity-loss. To further investigate this, we studied the effect of F on monocytes' cycle by means of flow cytometry. Apparently, F caused an arrest at S phase at 48h and it was not until 78h that cytotoxic effects started to be perceived. Considering that the assay was carried out at 1.3 μM of F (around 90% viability in THP1), it is consistent with the results of the apoptosis assay. Results should be confirmed with longer exposure times and more replicates. It would also be interesting to synchronize the cell culture before adding the ABC. In contrast, a research group had described that F and FOH at its IC50 induced G1 cell cycle arrest in PEL cell lines, although they only checked it after 24h. The same effects have been reported for HTLV-1-infected T-cell lines and lymphoma cell lines, also after 24h. Notably, in other cell types F has been shown to induce cell cycle arrest by upregulating p21(Cip1) and p27(Kip1). These factors are potent inhibitors of CDKs and cyclins in multiple cell types and also mediate the cell cycle arrest at G0/G1produced by GCs. We are currently working on the determination of the effect of F on different cell cycle regulatory proteins, to improve our understanding of the effects of the ABC. For instance, the activation of Chk2 kinase can lead to arrest at G1 or G2, among other functions. Preliminary results on THP1 suggest that F induced a partial inactivation of the protein, detected by Chk2 phosphorylation at T68. We have also detected a notable increase in the expression of Hsp60 when THP1 cells are incubated with F at its IC50 for 72h. Although it needs to be confirmed, this protein has been reported to accelerate the activation of caspase-3 during apoptosis in lymphocytes and is known to play different roles in cancer. Additionally, in an exploratory study F seemed to partially inhibit the Wnt-β-catenin pathway, measured by the expression of a reporter gene under control of the Lymphoid Enhancer Factor/ T-Cell Factor (LEF/TCF) response element in a colon cancer cell line. β-Catenin regulates cell-to-cell adhesion and has been associated with many types of cancers. In fact, it has been reported that F and F2 downregulate the expression of β-catenin in osteosarcoma and PEL cell lines, arguing that this event is related to the induction of apoptosis. F effects on the regulation of intracellular calcium levels could also be related to its influence on cell cycle.

ABCs are natural products known for being extremely hydrophobic molecules that rapidly undergo oxidation. Current formulations of ABCs are mostly in lipid-based compositions, which limits their administration to oral delivery. To allow new delivery routes and enhance bioavailability and stability, some efforts have been made to obtain a water-based ABC formulation. Emulsions, cross-linking agents and peptides have been tested with limited exit. In contrast, albumin NPs have been extensively studied as drug carriers with promising results. Albumin is the most abundant plasma protein in mammals. It possesses a large ligand binding capacity and is a natural transporter of some metabolites. We examined the possibility of using albumin as a delivery system for ABCs in an aqueous formulation. The F-BSA NPs obtained by the described desolvation method achieved total ABC solubilization in water, even at high concentrations. This represents an important improvement as it allows F to be administered intravenously and avoid the first-pass metabolism observed in oral administration.

A desolvation protocol for NP production was developed based on literature and the obtained NPs were characterized. Two of the different ratios of F:albumin tested resulted in small MPD (around 60 nm), homogenous size distribution and good entrapment of F. Among them, the ratio containing the lowest amount of albumin was selected, as it will probably ease the production process and enable a more economically viable procedure. Moreover, it will have special importance when BSA is substituted for HSA. Due to material availability, process development was not directly carried out with HSA. Despite BSA and HSA share a 75.6% sequence identity and a strongly similar three-dimensional structure, different epitopes have been identified that confer allergenicity. Although it is considered a safe ingredient in the food industry, its use is not suitable for intravenous administration. An initial test to substitute BSA with HSA gave promising results with our protocol. However, preparation procedure was only scaled up with BSA. Furthermore, the procedure needs to be scaled up to higher volumes than 10 mL to obtain enough material to carry out *in vivo* efficacy assays. It is of special importance the final filtration step, as it helps to ensure sample homogeneity, as well as it sterilizes the preparation. In prospect assays, free and bound albumin will also be measured to determine the ratio of F:bound-albumin and, thus, characterize the entrapment of the ABC. A first estimation could be obtained from the DLS measures. A better final characterization of the NPs is essential to ensure batch consistency.

Although extended stability studies are needed, data on F content of four different batches overt time was obtained. Unexpectedly, dried samples presented the highest degradation rates of the ABC. While it is true that the used drying method (vacuum-drying) can influence stability, we have hypothesized that ABC loss was caused by higher contact with oxygen. Degradation of F among dried samples was also higher with the increase in temperature, supposedly as major molecular mobility favors oxidation. Some batches have already been stored as powder under a nitrogen atmosphere and will be compared with these data to

prove the hypothesis. Alternative drying methods, as freeze-drying are also under evaluation.

So far, we concluded that around 30% of F is lost in the NPs suspended in water after 4 months, if samples are preserved at -20ºC or 4ºC and protected from light. Surprisingly, there were no major differences between storage temperatures in terms of ABC degradation among liquid samples. Presumably albumin stability would be limiting in this context, as NPs at RT experimented precipitation. Contamination of samples should also be assessed in the future, to discard its influence on the stability studies.

Other parameters that should be evaluated more carefully in stability studies are MPD and Z-potential (only preliminary results have been described). Changes in both physical parameters over time determine the stability of NPs. For instance, a progressive increase in MPD and decrease in the absolute value of the Z-potential could indicate gradual particle aggregation, which probably would lead to precipitation. Furthermore, changes in NP size, shape or surface can alter its biodistribution and clearance rate. It is also known that NPs up to 100 nm enter easily to cells, while slightly negative charged NPs tend to accumulate more efficiently in tumors. It would also be interesting to follow the stability in terms of aggregation of the F-BSA NPs in other environments, such as in plasma.

Importantly, F-BSA NPs were tested against GR in the same assays described in the first chapter. In particular, NPs proved to keep the inhibitory activity of F on GR(LBD) transcription in an assay that used a chimeric receptor and a fluorescent reporter gene. Results are not shown because assays were not performed with the final NP formulation (ratio F:BSA and concentration) and should be further confirmed.

Simultaneously to our development of the ABC-albumin NPs, a research group described the formation of similar NPs, which comprised F and albumin, β-lactoglobulin or α-lactoalbumin. This fact highlights the need to find a suitable carrier for F and ABCs in their use for human health applications. Interestingly, they explored in depth the interaction between F and albumin and determined that it occurred spontaneously and was driven by hydrogen bonds and van der Waals forces. They reported that BSA undergoes changes in secondary structure that lead to partial unfolding, which supports the idea that NPs are formed by aggregation and protein-protein interactions. Presumably, BSA presented only one binding site for F around an aromatic residue. They also defend that F binding affinity for BSA was higher than for other whey proteins, which would reinforce the idea that albumin would be a suitable nanocarrier. On the other hand, they tested F:BSA molar ratios ranging from 0.5:1 to 3:1; while we tested molar ratios from 5:1 to 100:1, concluding that 10:1 or 20:1 presented the best properties (corresponding to 1:5 and 1:10 w/w ratio). In this case, we have shown that the use of lower BSA amounts is possible. Increasing F loading in NPs enables to obtain a more concentrated formulation, which is beneficial for an easier administration. Although

both protocols include a final filtration step, they obtained NPs with a mean diameter of 200 to 300 nm with PDI around 0.3, whereas we obtained NPs around 65 nm with PDI below 0.2. The lowest molar ratio that we tested, 5:1 (equivalent to 1:20 w/w) is rather close to the ratios described. Interestingly, it displayed a biphasic distribution of diameters, similarly to their reported measures. It might indicate that low molar F:BSA ratios form NPs with wider particle size distributions and higher MPDs. In both cases control NPs presented low MPD and high PDI, presumably due to the presence of free albumin. Contrarily to their reports, we did not observe an increase in particle diameter with the increase in F concentration, except for the highest tested molar ratio of 100:1 (equivalent to 1:1 w/w). It could suggest that greater aggregation of albumin with increasing F concentrations can happen only at low or high molar ratios (below 3:1 and above 100:1).

After obtaining a nanoparticle aqueous formulation for F we studied its toxicity in mice. Repeated intravenous doses of the preparation were administered daily to immunocompetent mice for 5 days. In general, the formulation was well tolerated at the dose range tested and under the defined administration pattern. Therefore, the maximum tolerated dose could not be determined. NOAEL was established at 30 mg/kg/day. A research group had previously established that the 50% lethal dose in mice for orally administered F was above 2000 mg/kg in an acute administration, and above 1000 mg/kg/day in RDT studies. Although they did not study the bioavailability of F from their formulation, it is known that F is not well absorbed when administered orally. In fact, we observed very low concentrations of F in plasma in the pharmacokinetic studies after oral delivery, while metabolite levels achieved were of the same order as after intravenous administration. Evidently, the oral MTD is expected to be higher than the intravenous MTD. These results, along with the fact that F-containing algae are present in many diets, indicate that F is generally safe for both oral and intravenous administration.

The hematologic analysis of animals treated in the RTD assay revealed an imbalance in white cell population that involved no toxicity. The population of WBC was displaced towards granulocytes, in detriment of lymphocytes. Reduction of lymphocyte viability had been previously reported, but only for high concentrations of F in *in vitro* studies, as well as a modulating effect on their differentiation. Interestingly, lymphocytopenia is associated with the acute administration of GCs, mainly due to the redistribution of circulating lymphocytes and partially due to GC-induced apoptosis. The administration of GCs also induces a decrease in monocytes and eosinophils, contrarily to what we observed (although differences in medium size cells and granulocytes counts were not significant, it is probably due to the high variability present in this minor blood cell populations). Curiously, among

the tested HM cell lines, lymphocytes and its precursors were in general less sensitive to F than the myeloid lineage.

Another important finding associated with the treatment was a dose-dependent decrease of platelets, although values were inside the reference range. All associated morphological parameters were normal, discarding a defective production. Splenic enlargement was not observed post-mortem, so it was also rejected to have caused an increased breakdown of platelets. No more information is available to distinguish between decreased platelet production in bone marrow, increased peripheral destruction or abnormal distribution. Again, the behavior was contrary to effects of GCs, which are known to cause thrombocytosis.

In the same RDT study different metabolic parameters were measured. The major observed F effect was an important lipid mobilization with no concomitant change in body weight. Upon longer treatment times animals might experiment a suppression of body weight gain in comparison to control, as has been reported. Since in our study body weight was stable, changes in the plasma lipid profile must be related to liver function or hormonal alterations. Notably, differences in metabolism between species are high and it is difficult to correlate observed effects with potential consequences in humans. Indeed, F effects on lipid metabolism have been extensively reviewed. As reported, we detected a reduction in plasma triglycerides, along with a slight increase in total cholesterol. However, the distribution of cholesterol in the different lipoproteins was not characterized. A research group also described a rise in cholesterol and phospholipids in their oral RDT study, although they detected no alteration of triglycerides. Precisely, the administration of GCs induces cholesterol synthesis. In general, F has been described to regulate lipid and glucose metabolism and uptake in adipocytes, but also to inhibit intestinal lipid absorption. The lipid reduction is probably mediated by downregulation of hepatic fatty acid synthesis enzymes. Nevertheless, drug toxicity can also decrease triglyceride production by inducing liver vacuolation, which should be checked in a histology study. Lipid mobilization could also be related to the regulation of PPARγ, which is a key TRF of lipid metabolism. As exposed in Chapter 1, it has been described that F regulates its expression and we observed that F partially inhibited its transcriptional activity. GCs also have a permissive effect on the action of lipolytic hormones, as catecholamines, leading to the redistribution of fat. However, it usually happens upon long exposures to GCs.

Although F has been described to have protective effects against hepatotoxicity, we detected an increase in total bilirubin in mice treated with the highest dose. It was presumably caused by an increase in unconjugated bilirubin. Different processes can lead to this effect. RBC count and related parameters were normal, therefore an increased erythrocyte destruction cannot be the cause. Contrarily, it has been previously reported that

F causes eryptosis (suicidal death in erythrocytes). As the other liver function markers were normal, the most probable explanation is an altered bilirubin metabolism related to drug inhibition of metabolizing enzymes, as well as inhibition of glucuronidation and consequent bilirubin excretion. Therefore, the effect of F on the most common metabolizing enzymes should be assessed. In fact, a research group reported that Compound A is a potent inducer of CYP1A in rats, while in human hepatocytes it induces CYP3A4 and CYP2B6. Moreover, in the first chapter we described how F interacted with the PXR, which regulates the expression of CYP3A4. Cytochrome induction was also proposed to have caused liver weight gain in an oral toxicity study in mice. Although in this study an increase in bilirubin was also detected, it was suggested to be an artifact of the detection method. They postulated that F2 present in plasma had increased absorbance at 450 nm, where bilirubin was read. However, we determined bilirubin by a different method (Diazo method) with an endpoint at 540 nm, which showed no interference in the mentioned study. The low oral absorption of F in comparison with the intravenous delivery could be the cause of the observed differences in bilirubin quantification.

Again, it is not clear whether renal injury is altered or not in the highest dose treatment group. Albumin values are not reliable due to the composition of the injected formulation. Interestingly, plasma albumin has been reported to slightly decrease inside the normal range in oral RDT studies with F. Moreover, without a reference value of control animals no conclusions can be extracted. The analysis of urea would also help to clarify this, as alterations of blood urea nitrogen within normal limits have been reported in oral studies. In the same studies, no alteration of creatinine was reported. Oppositely, we detected an increase in creatinine, although it is not a highly reliable marker, as it is known to vastly depend on the diet and data on a control animal was not available. Moreover, creatinine determination was performed by Jaffe reaction, which is known to present many interferences. Determination by enzymatic reactions should be carried out, as it is generally more reliable.

Apart from the described findings, no major macroscopic changes were observed during animal necropsies. Biochemical and hematologic results should be accompanied by histopathological studies, especially from the liver and kidneys. However, no abnormalities are expected, as in previous oral studies no anomalies have been reported.

It is clear that extended toxicology studies are needed that include more animals per dosage, as well as that cover a wider range of doses. It would be interesting to perform the studies in rats, as the reference values are better established in this specie. Moreover, hematologic and biochemical analysis should be performed also around 7 days after last administration, in order to investigate whether the observed effects remain, or the animals recover rapidly. In addition, further toxic effects could also appear with longer exposures.

The last parameter analyzed in the RDT study was F biodistribution. Importantly, we detected the presence of F3 in the brain of mice treated with the highest dose. Although it has been previously suggested that F can cross the brain-blood barrier and exert protective effects on the brain, it is the first experimental direct evidence that supports this model. Other ABCs, such as Compound A, have also been shown to penetrate the barrier and accumulate in the brain. Further studies are needed to determine which compound (F, F2 or F3) crosses the brain-blood barrier and if any metabolic step takes place in the brain. It would be then necessary to assess whether the detected concentration of F or its metabolites is enough to exert protective or therapeutic effects and whether this concentration would also be reached after oral administration. We also detected the presence of F3 in mouse pancreas. In fact, it has been proposed that pancreatic esterases and lipases hydrolyze F into F2. Despite at present we have not been able to analyze other tissues, a research group reported that F and its two metabolites were detectable in different organs (liver, lung, kidney, heart, spleen and adipose tissue) after one week of oral administration. In contrast, F was not detected in plasma. Interestingly, we also have preliminary data on a pilot study were a MV-4-11 tumor was implanted subcutaneously to mice. Results indicate that intravenous daily administration of F at 30 mg/kg for 4 days leads to F3 being detected in the tumor in the order of 0.5 nmol/g. However, efficacy in tumor reduction has not yet been properly assessed.

Once established that F was not toxic up to 30 mg/kg by *in vitro* administration, we explored its pharmacokinetic profile in different formulations in oral and intravenous administration. The aqueous nanoparticle formulation presented clear advantages in intravenous administration when compared to PEG-DMA. Although this vehicle had been previously tested and reported no toxicity, when it was used for F administration the formulation caused necrosis in the tail of most animals, as well as the death of one of them before 48h. Presumably, it was caused by F precipitation in veins upon injection that might have led to thrombosis. In contrast, NPs ensured a good solubilization of F and caused no major adverse effects. The obtained pharmacokinetic profile for both formulations was very similar, although the resulting half-life of F and its metabolites was lower in the NPs. A research group published a pharmacokinetic study of F in rats after a single intravenous bolus administration at 2 mg/kg. Although they don't specify the formulation used, maximal concentration of F2 (1 μM) was achieved after 1h, whereas we observed a maximum peak after 3.7h for NPs and after 4.8h for PEG-DMA. By administering a 5 times higher dose of F, we achieved a C_{max} of the metabolite between 4 and 5 times higher. They also reported a half-life of 2.3h for F and of 11.9h for F2. In this case, values are similar to what we described for the NP formulation in mice.

In oral studies, F appeared to suffer first-pass metabolism: it was metabolized by the gut and liver before reaching systemic circulation. Therefore, very low concentrations of F were detected in plasma. In contrast, its metabolites were detected at similar levels as in intravenous administration. The low oral bioavailability will probably prevent F from reaching systemic effective concentrations by oral delivery. On the other hand, if the activity of metabolites is confirmed, it could still be a possible administration route. In this case, oil formulation showed better absorption of the compound than NPs, with higher maximum concentrations and extended apparent half-lives. Notably, the oil composition used was based on caprylic/capric triglyceride and contained C8 and C10 fatty acids that have been reported to increase absorption of ABCs. A research group also studied the pharmacokinetic parameters of F in rats after intragastrical administration. They administered F at 65 mg/kg in an undetermined formulation. After 7.7h a maximal concentration of 44 nM of F was detected, while F2 achieved a concentration ten-fold higher in 11h. In our experiments, absorption was faster and maximal F concentration was of 20-50 nM at 0.5-2h after administration, depending on the formulation. F2 also reached higher levels in plasma (around 800 nM in 3.7-5h), although initial dose was 6.5 times lower. Reported half-lives were similar to the parameters we obtained from the oil formulation 1.2h (F) and 9.3h (F2). A research group also administered 0.83 µmols of F to rats and reported a concentration of 274 pM of F2 after 8h. In our case, 8h after the administration of 0.46 µmols, F2 levels in plasma were 0.6-0.8 µM. All these differences in pharmacokinetics might be due to interspecies variances in metabolism. Pharmacokinetic studies of oral delivery to mice have also been published. In general, maximal concentrations of F and metabolites were achieved after 4-6h, although in some cases F was not detected. In these studies, F2 presented a half-life between 4-6h, while F3 lasted longer in plasma ($t_{½}$ 6-8h). In our case, however, very different half-lives were estimated (Table 35). In general, plasma concentrations of F3 were higher than F2, in agreement with our results.

Two studies have been published of oral administration to humans of F-containing algae**.** In both reports neither F nor F3 were detected in plasma, whereas F2 was present at maximal concentrations 4h after ingestion and with a half-life of 7h. Interestingly, differences between rodent and human F metabolism have been suggested. F3 has been reported to be a metabolite of F in rodents and to be also produced by human hepatocytes upon F incubation. However, it has not been detected *in vivo* in humans. Instead, the cis-isomer of F2 has been proposed as a possible alternative metabolite. Compound A, for instance, has been reported result in the production of different metabolites when administered to a cell culture or to rodents as a result of the induction of different cytochromes.

To sum up, F showed cytotoxic activity against several HM cell lines. It did not show synergy with tested standard of care drugs, but it could help to reduce their adverse effects by reducing the dosage needed. The metabolites F2 and F3 also presented activity in the same range in one tested cell line. Compound A and Compound B were the least active ABCs, which correlates with our findings in the inhibition of GR and AR transcriptional activity. It is not clear whether the observed cytotoxicity is due to apoptosis or cell cycle arrest and more investigation is needed regarding cell cycle markers. With the prospect of carrying out an *in vivo* efficacy assay of F in AML, we have developed a nanoparticle formulation of F that allows to deliver it in an aqueous preparation. Although extended stability studies of NPs are needed, preliminary data is favorable. The obtained formulation presumably allows a safe intravenous delivery, although an oil formulation proved to be more suitable for oral administration. No general toxic effects were observed due to the administration of up to 30 mg/kg/day of F. However, F effect on lymphocytes and platelets should be further evaluated. Bilirubin and creatinine determinations also need to be repeated to discard hepatoxicity and renal injury.

GENERAL DISCUSSION AND FUTURE PROSPECTS

In the last decade, the study of F has attracted considerable attention and it is now one of the most studied ABCs. It has been described to have many interesting properties with potential applications in human health. Nevertheless, there is no general agreement in its mechanism of action, since multiple signaling pathways have been reported to be involved in F actions. In this project, we proposed a new line of research by assessing the possibility that F acted as a NR modulator. We also pretended to confirm the potential application of F in the treatment of HMs. For that, we had to develop and test a new formulation of F based on albumin NPs.

In this work, we described how F and other ABCs modulate the transcriptional activity of different NRs in *in vitro* models. However, the mechanism of the modulation remains unclear, aside from the fact that F appears to interact with the LBD, albeit not in the steroid's pocket. It has not been confirmed either, whether this interaction takes place *in vivo* and to which extent it influences cell's functioning. Interestingly, in our assays, effective concentrations of NR inhibition in incubations up to 24h were within the low micromolar range, concurring with the estimated IC50s at 72h for several malignant cell lines. Indeed, several NR ligands, such as ATRA or RGZ, are known to induce apoptosis in HM cell lines. Nevertheless, we have not been able to correlate both events in the case of F. The activation of the apoptotic pathway in the observed cell death should also be further confirmed. Moreover, F affected both GR-sensitive and GR-insensitive lines, and no synergy has been observed between it and tested cytotoxic drugs, as happens with mifepristone or anti-androgens. In any case, F appears not to act as a classical GR ligand (agonist or antagonist), but to do so as a coregulator. It probably interacts with an unknown site in the LBD to inhibit receptor transactivation, although it does not affect nuclear translocation or intracellular levels of GR. F has been reported to have important anti-inflammatory effects, which could correspond to GR transrepression activity. In our set up, however, we could not confirm this activity beyond the inhibition of TNFα secretion. Most probably then, the observed effects are a combination of different mechanisms of action, among which there could be the modulation of different NRs. Indeed, in the past years different new mechanisms of action have been described for NRs. In the case of GR, F could be influencing its non-genomic effects or ligand-independent activation.

Independently of the mechanism of TNFα modulation, the combined properties of TNFα regulation and cytotoxicity on HM cells support the potential of the application of F in cancer prevention or treatment. It is widely described that inflammation is a critical component of tumor development and progression. Tumor microenvironments are largely created by inflammatory cells and mediators, which promote proliferation, survival and invasion. In fact, tumor cells use immune signaling molecules, such as chemokines and their receptors, for migration and metastasis. Inflammation is also a key factor in determining response to therapy. Nowadays, many new therapeutic approaches target inflammatory mediators or

seek an anti-inflammatory effect, both for prevention or treatment of cancer. In particular, in the case of hematologic malignancies, chronic inflammation is considered one of the possible causes of the disease development. Many inflammatory cytokines are characteristically high in patients with HMs and have been related to disease progression and worsened prognostic. TNFα, for instance, is one of the main factors of the inflammatory niche in the tumor microenvironment, where it is involved in cell transformation, proliferation and regulation of apoptosis of leukemia cells. Notably, its expression is enhanced in malignant cells. Therefore, the inhibition of TNFα secretion could contribute to F direct anti-carcinogenic activity *in vivo*. Other effects of F in the secretion of mediators in the tumor environment has not been discarded and could even be the result of an interaction with NRs. For instance, GR is known to induce the secretion of immunosuppressors that favor tumor progression.

Both in our results and in literature, F metabolites (F2 and F3) have shown to share some of F's bioactivities. In terms of inhibition of NR transcriptional activity, F and F3 showed higher effects on GR compared to F2. Contrarily, F3 was the most potent against AR and also showed the highest binding affinity, while F and F2 had comparable activities. F3 was also the most effective in inhibiting PR and MR. Curiously, F3 has been found to be more active in regulating adipogenesis and adipocyte differentiation than F2, partially because it accumulates in the adipose tissue. However, F3 showed the lowest cytotoxic potential when tested in THP1 cells, while F and F2 had the same effect. Accordingly, a research group described that F2, F and F3 had increasing IC50s in human prostate cancer cells. All these activities are of high interest given that F has been shown to have low oral bioavailability. Furthermore, according to our study in mice, F has a relatively short half-life in plasma after intravenous administration. Considering that we have observed that cytotoxic effects appear slowly (IC50 is not stable until 48h) and that TNFα inhibition is detected after 24h, it is probable that a single intravenous bolus is not enough to exert anti-cancer effects. However, the metabolites have shown much longer half-lives in plasma and have been described to accumulate in different tissues. Although F biodistribution and accumulation in tissues should be further assessed, the fact that the metabolites show comparable bioactivities could solve the issue of efficacy. Most of the existing *in vivo* assays are based on the oral administration of F. In view of the low oral bioavailability of the compound and that it has been described to be present only at low concentrations in tissues, it is possible that the multiple reported effects *in vivo* are mostly owed to the metabolites and not to F itself.

In addition to keep working with the metabolites, next steps in this ongoing work should include to gain more insight in F modulation of GR. F effects on GR knock-out cell models should be assessed. An interesting parameter to measure would be secreted and transmembrane TNFα, as well as examining intracellular TNFα levels. The crystal structures

of F and F3 in complex with GR and AR are currently being analyzed to establish their putative regions of interaction, which could help to better comprehend the modulation of the receptors. It could also shed some light on the ABC structural features that are implicated in the interaction. In this way, more potent, effective or selective derivatives might be designed. Furthermore, the interaction between F3 and AR presents many potential clinical applications, such as prostate cancer and breast cancer. Even in cosmetics, anti-androgens are promising compounds for the treatment of alopecia, hirsutism or acne.

Apart from that, we would also like to strengthen our understanding on the regulation of other NRs with potential applications in healthcare. It would be of special interest to further study F interaction with PPARγ, since it is a main regulator of lipid metabolism and we observed important effects on lipid mobilization *in vivo*.

Finally, to determine the applicability of F and its metabolites in the treatment of HMs, it is necessary to carry out an *in vivo* study of its efficacy. For the moment, we are testing further combinations of F with cytotoxic drugs. Since no synergy is expected, the efficacy assessment will be probably carried out with F in combination with a standard-of-care drug, with whom F had shown additive cytotoxicity. Testing other formulations, besides the albumin NPs, is also included in our agenda.

CONCLUSIONS

After discussing all the results of this thesis project, the following conclusions have been reached:

1. F inhibits the transcriptional activity of several NRs in *in vitro* models in the low micromolar range. It inhibits ERα, ERβ, ERRα, GR, MR, PPARγ and RXRα and, with less potency, AR, PR, RARγ and RXRβ.
2. F interacts with the dexamethasone-bound GR and the DHT-bound AR, but not with the Apo-GR. Results suggest that it binds to the LBD but not to the ligand pocket.
3. F interacts with PXR. Together with literature, it suggests a regulation of cytochrome expression.
4. F does not promote GR translocation and does not alter its expression or degradation in HaCat cells. F does not avoid dexamethasone-induced translocation of the receptor or affect receptor's levels when combined with dexamethasone.
5. F does not repress or activate the transcription of glucocorticoid-regulated anti-inflammatory genes in mouse macrophages. It does not antagonize dexamethasone activity either.
6. TNFα secretion in mouse macrophages and human monocytes is repressed by F, although not in a dose-dependent manner.
7. In *in vitro* models, F3 inhibits the transcriptional activity of steroid NRs (GR, AR, PR, MR and ERα) with different potencies and efficacies in the low micromolar range. Specifically, it interacts with the LBD of dexamethasone-bound GR, Apo-GR and DHT-bound AR.
8. F2, F4, L and N inhibit the transcriptional activity of the GR in the low micromolar range in an *in vitro* model.
9. Compound A and Compound B are the least active ABCs among the tested ones, in terms of *in vitro* inhibition of the transcriptional activity of GR and AR, as well as cytotoxicity on THP1 cells.
10. F has cytotoxic activity on hematologic malignant cells in the low micromolar range, independently of their glucocorticoid sensitivity. However, it does not show synergic cytotoxicity with cytarabine, 5-fluorouracil, daunorubicin, gemcitabine, lenalidomide, methotrexate, all-trans retinoic acid, calcipotriol or rosiglitazone in cell models of acute myeloid leukemia.
11. F3 has cytotoxic activity on cell models of acute myeloid leukemia but shows no synergy with cytarabine.
12. The described desolvation method plus a filtration step allow to solubilize F in water and to obtain a sterile and monodisperse NP formulation suitable for intravenous administration.
13. The described F:albumin NPs do not cause major adverse effects in mouse after 5 days of daily intravenous administration at 30 mg/kg. However, they have an

immunomodulatory effect by stimulating the proliferation of granulocytes in detriment of lymphocytes and dose-dependently down-regulating platelets. They also cause lipid mobilization by promoting an increase in total cholesterol, while reducing triglycerides.

14. F3 reaches the mouse brain after intravenous administration of F.
15. F formulation in caprylic/capric triglycerides shows a better pharmacokinetic profile in mouse than the described F:albumin NPs when administered orally. Albumin NPs, though, are more suitable for intravenous administration to mouse than the solubilization of F in a PEG-DMA vehicle.
16. F has a very low oral bioavailability. Results suggest that to reach effective F concentrations in plasma the administration should be intravenous.

REFERENCES

1. Sever R, Glass CK. Signaling by Nuclear Receptors. Cold Spring Harb Perspect Biol. 2013 Mar 1;5(3):a016709–a016709.

2. Francis GA, Fayard E, Picard F, Auwerx J. Nuclear Receptors and the Control of Metabolism. Annu Rev Physiol. 2003 Mar;65(1):261–311.

3. Perissi V, Rosenfeld MG. Controlling nuclear receptors: the circular logic of cofactor cycles. Nat Rev Mol Cell Biol. 2005 Jul;6(7):542–54.

4. Noy N. Ligand Specificity of Nuclear Hormone Receptors: Sifting through Promiscuity. Biochemistry. 2007 Nov;46(47):13461–7.

5. Bookout AL, Jeong Y, Downes M, Yu RT, Evans RM, Mangelsdorf DJ. Anatomical Profiling of Nuclear Receptor Expression Reveals a Hierarchical Transcriptional Network. Cell. 2006 Aug;126(4):789–99.

6. Laudet V, Auwerx J, Gustafsson J-A, Walter Wahli. A Unified Nomenclature System for the Nuclear Receptor Superfamily. Cell. 1999 Apr;97(2):161–3.

7. Patel HK, Bihani T. Selective estrogen receptor modulators (SERMs) and selective estrogen receptor degraders (SERDs) in cancer treatment. Pharmacol Ther. 2018 Jun;186:1–24.

8. Weikum ER, Knuesel MT, Ortlund EA, Yamamoto KR. Glucocorticoid receptor control of transcription: precision and plasticity via allostery. Nat Rev Mol Cell Biol. 2017 Mar 5;18(3):159–74.

9. Lewis-Tuffin LJ, Jewell CM, Bienstock RJ, Collins JB, Cidlowski JA. Human Glucocorticoid Receptor β Binds RU-486 and Is Transcriptionally Active. Mol Cell Biol. 2007;27(6):2266–82.

10. Kino T, Manoli I, Kelkar S, Wang Y, Su YA, Chrousos GP. Glucocorticoid receptor (GR) β has intrinsic, GRα-independent transcriptional activity. Biochem Biophys Res Commun. 2009;381(4):671–5.

11. Marino JS, Stechschulte LA, Stec DE, Nestor-Kalinoski A, Coleman S, Hinds TD. Glucocorticoid Receptor β Induces Hepatic Steatosis by Augmenting Inflammation and Inhibition of the Peroxisome Proliferator-activated Receptor (PPAR) α. J Biol Chem. 2016 Dec 9;291(50):25776–88.

12. He B, Cruz-Topete D, Oakley RH, Xiao X, Cidlowski A. Human Glucocorticoid Receptor beta Regulates Gluconeogenesis and inflammation in mouse liver. Mol Cell Biol. 2016;36(5):714–30.

13. Oakley RH, Jewell CM, Yudt MR, Bofetiado DM, Cidlowski JA. The Dominant Negative Activity of the Human Glucocorticoid Receptor β Isoform. J Biol Chem. 1999 Sep 24;274(39):27857–66.

14. Kino T, Su YA, Chrousos GP. Human glucocorticoid receptor isoform β: recent understanding of its potential implications in physiology and pathophysiology. Cell Mol Life Sci. 2009;66(21):3435–48.

15. Lange P De, Segeren CM, Koper JW, Cells T, Lange P De, Segeren CM, et al. Expression in Hematological Malignancies of a Glucocorticoid Receptor Splice Variant That Augments Glucocorticoid Receptor-mediated Effects in Transfected Cells Expression in Hematological Malignancies of a Glucocorticoid Receptor Splice Variant That Augm. Cancer Res. 2010;3937–41.

16. Beger C, Gerdes K, Lauten M, Tissing WJE, Fernandez-Munoz I, Schrappe M, et al. Expression and structural analysis of glucocorticoid receptor isoform gamma in human leukaemia cells using an isoform-specific real-time polymerase chain reaction approach. Br J Haematol. 2003 Jul;122(2):245–52.

17. Ramamoorthy S, Cidlowski JA. Exploring the Molecular Mechanisms of Glucocorticoid Receptor Action from Sensitivity to Resistance. In: Endocrine Development. 2013. p. 41–56.

18. Presul E, Schmidt S, Kofler R, Helmberg A. Identification, tissue expression, and glucocorticoid responsiveness of alternative first exons of the human glucocorticoid receptor. J Mol Endocrinol. 2007 Jan 1;38(1–2):79–90.

19. Kadmiel M, Cidlowski JA. Glucocorticoid receptor signaling in health and disease. Trends Pharmacol Sci. 2013;34(9):518–30.

20. Kirschke E, Goswami D, Southworth D, Griffin PR, Agard DA. Glucocorticoid receptor function regulated by coordinated action of the Hsp90 and Hsp70 chaperone cycles. Cell. 2014;157(7):1685–97.

21. Echeverria PC, Picard Didier D. Molecular chaperones, essential partners of steroid hormone receptors for activity and mobility. Biochim Biophys Acta - Mol Cell Res. 2010;1803(6):641–9.

22. Pratt WB, Galigniana MD, Harrell JM, DeFranco DB. Role of hsp90 and the hsp90-binding immunophilins in signalling protein movement. Cell Signal. 2004;16(8):857–72.

23. Pratt WB. The role of heat shock proteins in regulating the function, folding, and trafficking of the glucocorticoid receptor. J Biol Chem. 1993 Oct 15;268(29):21455–8.

24. Harrell JM, Murphy PJM, Morishima Y, Chen H, Mansfield JF, Galigniana MD, et al. Evidence for Glucocorticoid Receptor Transport on Microtubules by Dynein. J Biol Chem. 2004 Dec 24;279(52):54647–54.

25. Scheschowitsch K, Leite JA, Assreuy J. New Insights in Glucocorticoid Receptor Signaling—More Than Just a Ligand-Binding Receptor. Front Endocrinol (Lausanne). 2017 Feb 6;8(FEB):19–21.

26. Zhang X, Clark AF, Yorio T. Heat shock protein 90 is an essential molecular chaperone for nuclear transport of glucocorticoid receptor beta. Invest Ophthalmol Vis Sci. 2006;47(2):700–8.

27. Reddy TE, Pauli F, Sprouse RO, Neff NF, Newberry KM, Garabedian MJ, et al. Genomic determination of the glucocorticoid response reveals unexpected mechanisms of gene regulation. Genome Res. 2009 Dec 1;19(12):2163–71.

28. Bianchetti L, Wassmer B, Defosset A, Smertina A, Tiberti ML, Stote RH, et al. Alternative dimerization interfaces in the glucocorticoid receptor-α ligand binding domain. Biochim Biophys Acta - Gen Subj. 2018 May 1;

29. Presman DM, Ganguly S, Schiltz RL, Johnson TA, Karpova TS, Hager GL. DNA binding triggers tetramerization of the glucocorticoid receptor in live cells. Proc Natl Acad Sci. 2016 Jul 19;113(29):8236–41.

30. Presman DM, Hager GL. More than meets the dimer: What is the quaternary structure of the glucocorticoid receptor? Transcription. 2017 Jan 20;8(1):32–9.

31. Chinenov Y, Gupte R, Dobrovolna J, Flammer JR, Liu B, Michelassi FE, et al. Role of transcriptional coregulator GRIP1 in the anti-inflammatory actions of glucocorticoids. Proc Natl Acad Sci. 2012 Jul 17;109(29):11776–81.

32. Reichardt HM, Tuckermann JP, Göttlicher M, Vujic M, Weih F, Angel P, et al. Repression of inflammatory responses in the absence of DNA binding by the glucocorticoid receptor. EMBO J. 2001 Dec 17;20(24):7168–73.

33. Schiller BJ, Chodankar R, Watson LC, Stallcup MR, Yamamoto KR. Glucocorticoid receptor binds half sites as a monomer and regulates specific target genes. Genome Biol. 2014 Jul 31;15(8):418.

34. McKay LI, Cidlowski JA. Cross-Talk between Nuclear Factor-κB and the Steroid Hormone Receptors: Mechanisms of Mutual Antagonism. Mol Endocrinol. 1998 Jan;12(1):45–56.

35. Rauch A, Seitz S, Baschant U, Schilling AF, Illing A, Stride B, et al. Glucocorticoids suppress bone formation by attenuating osteoblast differentiation via the monomeric glucocorticoid receptor. Cell Metab. 2010;11(6):517–31.

36. Meyer T, Gustafsson JA, Carlstedt-Duke J. Glucocorticoid-dependent transcriptional repression of the

osteocalcin gene by competitive binding at the TATA box. DNA Cell Biol. 1997;16(8):919–27.

37. Watson LC, Kuchenbecker KM, Schiller BJ, Gross JD, Pufall MA, Yamamoto KR. The glucocorticoid receptor dimer interface allosterically transmits sequence-specific DNA signals. Nat Struct Mol Biol. 2013;20(7):876–83.

38. Thornton JW. Evolution of vertebrate steroid receptors from an ancestral estrogen receptor by ligand exploitation and serial genome expansions. Proc Natl Acad Sci. 2001 May 8;98(10):5671–6.

39. He Y, Yi W, Suino-Powell K, Zhou XE, Tolbert WD, Tang X, et al. Structures and mechanism for the design of highly potent glucocorticoids. Cell Res. 2014 Jun 25;24(6):713–26.

40. Ito K, Yamamura S, Essilfie-Quaye S, Cosio B, Ito M, Barnes PJ, et al. Histone deacetylase 2–mediated deacetylation of the glucocorticoid receptor enables NF-κB suppression. J Exp Med. 2006;203(1):7–13.

41. Nader N, Chrousos GP, Kino T. Circadian rhythm transcription factor CLOCK regulates the transcriptional activity of the glucocorticoid receptor by acetylating its hinge region lysine cluster: potential physiological implications. FASEB J. 2009;23(5):1572–83.

42. Galliher-Beckley AJ, Cidlowski JA. Emerging roles of glucocorticoid receptor phosphorylation in modulating glucocorticoid hormone action in health and disease. IUBMB Life. 2009 Oct;61(10):979–86.

43. Krstic MD, Rogatsky I, Yamamoto KR, Garabedian MJ. Mitogen-activated and cyclin-dependent protein kinases selectively and differentially modulate transcriptional enhancement by the glucocorticoid receptor. Mol Cell Biol. 1997 Jul;17(7):3947–54.

44. Miller AL, Webb MS, Copik AJ, Wang Y, Johnson BH, Kumar R, et al. p38 Mitogen-Activated Protein Kinase (MAPK) Is a Key Mediator in Glucocorticoid-Induced Apoptosis of Lymphoid Cells: Correlation between p38 MAPK Activation and Site-Specific Phosphorylation of the Human Glucocorticoid Receptor at Serine 211. Mol Endocrinol. 2005 Jun;19(6):1569–83.

45. Wang Z, Frederick J, Garabedian MJ. Deciphering the Phosphorylation “Code” of the Glucocorticoid Receptor in Vivo. J Biol Chem. 2002 Jul 19;277(29):26573–80.

46. Itoh M, Adachi M, Yasui H, Takekawa M, Tanaka H, Imai K. Nuclear Export of Glucocorticoid Receptor is Enhanced by c-Jun N-Terminal Kinase-Mediated Phosphorylation. Mol Endocrinol. 2002 Oct;16(10):2382–92.

47. Davies L, Paraskevopoulou E, Sadeq M, Symeou C, Pantelidou C, Demonacos C, et al. Regulation of Glucocorticoid Receptor Activity by a Stress Responsive Transcriptional Cofactor. Mol Endocrinol. 2011;25(1):58–71.

48. Kino T, Liou S-H. Glucocorticoid receptor mutants demonstrate increased motility inside the nucleus of living cells: time of fluorescence recovery after photobleaching (FRAP) is an integrated measure of receptor function. Mol Med. 2006;12(7–12):1.

49. Hua G, Paulen L, Chambon P. GR SUMOylation and formation of an SUMO-SMRT/NCoR1-HDAC3 repressing complex is mandatory for GC-induced IR nGRE-mediated transrepression. Proc Natl Acad Sci. 2016;113(5):E626–34.

50. Duma D, Silva-Santos JE, Assreuy J. Inhibition of glucocorticoid receptor binding by nitric oxide in endotoxemic rats. Crit Care Med. 2004 Nov;32(11):2304–10.

51. Kröncke KD, Carlberg C. Inactivation of zinc finger transcription factors provides a mechanism for a gene regulatory role of nitric oxide. FASEB J. 2000;14(1):166–73.

52. Heery DM, Kalkhoven E, Hoare S, Parker MG. A signature motif in transcriptional co-activators mediates binding to nuclear receptors. Nature. 1997;387(6634):733–6.

53. Hu X, Lazar MA. The CoRNR motif controls the recruitment of corepressors by nuclear hormone receptors. Nature. 1999;402(6757):93–6.

54. Khan SH, Awasthi S, Guo C, Goswami D, Ling J, Griffin PR, et al. Binding of the N-terminal region of coactivator TIF2 to the intrinsically disordered AF1 domain of the glucocorticoid receptor is accompanied by conformational reorganizations. J Biol Chem. 2012;287(53):44546–60.

55. Strehl C, Buttgereit F. Unraveling the functions of the membrane-bound glucocorticoid receptors: First clues on origin and functional activity. Ann N Y Acad Sci. 2014;1318(1):1–6.

56. Deng Q, Riquelme D, Trinh L, Low MJ, Tomic M, Stojilkovic S, et al. Rapid glucocorticoid feedback inhibition of ACTH secretion involves ligand-dependent membrane association of glucocorticoid receptors. Endocrinology. 2015;156(9):3215–27.

57. Norman AW, Mizwicki MT, Norman DPG. Steroid-hormone rapid actions, membrane receptors and a conformational ensemble model. Nat Rev Drug Discov. 2004;3(1):27–41.

58. Gruber CJ, Gruber DM, Gruber IML, Wieser F, Huber JC. Anatomy of the estrogen response element. Trends Endocrinol Metab. 2004;15(2):73–8.

59. Scheller K, Sekeris CE, Krohn G, Hock R, Hansen IA, Scheer U. Localization of glucocorticoid hormone receptors in mitochondria of human cells. Eur J Cell Biol. 2000 May;79(5):299–307.

60. Psarra A-MG, Sekeris CE. Glucocorticoids induce mitochondrial gene transcription in HepG2 cells. Biochim Biophys Acta - Mol Cell Res. 2011 Oct;1813(10):1814–21.

61. Talabér G, Boldizsár F, Bartis D, Pálinkás L, Szabó M, Berta G, et al. Mitochondrial translocation of the glucocorticoid receptor in double-positive thymocytes correlates with their sensitivity to glucocorticoid-induced apoptosis. Int Immunol. 2009 Nov;21(11):1269–76.

62. Sionov RV, Cohen O, Kfir S, Zilberman Y, Yefenof E. Role of mitochondrial glucocorticoid receptor in glucocorticoid-induced apoptosis. J Exp Med. 2006 Jan 23;203(1):189–201.

63. Furst R, Schroeder T, Eilken HM, Bubik MF, Kiemer AK, Zahler S, et al. MAPK phosphatase-1 represents a novel anti-inflammatory target of glucocorticoids in the human endothelium. FASEB J. 2006;21(1):74–80.

64. Mendes ES, Pereira A, Danta I, Duncan RC, Wanner A. Comparative bronchial vasoconstrictive efficacy of inhaled glucocorticosteroids. Eur Respir J. 2003;21(6):989–93.

65. Liu L, Wang YX, Zhou J, Long F, Sun HW, Liu Y, et al. Rapid non-genomic inhibitory effects of glucocorticoids on human neutrophil degranulation. Inflamm Res. 2005;54(1):37–41.

66. Long F, Wang YX, Liu L, Zhou J, Cui RY, Jiang CL. Rapid nongenomic inhibitory effects of glucocorticoids on phagocytosis and superoxide anion production by macrophages. Steroids. 2005;70(1):55–61.

67. Liu C, Zhou J, Zhang L-D, Wang Y-X, Kang Z-M, Chen Y-Z, et al. Rapid inhibitory effect of corticosterone on histamine release from rat peritoneal mast cells. Horm Metab Res. 2007;39(4):273–7.

68. Zhou J, Liu DF, Liu C, Kang ZM, Shen XH, Chen YZ, et al. Glucocorticoids inhibit degranulation of mast cells in allergic asthma via nongenomic mechanism. Allergy Eur J Allergy Clin Immunol. 2008;63(9):1177–85.

69. Lee SR, Kim HK, Youm JB, Dizon LA, Song IS, Jeong SH, et al. Non-genomic effect of glucocorticoids on cardiovascular system. Pflügers Arch - Eur J Physiol. 2012 Dec 23;464(6):549–59.

70. ZHANG T, SHI W-L, TASKER JG, ZHOU J-R, PENG Y-L, MIAO C-Y, et al. Dexamethasone induces rapid promotion of norepinephrine-mediated vascular smooth muscle cell contraction. Mol Med Rep. 2013 Feb;7(2):549–54.

71. Xu J, Wu R-C, O'Malley BW. Normal and cancer-related functions of the p160 steroid receptor co-activator (SRC) family. Nat Rev Cancer. 2009 Sep 1;9(9):615–30.

72. Walsh CA, Qin L, Tien JCY, Young LS, Xu J. The function of steroid receptor coactivator-1 in normal tissues and cancer. Int J Biol Sci. 2012;8(4):470–85.

73. Allen BL, Taatjes DJ. The Mediator complex: a central integrator of transcription. Nat Rev Mol Cell Biol. 2015 Mar 18;16(3):155–66.

74. Chodankar R, Wu D-Y, Schiller BJ, Yamamoto KR, Stallcup MR. Hic-5 is a transcription coregulator that acts before and/or after glucocorticoid receptor genome occupancy in a gene-selective manner. Proc Natl Acad Sci. 2014 Mar 18;111(11):4007–12.

75. Kim JH, Li H, Stallcup MR. CoCoA, a Nuclear Receptor Coactivator which Acts through an N-Terminal Activation Domain of p160 Coactivators. Mol Cell. 2003 Dec;12(6):1537–49.

76. King HA, Trotter KW, Archer TK. Chromatin remodeling during glucocorticoid receptor regulated transactivation. Biochim Biophys Acta - Gene Regul Mech. 2012 Jul;1819(7):716–26.

77. Stallcup MR, Kim JH, Teyssier C, Lee Y-H, Ma H, Chen D. The roles of protein–protein interactions and protein methylation in transcriptional activation by nuclear receptors and their coactivators. J Steroid Biochem Mol Biol. 2003 Jun;85(2–5):139–45.

78. Bittencourt D, Wu D-Y, Jeong KW, Gerke DS, Herviou L, Ianculescu I, et al. G9a functions as a molecular scaffold for assembly of transcriptional coactivators on a subset of Glucocorticoid Receptor target genes. Proc Natl Acad Sci. 2012 Nov 27;109(48):19673–8.

79. Fonte C, Trousson A, Grenier J, Schumacher M, Massaad C. Opposite effects of CBP and p300 in glucocorticoid signaling in astrocytes. J Steroid Biochem Mol Biol. 2007 May;104(3–5):220–7.

80. Ogryzko V V., Kotani T, Zhang X, Schiltz RL, Howard T, Yang X-J, et al. Histone-like TAFs within the PCAF Histone Acetylase Complex. Cell. 1998 Jul;94(1):35–44.

81. Guenther MG, Barak O, Lazar MA. The SMRT and N-CoR Corepressors Are Activating Cofactors for Histone Deacetylase 3. Mol Cell Biol. 2001 Sep 15;21(18):6091–101.

82. Wong MM, Guo C, Zhang J. Nuclear receptor corepressor complexes in cancer: mechanism, function and regulation. Am J Clin Exp Urol. 2014;2(3):169–87.

83. Ritter HD, Mueller CR. Expression microarray identifies the unliganded glucocorticoid receptor as a regulator of gene expression in mammary epithelial cells. BMC Cancer. 2014 Dec 22;14(1):275.

84. Sanchez ER. Heat shock induces translocation to the nucleus of the unliganded glucocorticoid receptor. J Biol Chem. 1992 Jan 5;267(1):17–20.

85. Ritter HD, Antonova L, Mueller CR. The Unliganded Glucocorticoid Receptor Positively Regulates the Tumor Suppressor Gene BRCA1 through GABP Beta. Mol Cancer Res. 2012 Apr 1;10(4):558–69.

86. Ji JY. Shear Stress Causes Nuclear Localization of Endothelial Glucocorticoid Receptor and Expression From the GRE Promoter. Circ Res. 2003 Feb 21;92(3):279–85.

87. Verhoog NJD, Du Toit A, Avenant C, Hapgood JP. Glucocorticoid-independent Repression of Tumor Necrosis Factor (TNF) α-stimulated Interleukin (IL)-6 Expression by the Glucocorticoid Receptor. J Biol Chem. 2011 Jun 3;286(22):19297–310.

88. Robertson S, Rohwer JM, Hapgood JP, Louw A. Impact of Glucocorticoid Receptor Density on Ligand-Independent Dimerization, Cooperative Ligand-Binding and Basal Priming of Transactivation: A Cell Culture Model. Chang AYW, editor. PLoS One. 2013 May 22;8(5):e64831.

89. Matthews L, Johnson J, Berry A, Trebble P, Cookson A, Spiller D, et al. Cell Cycle Phase Regulates

Glucocorticoid Receptor Function. Vanacker J-M, editor. PLoS One. 2011 Jul 29;6(7):e22289.

90. Hapgood JP, Avenant C, Moliki JM. Glucocorticoid-independent modulation of GR activity: Implications for immunotherapy. Pharmacol Ther. 2016 Sep;165:93–113.

91. Rang H, Dale M, Ritter M, Flower R, Henderson G. Rang and Dale's Pharmacology. 7th Editio. Elsevier Inc.; 2012.

92. Benedek TG. History of the development of corticosteroid therapy. Clin Exp Rheumatol. 1855;29(5 Suppl 68):S-5-12.

93. Schäcke H, Döcke WD, Asadullah K. Mechanisms involved in the side effects of glucocorticoids. Pharmacol Ther. 2002;96(1):23–43.

94. Clark R. Glucocorticoid Receptor Antagonists. Curr Top Med Chem. 2008;8(9):813–38.

95. Hattori T, Murase T, Iwase E, Takahashi K, Ohtake M, Tsuboi K, et al. Glucocorticoid-induced hypertension and cardiac injury: effects of mineralocorticoid and glucocorticoid receptor antagonism. Nagoya J Med Sci. 2013;75(1–2):81–92.

96. Wang J, Harris C. Glucocorticoid Signaling. Wang J-C, Harris C, editors. New York, NY: Springer New York; 2015. 235-239 p. (Advances in Experimental Medicine and Biology; vol. 872).

97. Garner B, Phillips L, Bendall S, Parslow R, Hetrick SE. Antiglucocorticoid and related treatments for psychosis. In: Garner B, editor. Cochrane Database of Systematic Reviews. Chichester, UK: John Wiley & Sons, Ltd; 2008.

98. Heath B, George W, Ann A. EP1127605 B1. 2006;99(19):1–8.

99. Alan F. Schatzberg JKB. US 6620802 B1. 2003;1(12).

100. Sonino N, Fava G. Psychiatric disorders associated with Cushing's syndrome. CNS Drugs. 2001;15(5):361–73.

101. Lutgendorf SK, Sood AK, Antoni MH. Host factors and cancer progression: Biobehavioral signaling pathways and interventions. J Clin Oncol. 2010;28(26):4094–9.

102. Sephton SE, Sapolsky RM, Kraemer HC, Spiegel D, Robert M, Kraemer HC. Diurnal Cortisol Rhythm as a Predictor of Breast Cancer Survival. J Natl Cancer Inst. 2000;92(12):994–1000.

103. Chen Z, Lan X, Wu D, Sunkel B, Ye Z, Huang J, et al. Ligand-dependent genomic function of glucocorticoid receptor in triple-negative breast cancer. Nat Commun. 2015;6:8323.

104. Reeder a, Attar M, Nazario L, Bathula C, Zhang a, Hochbaum D, et al. Stress hormones reduce the efficacy of paclitaxel in triple negative breast cancer through induction of DNA damage. Br J Cancer. 2015;112(9):1461–70.

105. Chen Y, Lyga J. Brain-skin connection: stress, inflammation and skin aging. Inflamm Allergy Drug Targets. 2014;13(3):177–90.

106. Denda M, Tsuchiya T, Elias PM, Feingold KR. Stress alters cutaneous permeability barrier homeostasis. Am J Physiol - Regul Integr Comp Physiol. 2000;278(2 47-2):R367–72.

107. Konturek PC, Brzozowski T, Konturek SJ, Konturek P.C., Brzozowski T. KSJ. Stress and the gut: pathophysiology, clinical consequences, diagnostic approach and treatment options. Am J Physiol. 2011 Dec;62(6):591–9.

108. Johanssen S, Allolio B. Mifepristone (RU 486) in Cushing's syndrome. Eur J Endocrinol. 2007;157(5):561–9.

109. Robert H. Howland M. Mifepristone as a therapeutic agent in psychiatry. J Psychosoc Nurs. 2013;51(6):11–4.

110. NICHD. Effects of the Glucocorticoid Antagonist, Mifepristone, on Glucose Intolerance in Obese and Overweight Individuals (Clinical Trial) [Internet]. [cited 2016 Mar 3]. Available from: https://clinicaltrials.gov/ct2/show/NCT01419535

111. Gross C, Blasey CM, Roe RL, Belanoff JK. Mifepristone reduces weight gain and improves metabolic abnormalities associated with risperidone treatment in normal men. Obesity (Silver Spring). 2010;18(12):2295–300.

112. Chu JW, Matthias DF, Belanoff J, Schatzberg A, Hoffman AR, Feldman D. Successful Long-Term Treatment of Refractory Cushing's Disease with High-Dose Mifepristone (RU 486). J Clin Endocrinol Metab. 2001;86(8):3568–73.

113. Fleseriu M, Biller BMK, Findling JW, Molitch ME, Schteingart DE, Gross C, et al. Mifepristone, a Glucocorticoid Receptor Antagonist, Produces Clinical and Metabolic Benefits in Patients with Cushing's Syndrome. J Clin Endocrinol Metab. 2012;97(6):2039–49.

114. Fein HG, Brooks T, Iii V, Kushner H, Cram D, Nguyen D. Sustained weight loss in patients treated with mifepristone for Cushing's syndrome: a follow-up analysis of the SEISMIC study and long-term extension. BMC Endocr Disord. 2015;15:1–7.

115. Ago Y, Arikawa S, Yata M, Yano K, Abe M, Takuma K, et al. Antidepressant-like effects of the glucocorticoid receptor antagonist RU-43044 are associated with changes in prefrontal dopamine in mouse models of depression. Neuropharmacology. 2008;55(8):1355–63.

116. De Bosscher K. Selective Glucocorticoid Receptor modulators. J Steroid Biochem Mol Biol. 2010;120(2–3):96–104.

117. Spiga F, Harrison LR, Wood S a., Atkinson HC, MacSweeney CP, Thomson F, et al. Effect of the glucocorticoid receptor antagonist Org 34850 on basal and stress-induced corticosterone secretion. J Neuroendocrinol. 2007;19(11):891–900.

118. Bachmann CG, Linthorst ACE, Holsboer F, Reul JMHM. Effect of chronic administration of selective glucocorticoid receptor antagonists on the rat hypothalamic-pituitary-adrenocortical axis. Neuropsychopharmacology. 2003;28(6):1056–67.

119. Beaudry JL, Dunford EC, Teich T, Zaharieva D, Hunt H, Belanoff JK, et al. Effects of Selective and Non-Selective Glucocorticoid Receptor II Antagonists on Rapid-Onset Diabetes in Young Rats. Tuckermann JP, editor. PLoS One. 2014 Mar 18;9(3):e91248.

120. Schacke H, Schottelius A, Docke W-D, Strehlke P, Jaroch S, Schmees N, et al. Dissociation of transactivation from transrepression by a selective glucocorticoid receptor agonist leads to separation of therapeutic effects from side effects. Proc Natl Acad Sci. 2004;101(1):227–32.

121. Schäcke H, Zollner TM, Döcke WD, Rehwinkel H, Jaroch S, Skuballa W, et al. Characterization of ZK 245186, a novel, selective glucocorticoid receptor agonist for the topical treatment of inflammatory skin diseases. Br J Pharmacol. 2009;158(4):1088–103.

122. Robertson S, Allie-Reid F, Berghe W Vanden, Visser K, Binder A, Africander D, et al. Abrogation of Glucocorticoid Receptor Dimerization Correlates with Dissociated Glucocorticoid Behavior of Compound A. J Biol Chem. 2010 Mar 12;285(11):8061–75.

123. Sundahl N, Bridelance J, Libert C, De Bosscher K, Beck IM. Selective glucocorticoid receptor modulation: New directions with non-steroidal scaffolds. Pharmacol Ther. 2015;152:28–41.

124. Kurimoto T, Tamai I, Miyai A, Kosugi Y, Nakagawa T, Yamamoto Y, et al. JTP-117968, a novel selective glucocorticoid receptor modulator, exhibits improved transrepression/transactivation dissociation.

Eur J Pharmacol. 2017;803(March):179–86.

125. Coghlan MJ, Jacobson PB, Lane B, Nakane M, Lin CW, Elmore SW, et al. A Novel Antiinflammatory Maintains Glucocorticoid Efficacy with Reduced Side Effects. Mol Endocrinol. 2003;17(5):860–9.

126. Rauch A, Gossye V, Bracke D, Gevaert E, Jacques P, Van Beneden K, et al. An anti-inflammatory selective glucocorticoid receptor modulator preserves osteoblast differentiation. FASEB J. 2011;25(4):1323–32.

127. Stock T, Fleishaker D, Wang X, Mukherjee A, Mebus C. Improved disease activity with fosdagrocorat (PF-04171327), a partial agonist of the glucocorticoid receptor, in patients with rheumatoid arthritis: a Phase 2 randomized study. Int J Rheum Dis. 2017 Aug;20(8):960–70.

128. Baiula M, Spampinato S. Mapracorat, a novel non-steroidal selective glucocorticoid receptor agonist for the treatment of allergic conjunctivitis. Inflamm Allergy Drug Targets. 2014;13(5):289–98.

129. Zhou J, Li M, Sheng CQ, Liu L, Li Z, Wang Y, et al. A novel strategy for development of glucocorticoids through non-genomic mechanism. Cell Mol Life Sci. 2011;68(8):1405–14.

130. Thermo Fisher. SelectScreen ™ Cell-Based Nuclear Receptor Profiling Service: Screening Protocol and Assay Conditions. 2018. p. 1–13.

131. Thermo Fisher. LanthaScreen™ TR-FRET Coregulator: Protocol and Assay Conditions. 2017. p. 1–7.

132. Thermo Fisher. LanthaScreen ™ TR-FRET Competitive Binding Assay: Screening Protocol and Assay Conditions. 2016. p. 1–5.

133. Ortlund EA, Bridgham JT, Redinbo MR, Thornton JW. Crystal Structure of an Ancient Protein: Evolution by Conformational Epistasis. Science (80-). 2007;317(5844):1544–8.

134. GE Healthcare. Biacore™ Assay Handbook. 29th-194th–0th ed. GE Healthcare Life Sciences;

135. Fernández-Rhodes LE, Kokkinis AD, White MJ, Watts CA, Auh S, Jeffries NO, et al. Efficacy and safety of dutasteride in patients with spinal and bulbar muscular atrophy: a randomised placebo-controlled trial. Lancet Neurol. 2011 Feb;10(2):140–7.

136. Thole Z, Manso G, Salgueiro E, Revuelta P, Hidalgo A. Hepatotoxicity induced by antiandrogens: A review of the literature. Urol Int. 2004;73(4):289–95.

137. Ronchetti S, Migliorati G, Riccardi C. GILZ as a Mediator of the Anti-Inflammatory Effects of Glucocorticoids. Front Endocrinol (Lausanne). 2015 Nov 9;6(NOV):1–6.

138. Korhonen R, Moilanen E. Mitogen-Activated Protein Kinase Phosphatase 1 as an Inflammatory Factor and Drug Target. Basic Clin Pharmacol Toxicol. 2014;114(1):24–36.

139. Altman A, Kong K. Protein Kinase C Enzymes in the Hematopoietic and Immune Systems. Annu Rev Immunol. 2016 May 20;34(1):511–38.

140. Baud V, Karin M. Signal transduction by tumor necrosis factor and its relatives. Trends Cell Biol. 2001 Sep;11(9):372–7.

141. Steer JH, Kroeger KM, Abraham LJ, Joyce DA. Glucocorticoids Suppress Tumor Necrosis Factor-α Expression by Human Monocytic THP-1 Cells by Suppressing Transactivation through Adjacent NF-κB and c-Jun-Activating Transcription Factor-2 Binding Sites in the Promoter. J Biol Chem. 2000 Jun 16;275(24):18432–40.

142. Joyce DA, Steer JH, Abraham LJ. Glucocorticoid modulation of human monocyte/macrophage function: Control of TNF-α secretion. Inflamm Res. 1997 Nov 1;46(11):447–51.

143. Coutinho AE, Chapman KE. The anti-inflammatory and immunosuppressive effects of glucocorticoids,

recent developments and mechanistic insights. Mol Cell Endocrinol. 2011;335(1):2–13.

144. Ayroldi E, Riccardi C. Glucocorticoid-induced leucine zipper (GILZ): a new important mediator of glucocorticoid action. FASEB J. 2009;23(11):3649–58.

145. Yang YH, Aeberli D, Dacumos A, Xue JR, Morand EF. Annexin-1 Regulates Macrophage IL-6 and TNF via Glucocorticoid-Induced Leucine Zipper. J Immunol. 2009 Jul 15;183(2):1435–45.

146. Oerlemans R, Vink J, Dijkmans BAC, Assaraf YG, van Miltenburg M, van der Heijden J, et al. Sulfasalazine sensitises human monocytic/macrophage cells for glucocorticoids by upregulation of glucocorticoid receptor and glucocorticoid induced apoptosis. Ann Rheum Dis. 2007 Oct 1;66(10):1289–95.

147. Deshantri AK, Varela Moreira A, Ecker V, Mandhane SN, Schiffelers RM, Buchner M, et al. Nanomedicines for the treatment of hematological malignancies. J Control Release. 2018 Oct;287(August):194–215.

148. Taylor J, Xiao W, Abdel-Wahab O. Diagnosis and classification of hematologic malignancies on the basis of genetics. Blood. 2017 Jul 27;130(4):410–23.

149. Krawczyk J, O'Dwyer M, Swords R, Freeman C, Giles FJ. The Role of Inflammation in Leukaemia. In: Advances in Experimental Medicine and Biology. 2014. p. 335–60.

150. Terwilliger T, Abdul-Hay M. Acute lymphoblastic leukemia: a comprehensive review and 2017 update. Blood Cancer J. 2017 Jun 30;7(6):e577.

151. Hallek M. Chronic lymphocytic leukemia: 2017 update on diagnosis, risk stratification, and treatment. Am J Hematol. 2017;92(9):946–65.

152. Ferrer G, Montserrat E. Critical molecular pathways in CLL therapy. Mol Med. 2018 Dec 15;24(1):9.

153. De Kouchkovsky I, Abdul-Hay M. 'Acute myeloid leukemia: a comprehensive review and 2016 update.' Blood Cancer J. 2016 Jul 1;6(7):e441–e441.

154. Watts J, Nimer S. Recent advances in the understanding and treatment of acute myeloid leukemia. F1000Research. 2018 Aug 6;7(0):1196.

155. Apperley JF. Chronic myeloid leukaemia. Lancet. 2015 Apr;385(9976):1447–59.

156. Ansell SM. Hodgkin lymphoma: 2016 update on diagnosis, risk-stratification, and management. Am J Hematol. 2016 Jun;91(4):434–42.

157. Luminari S, Bellei M, Biasoli I, Federico M. Follicular lymphoma. Rev Bras Hematol Hemoter. 2011;34(1):54–9.

158. Martelli M, Ferreri AJM, Agostinelli C, Di Rocco A, Pfreundschuh M, Pileri SA. Diffuse large B-cell lymphoma. Crit Rev Oncol Hematol. 2013;87(2):146–71.

159. Mehta GR, Suhail F, Haddad RY, Zalzaleh G, Lerma E V. Multiple myeloma. Disease-a-Month. 2014;60(10):483–8.

160. Hematopoiesis [Internet]. Clinical Gate. 2015 [cited 2018 Sep 7]. Available from: https://clinicalgate.com/hematopoiesis/

161. Spanish society of hematology and hemotherapy. Póster: Cáncer hematológico [Internet]. 2016. Available from: https://www.sehh.es/es/

162. Lee CK. Evolving Role of Radiation Therapy for Hematologic Malignancies. Hematol Oncol Clin North Am. 2006 Apr;20(2):471–503.

163. Baker M, Wang H, Rowley SD, Cai L, Pecora AL, Skarbnik A, et al. Comparative Outcomes after

Haploidentical or Unrelated Donor Bone Marrow or Blood Stem Cell Transplantation in Adult Patients with Hematological Malignancies. Biol Blood Marrow Transplant. 2016 Nov;22(11):2047–55.

164. Ottmann O, Saglio G, Apperley JF, Arthur C, Bullorsky E, Charbonnier A, et al. Long-term efficacy and safety of dasatinib in patients with chronic myeloid leukemia in accelerated phase who are resistant to or intolerant of imatinib. Blood Cancer J. 2018 Sep 3;8(9):88.

165. Rosti G, Castagnetti F, Gugliotta G, Baccarani M. Tyrosine kinase inhibitors in chronic myeloid leukaemia: which, when, for whom? Nat Rev Clin Oncol. 2017 Mar 18;14(3):141–54.

166. Walasek A. The new perspectives of targeted therapy in acute myeloid leukemia. Adv Clin Exp Med. 2018 Aug 24;

167. Im A, Pavletic SZ. Immunotherapy in hematologic malignancies: past, present, and future. J Hematol Oncol. 2017 Dec 24;10(1):94.

168. Iwai Y, Terawaki S, Honjo T. PD-1 blockade inhibits hematogenous spread of poorly immunogenic tumor cells by enhanced recruitment of effector T cells. Int Immunol. 2004 Dec 20;17(2):133–44.

169. Constantinidou A, Alifieris C, Trafalis DT. Targeting Programmed Cell Death -1 (PD-1) and Ligand (PD-L1): A new era in cancer active immunotherapy. Pharmacol Ther. 2018 Sep;1.

170. Rescigno M, Avogadri F, Curigliano G. Challenges and prospects of immunotherapy as cancer treatment. Biochim Biophys Acta - Rev Cancer. 2007 Sep;1776(1):108–23.

171. Buie LW, Pecoraro JJ, Horvat TZ, Daley RJ. Blinatumomab: A First-in-Class Bispecific T-Cell Engager for Precursor B-Cell Acute Lymphoblastic Leukemia. Ann Pharmacother. 2015;49(9):1057–67.

172. Tasian SK, Gardner RA. CD19-redirected chimeric antigen receptor-modified T cells: A promising immunotherapy for children and adults with B-cell acute lymphoblastic leukemia (ALL). Ther Adv Hematol. 2015;6(5):228–41.

173. Grillo-Lopez A, White C, Dallaire B, Varns C, Shen C, Wei A, et al. Rituximab The First Monoclonal Antibody Approved for the Treatment of Lymphoma. Curr Pharm Biotechnol. 2000 Jul 1;1(1):1–9.

174. Teeling JL. Characterization of new human CD20 monoclonal antibodies with potent cytolytic activity against non-Hodgkin lymphomas. Blood. 2004 Sep 15;104(6):1793–800.

175. Grillo-López AJ. Zevalin: the first radioimmunotherapy approved for the treatment of lymphoma. Expert Rev Anticancer Ther. 2002 Oct 10;2(5):485–93.

176. Medinger M, Passweg J. Role of tumour angiogenesis in haematological malignancies. Swiss Med Wkly. 2014 Nov 6;144(November):1–12.

177. Doxil®: FDA Approved Drug Products [Internet]. [cited 2018 Sep 10]. Available from: https://www.accessdata.fda.gov/scripts/cder/daf/index.cfm?event=overview.process&ApplNo=050718

178. Marqibo®: FDA Approved Drug Products [Internet]. [cited 2018 Sep 10]. Available from: https://www.accessdata.fda.gov/scripts/cder/daf/index.cfm?event=overview.process&ApplNo=202497

179. DaunoXome®: FDA Approved Drug Products [Internet]. [cited 2018 Sep 10]. Available from: https://www.accessdata.fda.gov/scripts/cder/daf/index.cfm?event=overview.process&ApplNo=050704

180. VYXEOS™: FDA Approved Drug Products [Internet]. [cited 2018 Sep 10]. Available from: https://www.accessdata.fda.gov/scripts/cder/daf/index.cfm?event=overview.process&ApplNo=209401

181. A Evaluation of the Safety of Oncocort IV Pegylated Liposomal Dexamethasone Phosphate in Patients With Progressive Multiple Myeloma - ClinicalTrials.gov [Internet]. 2017 [cited 2018 Sep 9]. Available from: https://clinicaltrials.gov/ct2/show/NCT03033316?cond=NCT03033316&rank=1

182. Krishnan V, Xu X, Barwe SP, Yang X, Czymmek K, Waldman SA, et al. Dexamethasone-Loaded Block Copolymer Nanoparticles Induce Leukemia Cell Death and Enhance Therapeutic Efficacy: A Novel Application in Pediatric Nanomedicine. Mol Pharm. 2013 Jun 3;10(6):2199–210.

183. Moehler T., Ho A., Goldschmidt H, Barlogie B. Angiogenesis in hematologic malignancies. Crit Rev Oncol Hematol. 2003 Mar;45(3):227–44.

184. Sarin H. Physiologic upper limits of pore size of different blood capillary types and another perspective on the dual pore theory of microvascular permeability. J Angiogenes Res. 2010;2(1):14.

185. Tardi P, Wan CPL, Mayer L. Passive and semi-active targeting of bone marrow and leukemia cells using anionic low cholesterol liposomes. J Drug Target. 2016 Oct 20;24(9):797–804.

186. Paclitaxel Albumin-Stabilized Nanoparticle Formulation in Treating Patients With Relapsed or Refractory Multiple Myeloma - Clinical trial [Internet]. 2012 [cited 2018 Sep 10]. Available from: https://clinicaltrials.gov/ct2/show/NCT01646762?cond=NCT01646762&rank=1

187. Phase I/II Trial of the Combination of Lenalidomide (Revlimid) and Nab-paclitaxel (Abraxane) in the Treatment of Relapsed/Refractory Multiple Myeloma - Clinical trials [Internet]. 2014 [cited 2018 Sep 10]. Available from: https://clinicaltrials.gov/ct2/show/NCT02075021?cond=NCT02075021&rank=1

188. A Phase 1 Trial of ABI-011 in Patients With Advanced Solid Tumors or Lymphomas - Clinical trial [Internet]. 2010 [cited 2018 Sep 10]. Available from: https://clinicaltrials.gov/ct2/show/NCT01163071?cond=NCT01163071&rank=1

189. Doweyko AM. Steroid nuclear hormone receptors: The allosteric conversation. Drug Dev Res. 2007 May;68(3):95–106.

190. Coombs CC, Tavakkoli M, Tallman MS. Acute promyelocytic Leukemia: Where did we start, where are we now, and the future. Blood Cancer J. 2015;5(4):e304-9.

191. Greenstein S, Ghias K, Krett NL, Rosen ST. Mechanisms of glucocorticoid-mediated apoptosis in hematological malignancies. Clin Cancer Res. 2002 Jun;8(6):1681–94.

192. Wang Z, Malone MH, He H, McColl KS, Distelhorst CW. Microarray Analysis Uncovers the Induction of the Proapoptotic BH3-only Protein Bim in Multiple Models of Glucocorticoid-induced Apoptosis. J Biol Chem. 2003 Jun 27;278(26):23861–7.

193. Inaba H, Pui C-H. Glucocorticoid use in acute lymphoblastic leukaemia. Lancet Oncol. 2010 Nov;11(11):1096–106.

194. Tsao T, Kornblau S, Safe S, Watt JC, Ruvolo V, Chen W, et al. Role of peroxisome proliferator-activated receptor-gamma and its coactivator DRIP205 in cellular responses to CDDO (RTA-401) in acute myelogenous leukemia. Cancer Res. 2010;70(12):4949–60.

195. Asou H, Verbeek W, Williamson E, Elstner E, Kubota T, Kamada N, et al. Growth inhibition of myeloid leukemia cells by troglitazone, a ligand for peroxisome proliferator activated receptor gamma, and retinoids. IntJOncol. 1999;15:1027–31.

196. Yavasoglu I, Sargin G, Kadikoylu G, Karul A, Bolaman Z. The activity of atorvastatin and rosiglitazone on CD38, ZAP70 and apoptosis in lymphocytes of B-cell chronic lymphocytic leukemia in vitro. Med Oncol. 2013 Sep 19;30(3):603.

197. Cetinkalp S, Simsir IY, Sahin F, Saydam G, Ural AU, Yilmaz C. Can an oral antidiabetic (rosiglitazone) be of benefit in leukemia treatment? Saudi Pharm J. 2015 Jan;23(1):14–21.

198. Liu J-J, Hu T, Wu X-Y, Wang C-Z, Xu Y, Zhang Y, et al. Peroxisome Proliferator-Activated Receptor-γ Agonist Rosiglitazone– Induced Apoptosis in Leukemia K562 Cells and Its Mechanisms of Action. Int J Toxicol. 2009 Mar 13;28(2):123–31.

199. Pan J, Chen C, Jin Y, Fuentes-Mattei E, Velazquez-Tores G, Benito JM, et al. Differential impact of structurally different anti-diabetic drugs on proliferation and chemosensitivity of acute lymphoblastic leukemia cells. Cell Cycle. 2012 Jun 15;11(12):2314–26.

200. Yasugi E, Horiuchi A, Uemura I, Okuma E, Nakatsu M, Saeki K, et al. Peroxisome proliferator-activated receptor γ ligands stimulate myeloid differentiation and lipogenensis in human leukemia NB4 cells. Dev Growth Differ. 2006;48(3):177–88.

201. Bruns H, Büttner M, Fabri M, Mougiakakos D, Bittenbring JT, Hoffmann MH, et al. Vitamin D–dependent induction of cathelicidin in human macrophages results in cytotoxicity against high-grade B cell lymphoma. Sci Transl Med. 2015 Apr 8;7(282):282ra47-282ra47.

202. Pepper C. The vitamin D3 analog EB1089 induces apoptosis via a p53-independent mechanism involving p38 MAP kinase activation and suppression of ERK activity in B-cell chronic lymphocytic leukemia cells in vitro. Blood. 2003 Apr 1;101(7):2454–9.

203. Renné C, Benz AH, Hansmann ML. Vitamin D3receptor is highly expressed in Hodgkin's lymphoma. BMC Cancer. 2012 Dec 6;12(1):215.

204. Kulling PM, Olson KC, Olson TL, Feith DJ, Loughran TP. Vitamin D in hematological disorders and malignancies. Eur J Haematol. 2017;98(3):187–97.

205. Hickish T, Cunningham D, Colston K, Millar BC, Sandle J, Mackay AG, et al. The effect of 1,25-dihydroxyvitamin D3 on lymphoma cell lines and expression of vitamin D receptor in lymphoma. Br J Cancer. 1993 Oct;68(4):668–72.

206. Consolini R, Pala S, Legitimo A, Crimaldi G, Ferrari S, Ferrari S. Effects of vitamin D on the growth of normal and malignant B-cell progenitors. Clin Exp Immunol. 2001 Nov;126(2):214–9.

207. Mellibovsky RR, Díez, Pérez-Vila, Serrano, Nacher, AubÍa, et al. Vitamin D treatment in myelodysplastic syndromes. Br J Haematol. 1998;100(3):516–20.

208. Gallastegui N, Mackinnon JAG, Fletterick RJ, Estébanez-Perpiña E. Advances in our structural understanding of orphan nuclear receptors. Trends Biochem Sci. 2015;40(1):25–35.

209. Safe S, Jin U-H, Morpurgo B, Abudayyeh A, Singh M, Tjalkens RB. Nuclear receptor 4A (NR4A) family – orphans no more. J Steroid Biochem Mol Biol. 2016 Mar;157:48–60.

210. Zhao Y, Bruemmer D. NR4A Orphan Nuclear Receptors. Arterioscler Thromb Vasc Biol. 2010 Aug;30(8):1535–41.

211. Mullican SE, Zhang S, Konopleva M, Ruvolo V, Andreeff M, Milbrandt J, et al. Abrogation of nuclear receptors Nr4a3 andNr4a1 leads to development of acute myeloid leukemia. Nat Med. 2007 Jun 21;13(6):730–5.

212. Sirin O, Lukov GL, Mao R, Conneely OM, Goodell MA. The orphan nuclear receptor Nurr1 restricts the proliferation of haematopoietic stem cells. Nat Cell Biol. 2010 Dec 14;12(12):1213–9.

213. Deutsch AJA, Rinner B, Wenzl K, Pichler M, Troppan K, Steinbauer E, et al. NR4A1-mediated apoptosis suppresses lymphomagenesis and is associated with a favorable cancer-specific survival in patients with aggressive B-cell lymphomas. Blood. 2014;123(15):2367–77.

214. Grignani F, De Matteis S, Nervi C, Tomassoni L, Gelmetti V, Cioce M, et al. Fusion proteins of the retinoic acid receptor-alpha recruit histone deacetylase in promyelocytic leukaemia. Nature. 1998;391(6669):815–8.

215. Hong SH, David G, Wong CW, Dejean A, Privalsky ML. SMRT corepressor interacts with PLZF and with the PML-retinoic acid receptor alpha (RARalpha) and PLZF-RARalpha oncoproteins associated with acute promyelocytic leukemia. Proc Natl Acad Sci U S A. 1997;94(17):9028–33.

216. Racanicchi S, Maccherani C, Liberatore C, Billi M, Gelmetti V, Panigada M, et al. Targeting fusion protein/corepressor contact restores differentiation response in leukemia cells. EMBO J. 2005;24(6):1232–42.

217. Hug BA, Lazar MA. ETO interacting proteins. Oncogene. 2004 May 24;23(24):4270–4.

218. Zhang J, Hug BA, Huang EY, Chen CW, Gelmetti V, Maccarana M, et al. Oligomerization of ETO Is Obligatory for Corepressor Interaction. Mol Cell Biol. 2001 Jan 1;21(1):156–63.

219. Malam Y, Loizidou M, Seifalian AM. Liposomes and nanoparticles: nanosized vehicles for drug delivery in cancer. Trends Pharmacol Sci. 2009;30(11):592–9.

220. Chou T-C. Drug Combination Studies and Their Synergy Quantification Using the Chou-Talalay Method. Cancer Res. 2010 Jan 15;70(2):440–6.

221. Zhou G, Jin X, Zhu P, Yao JU, Zhang Y, Teng L, et al. Human Serum Albumin Nanoparticles as a Novel Delivery System for Cabazitaxel. Anticancer Res. 2016;36(4):1649–56.

222. Shargel L, Wu-Pong S, Yu ABC. Applied Biopharmaceutics and Pharmacokinetics, Leon Shargel and Andrew B. C. Yu. 5th editio. McGraw-Hill's; 2004.

223. Cho S, Yoon Y-R. Understanding the pharmacokinetics of prodrug and metabolite. Transl Clin Pharmacol. 2018;26(1):1.

224. Stetefeld J, McKenna SA, Patel TR. Dynamic light scattering: a practical guide and applications in biomedical sciences. Biophys Rev. 2016 Dec;8(4):409–27.

225. Bhattacharjee S. DLS and zeta potential – What they are and what they are not? J Control Release. 2016 Aug;235:337–51.

226. York MJ. Clinical Pathology. In: A Comprehensive Guide to Toxicology in Nonclinical Drug Development. Elsevier; 2017. p. 325–74.

227. Aulbach AD, Amuzie CJ. Biomarkers in Nonclinical Drug Development. In: A Comprehensive Guide to Toxicology in Nonclinical Drug Development. Elsevier; 2017. p. 447–71.